

Six-Wave Systems In One-Dimensional Wave Turbulence

by

Jason Paul Laurie

Thesis

Submitted to the University of Warwick

for the degree of

Doctor of Philosophy

Mathematics Institute

September 2010

THE UNIVERSITY OF
WARWICK

Contents

List of Figures	v
Acknowledgments	xi
Declarations	xii
Abstract	xiii
Abbreviations	xiv
Chapter 1 Introduction	1
1.1 Wave Turbulence	1
1.2 One-Dimensional Wave Turbulence	3
1.3 Layout of Thesis	4
Chapter 2 Wave Turbulence Theory	6
2.1 The Statistical Setup	7
2.2 Random Phase and Amplitude Fields	8
2.3 The Generating Functional	10
2.4 The Hamiltonian Formulation	11
2.5 The Canonical Transformation	13
2.6 The Weak Nonlinearity Expansion	21
2.7 Calculation of the Generating Functional	26
2.8 Phase Averaging	28
2.9 Amplitude Averaging	29

2.10	The Large Box and The Long Evolution Limits	30
2.11	Moments of the Wave Intensity $J_{\mathbf{k}}$	32
2.12	The One-Mode Amplitude Probability Density Function	33
2.13	The Kinetic Equation	35
2.14	The Fjørtoft Argument	36
2.15	The Zakharov Transform	38
2.16	Locality of the Kolmogorov-Zakharov Solutions	42
2.16.1	Convergence in the Infrared Region	43
2.16.2	Convergence in the Ultraviolet Region	44
2.17	Linear and Nonlinear Transfer Times and The Critical Balance Regime .	45
2.18	The Differential Approximation for the Kinetic Equation	47
2.19	The Gallavotti-Cohen Fluctuation Relation	49
Chapter 3	Kelvin Waves in Quantum Turbulence	52
3.1	Introduction to Quantum Turbulence	52
3.2	Kelvin Waves and Quantised Vortices	53
3.3	The Local Induction Approximation and Biot-Savart Hamiltonians . .	55
3.4	The Λ^{-1} -Expansion of the Six-Wave Interaction Coefficient $\mathcal{W}_{4,5,6}^{1,2,3}$. . .	59
3.5	Correction to the Local Induction Approximation Resonance Condition .	61
3.6	Asymptotics of ${}^c\mathcal{W}_{4,5,6}^{1,2,3}$	63
3.7	The Local Nonlinear Equation	64
3.8	The Truncated Local Induction Approximation Model	65
3.9	The Kozik-Svistunov Spectrum	66
3.10	Non-locality of Kelvin Wave Turbulence	66
3.10.1	Infrared Convergence	67
3.10.2	Ultraviolet Convergence	67
3.11	Logarithmic Corrections to the Inverse Wave Action Spectrum	68
3.12	The L'vov-Nazarenko Spectrum	68
3.13	Numerical Results	70
3.13.1	The Truncated Local Induction Approximation Model	70
3.13.2	The Local Nonlinear Equation	74

Chapter 4 Optical Wave Turbulence	80
4.1 The Experimental Setup	83
4.2 Equations for Optical Wave Turbulence	85
4.2.1 The Evolution Equation	85
4.2.2 The Long-Wave Equation	86
4.2.3 The Short-Wave Equation	87
4.3 The Hamiltonian Formulation	88
4.4 The Hamiltonian Representation for the Evolution Equation	90
4.5 The Nonlinearity Parameter	90
4.6 Scale Invariance of $\mathcal{W}_{4,5,6}^{1,2,3}$	91
4.7 The Kolmogorov-Zakharov Solutions of Optical Wave Turbulence	93
4.8 Locality of Optical Wave Turbulence	93
4.9 Logarithmic Corrections to the Direct Energy Spectrum	95
4.10 Flux Directions in Optical Wave Turbulence	96
4.11 Modulational Instability and the Creation of Solitons in the Long-Wave Equation	98
4.12 The Numerical Method	102
4.13 Results	104
4.13.1 The Long-Wave Equation	105
4.13.2 The Short-Wave Equation	125
Chapter 5 Conclusions	131
Appendix A The Canonical Transformation	136
Appendix B The Zakharov Transform	138
Appendix C Derivation of the Interaction Coefficients for the Biot-Savart Equation	140
C.1 The Four-Wave Function $\mathcal{F}_{3,4}^{1,2}$	143
C.2 The Six-Wave Function $\mathcal{G}_{4,5,6}^{1,2,3}$	144

Appendix D The Asymptotic Expansion of ${}^c\mathcal{W}_{4,5,6}^{1,2,3}$	145
D.1 The Analytical Expression for ${}^c\mathcal{W}_{4,5,6}^{1,2,3}$ with Two Small Wave Numbers	145
D.2 The Analytical Expression for ${}^c\mathcal{W}_{4,5,6}^{1,2,3}$ with Four Small Wave Numbers	148
Appendix E The Intensity Spectrum	149
Appendix F Non-Dimensionalisation of the Optical Wave Turbulence Models	152
Bibliography	153

List of Figures

2.1	We plot a graphical representation of the four-wave resonance condition [1]. The four-wave resonance condition is satisfied at points where the green and blue lines intersect, (shown by the black dot). However, for dispersion relations $\omega_k \propto k^\alpha$, with $\alpha > 1$, there can only be one intersection, corresponding to the trivial wave resonance: $\mathbf{k}_1 = \mathbf{k}_4$ and $\mathbf{k}_2 = \mathbf{k}_3$ (see text for details).	16
2.2	An illustration to show the four-wave interaction, $T_{3,4}^{1,2}$, and the six-wave interaction, $\mathcal{W}_{4,5,6}^{1,2,3}$, after the CT. The six-wave interaction term (sextet) is a sum of a $3 \rightarrow 3$ wave process and the contribution arising from two coupled four-wave interaction via a virtual wave.	21
2.3	A Graphic to show the development of the the dual cascade regime. . .	38
3.1	The averaged wave number spectrum $n_{\mathbf{k}}$ for a simulation of the direct cascade in stationary conditions, courtesy of Davide Dezzani. The straight line represents the KE prediction $n_{\mathbf{k}} \propto k^{-17/5}$. The inset shows the spectrum compensated with the theoretical prediction.	72
3.2	The averaged wave number spectrum, $n_{\mathbf{k}}$, for a simulation of the inverse cascade in stationary conditions, courtesy of Davide Dezzani. The straight line represents the KE prediction, $n_{\mathbf{k}} \propto k^{-3}$. The inset shows the spectrum compensated with the theoretical prediction.	73

3.3	We plot the magnitude of the linear, \mathcal{H}_2 , the nonlinear, \mathcal{H}_4 , and the total, \mathcal{H} energies of the simulation at late times in units of the linear timescale of the forcing mode, τ . Note that \mathcal{H}_2 is strictly non-negative and \mathcal{H}_4 is strictly non-positive. We observe a statistically stationary state of the energy. However, we also observe sharp jumps, peaks and troughs in the energy values.	75
3.4	Averaged wave action spectrum n_k for the LNE compensated by $k^{11/3}$. The spectrum has been averaged over a long time window once the steady state is reached. We plot the theoretical predictions of the KS and LN spectra.	76
3.5	We plot the wave action spectrum, n_k , at two times $\tau = 84$ and $\tau = 100$, where the energy at peka and in a trough respectively. We compare these two spectra with the fully averaged wave action spectrum of Figure 3.4.	77
3.6	We plot the averaged linear energy flux, P_k , verses k in a stationary state. We observe a short inertial range where P_k is constant corresponding to the KZ solution.	78
3.7	We plot the PDF of the intensity of the wave field from physical space. We compare with the Gaussian fit of a straight line.	78
3.8	We plot the GCFR for the LNE for time fluctuations in the energy flux P_k . We superimpose a straight line corresponding to Relation (2.141). The length of the average τ is taken over a window corresponding to 285 linear time periods of the mode $k = 32$	79
4.1	a) Sketch of the experimental setup: a laminar shaped input beam propagates inside the LC layer; random phase modulations are imposed at the entrance of the cell by means of a SLM. b) Schematic of the LC cell. Figure courtesy of Umberto Bortolozzo and Stefania Residori.	84
4.2	Detailed representation of the experimental setup, showing the initialisation of the input laser beam. Figure courtesy of Umberto Bortolozzo and Stefania Residori.	84

4.3	Plot of the energy flux P_ω and wave action flux Q_ω against the exponent x of the power law distribution of $n_\omega = C\omega^{-x/2}$ in the DAM representation of the LWE.	97
4.4	Intensity profile of the 1D NLSE soliton profile given in Equation (4.31).	99
4.5	The corresponding wave action spectrum for the soliton profile in Figure 4.4100	
4.6	Numerical spectrum of the wave action, n_k , at distances $z = 0 \text{ mm}$ and $z = 63 \text{ mm}$	107
4.7	Experimental spectrum of the light intensity, $N_k = I_k ^2$ at two different distances z . Figure courtesy of Umberto Bortolozzo and Stefania Residori.	108
4.8	Numerical spectrum of the light intensity, $N_k = I_k ^2$ at two different distances z . Averaging is done over a small finite time window and over ten realisations.	108
4.9	Intensity distribution $I(x, z)$ showing the beam evolution during propagation; a) linear case, b) weakly nonlinear case. Figure courtesy of Umberto Bortolozzo and Stefania Residori.	109
4.10	Two intensity profiles $I(x)$ recorded at $z = 0$ and $z = 1.9 \text{ mm}$ in the weakly nonlinear regime, with $V = 2.5 \text{ V}$, showing the smoothing associated with the inverse cascade. Figure courtesy of Umberto Bortolozzo and Stefania Residori.	109
4.11	Experimental results for intensity distribution $I(x, z)$. The area marked by the dashed line is shown at a higher resolution (using a larger magnification objectif). Figure courtesy of Umberto Bortolozzo and Stefania Residori.	110
4.12	Numerical results for intensity distribution $I(x, z)$. The frame on the left is a magnified section of the initial propagation of the beam.	110
4.13	Linear intensity profiles $I(x)$ taken at different propagation distances, $z = 0.3, 4.5$ and 7.5 mm . Figure courtesy of Umberto Bortolozzo and Stefania Residori.	111

4.14 PDFs of the wave intensity within the experimental cell at three different distances along the cell, $z = 0 \text{ mm}$, $z = 3 \text{ mm}$ and $z = 8 \text{ mm}$. Straight lines have been fitted to each PDF to show Gaussianity. Figure courtesy of Umberto Bortolozzo and Stefania Residori.	112
4.15 PDFs of the wave intensity within the numerical cell at three different distances along the cell, $z = 0 \text{ mm}$, 31 mm and $z = 63 \text{ mm}$. Straight lines have been fitted to each PDF to show Gaussianity.	112
4.16 The (\mathbf{k}, ω) -plot of the wave field at $z = 10 \text{ m}$. The Bogoliubov dispersion relation is shown by the solid green line.	113
4.17 Plot of the intensity profile at $z = 10 \text{ m}$ of both the soliton and wave components	115
4.18 The wave action spectrum of both soliton and wave components of the spectrum, with the KZ prediction for comparison.	116
4.19 Numerically obtained (x, z) -plot for a long time simulation with a low intensity initial condition to see the inverse cascade and soliton merging. .	117
4.20 Three close-ups at different propagation distances showing solitons a) passing through each other, b) merging and c) dissipating.	118
4.21 Plot of the maximum of the wave intensity in physical space versus z . .	118
4.22 Plot of the magnitude of the energies for the long time simulation. We see the conservation of the total energy, the growth of the linear and both nonlinear energies (corresponding to the two nonlinear terms in equation (4.10a)). Note that the first nonlinear energy is strictly a non-positive quantity, therefore we have plotted the magnitude of the value in this Figure.	119
4.23 We plot the intensity PDF for variable $s_{\mathbf{k}} = J_{\mathbf{k}}$, at two wave numbers, $k = 9.8 \text{ mm}^{-1}$, and $k = 3.8 \times 10^2 \text{ mm}^{-1}$. We fit a black dashed straight line that corresponds to a Gaussian wave field.	120

4.24 We depict the WTLC for 1D OWT. High wave number forcing injects wave action, that subsequently gets transferred to low \mathbf{k} by the inverse cascade. At low \mathbf{k} , solitons form resulting in a $n_{\mathbf{k}} \propto k^0$ spectrum. The emission of waves from merging or dissipating solitons re-injects wave action at low intensities.	121
4.25 The wave action spectrum $n_{\mathbf{k}}$ in a statistically non-equilibrium stationary state for the direct cascade simulation of the long-wave equation (LWE). The straight line represents the WT prediction of the KZ solution of $n_{\mathbf{k}} \propto k^{-1} \ln(k\ell)$	122
4.26 The wave action spectrum, $n_{\mathbf{k}}$, in a statistically non-equilibrium stationary state for the inverse cascade simulation of the LWE. The straight line represents the WT prediction of the KZ solution of $n_{\mathbf{k}} \propto k^{-3/5}$	122
4.27 Averaged energy flux $P_{\mathbf{k}}$ versus wave number k in the direct cascade simulation of the LWE. A KZ solution implies that $P_{\mathbf{k}}$ should be a non-zero constant in the inertial range	124
4.28 Averaged wave action flux $Q_{\mathbf{k}}$ versus wave number k in the inverse cascade simulation of the LWE. A KZ solution implies that $Q_{\mathbf{k}}$ should be a non-zero constant in the inertial range	124
4.29 PDF of the wave intensity in the direct cascade simulation of the LWE. The straight line corresponds to a Gaussian distribution predicted by WT theory.	125
4.30 PDF of the wave intensity in the inverse cascade simulation of the LWE. The straight line corresponds to a Gaussian distribution predicted by WT theory.	126
4.31 The wave action spectrum $n_{\mathbf{k}}$ in a statistically non-equilibrium stationary state for the direct cascade simulation of the short-wave equation (SWE). The straight line represents the WT prediction of the KZ solution of $n_{\mathbf{k}} \propto k^{7/5}$	126

4.32 Averaged energy flux P_k versus wave number k in the direct cascade simulation of the SWE. A KZ solution implies that P_k should be a non-zero constant in the inertial range	127
4.33 The wave action spectrum n_k in a statistically non-equilibrium stationary state for the inverse cascade simulation for the SWE. The straight line represents the WT prediction of the KZ solution of $n_k \propto k^{9/5}$	128
4.34 Averaged wave action flux Q_k versus wave number k for the inverse cascade simulation of the SWE. A KZ solution implies that Q_k should be a non-zero constant in the inertial range	129
4.35 PDF of the wave intensity in the direct cascade simulation of the SWE. The straight line corresponds to a Gaussian distribution predicted by WT theory.	129
4.36 PDF of the wave intensity in the inverse cascade simulation of the SWE. The straight line corresponds to a Gaussian distribution predicted by WT theory.	130

Acknowledgments

I would like to thank my supervisor and friend Sergey Nazarenko, whose patience, support, guidance and most importantly his enthusiasm, has kept me focused and motivated during my PhD. Also I must acknowledge all my collaborators, Guido Boffetta, Umberto Bortolozzo, Antonio Celani, Davide Dezzani, Victor L'vov, Stefania Residori and Oleksii Rudenko, who have helped me to understand and overcome difficulties during my PhD. In addition, I would like to thank Colm Connaughton, for his advice on numerical techniques and I am especially grateful to Zoe Gumm and Thorwald Stein for their help in proof reading my thesis.

My time at Warwick would not have been so enjoyable without my colleagues, Paul Clifford, Dana Elam, Andrew Ferguson, Amar Parmer, Brenda Quinn and Thorwald Stein, who have been great friends and good listeners throughout the years.

Finally, I must mention my family for all the support they have given me during my time at university.

Declarations

I wish to declare, that the work contained in this thesis is my own except where stated otherwise. Chapter 1 gives a brief review on the history and applications of the theory and contains no original work.

Chapter 2, begins by introducing the fundamental properties of the wave field and various definitions required for the application of WT theory. These can all be found in References [2, 3, 4, 5, 1]. However, the consideration to a general six-wave system is original work conducted by myself. The CT, is not a new procedure [6], however its application to the removal of non-resonant four-wave interactions was first implemented by myself, and has been published in various journal articles with my collaborators [7, 8, 9]. The locality analysis for the KZ solutions to the six-wave KE is original work, being jointly conducted by myself, Sergey Nazarenko, Victor L'vov and Oleksii Rudenko [9].

Chapter 3, consists of original results, except for the derivation of the BSE Hamiltonian and subsequent cosine formulation of the interaction coefficients [10, 11]. The numerical computation of the TLIA model and Figures 3.1 and 3.2 were done by one of my collaborators, Davide Dezzani, and have appeared in [7].

The experimental setup and Figures 4.1, 4.2, 4.7, 4.9, 4.10, 4.11, 4.13 and 4.14 in Chapter 4 were produced by my collaborators, Umberto Bortolozzo and Stefania Residori, and have been published in [8].

I state that this thesis has not been submitted for a degree at another university.

Abstract

We investigate one-dimensional (1D) wave turbulence (WT) systems that are characterised by six-wave interactions. We begin by presenting a brief introduction to WT theory - the study of the non-equilibrium statistical mechanics of nonlinear random waves, by giving a short historical review followed by a discussion on the physical applications.

We implement the WT description to a general six-wave Hamiltonian system that contains two invariants, namely, energy and wave action. This enables the subsequent derivations for the evolutions equations of the one-mode amplitude probability density function (PDF) and kinetic equation (KE). Analysis of the stationary solutions of these equations are made with additional checks on their underlying assumptions for validity. Moreover, we derive a differential approximation model (DAM) to the KE for super-local wave interactions and investigate the possible occurrence of a fluctuation relation. We then consider these results in the context of two physical systems - Kelvin waves in quantum turbulence (QT) and optical wave turbulence (OWT).

We discuss the role of Kelvin waves in decaying QT, and show that they can be described by six-wave interactions. We explicitly compute the interaction coefficients for the Biot-Savart equation (BSE) Hamiltonian and represent the Kelvin wave dynamics in the form of a KE. The resulting non-equilibrium Kolmogorov-Zakharov (KZ) solutions to the KE are shown to be non-local, thus a new non-local theory for Kelvin wave interactions is discussed. A local equation for the dynamics of Kelvin waves, the local nonlinear equation (LNE), is derived from the BSE in the asymptotic limit of one long Kelvin wave. Numerical computation of the LNE leads to an agreement with the non-local Kelvin wave theory.

Finally, we consider 1D OWT. We present the first experimental implementation of OWT and provide a comparable decaying numerical simulation for verification. We show that 1D OWT is described by a six-wave process and that the inverse cascade state leads to the development of coherent solitons at large scales. Further investigation is conducted into the behaviour of solitons and their impact to the WT description. Analysis of the fluxes and intensity PDFs lead to the development of a wave turbulence life cycle (WTLC), explaining the coexistence between coherent solitons and incoherent waves. Additional numerical simulations are performed in non-equilibrium stationary regimes to determine if a pure KZ state can be realised.

Abbreviations

WT wave turbulence	1
KE kinetic equation	1
PDF probability density function	1
KZ Kolmogorov-Zakharov.....	1
BEC Bose-Einstein condensate	2
WTLC wave turbulence life cycle.....	2
1D one-dimensional.....	3
MMT Majda-McLaughlin-Tabak	4
OWT optical wave turbulence.....	4

QT quantum turbulence	4
RPA random phase and amplitude	4
GF generating functional	4
CT canonical transformation	4
DAM differential approximation model	5
LNE local nonlinear equation	5
TLIA truncated local induction approximation	5
BSE Biot-Savart equation	5
LWE long-wave equation	5
SWE short-wave equation	5
NLSE nonlinear Schrödinger equation	5
2D two-dimensional	36
ZT Zakharov transform	38

IR infrared	42
UV ultraviolet	42
5D five-dimensional	42
3D three-dimensional	42
CB critical balance	22
GCFR Gallavotti-Cohen fluctuation relation	50
GPE Gross-Pitaevskii equation	53
LIA local induction approximation	57
KS Kozik-Svistunov	66
LN L'vov-Nazarenko	68
LC liquid crystal	81
MI modulational instability	81
SLM spatial light modulator	83

CFL Courant-Friedrichs-Lowy	103
--	-----

Chapter 1

Introduction

1.1 Wave Turbulence

We define wave turbulence (WT) theory as the study of the non-equilibrium statistical mechanics of random nonlinear waves [6, 1], consisting of a large number of random wave modes evolving far from their thermodynamic equilibrium. Hence, a non-equilibrium statistical description is preferred over a deterministic one. The origins of WT theory began in 1929, when Rudolph Peierls investigated the kinetics of phonons in anharmonic crystals [12]. In his work, he derived evolution equations for the wave action density, now known as the kinetic equation (KE), and for the wave amplitude probability density function (PDF), with the subsequent description of their thermodynamic equilibrium solutions. Whilst significant progress in the field has been made since 1929, these two equations remain the key focal points in the theory.

It was not until the 1960s that WT theory gained increased attention from the physics community, with its application to plasma physics [13, 14] and water waves [15, 16, 17, 18, 19, 20]. One of the major reasons for this new interest, was the discovery of a new type of solution to the KE describing a non-equilibrium turbulent cascade. These new solutions were discovered by Vladimir Zakharov in 1965, and correspond to states defined by a constant flux of a cascading invariant through scales [21]. They are known as Kolmogorov-Zakharov (KZ) solutions, due to their analogy with the Kolmogorov energy spectrum of hydrodynamical turbulence [22].

Since the pioneering work of Zakharov, there have been many physical systems that lend themselves to the application of WT theory including water surface gravity and capillary waves in oceans [19, 20, 6, 23, 24, 25, 26, 27, 28, 29, 30, 31, 32, 33, 34, 35]; internal, inertial, and Rossby waves in atmospheres and oceans [36, 37, 38, 39, 40, 41, 42, 43, 44]; Alfvén waves in solar wind and interstellar turbulence [45, 46, 47, 48, 49, 50, 51, 52, 53, 54, 55, 56]; Kelvin waves on quantised vortex lines in superfluid helium [57, 11, 58, 59, 60, 61, 9]; waves in Bose-Einstein condensates (BECs) and nonlinear optics [62, 63, 64, 65, 8]; waves in fusion plasmas [13, 66, 14, 6]; and waves on vibrating, elastic plates [67].

WT theory is often associated with weakly nonlinear dispersive waves, where the theory enables the description of weakly interacting random waves and the prediction of KZ cascade states. In this case, WT is referred to as *weak* WT. However, when wave amplitudes become large, and the nonlinearity is strong, the weak WT description fails, resulting in a regime of strong WT. In strong WT regimes, we observe a suppression of the KZ states with the development of non-universal features, such as shocks [68], vortices [69, 70, 62], condensates [62, 64], and solitons [8]. Strong WT descriptions have been proposed for several wave systems, usually resulting in the formation of a wave turbulence life cycle (WTLC) [71, 1]. The WTLC presents a qualitative description of the mutual coexistence of random waves, coherent structures, and the energy exchange between them.

It is the weak WT description that allows for the systematic evaluation of the nonlinear evolution of a WT system. When the nonlinearity of a system is weak, the small amplitudes of weakly nonlinear random waves are approximately time-independent, and thus the waves evolve close to the linear theory. However, over long times, these amplitudes gradually evolve, and the nonlinear interactions between weakly nonlinear random waves become apparent. It is this separation of the characteristic linear timescale, T_L , and the nonlinear evolution timescale, T_{NL} , that allows for an ensemble average to be taken over the linear timescale and for a prediction to the nonlinear evolution to be made.

Recently, improved experimental and numerical simulations of WT systems have,

in many situations, indicated towards deviations in the WT predictions [72, 64, 73]. This has led to an emphasis on the verification of the weak WT assumptions, the investigation of strong WT effects, and the role of turbulent intermittency. Discreteness of wave modes - a fact arising from the consideration of a finite box, has led many theorists to examine if the infinite box assumption of WT theory is consistent with experimental and numerical observations. This discreteness imposes restrictions to the number of wave resonances that can occur. If the nonlinearity of the system is too low, then only *exact* wave resonances can satisfy the resonance condition¹, which subsequently leads to the development of *discrete* WT [74, 75, 76, 77, 78, 79, 80]. In such circumstances, isolated clusters of exact wave resonances are formed. When the nonlinear frequency broadening is of the same order as the frequency spacing, isolated clusters of interacting waves can become connected, but still being of insufficient size for the transfer of energy to the dissipation scale. Such situations are known as *frozen turbulence* [81]. If a frozen turbulent system is under continuous forcing, then we can observe intermittent cascade bursts or sand-pile behaviour. This is formally known as *mesoscopic* WT [82, 27, 31, 52, 83]. If the nonlinear frequency broadening is larger than the frequency grid spacing, then the system is in a *kinetic* WT regime and is described by WT theory. However, the infinite size box assumption is only really applicable to systems present in nature. Therefore the understanding of discreteness effects is of fundamental importance in WT modelling.

1.2 One-Dimensional Wave Turbulence

Interestingly, one-dimensional (1D) WT systems can be highly complex, even more so than WT systems in higher dimensions. This is because the one-dimensionality of \mathbf{k} -space imposes more restrictions than simplifications, i.e. resonant interactions on a 1D line are much harder to satisfy than on a multi-dimensional grid. Moreover, certain wave frequency structures can further restrict wave resonances. That said, there are not many physical examples of 1D WT systems and therefore the motivation for their

¹This is when the nonlinear frequency broadening, approximately the inverse of the nonlinear timescale T_{NL} , is smaller than the frequency spacing in the finite box.

investigation has been limited until recently. Most notably was the introduction of an artificial equation called the Majda-McLaughlin-Tabak (MMT) model. The MMT model is a 1D wave equation containing several adjustable parameters, that give rise to a whole family of new 1D four-wave WT systems [72, 84, 73]. Interestingly, the MMT model, was initially used as a model for the verification of weak WT assumptions. However, it was subsequently found to produce results that were not fully consistent with the WT predictions [72]. This has again motivated the investigation into the validity of the WT assumptions.

In this thesis, we will discuss two examples of 1D WT. First, we consider the role of Kelvin waves on 1D quantised vortex lines in superfluid helium quantum turbulence (QT) [11], and secondly, waves in 1D optical wave turbulence (OWT) [8]. Both of these systems are defined by six-wave interactions that arise due to the inability of the system to support four-wave interactions. This lack of four-wave resonance is down to the structure of the linear wave frequency, which only permits trivial wave number pairings to the four-wave resonance condition.

1.3 Layout of Thesis

In this thesis, we investigate 1D wave turbulent systems, with emphasis on systems that are described by six-wave interactions. There have been many studies in WT in three-, four- and five-wave interaction systems, however, there has been little investigation into the consideration of six-wave systems.

In Chapter 2, we develop the WT description for a general six-wave system. We begin by presenting the WT statistical setup. We introduce the definitions of the random phase and amplitude (RPA) field, the generating functional (GF), the canonical transformation (CT), and finally apply the WT description to a general six-wave Hamiltonian. This enables the formulation of the GF for the six-wave system, which leads to construction of evolution equations for the amplitude PDF, and KE. The main focus of WT theory has been predominantly on the KE and its solutions. However, we emphasise the importance of the amplitude PDF, which subsequently allows for the investigation

into intermittency and strong WT. Towards the end of Chapter 2, we concentrate on the solutions of the KE, and check the locality assumption of the derived KZ solutions. Finally, we introduce the differential approximation model (DAM) for strongly local wave interactions as a means to investigate the energy and wave action fluxes.

With the main generalised results already derived in Chapter 2, we proceed by considering applications to QT in Chapter 3. Six-wave theory for Kelvin waves was originally developed by Kozik and Svistunov [11]. However, their initial work failed to fully check the validity of the underlying WT assumptions. Therefore, we present a detailed and thorough analysis of the Biot-Savart equation (BSE) Hamiltonian description for Kelvin waves and investigate the legitimacy of the local wave interaction assumption for the KZ solutions. Moreover, we examine two simplified models for Kelvin waves interactions: the local nonlinear equation (LNE) and the truncated local induction approximation (TLIA) model. Both greatly reduce the computational expense of the BSE, whilst maintaining the same WT characteristics. We perform numerical simulations of the LNE and TLIA model and compare the results with the local [11], and recently proposed non-local [85] Kelvin WT theories.

In Chapter 4, we present an experimental setup for 1D OWT, and verify our observations with comparisons to numerical simulations and the WT predictions of Chapter 2. We examine OWT in two limits of \mathbf{k} -space and derive the long-wave equation (LWE) and the short-wave equation (SWE). The LWE, which models the experimental setup, is similar to the integrable 1D nonlinear Schrödinger equation (NLSE) and therefore contains soliton-like solutions. These coherent structures appear after an inverse cascade in the decaying OWT setup. However, the presence of a large number of solitons in the system can inhibit the weak WT regime and invalidate the kinetic description. This behaviour can be understood with the aid of the WTLC. We perform additional numerical simulations of both the LWE and the SWE in non-equilibrium stationary states to compare with the theoretical KZ predictions.

Finally, in Chapter 5 we conclude with a discussion of the results from Chapters 3 and 4 and highlight areas where further investigation is needed.

Chapter 2

Wave Turbulence Theory

There have been several approaches to the description of WT statistics, first using a diagrammatic approach [86, 87, 88], then by cumulants expansions [17, 18, 89, 90, 91], and finally by the use of the random phase approximation [6, 20]. However, the random phase approximation is insufficient for a rigorous treatment of WT theory - the wave amplitudes must also be random independent variables¹. This was the approach that was recently developed in [2, 3, 4, 5, 1], using RPA wave fields. The RPA field approach is what we shall consider in this thesis. Moreover, it allows for the derivation of not only the KE, but of Peierls' equation for the PDF, and for the ability of considering non-Gaussian wave fields. These provide a formulation for the study of the underlying WT assumptions, the phenomena of turbulence intermittency, and the presence of coherent structures.

In this Chapter, we will present the bulk of the mathematics within this thesis. We will lay down the necessary statistical foundations before developing the RPA field approach to a general six-wave Hamiltonian system. WT theory has been applied on several occasions to six-wave systems [11, 7, 8, 9], however, this is the first time the detailed derivation to a general six-wave system using the RPA field approach has been considered.

¹The wave amplitudes do not necessarily have to be Gaussian.

2.1 The Statistical Setup

To set the foundations for the WT description, we need to present a few concepts and definitions that will aid us in the development of the theory [1]. The vast number of degrees of freedom in a wave turbulent system implies that a deterministic approach is inconvenient and far too cumbersome. Therefore we find that a statistical strategy is more suitable. The non-equilibrium nature of turbulence means that applying a naïve thermodynamic approach of defining temperature as energy per degree of freedom, would lead to an absurdly high temperature for the system. Therefore, WT theory is based upon non-equilibrium states defined by fluxes through scales. The most fundamental and universal of these statistical quantities is the PDF of the wave field, containing all the information of the system.

Let us consider a 1D wave field, $a(x, t)$, in a periodic box of length L , and let the Fourier transform of this field be represented by Fourier amplitudes $a_l(t) = a(\mathbf{k}_l, t)$, with wave number, $\mathbf{k}_l = 2\pi l/L$, where l is taken from a finite box $\mathcal{B}_N \subset \mathbb{Z}$, centred around zero. Finiteness of the number of wave modes, implies that there exists a maximal wave number, k_{max} , such that the total number of modes is defined by $N = k_{max} L/\pi$. The strategy we shall take will be to consider the system in a finite box of N wave modes, and then take the large box and long evolution time limits towards the end.

In addition, let us consider an amplitude and phase factor decomposition of wave mode $a_l(t) = A_l(t)\psi_l(t)$, such that A_l is a real positive amplitude and ψ_l is a phase factor that takes values on the unit circle in the complex plane ($\in \mathbb{T}$). The reason why we take phase factors, ψ_l , and not phases, ϕ_l , with $\psi_l = e^{i\phi_l}$, is because phase factors remain independent up to the nonlinear evolution time, whereas phases do not. Correlation of phases would result in breakdown of the random phase assumption [92, 2].

We now introduce some important definitions to the theory:

Definition 1. *The N -mode joint PDF, $\mathcal{P}^{(N)}\{s, \xi\}$, is the probability for wave intensities $J_l = |A_l|^2$ to be in the range $(s_l, s_l + ds_l)$, and for the phase factors, ψ_l , to be on the unit circle segment, $(\xi_l, \xi_l + d\xi_l)$, for all $l \in \mathcal{B}_N$. We have used the notation that $\{s, \xi\} = \{s_l, \xi_l : l \in \mathcal{B}_N\}$.*

Definition 2. *The full joint PDF of the wave field, $a(x, t)$, is defined as the large box limit of the N -mode joint PDF:*

$$\mathcal{P}\{s, \xi\} = \lim_{N \rightarrow \infty} \mathcal{P}^{(N)}\{s, \xi\}. \quad (2.1)$$

The joint PDFs above, contain all the information of the system. However, we can consider the PDF of the wave amplitudes of the field $a(x, t)$ by averaging over phase factors,

Definition 3. *$\mathcal{P}^{(N,a)}\{s\}$, is known as the N -mode amplitude PDF, and is defined by integration of the N -mode joint PDF over all phase factors:*

$$\mathcal{P}^{(N,a)}\{s\} = \prod_{l \in \mathcal{B}_N} \oint_{\mathcal{S}^1} \mathcal{P}^{(N)}\{s, \xi\} |d\xi_l|. \quad (2.2)$$

Moreover, we can define the amplitude PDF of a smaller subset of M modes, called the M -mode joint amplitude PDF, where $M < N$, by integrating the N -mode amplitude PDF over all but M amplitudes.

Definition 4. *The M -mode amplitude PDF is defined as*

$$\mathcal{P}^{(M,a)}\{s\} = \prod_{l \neq l_1, l_2, \dots, l_M} \int_{\mathbb{R}^+} \mathcal{P}^{(N,a)}\{s\} ds_l, \quad (2.3)$$

where we have labelled the M modes as l_1, l_2, \dots, l_M .

2.2 Random Phase and Amplitude Fields

Let us introduce the RPA field strategy by first beginning with the definition of an *ideal* RPA field [3, 93, 2, 4].

Definition 5. *We say a wave field, $a(x, t)$, is an ideal RPA field, if it possesses the following statistical properties:*

- All amplitudes, A_l , and phase factors, ψ_l , are independent random variables. Therefore, the N -mode joint PDF is equal to the product of the one-mode PDFs

of each amplitude and phase factor:

$$\mathcal{P}^{(N)}\{s, \xi\} = \prod_{l \in \mathcal{B}_N} \mathcal{P}_l^{(1,a)}(s_l) \mathcal{P}_l^{(1,\psi)}(\xi_l). \quad (2.4)$$

- The phase factors, ψ_l , are uniformly distributed on the unit circle. Hence, for any mode l we have

$$\mathcal{P}_l^{(1,\psi)}(\xi_l) = \begin{cases} \frac{1}{2\pi} & \text{if } 0 \leq \xi_l < 2\pi \\ 0 & \text{otherwise.} \end{cases} \quad (2.5)$$

A consequence of an ideal RPA field is that we can write the N -mode amplitude PDF, $\mathcal{P}^{(N,a)}\{s\}$, as a product of N one-mode amplitude PDFs:

$$\mathcal{P}^{(N,a)}\{s\} = \prod_{l \in \mathcal{B}_N} \mathcal{P}_l^{(1,a)}(s_l). \quad (2.6)$$

We remark, that the ideal RPA field does not require us to fix the shape of the amplitude PDF, and therefore, we can deal with strongly non-Gaussian wave fields. However, the ideal RPA field does not hold precisely, but only approximately, up to the nonlinear evolution time [93, 2, 3]. Fortunately, the WT closure is still valid if we use a weaker definition of an ideal RPA field - an *essentially* RPA field:

Definition 6. We say that the field, $a(x, t)$, is an *essentially* RPA field if:

- The phase factors are statistically independent and uniformly distributed variables up to $\mathcal{O}(\epsilon^2)$ corrections with:

$$\mathcal{P}^{(N)}\{s, \xi\} = \frac{1}{(2\pi)^N} \mathcal{P}^{(N,a)}\{s\} [1 + \mathcal{O}(\epsilon^2)]. \quad (2.7)$$

- The amplitude variables are almost independent, in the sense that for a subset of modes of number $M \ll N$, the M -mode amplitude PDF is equal to the product of the M one-mode amplitude PDFs up to an accuracy of $\mathcal{O}(M/N)$ and $\mathcal{O}(\epsilon^2)$ with:

$$\mathcal{P}_{l_1, l_2, \dots, l_M}^{(M)} = \left(\prod_{j=1}^M \mathcal{P}_{l_j}^{(1,a)} \right) \left[1 + \mathcal{O}\left(\frac{M}{N}\right) + \mathcal{O}(\epsilon^2) \right]. \quad (2.8)$$

With this weaker definition, the phase factors are independent from each other by $\mathcal{O}(\epsilon^2)$ corrections, where ϵ is a formal parameter quantifying the weak nonlinearity of the system ($\epsilon \ll 1$). Moreover, there is only the independence of M wave amplitudes up to a correction of $\mathcal{O}(M/N)$ for $M \ll N$, but this is still sufficient for the WT closure.

2.3 The Generating Functional

The GF provides a useful tool in deriving the evolution equations for all the statistical quantities of the wave system.

Definition 7. *The N -mode GF is defined as*

$$\mathcal{Z}^{(N)}\{\lambda, \mu\} = \left\langle \prod_{l \in \mathcal{B}_N} e^{(\frac{L}{2\pi})\lambda_l J_l} \psi_l^{\mu_l} \right\rangle, \quad (2.9)$$

where $\{\lambda, \mu\} = \{\lambda_l, \mu_l : l \in \mathcal{B}_N\}$ is a set of parameters such that $\lambda_l \in \mathbb{R}$ and $\mu_l \in \mathbb{Z}$. Here $\langle \cdot \rangle = \langle \cdot \rangle_{J, \psi}$ represents the ensemble amplitude and phase averages with respect to J and ψ .

Due to the statistical independence of the amplitudes, A_l , to the phase factors, ψ_l , we can define the N -mode amplitude GF.

Definition 8. *The N -mode amplitude GF is defined as*

$$\mathcal{Z}^{(N,a)}\{\lambda\} = \left\langle \prod_{l \in \mathcal{B}_N} e^{(\frac{L}{2\pi})\lambda_l J_l} \right\rangle = \mathcal{Z}^{(N)}\{\lambda, \mu\}|_{\mu=0}. \quad (2.10)$$

We will only concentrate on the one-mode statistics of the system for brevity². Therefore, we will only need to consider the one-mode amplitude GF, $\mathcal{Z}_{\mathbf{k}}^{(1,a)}(\lambda_{\mathbf{k}})$.

Definition 9. *The one-mode amplitude GF is defined as*

$$\mathcal{Z}_{\mathbf{k}}^{(1,a)}(\lambda_{\mathbf{k}}) = \left\langle e^{(\frac{L}{2\pi})\lambda_{\mathbf{k}} J_{\mathbf{k}}} \right\rangle, \quad (2.11)$$

for wave number \mathbf{k} .

²There exist several papers that consider the full N -mode statistics of three-wave and four-wave systems, for instance see [2, 3].

We can reconstruct the one-mode amplitude PDF for wave intensities, $s_{\mathbf{k}} = J_{\mathbf{k}}$, by taking the inverse Laplace transform of the one-mode amplitude GF:

$$\mathcal{P}_{\mathbf{k}}^{(1,a)}(s_{\mathbf{k}}) = \frac{1}{2\pi i} \int_{-i\infty+c}^{i\infty+c} e^{-\left(\frac{L}{2\pi}\right)\lambda_{\mathbf{k}} s_{\mathbf{k}}} \mathcal{Z}_{\mathbf{k}}^{(1,a)}(\lambda_{\mathbf{k}}) d\lambda_{\mathbf{k}}, \quad (2.12)$$

where c is a constant greater than the real part of all singularities of $\mathcal{Z}_{\mathbf{k}}^{(1,a)}(\lambda_{\mathbf{k}})$.

2.4 The Hamiltonian Formulation

Many systems that contain waves are described by different natural variables, which pose a problem if we would like to apply a universal wave theory. Fortunately, most of these systems possess a Hamiltonian structure, arising from the fact that most of these equations can be derived from the initial microscopic Hamiltonian equations of motion. If we are only interested in small amplitude waves, then all the information describing the propagation of non-interacting waves is fully contained in the *linear dispersion relation* $\omega(\mathbf{k})$. Furthermore, in the weakly nonlinear regime, the Hamiltonian structure can be represented as a power series in terms of the complex amplitudes of these waves, with the leading quadratic order describing non-interacting linear waves. Subsequently, the higher order terms then describe the nonlinear interactions of these waves.

To begin with, the simplest Hamiltonian structure can be defined by a pair of canonical variables, usually defined as the coordinate, $q(x, t)$, and the momentum, $p(x, t)$, with the canonical equations of motion expressed as

$$\frac{\partial q(x, t)}{\partial t} = \frac{\delta \mathcal{H}}{\delta p(x, t)}, \quad (2.13a)$$

$$\frac{\partial p(x, t)}{\partial t} = -\frac{\delta \mathcal{H}}{\delta q(x, t)}. \quad (2.13b)$$

The Hamiltonian \mathcal{H} is a functional, dependent on the variables, $q(x, t)$, and, $p(x, t)$, with $\delta/\delta q$ and $\delta/\delta p$ denoting variational derivatives. The advantage of the Hamiltonian formulation is the symmetry it possesses between $q(x, t)$ and $p(x, t)$. If we define new canonical variables, $\tilde{q} = \lambda^* q$, and, $\tilde{p} = p/\lambda^*$, choosing the dimensional factor λ^* such

that both \tilde{q} and \tilde{p} have the same dimensions, then one can introduce the complex variables

$$a(x, t) = \frac{\tilde{q} + i\tilde{p}}{\sqrt{2}}, \quad (2.14a)$$

$$a^*(x, t) = \frac{\tilde{q} - i\tilde{p}}{\sqrt{2}}. \quad (2.14b)$$

Subsequently, the Hamiltonian (2.13) can be expressed as

$$i \frac{\partial a(x, t)}{\partial t} = \frac{\delta \mathcal{H}}{\delta a^*(x, t)}, \quad (2.15a)$$

$$-i \frac{\partial a^*(x, t)}{\partial t} = \frac{\delta \mathcal{H}}{\delta a(x, t)}. \quad (2.15b)$$

Equation (2.15b) follows from (2.15a) by complex conjugation. Hence we have obtained one complex equation out of two real equations, (2.13). It should be noted that variables $a(x, t)$ and $a^*(x, t)$ are not the only canonical variables to choose from. The Hamiltonian structure can be significantly simplified if one considers (2.15) in Fourier space. The wave interaction variable $a_{\mathbf{k}} = a(\mathbf{k}, t)$ is defined as the Fourier representation of the wave field $a(x, t)$ such that

$$a(\mathbf{k}, t) = \frac{1}{L} \int_{Box} a(x, t) e^{i\mathbf{k}x} dx. \quad (2.16)$$

Subsequently, the Hamiltonian equations (2.15) can be represented as

$$i \frac{\partial a_{\mathbf{k}}}{\partial t} = \frac{\delta \mathcal{H}}{\delta a_{\mathbf{k}}^*}. \quad (2.17)$$

In the limit of small amplitude waves (i.e. $|a_{\mathbf{k}}|^2 \ll 1$), we can expand the Hamiltonian \mathcal{H} in powers of $a_{\mathbf{k}}$ and $a_{\mathbf{k}}^*$:

$$\mathcal{H} = \mathcal{H}_2 + \mathcal{H}_{int}, \quad (2.18a)$$

$$\mathcal{H}_{int} = \mathcal{H}_3 + \mathcal{H}_4 + \mathcal{H}_5 + \dots, \quad (2.18b)$$

such that $\mathcal{H}_2 \gg \mathcal{H}_3 \gg \mathcal{H}_4 \gg \dots$. Here, \mathcal{H}_2 is the quadratic part of the Hamiltonian, describing the free non-interacting propagation of linear waves and \mathcal{H}_{int} is the *interaction*

Hamiltonian, containing all terms that describe the nonlinear interaction of waves. The subscript i in each term \mathcal{H}_i defines the order of the interaction process with respect to the canonical variables $a_{\mathbf{k}}$ and $a_{\mathbf{k}}^*$.

The most general form³ of the quadratic Hamiltonian, \mathcal{H}_2 , is given by

$$\mathcal{H}_2 = \sum_{\mathbf{k}} A(\mathbf{k}) a_{\mathbf{k}} a_{\mathbf{k}}^* + \frac{1}{2} [B(\mathbf{k}) a_{\mathbf{k}} a_{-\mathbf{k}} + B^*(\mathbf{k}) a_{\mathbf{k}}^* a_{-\mathbf{k}}^*], \quad (2.19)$$

with the restrictions that $A(\mathbf{k})$ be a real function and $B(\mathbf{k})$ be an even function ($B(\mathbf{k}) = B(-\mathbf{k})$) imposed by the Hamiltonian \mathcal{H} being real. In addition, the presence of negative wave numbers is for \mathcal{H}_2 to satisfy the conservation of momentum (see Equation (2.21a) below).

However, one would like to diagonalise (2.19) into the form

$$\mathcal{H}_2 = \sum_{\mathbf{k}} \omega(\mathbf{k}) \tilde{a}_{\mathbf{k}} \tilde{a}_{\mathbf{k}}^*, \quad (2.20)$$

where $\tilde{a}_{\mathbf{k}}$ and $\tilde{a}_{\mathbf{k}}^*$ are new canonical variables and $\omega(\mathbf{k})$ is the linear frequency or dispersion relation. This is because we would like variable $\tilde{a}_{\mathbf{k}}$ to correspond to a single mode with frequency ω_k and not a linear combination of modes⁴. This can be done with the aid of the Bogoliubov transformation, that we omit from this thesis for brevity, (see [6] for an overview). Once diagonalised, we can proceed with the application of WT theory.

2.5 The Canonical Transformation

Nonlinear wave interactions can only occur if the waves satisfy a resonance condition. For an $N \leftrightarrow M$ wave scattering event in an $N + M$ -wave process, this resonance condition is defined as

$$\mathbf{k}_1 + \cdots + \mathbf{k}_N = \mathbf{k}_{N+1} + \cdots + \mathbf{k}_{N+M}, \quad (2.21a)$$

$$\omega(\mathbf{k}_1) + \cdots + \omega(\mathbf{k}_N) = \omega(\mathbf{k}_{N+1}) + \cdots + \omega(\mathbf{k}_{N+M}), \quad (2.21b)$$

³This generality arises from the possible combinations of $a_{\mathbf{k}}$ and $a_{\mathbf{k}}^*$ up to the quadratic order in $a_{\mathbf{k}}$.

⁴From this point on, we omit tildes, and assume that the system is already diagonalised.

where \mathbf{k}_i is the wave number and $\omega(\mathbf{k}_i) = \omega_i$ is the frequency of wave i . Waves with index $i = 1, \dots, N$, on the left-hand side of (2.21), are incoming waves to the interaction, whereas waves with index $i = N + 1, \dots, N + M$, on the right-hand side determine outgoing waves.

WT theory automatically implies the conservation of the linear energy \mathcal{H}_2 and momentum \mathcal{M} :

$$\mathcal{M} = \sum_{\mathbf{k}} \mathbf{k} a_{\mathbf{k}} a_{\mathbf{k}}^*. \quad (2.22)$$

This is reflected in the resonance condition (2.21), where Relation (2.21a), corresponds to the conservation of momentum in the wave interaction, and (2.21b), the conservation of linear energy⁵. In special situations, there can be additional conserved quantities or invariants. An additional conserved quantity (or even two) would allow for a dual (triple) cascade scenario, with the cascading invariants being transferred to separate regions of Fourier space [65, 62, 63, 8, 7, 44, 94]. For instance, in this thesis we are primarily concerned with dual cascade systems with an additional invariant arising from the conservation of the total number of waves in the system. Systems of this form are seen in nonlinear optics/BECs [65, 62, 63, 8] and in Kelvin waves in QT [7, 9]⁶. Therefore, we consider systems of only even order wave interactions where the number of waves before and after interaction are the same, i.e. four-wave and six-wave interactions, which result from $2 \leftrightarrow 2$ and $3 \leftrightarrow 3$ wave scattering processes respectively. When N and M in (2.21) are equal, we have that the total number of waves, that is the wave action \mathcal{N} , is conserved, where \mathcal{N} is defined as

$$\mathcal{N} = \sum_{\mathbf{k}} a_{\mathbf{k}} a_{\mathbf{k}}^*. \quad (2.23)$$

Aside from wave action, other invariants have been found in systems, such as enstrophy and zonostrophy [95, 44]. But as we are only considering systems that conserve wave action, our general system will only contain even order wave interactions. Therefore, all terms of odd order in the Hamiltonian expansion (2.18), (\mathcal{H}_3 , \mathcal{H}_5 , etc.) will vanish.

⁵In the weak nonlinearity limit, one can approximate the conservation of energy with the conservation of linear energy. This approximation is vital in WT theory.

⁶The majority of WT systems are defined by three-wave interactions

Hence, (2.18) becomes

$$\mathcal{H} = \mathcal{H}_2 + \mathcal{H}_4 + \mathcal{H}_6 + \dots . \quad (2.24)$$

Let us consider a general Hamiltonian up to order \mathcal{H}_6 that conserves wave action, as well as the energy and momentum, in the form of

$$\mathcal{H} = \sum_{\mathbf{k}} \omega_k a_{\mathbf{k}} a_{\mathbf{k}}^* + \frac{1}{4} \sum_{1,2,3,4} T_{3,4}^{1,2} a_1 a_2 a_3^* a_4^* \delta_{3,4}^{1,2} + \frac{1}{36} \sum_{1,2,3,4,5,6} W_{4,5,6}^{1,2,3} a_1 a_2 a_3 a_4^* a_5^* a_6^* \delta_{4,5,6}^{1,2,3}, \quad (2.25)$$

where $\delta_{3,4}^{1,2} = \delta(\mathbf{k}_1 + \mathbf{k}_2 - \mathbf{k}_3 - \mathbf{k}_4)$ is a Kronecker delta function and $T_{3,4}^{1,2} = T(\mathbf{k}_1, \mathbf{k}_2, \mathbf{k}_3, \mathbf{k}_4)$ and $W_{4,5,6}^{1,2,3} = W(\mathbf{k}_1, \mathbf{k}_2, \mathbf{k}_3, \mathbf{k}_4, \mathbf{k}_5, \mathbf{k}_6)$ are the interaction coefficients for the $2 \leftrightarrow 2$ and $3 \leftrightarrow 3$ wave scatterings respectively. Their structures determine the wave interaction for their corresponding wave scattering process. The Hamiltonian (2.25) represents the total energy of the system and therefore is real. Moreover, its value should not change if we permute certain wave numbers, i.e. $\mathbf{k}_1 \leftrightarrow \mathbf{k}_2$ etc. This property establishes symmetries on the interaction coefficients:

$$T_{3,4}^{1,2} = T_{3,4}^{2,1} = T_{4,3}^{1,2} = (T_{1,2}^{3,4})^*, \quad (2.26a)$$

$$W_{4,5,6}^{1,2,3} = W_{4,5,6}^{2,1,3} = W_{4,5,6}^{3,2,1} = W_{5,4,6}^{1,2,3} = W_{6,5,4}^{1,2,3} = (W_{1,2,3}^{4,5,6})^*. \quad (2.26b)$$

In the limit of $|a_{\mathbf{k}}| \ll 1$, the leading contribution to the interaction Hamiltonian of (2.25) are the $2 \leftrightarrow 2$ wave interactions defined by \mathcal{H}_4 . These occur if the wave numbers satisfy the $2 \leftrightarrow 2$ wave resonant condition:

$$\mathbf{k}_1 + \mathbf{k}_2 = \mathbf{k}_3 + \mathbf{k}_4, \quad (2.27a)$$

$$\omega(\mathbf{k}_1) + \omega(\mathbf{k}_2) = \omega(\mathbf{k}_3) + \omega(\mathbf{k}_4). \quad (2.27b)$$

We will limit ourselves to 1D systems that possess waves with linear dispersion relations of the form

$$\omega(\mathbf{k}) = Ck^2, \quad (2.28)$$

where C is a real constant and we use the notation $k = |\mathbf{k}|$ for the magnitude of the

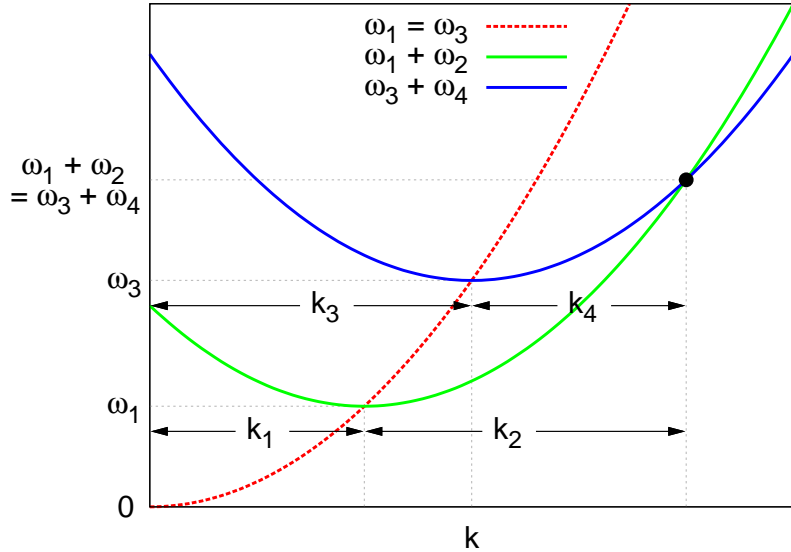


Figure 2.1: We plot a graphical representation of the four-wave resonance condition [1]. The four-wave resonance condition is satisfied at points where the green and blue lines intersect, (shown by the black dot). However, for dispersion relations $\omega_k \propto k^\alpha$, with $\alpha > 1$, there can only be one intersection, corresponding to the trivial wave resonance: $\mathbf{k}_1 = \mathbf{k}_4$ and $\mathbf{k}_2 = \mathbf{k}_3$ (see text for details).

wave number. Indeed, dispersion relations in 1D of the form $\omega(\mathbf{k}) \propto k^\alpha$ with $\alpha > 1$ cannot satisfy the four-wave resonant condition (2.27). This can be understood by a simple diagrammatic representation presented in Figure 2.1 [13, 1]. In Figure 2.1 we observe the red dashed curve representing the dispersion relation $\omega_k = Ck^\alpha$ with $\alpha > 1$. At two points along this curve (at $\mathbf{k} = \mathbf{k}_1$ and $\mathbf{k} = \mathbf{k}_3$), two further dispersion curves (the green and blue solid lines) are produced at points (\mathbf{k}_1, ω_1) and at (\mathbf{k}_3, ω_3) respectively. These subsequent lines represent the wave frequencies of $\omega_1 + \omega_2$ and $\omega_3 + \omega_4$, where \mathbf{k}_1 and \mathbf{k}_3 are now fixed and along the green solid line, \mathbf{k}_2 is varying and along the blue line, \mathbf{k}_4 is varying. If the green and blue lines intersect, it will be when Equations (2.27) are satisfied (the four-wave resonance condition) at the point $(\mathbf{k}_1 + \mathbf{k}_2, \omega_1 + \omega_2) = (\mathbf{k}_3 + \mathbf{k}_4, \omega_3 + \omega_4)$. In Figure 2.1 this occurs once, and it can be clearly seen that $\mathbf{k}_1 = \mathbf{k}_4$ and $\mathbf{k}_2 = \mathbf{k}_3$, corresponding to a trivial pairing of wave numbers, which will not provide any nonlinear energy exchange between wave modes. As a consequence, resonant four-wave interactions are absent in the system. However,

there exists a weakly nonlinear CT that allows us to change to new canonical variables to remove the non-resonant wave interactions. The side effect of this is the introduction of a new additional term that describes the next order of wave interaction [6]. This strategy was recently applied to four-wave systems in the context of Kelvin waves in QT [7, 9] and nonlinear optics [8]. This technique has also been previously applied to surface gravity waves [96, 97]. The CT can be re-iterated until one gets a leading order resonant wave interaction.

The first step of the CT is to define a new canonical interaction variable, c_k , such that it satisfies an auxiliary Hamiltonian \mathcal{H}_{aux} , Equation (2.29), which contains arbitrary interaction coefficients at all orders⁷. The auxiliary Hamiltonian for c_k is of the form:

$$\begin{aligned}
\mathcal{H}_{aux} = & \frac{1}{2} \sum_{1,2,3} \tilde{V}_3^{1,2} \delta_3^{1,2} (c_1 c_2 c_3^* + \text{c.c.}) + \frac{1}{6} \sum_{1,2,3} \tilde{U}^{1,2,3} \delta^{1,2,3} (c_1 c_2 c_3 + \text{c.c.}) \\
& + \frac{1}{4} \sum_{1,2,3,4} \tilde{T}_{3,4}^{1,2} \delta_{3,4}^{1,2} c_1 c_2 c_3^* c_4^* + \frac{1}{6} \sum_{1,2,3,4} \tilde{X}_4^{1,2,3} \delta_4^{1,2,3} (c_1 c_2 c_3 c_4^* + \text{c.c.}) \\
& + \frac{1}{24} \sum_{1,2,3,4} \tilde{Y}^{1,2,3,4} \delta^{1,2,3,4} (c_1 c_2 c_3 c_4 + \text{c.c.}) \\
& + \frac{1}{120} \sum_{1,2,3,4,5} \tilde{A}^{1,2,3,4,5} \delta^{1,2,3,4,5} (c_1 c_2 c_3 c_4 c_5 + \text{c.c.}) \\
& + \frac{1}{24} \sum_{1,2,3,4,5} \tilde{B}_5^{1,2,3,4} \delta_5^{1,2,3,4} (c_1 c_2 c_3 c_4 c_5^* + \text{c.c.}) \\
& + \frac{1}{12} \sum_{1,2,3,4,5} \tilde{C}_{4,5}^{1,2,3} \delta_{4,5}^{1,2,3} (c_1 c_2 c_3 c_4^* c_5^* + \text{c.c.}) \\
& + \frac{1}{36} \sum_{1,2,3,4,5,6} \tilde{W}_{4,5,6}^{1,2,3} \delta_{4,5,6}^{1,2,3} c_1 c_2 c_3 c_4^* c_5^* c_6^* \\
& + \frac{1}{120} \sum_{1,2,3,4,5,6} \tilde{Q}_6^{1,2,3,4,5} \delta_6^{1,2,3,4,5} (c_1 c_2 c_3 c_4 c_5 c_6^* + \text{c.c.}) \\
& + \frac{1}{48} \sum_{1,2,3,4,5,6} \tilde{R}_{5,6}^{1,2,3,4} \delta_{5,6}^{1,2,3,4} (c_1 c_2 c_3 c_4 c_5^* c_6^* + \text{c.c.}) \\
& + \frac{1}{36} \sum_{1,2,3,4,5,6} \tilde{S}^{1,2,3,4,5,6} \delta^{1,2,3,4,5,6} (c_1 c_2 c_3 c_4 c_5 c_6 + \text{c.c.}),
\end{aligned} \tag{2.29}$$

⁷We have defined the auxiliary Hamiltonian up to six-wave interactions, which is sufficient for our CT. This will be verified *a posteriori*.

where c.c. means complex conjugate. The auxiliary Hamiltonian is completely arbitrary and as such we denote all interaction coefficients with tildes to emphasise this. The original Hamiltonian (2.25) will fix certain auxiliary interaction coefficients, whilst allowing us to explicitly choose the remaining arbitrary coefficients to eliminate the non-resonant interaction terms.

The CT is weakly nonlinear, thus preserving the linear dynamics of the system. We use the fact that the time evolution operator is canonical, and use the Taylor expansion of $a(\mathbf{k}, t)$ around $a(\mathbf{k}, 0) = c(\mathbf{k}, 0)$ giving

$$a(\mathbf{k}, t) = c(\mathbf{k}, 0) + t \left(\frac{\partial c(\mathbf{k}, t)}{\partial t} \right) \Big|_{t=0} + \frac{t^2}{2} \left(\frac{\partial^2 c(\mathbf{k}, t)}{\partial t^2} \right) \Big|_{t=0} + \dots \quad (2.30)$$

The coefficients of the CT, (2.30), can be calculated using Relation (2.17) applied to the auxiliary Hamiltonian, (2.29), i.e.

$$\left(\frac{\partial c_{\mathbf{k}}}{\partial t} \right)_{t=0} = -i \frac{\delta \mathcal{H}_{aux}}{\delta c_{\mathbf{k}}^*}, \quad (2.31a)$$

$$\left(\frac{\partial^2 c_{\mathbf{k}}}{\partial t^2} \right)_{t=0} = -i \frac{\partial}{\partial t} \frac{\delta \mathcal{H}_{aux}}{\delta c_{\mathbf{k}}^*}. \quad (2.31b)$$

These coefficients will be of the form of summations, involving variable $c_{\mathbf{k}}$ and the interaction coefficients from the auxiliary Hamiltonian. Once coefficients (2.31) have been found, we then substitute transformation, (2.30), into Hamiltonian (2.25). This will result in a new Hamiltonian expressed in terms of the new interaction representation variable, $c_{\mathbf{k}}$, involving the interaction coefficients from the auxiliary Hamiltonian (containing tildes), $T_{3,4}^{1,2}$ and $W_{4,5,6}^{1,2,3}$. The aim is to eliminate the four-wave interaction contribution by selecting the values of the arbitrary interaction coefficients. Because in this specific case, we are considering an even N -wave system that conserves wave action, we find that the CT does not result in any additional odd N -wave contributions. Hence, all arbitrary interaction coefficients for odd orders are zero.

Elimination of all four-wave contributions can be achieved by selecting

$$\tilde{T}_{3,4}^{1,2} = \frac{-4i \left(T_{3,4}^{1,2} \right)^*}{\omega_1 + \omega_2 - \omega_3 - \omega_4}. \quad (2.32)$$

Relation (2.32) is valid because the denominator does not vanish due to a lack resonant four-wave interactions. After selecting (2.32), we find that Hamiltonian (2.25) reduces to

$$\begin{aligned} \mathcal{H} = & \sum_{\mathbf{k}} \omega_{\mathbf{k}} c_{\mathbf{k}} c_{\mathbf{k}}^* + \frac{1}{36} \sum_{1,2,3,4,5,6} \left[\mathcal{W}_{4,5,6}^{1,2,3} - i(\omega_1 + \omega_2 + \omega_3 - \omega_4 - \omega_5 - \omega_6) \right. \\ & \times \tilde{W}_{4,5,6}^{1,2,3} \left. \right] \delta_{4,5,6}^{1,2,3} c_1 c_2 c_3 c_4^* c_5^* c_6^*. \end{aligned} \quad (2.33)$$

Hamiltonian (2.33) represents Hamiltonian (2.25) in the new canonical variable $c_{\mathbf{k}}$, up to the leading resonant wave interaction, in this case being of order six. Notice, that within the six-wave contribution there is still an arbitrary contribution, $\tilde{W}_{4,5,6}^{1,2,3}$, that arises from the auxiliary Hamiltonian (2.29). However, its prefactor, $\omega_1 + \omega_2 + \omega_3 - \omega_4 - \omega_5 - \omega_6$ vanishes when the six-wave resonance condition

$$\mathbf{k}_1 + \mathbf{k}_2 + \mathbf{k}_3 = \mathbf{k}_4 + \mathbf{k}_5 + \mathbf{k}_6, \quad (2.34a)$$

$$\omega(\mathbf{k}_1) + \omega(\mathbf{k}_2) + \omega(\mathbf{k}_3) = \omega(\mathbf{k}_4) + \omega(\mathbf{k}_5) + \omega(\mathbf{k}_6), \quad (2.34b)$$

is satisfied. Hence, $\tilde{W}_{4,5,6}^{1,2,3}$ does not provide a contribution to the nonlinear wave dynamics. We can select $\tilde{W}_{4,5,6}^{1,2,3}$ to equal minus the difference of $\mathcal{W}_{4,5,6}^{1,2,3}$ from its value taken when the resonance condition, (2.34), is satisfied. For instance, if we decompose $\mathcal{W}_{4,5,6}^{1,2,3}$ into two parts, the first being its value when the resonant condition is satisfied, say ${}^R\mathcal{W}_{4,5,6}^{1,2,3}$ and the second being its residual ${}^\perp\mathcal{W}_{4,5,6}^{1,2,3} = \mathcal{W}_{4,5,6}^{1,2,3} - {}^R\mathcal{W}_{4,5,6}^{1,2,3}$, we can then express

$$\mathcal{W}_{4,5,6}^{1,2,3} = {}^R\mathcal{W}_{4,5,6}^{1,2,3} + {}^\perp\mathcal{W}_{4,5,6}^{1,2,3}. \quad (2.35)$$

By choosing

$$\tilde{W}_{4,5,6}^{1,2,3} = \frac{-i {}^\perp\mathcal{W}_{4,5,6}^{1,2,3}}{\omega_1 + \omega_2 + \omega_3 - \omega_4 - \omega_5 - \omega_6}, \quad (2.36)$$

the arbitrary interaction coefficient, $\tilde{W}_{4,5,6}^{1,2,3}$, directly cancels with the residual contribu-

tion of $\mathcal{W}_{4,5,6}^{1,2,3}$. Therefore, the resulting transformed Hamiltonian reads

$$\mathcal{H} = \sum_{\mathbf{k}} \omega_{\mathbf{k}} c_{\mathbf{k}} c_{\mathbf{k}}^* + \frac{1}{36} \sum_{1,2,3,4,5,6} \mathcal{W}_{4,5,6}^{1,2,3} \delta_{4,5,6}^{1,2,3} c_1 c_2 c_3 c_4^* c_5^* c_6^*, \quad (2.37)$$

where the explicit formula for $\mathcal{W}_{4,5,6}^{1,2,3}$ stemming from the CT is given by

$$\mathcal{W}_{4,5,6}^{1,2,3} = {}^R W_{4,5,6}^{1,2,3} - \frac{1}{8} \sum_{\substack{i,j,m=1 \\ i \neq j \neq m \neq i}}^3 \sum_{\substack{p,q,r=4 \\ p \neq q \neq r \neq p}}^6 \frac{T_{p,q}^{p+q-i,i} T_{j,m}^{j+m-r,r}}{\omega_{j,m}^{j+m-r,r}} + \frac{T_{i,j}^{i+j-p,p} T_{q,r}^{q+r-m,m}}{\omega_{q,r}^{q+r-m,m}}, \quad (2.38)$$

where we have use the notation of $\omega_{3,4}^{1,2} = \omega_1 + \omega_2 - \omega_3 - \omega_4$. The second contribution to the right-hand side of Equation (2.38) is an additional term arising from the CT describing the sub-leading contribution of the four-wave dynamics. This term adds to the resonant six-wave dynamics with the consideration of two coupled four-wave interactions.

Hamiltonian (2.37) represents the the original Hamiltonian system (2.25) in the new canonical variable $c_{\mathbf{k}}$. However, the interaction Hamiltonian has now been transformed from having a leading non-resonant four-wave interaction term into one with a leading resonant six-wave interaction contribution. From the formula of the new six-wave interaction coefficient (2.38), the six-wave interaction stems from the coupling of two non-resonant four-wave interactions connected by a *virtual* wave, see Figure 2.2.

By applying Relation (2.17) to Hamiltonian (2.37), we get an equation for the time evolution of the wave interaction variable $c_{\mathbf{k}}$, where

$$i\dot{c}_{\mathbf{k}} = \omega_{\mathbf{k}} c_{\mathbf{k}} + \frac{1}{12} \sum_{2,3,4,5,6} \mathcal{W}_{4,5,6}^{\mathbf{k},2,3} c_2^* c_3^* c_4 c_5 c_6 \delta_{4,5,6}^{\mathbf{k},2,3}. \quad (2.39)$$

This equation is the starting point for WT theory. This is the six-wave analogue of the Zakharov equation, which describes four-wave interactions of water surface waves [98].

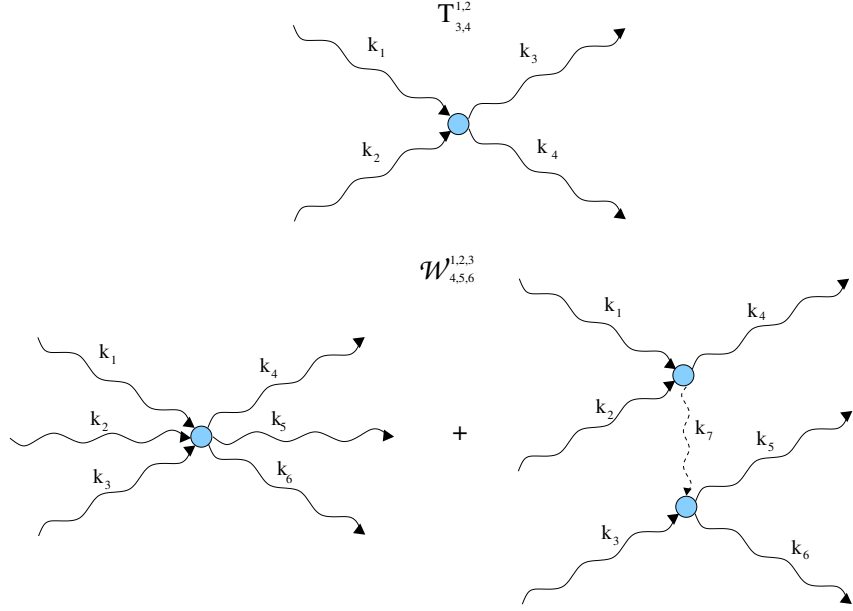


Figure 2.2: An illustration to show the four-wave interaction, $T_{3,4}^{1,2}$, and the six-wave interaction, $\mathcal{W}_{4,5,6}^{1,2,3}$, after the CT. The six-wave interaction term (sextet) is a sum of a $3 \rightarrow 3$ wave process and the contribution arising from two coupled four-wave interaction via a virtual wave.

2.6 The Weak Nonlinearity Expansion

The approach of WT theory is established by a separation of the linear and nonlinear dynamics. i.e. when considering a weakly nonlinear regime, (when wave amplitudes are small), the linear evolution time, T_L , defined as

$$T_L = \frac{2\pi}{\omega_k}, \quad (2.40)$$

is smaller than the nonlinear evolution time, T_{NL} - the time for the nonlinear energy transfer between waves, i.e.

$$T_L \ll T_{NL}. \quad (2.41)$$

This separation of timescales allows for an ensemble average over the fast linear timescale and for the description of the nonlinear evolution of the wave system. For WT systems, T_L and T_{NL} are usually wave number dependent, hence it is likely for (2.41) to be

violated in some region of Fourier space. For instance, it was predicted that Condition (2.41) would break down at small wave numbers in OWT [65], for Kelvin waves in QT [99], and for capillary waves [6, 100]. Alternatively, a break down is predicted at large wave numbers for gravity waves [6, 100] and Rossby/drift waves [94]. We will observe later in this thesis, that (2.41) will almost always be violated in some region of Fourier space resulting in the formation of coherent structures, strong turbulence, or a critical balance (CB) regime.

For small wave amplitudes, $|c_k| \ll 1$, we can re-scale c_k by the introduction of a small nonlinearity parameter $\epsilon \in \mathbb{R}^+$. Therefore, we can express wave amplitudes in terms of a new canonical variable $b_k \sim \mathcal{O}(1)$ and ϵ . By introducing ϵ , it allows us to easily distinguish between the linear and nonlinear timescales. The nonlinear timescale for a six-wave process is of the order $T_{NL} \sim 2\pi/\epsilon^8\omega_k$, which will be verified *a posteriori*, and hence we seek a solution at an intermediate time, T , where

$$T_L \ll T \ll T_{NL}. \quad (2.42)$$

Trivial pairings of wave numbers in Equation (2.39), do not contribute to the nonlinear exchange of energy between wave modes, but they do provide an additional contribution to the frequency. Therefore, before we can proceed, we must first consider this contribution. This ensures that the weak nonlinearity expansion will be defined in a self-consistent way [2]. By separating the diagonal terms from the main summation, Equation (2.39) can be expressed as

$$i\dot{c}_k = (\omega_k + \Omega_k^c) c_k + \frac{1}{12} \sum_{\mathcal{K}_{4,5,6}^{2,3}} \mathcal{W}_{4,5,6}^{\mathbf{k},2,3} c_2^* c_3^* c_4 c_5 c_6 \delta_{4,5,6}^{\mathbf{k},2,3}, \quad (2.43)$$

where

$$\Omega_k^c = \frac{1}{2} \sum_{7,8} \mathcal{W}_{k,7,8}^{\mathbf{k},7,8} |c_7|^2 |c_8|^2. \quad (2.44)$$

The summation in (2.43) is now taken over the set $\mathcal{K}_{4,5,6}^{2,3} = \{\mathbf{k}_2, \mathbf{k}_3, \mathbf{k}_4, \mathbf{k}_5, \mathbf{k}_6 : \mathbf{k}, \mathbf{k}_2, \mathbf{k}_3 \neq \mathbf{k}_4, \mathbf{k}_5, \mathbf{k}_6\}$. We see that the nonlinear frequency, Ω_k^c , acts as a correction to the linear wave frequency, and subsequently, the system is modified to a new

frequency $\tilde{\omega}_k = \omega_k + \Omega_k^c$.

Let us define the interaction variable $b_{\mathbf{k}}$, such that all smallness of the wave amplitude $c_{\mathbf{k}}$ is represented by the parameter ϵ . In addition, we shall incorporate the new system frequency, $\tilde{\omega}_k$, into variable $b_{\mathbf{k}}$. Therefore, we define $b_{\mathbf{k}}$ as

$$b_{\mathbf{k}} = \frac{c_{\mathbf{k}}}{\epsilon} e^{i\omega_k t + i \int_0^t \Omega_k dt'}. \quad (2.45)$$

In (2.45), time-dependence of the nonlinear frequency correction, Ω_k^c , must be taken into account, and consequently, there remains an integration in the phase. In terms of variable $b_{\mathbf{k}}$, the nonlinear frequency correction can be expressed as

$$\Omega_k^b = \frac{\epsilon^4}{2} \sum_{7,8} \mathcal{W}_{\mathbf{k},7,8}^{\mathbf{k},7,8} |b_7|^2 |b_8|^2 = \epsilon^4 \Omega_k^c. \quad (2.46)$$

The change of variable introduces an extra prefactor of ϵ^4 . From now on, we will omit the superscript in (2.46), thus Ω_k^b will become Ω_k .

Substitution of Formula (2.45) into Equation (2.43) implies that

$$i\dot{b}_{\mathbf{k}} = \frac{\epsilon^4}{12} \sum_{\mathcal{K}_{4,5,6}^{2,3}} \mathcal{W}_{4,5,6}^{\mathbf{k},2,3} b_2^* b_3^* b_4 b_5 b_6 \delta_{4,5,6}^{\mathbf{k},2,3} e^{i\omega_{4,5,6}^{k,2,3} t + i\epsilon^4 \int_0^t \Omega_{4,5,6}^{k,2,3} dt'}. \quad (2.47)$$

As the nonlinear frequency correction is time-dependent, extra care should be taken when considering its contribution to (2.47). Therefore, we expand the last exponential in Equation (2.47) as

$$e^{i\epsilon^4 \int_0^t \Omega_{4,5,6}^{k,2,3} dt'} = 1 + i\epsilon^4 \int_0^t \Omega_{4,5,6}^{k,2,3} dt' - \frac{\epsilon^8}{2} \left(\int_0^t \Omega_{4,5,6}^{k,2,3} dt' \right)^2 + \dots \quad (2.48)$$

The main objective is to seek a solution of $b_{\mathbf{k}}(T)$, where T is our intermediate scale defined in (2.42). Let us consider an ϵ -expansion of $b_{\mathbf{k}}(T)$ of the form

$$b_{\mathbf{k}}(T) = b_{\mathbf{k}}^{(0)} + \epsilon^4 b_{\mathbf{k}}^{(1)} + \epsilon^8 b_{\mathbf{k}}^{(2)} + \dots, \quad (2.49)$$

and then solve each ϵ -order of $b_{\mathbf{k}}(T)$ by an iterative method using evolution Equation

(2.47). Expansion (2.49) is in powers of ϵ^4 because this is determined by the evolution equation (2.47), which will only contribute at every fourth order of ϵ . We substitute (2.49) into (2.47), and equate ϵ -orders. The leading $\mathcal{O}(\epsilon^0)$ contribution implies

$$i\dot{b}_{\mathbf{k}}^{(0)} = 0. \quad (2.50)$$

Integration of (2.50), with respect to time gives

$$b_{\mathbf{k}}^{(0)}(T) = b_{\mathbf{k}}^{(0)}(0). \quad (2.51)$$

Result (2.51), implies that at leading order, the wave amplitude $b_{\mathbf{k}}(T)$ is time-independent.

Consideration of the following order, $\mathcal{O}(\epsilon^4)$, implies that

$$\epsilon^4 i\dot{b}_{\mathbf{k}}^{(1)} = \frac{\epsilon^4}{12} \sum_{\kappa_{4,5,6}^{2,3}} \mathcal{W}_{4,5,6}^{\mathbf{k},2,3} b_2^{(0)*} b_3^{(0)*} b_4^{(0)} b_5^{(0)} b_6^{(0)} \delta_{4,5,6}^{\mathbf{k},2,3} e^{i\omega_{4,5,6}^{k,2,3} t}. \quad (2.52)$$

The nonlinear frequency correction does not contribute to (2.52), as it contains an additional ϵ^4 prefactor. Therefore, integration with respect to time yields

$$b_{\mathbf{k}}^{(1)}(T) = -\frac{i}{12} \sum_{\kappa_{4,5,6}^{2,3}} \mathcal{W}_{4,5,6}^{\mathbf{k},2,3} b_2^{(0)*} b_3^{(0)*} b_4^{(0)} b_5^{(0)} b_6^{(0)} \delta_{4,5,6}^{\mathbf{k},2,3} \Delta_T \left(\omega_{4,5,6}^{k,2,3} \right). \quad (2.53)$$

Here we have used that $b_{\mathbf{k}}^{(1)}(0) = 0$ and have defined

$$\Delta_T(x) = \int_0^T e^{ixt} dt. \quad (2.54)$$

Note that if we conjugate (2.54), we get that $\Delta_T^*(x) = \Delta_T(-x)$. Finally, we use

formulae (2.51) and (2.53) to determine $b_{\mathbf{k}}^{(2)}(T)$:

$$\begin{aligned} \epsilon^8 i b_{\mathbf{k}}^{(2)} &= \frac{\epsilon^8}{12} \sum_{\mathcal{K}_{4,5,6}^{2,3}} \mathcal{W}_{4,5,6}^{\mathbf{k},2,3} \delta_{4,5,6}^{\mathbf{k},2,3} \left(2 b_2^{(1)*} b_3^{(0)*} b_4^{(0)} b_5^{(0)} b_6^{(0)} + 3 b_2^{(0)*} b_3^{(0)*} b_4^{(1)} b_5^{(0)} b_6^{(0)} \right) \\ &\quad \times e^{i\omega_{4,5,6}^{k,2,3} t} \\ &+ \frac{\epsilon^8}{12} \sum_{\mathcal{K}_{4,5,6}^{2,3}} \mathcal{W}_{4,5,6}^{\mathbf{k},2,3} \delta_{4,5,6}^{\mathbf{k},2,3} b_2^{(0)*} b_3^{(0)*} b_4^{(0)} b_5^{(0)} b_6^{(0)} e^{i\omega_{4,5,6}^{k,2,3} t} {}^{(0)}\Omega_{4,5,6}^{k,2,3} t, \end{aligned} \quad (2.55)$$

where

$${}^{(0)}\Omega_k = \frac{\epsilon^4}{2} \sum_{7,8} \mathcal{W}_{\mathbf{k},7,8}^{\mathbf{k},7,8} |b_7^{(0)}|^2 |b_8^{(0)}|^2, \quad (2.56)$$

and ${}^{(0)}\Omega_{4,5,6}^{k,2,3} = {}^{(0)}\Omega_k + {}^{(0)}\Omega_2 + {}^{(0)}\Omega_3 - {}^{(0)}\Omega_4 - {}^{(0)}\Omega_5 - {}^{(0)}\Omega_6$. The last contribution in Equation (2.55), stems from the nonlinear frequency correction and can be integrated as $b_{\mathbf{k}}^{(0)}$ is time-independent. Substitution of the expression for $b_{\mathbf{k}}^{(1)}$ into Equation (2.55) and integrating gives

$$\begin{aligned} b_{\mathbf{k}}^{(2)} &= \frac{1}{12} \sum_{\mathcal{K}_{4,5,6}^{2,3}, \mathcal{K}_{9,10,11}^{7,8}} \left[2 \mathcal{W}_{4,5,6}^{\mathbf{k},2,3} \left(\mathcal{W}_{9,10,11}^{2,7,8} \right)^* b_3^{(0)*} b_9^{(0)*} b_{10}^{(0)*} b_{11}^{(0)*} b_4^{(0)} b_5^{(0)} b_6^{(0)} b_7^{(0)} b_8^{(0)} \right. \\ &\quad \times \delta_{4,5,6}^{\mathbf{k},2,3} \delta_{9,10,11}^{2,7,8} E_T \left(\left(\omega_{9,10,11}^{2,7,8} \right)^*, \omega_{4,5,6}^{k,2,3} \right) - 3 \mathcal{W}_{4,5,6}^{\mathbf{k},2,3} \mathcal{W}_{9,10,11}^{4,7,8} \\ &\quad \times b_2^{(0)*} b_3^{(0)*} b_7^{(0)*} b_8^{(0)*} b_5^{(0)} b_6^{(0)} b_9^{(0)} b_{10}^{(0)} b_{11}^{(0)} \delta_{4,5,6}^{\mathbf{k},2,3} \delta_{9,10,11}^{4,7,8} E_T \left(\omega_{9,10,11}^{4,7,8}, \omega_{4,5,6}^{k,2,3} \right) \Big] \\ &+ \frac{\epsilon^8}{12} \sum_{\mathcal{K}_{4,5,6}^{2,3}} \mathcal{W}_{4,5,6}^{\mathbf{k},2,3} \delta_{4,5,6}^{\mathbf{k},2,3} b_2^{(0)*} b_3^{(0)*} b_4^{(0)} b_5^{(0)} b_6^{(0)} e^{i\omega_{4,5,6}^{k,2,3} t} {}^{(0)}\Omega_{4,5,6}^{k,2,3} t, \end{aligned} \quad (2.57)$$

where we have defined $E_T(x, y)$ as

$$E_T(x, y) = \int_0^T \Delta_t(x) e^{i \int_0^t y dt'} dt'. \quad (2.58)$$

Symmetry of $\Delta_T(x)$ implies that $E_T(x^*, y) = E_T(-x, y)$. With Equations (2.51), (2.53) and (2.57), we have calculated the ϵ -expansion of $b_{\mathbf{k}}$ up to $\mathcal{O}(\epsilon^8)$ ⁸. The next objective is to define the GF, this provides a clear and concise way to describe the evolution of all the statistical quantities in WT.

⁸We will find that this order is sufficient for all the analysis contained within this thesis.

2.7 Calculation of the Generating Functional

The N -mode GF defines all the joint statistics in the system. The N -mode statistics are essential if we are interested in verifying the WT assumptions of the system. However, for the application of WT theory, the one-mode statistics are sufficient. Although wave amplitudes will eventually become correlated as we approach the nonlinear evolution time, any pair of wave modes will remain independent, up to an accuracy of $\mathcal{O}(\epsilon^2)$ [2, 4]. This implies that for the description of WT theory (and to form the WT closure) one-mode statistical objects are adequate. With this in mind, we will restrict ourselves to only considering the one-mode amplitude GF $\mathcal{Z}_k^{(1,a)}(\lambda_k)$.

Recall that the one-mode amplitude GF (2.11) is defined as

$$\mathcal{Z}_k(\lambda_k) = \left\langle e^{\left(\frac{L}{2\pi}\right)\lambda_k|b_k|^2} \right\rangle. \quad (2.59)$$

Here, we have dropped the superscript from the one-mode amplitude GF from definition (2.11) for clarity. The aim is to calculate the ϵ -expansion of \mathcal{Z}_k at the intermediate time, T , and subsequently, derive an evolution equation, using Equations (2.51), (2.53) and (2.57) for b_k . Assume that we can represent the GF in powers of ϵ , as

$$\mathcal{Z}_k = \mathcal{Z}_k^{(0)} + \epsilon^4 \mathcal{Z}_k^{(1)} + \epsilon^8 \mathcal{Z}_k^{(2)} + \dots \quad (2.60)$$

Then to calculate the GF, (2.59), we must average over random amplitudes, $\langle \cdot \rangle_J$, and random phases, $\langle \cdot \rangle_\phi$, in an RPA field. Once we have performed these, we can derive the evolution equation for \mathcal{Z}_k , and thus any of the one-mode statistical objects we require.

To begin, we substitute the ϵ -expansion of b_k , (2.49), into Definition (2.59) and consider terms up to $\mathcal{O}(\epsilon^8)$:

$$\mathcal{Z}_k = \langle e^{\left(\frac{L}{2\pi}\right)\lambda_k|b_k^{(0)} + \epsilon^4 b_k^{(1)} + \epsilon^8 b_k^{(2)}|^2} \rangle + \mathcal{O}(\epsilon^{12}). \quad (2.61)$$

Expression (2.61) can be further simplified using a Taylor expansion for each exponent-

tial⁹, thus obtaining

$$\begin{aligned} \mathcal{Z}_{\mathbf{k}} = & \left\langle e^{\left(\frac{L}{2\pi}\right)\lambda_{\mathbf{k}}|b_{\mathbf{k}}^{(0)}|^2} \left[1 + \epsilon^4 \left(\frac{L}{2\pi}\right) \lambda_{\mathbf{k}} \left(b_{\mathbf{k}}^{(0)} b_{\mathbf{k}}^{(1)*} + b_{\mathbf{k}}^{(0)*} b_{\mathbf{k}}^{(1)} \right) \right. \right. \\ & + \epsilon^8 \left(\left(\frac{L}{2\pi}\right) \lambda_{\mathbf{k}} \left(|b_{\mathbf{k}}^{(1)}|^2 + b_{\mathbf{k}}^{(0)} b_{\mathbf{k}}^{(2)*} + b_{\mathbf{k}}^{(0)*} b_{\mathbf{k}}^{(2)} \right) \right. \\ & \left. \left. + \left(\frac{L}{2\pi}\right)^2 \frac{\lambda_{\mathbf{k}}^2}{2} \left(b_{\mathbf{k}}^{(0)} b_{\mathbf{k}}^{(1)*} + b_{\mathbf{k}}^{(0)*} b_{\mathbf{k}}^{(1)} \right)^2 \right) \right\rangle + \mathcal{O}(\epsilon^{12}). \end{aligned} \quad (2.62)$$

We now proceed by performing amplitude and phase averaging of each term in Expansion (2.62). The leading $\mathcal{O}(\epsilon^0)$ contribution of $\mathcal{Z}_{\mathbf{k}}$ is

$$\mathcal{Z}_{\mathbf{k}}^{(0)} = \left\langle e^{\left(\frac{L}{2\pi}\right)\lambda_{\mathbf{k}}|b_{\mathbf{k}}^{(0)}|^2} \right\rangle = \left\langle e^{\left(\frac{L}{2\pi}\right)\lambda_{\mathbf{k}}J_{\mathbf{k}}^{(0)}} \right\rangle = \mathcal{Z}_{\mathbf{k}}(0), \quad (2.63)$$

where $J_{\mathbf{k}}^{(0)} = |b_{\mathbf{k}}^{(0)}|^2$ is the amplitude of the interaction variable $b_{\mathbf{k}}^{(0)}$. For clarity, we shall omit the superscript of $J_{\mathbf{k}}^{(0)}$ which will thus become $J_{\mathbf{k}}$ ¹⁰. We have labelled the leading order of the ϵ -expansion as $\mathcal{Z}_{\mathbf{k}}(0)$, corresponding to the initial value of the GF. The next order yields

$$\mathcal{Z}_{\mathbf{k}}^{(1)} = \left\langle \left(\frac{L}{2\pi}\right) \lambda_{\mathbf{k}} e^{\left(\frac{L}{2\pi}\right)\lambda_{\mathbf{k}}J_{\mathbf{k}}} \left(b_{\mathbf{k}}^{(0)} b_{\mathbf{k}}^{(1)*} + b_{\mathbf{k}}^{(0)*} b_{\mathbf{k}}^{(1)} \right) \right\rangle, \quad (2.64)$$

and subsequently at the final order to be considered, we obtain

$$\begin{aligned} \mathcal{Z}_{\mathbf{k}}^{(2)} = & \left\langle \left(\frac{L}{2\pi}\right) \lambda_{\mathbf{k}} e^{\left(\frac{L}{2\pi}\right)\lambda_{\mathbf{k}}J_{\mathbf{k}}} \left[|b_{\mathbf{k}}^{(1)}|^2 + b_{\mathbf{k}}^{(0)} b_{\mathbf{k}}^{(2)*} + b_{\mathbf{k}}^{(0)*} b_{\mathbf{k}}^{(2)} \right. \right. \\ & \left. \left. + \left(\frac{L}{2\pi}\right) \frac{\lambda_{\mathbf{k}}}{2} \left(2J_{\mathbf{k}}|b_{\mathbf{k}}^{(1)}|^2 + \left(b_{\mathbf{k}}^{(0)} b_{\mathbf{k}}^{(1)*}\right)^2 + \left(b_{\mathbf{k}}^{(0)*} b_{\mathbf{k}}^{(1)}\right)^2 \right) \right] \right\rangle. \end{aligned} \quad (2.65)$$

Having expressed $\mathcal{Z}_{\mathbf{k}}$ in terms of $b_{\mathbf{k}}$, we now proceed by evaluating the ensemble averages.

⁹This will not alter the the accuracy of the derivation.

¹⁰Note that now $J_{\mathbf{k}}$ is not the amplitude of the *full* interaction variable $b_{\mathbf{k}}$, as defined in Section 2.1.

2.8 Phase Averaging

The next step is to evaluate the amplitude and phase average of each term in the GF. We can identify three types of terms that appear in our expansion for the GF, these are $\langle b_{\mathbf{k}}^{(0)} b_{\mathbf{k}}^{(1)*} \rangle$, $\langle |b_{\mathbf{k}}^{(1)}|^2 \rangle$, and $\langle b_{\mathbf{k}}^{(0)} b_{\mathbf{k}}^{(2)*} \rangle$. We will begin by considering the phase average of these quantities.

From formula (2.53), we have that

$$\langle b_{\mathbf{k}}^{(0)} b_{\mathbf{k}}^{(1)*} \rangle_{\phi} = \frac{i}{12} \sum_{\mathcal{K}_{4,5,6}^{2,3}} \left(\mathcal{W}_{4,5,6}^{\mathbf{k},2,3} \right)^* \left\langle b_{\mathbf{k}}^{(0)} b_2^{(0)} b_3^{(0)} b_4^{(0)*} b_5^{(0)*} b_6^{(0)*} \right\rangle_{\phi} \delta_{4,5,6}^{\mathbf{k},2,3} \Delta_T(\omega_{4,5,6}^{k,2,3}). \quad (2.66)$$

To compute the phase average of (2.66), we implement Wick's rule, i.e. we consider all possible pairings of wave numbers that are allowed by the summation. However, due to the trivial pairings leading to the nonlinear frequency correction, we are restricted to which wave numbers can be matched¹¹. Consequently, no pairings can occur, and thus, the average (2.66) is zero. This is also the case for $\langle \left(b_{\mathbf{k}}^{(0)} b_{\mathbf{k}}^{(1)*} \right)^2 \rangle_{\phi}$, which also results in no contribution for the same reason.

In $\mathcal{Z}_{\mathbf{k}}^{(2)}$, we have the term

$$\begin{aligned} \left\langle |b_{\mathbf{k}}^{(1)}|^2 \right\rangle_{\phi} &= \frac{1}{144} \sum_{\mathcal{K}_{4,5,6}^{2,3}, \mathcal{K}_{9,10,11}^{7,8}} \mathcal{W}_{4,5,6}^{\mathbf{k},2,3} \left(\mathcal{W}_{9,10,11}^{\mathbf{k},7,8} \right)^* \\ &\times \left\langle b_2^{(0)*} b_3^{(0)*} b_9^{(0)*} b_{10}^{(0)*} b_{11}^{(0)*} b_4^{(0)*} b_5^{(0)*} b_6^{(0)*} b_7^{(0)*} b_8^{(0)} \right\rangle_{\phi} \\ &\times \delta_{4,5,6}^{\mathbf{k},2,3} \delta_{9,10,11}^{\mathbf{k},7,8} \Delta_T(\omega_{4,5,6}^{k,2,3}) \Delta_T^*(\omega_{9,10,11}^{k,7,8}). \end{aligned} \quad (2.67)$$

In this case, we are able to match the wave numbers in such a way as to not contradict the restrictions of the summations. Using Wick's rule, we find that

$$\begin{aligned} \left\langle b_2^{(0)*} b_3^{(0)*} b_9^{(0)*} b_{10}^{(0)*} b_{11}^{(0)*} b_4^{(0)*} b_5^{(0)*} b_6^{(0)*} b_7^{(0)*} b_8^{(0)} \right\rangle_{\phi} &= (\delta_7^2 \delta_8^3 + \delta_8^2 \delta_7^3) \\ &\times [\delta_9^4 (\delta_{10}^5 \delta_{11}^6 + \delta_{11}^5 \delta_{10}^6) + \delta_{10}^4 (\delta_9^5 \delta_{11}^6 + \delta_{11}^5 \delta_9^6) + \delta_{11}^4 (\delta_9^5 \delta_{10}^6 + \delta_{10}^5 \delta_9^6)]. \end{aligned} \quad (2.68)$$

¹¹See the definition of set $\mathcal{K}_{4,5,6}^{2,3}$.

This simplifies Equation (2.67) to give

$$\left\langle |b_{\mathbf{k}}^{(1)}|^2 \right\rangle_{\phi} = \frac{1}{12} \sum_{\mathcal{K}_{4,5,6}^{2,3}} |\mathcal{W}_{4,5,6}^{\mathbf{k},2,3}|^2 J_2 J_3 J_4 J_5 J_6 \delta_{4,5,6}^{\mathbf{k},2,3} |\Delta_T(\tilde{\omega}_{4,5,6}^{k,2,3})|^2. \quad (2.69)$$

Applying a similar approach to $\langle b_{\mathbf{k}}^{(0)} b_{\mathbf{k}}^{(2)*} \rangle_{\phi}$ we arrive at

$$\begin{aligned} \langle b_{\mathbf{k}}^{(0)} b_{\mathbf{k}}^{(2)*} \rangle_{\phi} &= \frac{1}{12} \sum_{\mathcal{K}_{4,5,6}^{2,3}} |\mathcal{W}_{4,5,6}^{\mathbf{k},2,3}|^2 J_{\mathbf{k}} (J_2 + J_3) J_4 J_5 J_6 \delta_{4,5,6}^{\mathbf{k},2,3} E_T \left(\left(\omega_{4,5,6}^{k,2,3} \right)^*, \omega_{4,5,6}^{k,2,3} \right) \\ &\quad - \frac{1}{12} \sum_{\mathcal{K}_{4,5,6}^{2,3}} |\mathcal{W}_{4,5,6}^{\mathbf{k},2,3}|^2 J_{\mathbf{k}} J_2 J_3 (J_4 J_5 + J_4 J_6 + J_5 J_6) \delta_{4,5,6}^{\mathbf{k},2,3} \\ &\quad \times E_T^* \left(\omega_{k,2,3}^{4,5,6}, \omega_{4,5,6}^{k,2,3} \right). \end{aligned} \quad (2.70)$$

Note that the last term in Equation (2.57), corresponds to the nonlinear frequency correction and averages to zero.

2.9 Amplitude Averaging

So far, we have taken the phase average, now we must perform the amplitude average over the $J_{\mathbf{k}}$ s. Recalling Equations (2.62-2.65), we see that $\mathcal{Z}_{\mathbf{k}}^{(1)}$ is zero, as (2.66) vanishes, and thus, the ϵ -expansion of the GF can be expressed as

$$\begin{aligned} \mathcal{Z}_{\mathbf{k}}(T) &= \mathcal{Z}_{\mathbf{k}}(0) + \frac{\epsilon^8}{12} \sum_{\mathcal{K}_{4,5,6}^{2,3}} |\mathcal{W}_{4,5,6}^{\mathbf{k},2,3}|^2 \delta_{4,5,6}^{\mathbf{k},2,3} \left[\left\langle \left(\left(\frac{L}{2\pi} \right) \lambda_{\mathbf{k}} + \left(\frac{L}{2\pi} \right)^2 \lambda_{\mathbf{k}}^2 J_{\mathbf{k}} \right) \right. \right. \\ &\quad \times e^{\left(\frac{L}{2\pi} \right) \lambda_{\mathbf{k}} J_{\mathbf{k}}} J_2 J_3 J_4 J_5 J_6 \left. \right\rangle_J |\Delta_T(\tilde{\omega}_{4,5,6}^{k,2,3})|^2 \\ &\quad + 2 \left\langle \left(\frac{L}{2\pi} \right) \lambda_{\mathbf{k}} e^{\left(\frac{L}{2\pi} \right) \lambda_{\mathbf{k}} J_{\mathbf{k}}} J_{\mathbf{k}} (J_2 + J_3) J_4 J_5 J_6 \right\rangle_J \Re \left[E_T \left(\left(\omega_{4,5,6}^{k,2,3} \right)^*, \omega_{4,5,6}^{k,2,3} \right) \right] \\ &\quad - 2 \left\langle \left(\frac{L}{2\pi} \right) \lambda_{\mathbf{k}} e^{\left(\frac{L}{2\pi} \right) \lambda_{\mathbf{k}} J_{\mathbf{k}}} J_{\mathbf{k}} J_2 J_3 (J_4 J_5 + J_4 J_6 + J_5 J_6) \right\rangle_J \\ &\quad \times \Re \left[E_T^* \left(\omega_{k,2,3}^{4,5,6}, \omega_{4,5,6}^{k,2,3} \right) \right], \end{aligned} \quad (2.71)$$

where $\Re[\cdot]$ denotes the real part. To calculate the amplitude averages, we can use the independence of amplitudes and the fact that all wave numbers are non-identical due to the restriction of trivial pairings within the summation. For example, for three wave numbers, $\mathbf{k} \neq \mathbf{k}_2 \neq \mathbf{k}_3 \neq \mathbf{k}$, we can split an amplitude average as

$$\langle J_{\mathbf{k}} J_2 e^{\lambda_2 J_2} e^{\lambda_3 J_3} \rangle_J = \langle J_{\mathbf{k}} \rangle_J \langle J_2 e^{\lambda_2 J_2} \rangle_J \langle e^{\lambda_3 J_3} \rangle_J. \quad (2.72)$$

We can define the wave action spectrum $n_{\mathbf{k}}$, and the derivative of the GF with respect to $\lambda_{\mathbf{k}}$ as

$$n_{\mathbf{k}} = \left(\frac{L}{2\pi} \right) \langle J_{\mathbf{k}} \rangle_J, \quad (2.73a)$$

$$\frac{\partial \mathcal{Z}_{\mathbf{k}}}{\partial \lambda_{\mathbf{k}}} = \frac{\partial}{\partial \lambda_{\mathbf{k}}} \left\langle e^{\left(\frac{L}{2\pi}\right) \lambda_{\mathbf{k}} J_{\mathbf{k}}} \right\rangle_J = \left\langle \left(\frac{L}{2\pi} \right) J_{\mathbf{k}} e^{\left(\frac{L}{2\pi}\right) \lambda_{\mathbf{k}} J_{\mathbf{k}}} \right\rangle_J. \quad (2.73b)$$

Therefore, Equation (2.71) can be written in the form,

$$\begin{aligned} \mathcal{Z}_{\mathbf{k}}(T) - \mathcal{Z}_{\mathbf{k}}(0) &= \left(\frac{2\pi}{L} \right)^4 \frac{\epsilon^8}{12} \sum_{\mathcal{K}_{4,5,6}^{2,3}} |\mathcal{W}_{4,5,6}^{\mathbf{k},2,3}|^2 \delta_{4,5,6}^{\mathbf{k},2,3} \left[\left(\lambda_{\mathbf{k}} \mathcal{Z}_{\mathbf{k}} + \lambda_{\mathbf{k}}^2 \frac{\partial \mathcal{Z}_{\mathbf{k}}}{\partial \lambda_{\mathbf{k}}} \right) \right. \\ &\quad \times n_2 n_3 n_4 n_5 n_6 \left| \Delta_T \left(\omega_{4,5,6}^{k,2,3} \right) \right|^2 \\ &\quad + 2 \lambda_{\mathbf{k}} \frac{\partial \mathcal{Z}_{\mathbf{k}}}{\partial \lambda_{\mathbf{k}}} (n_2 + n_3) n_4 n_5 n_6 \Re \left[E_T \left(\left(\omega_{4,5,6}^{k,2,3} \right)^*, \omega_{4,5,6}^{k,2,3} \right) \right] \\ &\quad - 2 \lambda_{\mathbf{k}} \frac{\partial \mathcal{Z}_{\mathbf{k}}}{\partial \lambda_{\mathbf{k}}} n_2 n_3 (n_4 n_5 + n_4 n_6 + n_5 n_6) \\ &\quad \left. \times \Re \left[E_T^* \left(\omega_{k,2,3}^{4,5,6}, \omega_{4,5,6}^{k,2,3} \right) \right] \right]. \end{aligned} \quad (2.74)$$

2.10 The Large Box and The Long Evolution Limits

Next we consider the limits of both an infinite box and long evolution time to Equation (2.74). However, the order in which the limits are taken is essential. We must take the large box limit, $N \rightarrow \infty$, before the limit of long time behaviour, $T \sim 1/\epsilon^4 \rightarrow \infty$, otherwise the width of the nonlinear resonance broadening will be smaller than the frequency grid spacing, and therefore resulting in a zero contribution. In the $N \rightarrow \infty$ limit

we have

$$\lim_{N \rightarrow \infty} \sum_{2,3,4,5,6} = \left(\frac{L}{2\pi} \right)^5 \int d\mathbf{k}_2 d\mathbf{k}_3 d\mathbf{k}_4 d\mathbf{k}_5 d\mathbf{k}_6, \quad (2.75a)$$

$$\lim_{N \rightarrow \infty} \text{Kronecker } \delta = \left(\frac{2\pi}{L} \right) \times \text{Dirac } \delta. \quad (2.75b)$$

Now, we consider the limit of long time behaviour, $T \rightarrow \infty$. Only the functions $\Delta_T(\cdot)$ and $E_T(\cdot, \cdot)$ depend on time T . Hence, we much evaluate the asymptotic limit of these functions as $T \rightarrow \infty$. Relation (2.54) implies that

$$|\Delta_T(x)|^2 = \frac{|e^{ixT/2} - e^{-ixT/2}|^2}{x^2} = \frac{4 \sin^2 \left(\frac{xT}{2} \right)}{x^2}, \quad (2.76)$$

and therefore,

$$\lim_{T \rightarrow \infty} |\Delta_T(x)|^2 = 2\pi T \delta(x). \quad (2.77)$$

Similarly for $E_T(-x, x)$ we have

$$E_T(-x, x) = \int_0^T \frac{1 - e^{-ixt}}{ix} e^{ixt} dt = \frac{1 - e^{ixT}}{x^2} + \frac{iT}{x}, \quad (2.78)$$

therefore,

$$\lim_{T \rightarrow \infty} \Re[E_T(-x, x)] = \lim_{T \rightarrow \infty} \frac{1 - \cos(xT)}{x^2} = \lim_{T \rightarrow \infty} \frac{2 \sin^2 \left(\frac{xT}{2} \right)}{x^2} = \pi T \delta(x). \quad (2.79)$$

As the intermediate time, T , is smaller than the nonlinear evolution time, T_{NL} , we can approximate the time derivative of $\mathcal{Z}_{\mathbf{k}}$ by

$$\dot{\mathcal{Z}}_{\mathbf{k}} \approx \frac{\mathcal{Z}_{\mathbf{k}}(T) - \mathcal{Z}_{\mathbf{k}}(0)}{T}. \quad (2.80)$$

Therefore, using Results (2.75), (2.77), (2.79) and (2.80), we derive a continuous evolution equation for the GF:

$$\dot{\mathcal{Z}}_{\mathbf{k}} = \lambda_{\mathbf{k}} \eta_{\mathbf{k}} \mathcal{Z}_{\mathbf{k}} + (\lambda_{\mathbf{k}}^2 \eta_{\mathbf{k}} - \lambda_{\mathbf{k}} \gamma_{\mathbf{k}}) \frac{\partial \mathcal{Z}_{\mathbf{k}}}{\partial \lambda_{\mathbf{k}}}, \quad (2.81)$$

where

$$\eta_{\mathbf{k}} = \frac{\epsilon^8 \pi}{6} \int |\mathcal{W}_{4,5,6}^{\mathbf{k},2,3}|^2 \delta_{4,5,6}^{\mathbf{k},2,3} \delta(\omega_{4,5,6}^{k,2,3}) n_2 n_3 n_4 n_5 n_6 d\mathbf{k}_2 d\mathbf{k}_3 d\mathbf{k}_4 d\mathbf{k}_5 d\mathbf{k}_6, \quad (2.82a)$$

and

$$\begin{aligned} \gamma_{\mathbf{k}} = & \frac{\epsilon^8 \pi}{6} \int |\mathcal{W}_{4,5,6}^{\mathbf{k},2,3}|^2 \delta_{4,5,6}^{\mathbf{k},2,3} \delta(\omega_{4,5,6}^{k,2,3}) [(n_2 + n_3) n_4 n_5 n_6 \\ & - n_2 n_3 (n_4 n_5 + n_4 n_6 + n_5 n_6)] d\mathbf{k}_2 d\mathbf{k}_3 d\mathbf{k}_4 d\mathbf{k}_5 d\mathbf{k}_6. \end{aligned} \quad (2.82b)$$

2.11 Moments of the Wave Intensity $J_{\mathbf{k}}$

Moments of $J_{\mathbf{k}}$, defined as $M_{\mathbf{k}}^{(p)} = (\frac{L}{2\pi})^p \langle J_{\mathbf{k}}^p \rangle$, can be easily found by differentiating the GF p times with respect to $\lambda_{\mathbf{k}}$ and evaluating at $\lambda_{\mathbf{k}} = 0$:

$$M_{\mathbf{k}}^{(p)} = \left. \frac{\partial^p}{\partial \lambda_{\mathbf{k}}^p} \mathcal{Z}_{\mathbf{k}} \right|_{\lambda_{\mathbf{k}}=0}. \quad (2.83)$$

Therefore, the evolution equation for $M_{\mathbf{k}}^{(p)}$ can be found directly from (2.81) using Formula (2.83), giving

$$\dot{M}_{\mathbf{k}}^{(p)} = -p \gamma_{\mathbf{k}} M_{\mathbf{k}}^{(p)} + p^2 \eta_{\mathbf{k}} M_{\mathbf{k}}^{(p-1)}. \quad (2.84)$$

For Gaussian wave fields we find that the p -th order moment is given by

$$M_{\mathbf{k}}^{(p)} = p! n_{\mathbf{k}}^p. \quad (2.85)$$

However, these solutions are invalid at small $\lambda_{\mathbf{k}}$ and at high p , as large amplitudes for which nonlinearity is no longer weak have a strong contribution to their value. Therefore, it is more suitable to consider quantities that are local in $J_{\mathbf{k}}$, such as the amplitude PDF.

The evolution equation for the first order moment, $M_{\mathbf{k}}^{(1)} = n_{\mathbf{k}}$, known as the KE, is given by

$$\dot{n}_{\mathbf{k}} = \eta_{\mathbf{k}} - \gamma_{\mathbf{k}} n_{\mathbf{k}}, \quad (2.86)$$

where η_k and γ_k are given in equations (2.82a) and (2.82b). From (2.86), we see that any stationary solution of the KE satisfies the relation:

$$n_k = \frac{\eta_k}{\gamma_k}. \quad (2.87)$$

We will consider the KE in more detail later, however, let us first investigate the one-mode amplitude PDF.

2.12 The One-Mode Amplitude Probability Density Function

Recall, that the one-mode amplitude PDF¹², $\mathcal{P}_k^{(1,a)}$, can be found by applying the inverse Laplace transform, (2.12), to the GF, \mathcal{Z}_k . By applying the inverse Laplace transform to Equation (2.81), we arrive at the equation for the evolution of the PDF:

$$\dot{\mathcal{P}}_k = -\frac{\partial \mathcal{F}_k}{\partial s_k}, \quad (2.88a)$$

where we have introduced a probability space flux \mathcal{F}_k defined as

$$\mathcal{F}_k = - \left(s_k \gamma_k \mathcal{P}_k + s_k \eta_k \frac{\partial \mathcal{P}_k}{\partial s_k} \right). \quad (2.88b)$$

If the PDF reaches thermodynamic equilibrium, then the probability space flux \mathcal{F}_k will vanish. In this situation, the PDF can be calculated from (2.88). This homogeneous solution, we denote \mathcal{P}_{hom} , corresponds to the thermodynamic equilibrium distribution of

$$\mathcal{P}_k = \mathcal{P}_{\text{hom}} = \frac{1}{n_k} e^{-\frac{s_k}{n_k}}, \quad (2.89)$$

where n_k corresponds to any stationary state of the KE satisfying (2.87). Solution \mathcal{P}_{hom} , is the Rayleigh distribution. A solution to Equation (2.88) was obtained for a

¹²For clarity, we will omit the superscript.

constant non-zero flux, $\mathcal{F}_k = \mathcal{F} \neq 0$ [3], of the form

$$\mathcal{P}_k = \mathcal{P}_{\text{hom}} + \mathcal{P}_{\text{part}}, \quad (2.90a)$$

where $\mathcal{P}_{\text{part}}$ is a particular solution to Equation (2.88), given by

$$\mathcal{P}_{\text{part}} = -\frac{\mathcal{F}}{\eta_k} Ei\left(\frac{s_k}{n_k}\right) e^{-\frac{s_k}{n_k}}, \quad (2.90b)$$

where function $Ei(x)$ is the exponential integral function

$$Ei(x) = \int_{-\infty}^x \frac{e^t}{t} dt. \quad (2.91)$$

The particular solution is a correction due to the presence of a non-zero flux. In the region of the PDF tail, where $n_k \ll s_k$, we can expand $\mathcal{P}_{\text{part}}$ in powers of n_k/s_k :

$$\mathcal{P}_{\text{part}} = -\frac{\mathcal{F}}{s_k \gamma_k} - \frac{\eta_k \mathcal{F}}{(s_k \gamma_k)^2} - \dots. \quad (2.92)$$

Thus, at leading order, the PDF tail has algebraic decay $\sim \mathcal{O}(1/s_k)$. This behaviour corresponds to the presence of strong intermittency of WT [3]. However, it was also noted in [3], that if the weak nonlinearity assumption was valid, uniformly on the whole of s_k -space, up to $s_k = \infty$, then the probability flux, \mathcal{F}_k , is forced to equal zero, to ensure positivity of \mathcal{P}_k and convergence of its normalisation:

$$\int_0^\infty \mathcal{P}_k ds_k = 1. \quad (2.93)$$

Hence, for a finite flux solution to exist, there must be a cut-off in s_k -space, for which the PDF vanishes. This can be viewed as a wave breaking process, which does not allow wave amplitudes to exceed a critical value [3]. The wave breaking process is essential for the presence of WT intermittency. The sign of the flux \mathcal{F} , determines whether the tail of the amplitude PDF is greater or less than the Rayleigh distribution. From Equation (2.92), we observe that a negative \mathcal{F} implies an increase in the probability of high intensity events. Subsequently, a positive flux, \mathcal{F} , would imply that we are less

likely to observe high intensity structures than what is predicted by a Gaussian wave field. In wave turbulent systems, we expect to observe signs of WT intermittency, as it is a result of a WT cascade being inhibited by the breakdown of the WT description through a wave breaking process.

2.13 The Kinetic Equation

The KE is one of the key objects in WT theory, it describes the evolution of the wave action density, which corresponds to distribution of wave action within \mathbf{k} -space. The evolution of $n_{\mathbf{k}}$ is given by the evolution equation of the first moment (2.86), and written in its full form, using the definitions for $\eta_{\mathbf{k}}$, (2.82a), and $\gamma_{\mathbf{k}}$, (2.82b), it is expressed as

$$\begin{aligned} \dot{n}_{\mathbf{k}} = & \frac{\epsilon^8 \pi}{6} \int |\mathcal{W}_{4,5,6}^{\mathbf{k},2,3}|^2 \delta_{4,5,6}^{\mathbf{k},2,3} \delta(\omega_{4,5,6}^{k,2,3}) n_{\mathbf{k}} n_2 n_3 n_4 n_5 n_6 \\ & \times (n_{\mathbf{k}}^{-1} + n_2^{-1} + n_3^{-1} - n_4^{-1} - n_5^{-1} - n_6^{-1}) d\mathbf{k}_2 d\mathbf{k}_3 d\mathbf{k}_4 d\mathbf{k}_5 d\mathbf{k}_6. \end{aligned} \quad (2.94)$$

The integral on the right hand side of the KE, (2.94), is known as the *collision integral*. Stationary solutions of the KE are solutions that make the collision integral zero. These stationary solutions of the KE satisfy Relation (2.87).

As previously mentioned in Chapter 1, there exist two types of solutions to the KE. The first type are referred to as the thermodynamic equilibrium solutions. These describe the profile of the wave action density, $n_{\mathbf{k}}$, when the system relaxes to its thermodynamic equilibrium. The thermodynamic solutions correspond to an equilibrated system and thus correspond to an absence of flux for the conserved quantities, (in our case, energy, \mathcal{H} , and total wave action, \mathcal{N}). The second type are known as the KZ solutions. They correspond to non-equilibrium stationary states determined by the transfer of constant non-zero flux. They arise when the system is in the presence of forcing and dissipation, where there exists some intermediate range of scales, known as the *inertial range*, where neither forcing nor dissipation influences the transfer of the cascading invariant. The discovery of the KZ solutions for the KE has been one of the major achievements of WT theory, and as such these solutions have received a large amount of attention within the community. In systems that possess more than

one invariant, the KZ solutions describe the transfer of invariants to distinct regions of \mathbf{k} -space [6]. For many systems, these regions are usually the low and high wave number areas of \mathbf{k} -space, however this is not necessarily the case [94]. The directions in which the invariants cascade can be discovered by following a Fjørtoft argument.

2.14 The Fjørtoft Argument

As we are considering a WT system with two invariants, there are two KZ solutions of the KE, each defined by the transfer with constant flux of either invariant. This is analogous to two-dimensional (2D) turbulence, where the enstrophy, (the sum of the square of vorticity), cascades towards small scales and energy towards large scales [101, 102]. Weak nonlinearity of the system implies that in a non-equilibrium statistical steady state, where the total energy \mathcal{H} is conserved, we can approximate the total energy conservation with the conservation of the linear energy ($\mathcal{H} \approx \mathcal{H}_2$). Consequently, it allows for the formation of a Fjørtoft argument [103]. This argument was originally derived in the context of 2D turbulence, and does not require any assumptions on the locality of wave interactions. Firstly, let us define the (linear) energy flux $P(\mathbf{k}, t) = P_{\mathbf{k}}$ and wave action flux $Q(\mathbf{k}, t) = Q_{\mathbf{k}}$:

$$\frac{\partial \epsilon_{\mathbf{k}}}{\partial t} = -\frac{\partial P_{\mathbf{k}}}{\partial \mathbf{k}}, \quad (2.95a)$$

$$\frac{\partial n_{\mathbf{k}}}{\partial t} = -\frac{\partial Q_{\mathbf{k}}}{\partial \mathbf{k}}, \quad (2.95b)$$

where the energy density in Fourier space is defined as $\epsilon_{\mathbf{k}} = \omega_k n_{\mathbf{k}}$, such that $\mathcal{H}_2 = \int \epsilon_{\mathbf{k}} d\mathbf{k}$. Below, we will outline the Fjørtoft argument in the context of our six-wave system.

We should assume that the system has reached a steady state, therefore the total amount of energy flux, $P_{\mathbf{k}}$, and wave action flux, $Q_{\mathbf{k}}$, contained within the system must be zero, i.e. $\int P_{\mathbf{k}} d\mathbf{k} = 0$, and $\int Q_{\mathbf{k}} d\mathbf{k} = 0$ respectively - this corresponds to the input of flux into the system equalling the output. Then, let the system be forced by a narrowband forcing at a specific intermediate scale, say \mathbf{k}_f , with both energy and wave

action fluxes being generated into the system at rates P_f and Q_f . Moreover, let there exist two sinks, one towards small scales, say at $k_+ \gg k_f$, with energy and wave action being dissipated at rates P_+ and Q_+ , and one at the large scales, say at $k_- \ll k_f$, dissipated at rates P_- and Q_- ¹³. Therefore, in between the forcing and dissipation, there exist two distinct inertial ranges where neither forcing nor dissipation takes effect. In the weakly nonlinear regime, the energy flux is related to the wave action flux by $P_k \approx \omega_k Q_k \approx k^2 Q_k$. In a steady state system, the energy and wave action balance implies that

$$P_f = P_- + P_+, \quad (2.96a)$$

$$Q_f = Q_- + Q_+. \quad (2.96b)$$

Therefore, approximately we have

$$P_f \approx k_f^2 Q_f, \quad (2.97a)$$

$$P_- \approx k_-^2 Q_-, \quad (2.97b)$$

$$P_+ \approx k_+^2 Q_+. \quad (2.97c)$$

Subsequently, the balance Equations (2.96) imply

$$k_f^2 Q_f \approx k_-^2 Q_- + k_+^2 Q_+, \quad (2.98a)$$

$$Q_f = Q_- + Q_+. \quad (2.98b)$$

Re-arranging Equations (2.98) enables us to predict at what rates the energy and wave action fluxes are dissipated at the two sinks. From Equations (2.98) we obtain

$$Q_+ \approx \frac{k_f^2 - k_-^2}{k_+^2 - k_-^2} Q_f, \quad (2.99a)$$

$$Q_- \approx \frac{k_f^2 - k_+^2}{k_-^2 - k_+^2} Q_f. \quad (2.99b)$$

¹³The dissipation mechanism could be natural in the system, i.e. friction with the box or fluid viscosity. However, (especially in numerical simulations) this could be artificial, i.e. hypo- and hyper-viscosities or large scale friction to enforce a statistical non-equilibrium stationary state.

If we consider the region around large scales, $k_- \ll k_f < k_+$, then Equation (2.99a) implies

$$k_f^2 Q_f \approx k_+^2 Q_+, \quad (2.100)$$

i.e. that energy is mostly absorbed at the region around k_+ . Furthermore, considering the region around small scales, $k_- < k_f \ll k_+$, (2.99b) implies that

$$Q_f \approx Q_-, \quad (2.101)$$

i.e. that wave action is mostly absorbed at regions around k_- . If we force the system at an intermediate scale, where there exists two inertial ranges either side of k_f , we should have the majority of the energy flowing towards small scales and the majority of the wave action flowing towards large scales. This determines the dual cascade picture of the six-wave system, illustrated in Figure 2.3.

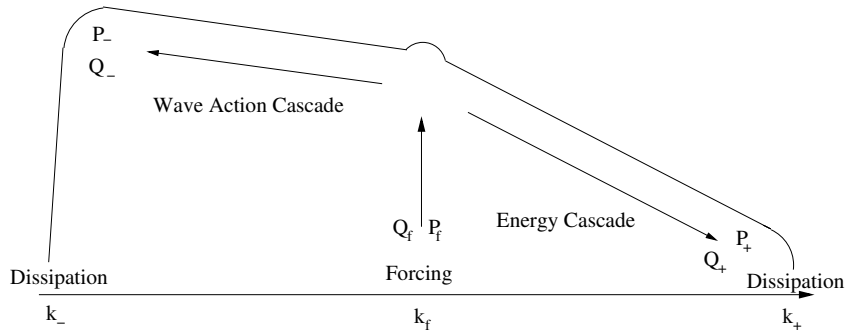


Figure 2.3: A Graphic to show the development of the the dual cascade regime.

2.15 The Zakharov Transform

To formally derive the thermodynamic and KZ solutions of the KE we will use the Zakharov transform (ZT). However this requires that the interaction coefficients of the system are *scale invariant*. Scale invariance of an interaction coefficient is a self-similar property of the structure when the length scales are multiplied by a common factor. i.e for any real number λ , we say that an interaction coefficient is scale invariant with a

homogeneity coefficient, $\beta \in \mathbb{R}$, if

$$\mathcal{W}(\lambda\mathbf{k}_1, \lambda\mathbf{k}_2, \lambda\mathbf{k}_3, \lambda\mathbf{k}_4, \lambda\mathbf{k}_5, \lambda\mathbf{k}_6) = \lambda^\beta \mathcal{W}(\mathbf{k}_1, \mathbf{k}_2, \mathbf{k}_3, \mathbf{k}_4, \mathbf{k}_5, \mathbf{k}_6). \quad (2.102)$$

For example, in 1D OWT, $\mathcal{W}_{4,5,6}^{1,2,3} = \text{const.}$ then trivially $\beta = 0$. If the six-wave interaction coefficient was a product of six wave numbers (i.e. the TLIA model for Kelvin waves in QT), i.e. $\mathcal{W}_{4,5,6}^{1,2,3} = \mathbf{k}_1\mathbf{k}_2\mathbf{k}_3\mathbf{k}_4\mathbf{k}_5\mathbf{k}_6$, then $\beta = 6$. Moreover, the frequency $\omega(\mathbf{k})$ must also possess the scale invariant property, i.e.

$$\omega(\lambda\mathbf{k}) = \lambda^\alpha \omega(\mathbf{k}), \quad (2.103)$$

with some $\alpha \in \mathbb{R}$. In this thesis, we are only considering systems that possess dispersion relations of the form of Relation (2.28), therefore α will always be $\alpha = 2$. In addition, we seek solutions of the KE with power-law form, with respect to wave number \mathbf{k} , i.e.

$$n_{\mathbf{k}} = Ck^{-x}, \quad (2.104)$$

where C is the constant prefactor of the spectrum, usually determined by the dimensional quantities within the system, and x is the exponent of the spectrum.

An informal way of determining exponent x of the KZ and thermodynamic solutions is to apply a dimensional analysis argument. For the thermodynamic equilibrium solutions, we assume a zero flux, i.e. that both $\epsilon_{\mathbf{k}}$ and $n_{\mathbf{k}}$ are scale independent. Conversely, for the derivation of the KZ solutions, we want to consider a wave action density scaling that implies a constant flux of the cascading invariant. This is achieved by considering $P_{\mathbf{k}}, Q_{\mathbf{k}} \propto k^0$ in Equations

$$P_{\mathbf{k}} = \int^{\mathbf{k}} \frac{\partial \epsilon_{\mathbf{k}'} }{\partial t} d\mathbf{k}', \quad (2.105a)$$

$$Q_{\mathbf{k}} = \int^{\mathbf{k}} \frac{\partial n_{\mathbf{k}'} }{\partial t} d\mathbf{k}', \quad (2.105b)$$

derived from Equations (2.95), using (2.104) and the KE, (2.94). However, this method is not mathematically precise and does not allow for the evaluation of the prefactor in

(2.104). Therefore, we will now describe the formal way of calculating such solutions by using the ZT. The ZT expresses the KE in such a way that it overlaps sub-regions of the KE's domain, thus at each solution, the integrand of the collision integral is set to zero over the whole domain [6]. The ZT takes advantage of the symmetries possessed within the KE by a change of variables. In our case, this results in dividing the domain of the KE into six sub-regions.

Applicability of the ZT requires locality of wave interactions. This means that wave interactions are local in \mathbf{k} -space, i.e. only waves with a similar order of wave number can interact. The criterion of locality is equivalent to the convergence of the collision integral [6]. Locality of these solutions will be checked in the following section.

The ZT is a change of variables on certain sub-regions of the domain, one such sub-region is transformed by¹⁴

$$\mathbf{k}_2 = \frac{\mathbf{k}^2}{\tilde{\mathbf{k}}_2}, \quad \mathbf{k}_3 = \frac{\mathbf{k}\tilde{\mathbf{k}}_3}{\tilde{\mathbf{k}}_2}, \quad \mathbf{k}_4 = \frac{\mathbf{k}\tilde{\mathbf{k}}_4}{\tilde{\mathbf{k}}_2}, \quad \mathbf{k}_5 = \frac{\mathbf{k}\tilde{\mathbf{k}}_5}{\tilde{\mathbf{k}}_2} \quad \text{and} \quad \mathbf{k}_6 = \frac{\mathbf{k}\tilde{\mathbf{k}}_6}{\tilde{\mathbf{k}}_2}, \quad (2.106)$$

with the Jacobian of the transformation $J = -(\mathbf{k}/\tilde{\mathbf{k}}_2)^6$. We must apply four similar transformations, to each of the remaining sub-regions, (see Appendix B).

Using the scale invariant properties of the interaction coefficients and frequency, and the fact that a Dirac delta function scales as

$$\delta((\lambda\mathbf{k})^\alpha) = \lambda^{-\alpha}\delta(\mathbf{k}^\alpha), \quad (2.107)$$

the ZT implies that the KE can be expressed as

$$\begin{aligned} \dot{n}_{\mathbf{k}} &= \frac{C^5 \epsilon^8 \pi}{6} \int |\mathcal{W}_{4,5,6}^{\mathbf{k},2,3}|^2 |\mathbf{k}\mathbf{k}_2\mathbf{k}_3\mathbf{k}_4\mathbf{k}_5\mathbf{k}_6|^{-x} (k^x + k_2^x + k_3^x - k_4^x - k_5^x - k_6^x) \\ &\times \left[1 + \left(\frac{k_2}{k} \right)^y + \left(\frac{k_3}{k} \right)^y - \left(\frac{k_4}{k} \right)^y - \left(\frac{k_5}{k} \right)^y - \left(\frac{k_6}{k} \right)^y \right] \\ &\times \delta_{4,5,6}^{\mathbf{k},2,3} \delta(\omega_{4,5,6}^{k,2,3}) d\mathbf{k}_2 d\mathbf{k}_3 d\mathbf{k}_4 d\mathbf{k}_5 d\mathbf{k}_6, \end{aligned} \quad (2.108)$$

where we have omitted the tildes and $y = 5x - 3 - 2\beta$. We see that if $x = 0$ or $x = 2$, the

¹⁴The ZT is only defined for scalars. Our notation is that \mathbf{k} is a 1D variable $\in \mathbb{R}$ and not a multi-dimensional vector. In this case, one would need to apply the ZT to k and not \mathbf{k} .

integrand will be zero as we either have zero by cancellation of the third term within the integral or via the Dirac delta function involving frequencies. In particular, when $x = 0$ or $x = 2$, the solutions will correspond to thermodynamic equilibria of the equipartition of the wave action and the energy respectively:

$$n_{\mathbf{k}}^T = C_{\mathcal{N}}^T k^0, \quad (2.109a)$$

$$n_{\mathbf{k}}^T = C_{\mathcal{H}}^T k^{-2}. \quad (2.109b)$$

Solutions (2.109) correspond to zero flux states - in fact both energy and wave action fluxes, $P_{\mathbf{k}}$ and $Q_{\mathbf{k}}$, are identically equal to zero on both equilibrium solutions. Spectra (2.109) are two limiting cases in low and high wave number regions of the more general thermodynamic equilibrium Rayleigh-Jeans solution, $n_{\mathbf{k}}^{RJ}$, where

$$n_{\mathbf{k}}^{RJ} = \frac{T_c}{\omega_k + \mu}. \quad (2.110)$$

T_c is the characteristic temperature of the system, and μ is a chemical potential.

In addition to these thermodynamic solutions, our system possesses two non-equilibrium KZ solutions. The KZ solutions are obtained from Equation (2.108) when either $y = 0$ or $y = 2$. When either condition is met, the integrand in Equation (2.108) vanishes due to cancellation in the square bracket. The corresponding solution for the direct energy cascade from low to high wave numbers is obtained when $y = 2$, this gives the following wave action spectrum scaling:

$$n_{\mathbf{k}}^{\mathcal{H}} = C_{\mathcal{H}} k^{-\frac{5+2\beta}{5}}. \quad (2.111a)$$

The wave action spectrum (2.111a) implies that the energy flux $P_{\mathbf{k}}$ is \mathbf{k} -independent and non-zero. The solution for the inverse wave action cascade from high to low wave numbers is obtained when one sets $y = 0$, and is of the form

$$n_{\mathbf{k}}^{\mathcal{N}} = C_{\mathcal{N}} k^{-\frac{3+2\beta}{5}}. \quad (2.111b)$$

On each KZ solution, the respective flux is a non-zero constant - reflecting the Kolmogorov scenario, whilst the flux of the second invariant is absent. However, we emphasise that the KZ solutions are only valid if they correspond to local wave interactions - an assumption in the ZT.

2.16 Locality of the Kolmogorov-Zakharov Solutions

The KZ solutions can only be realised if they correspond to local, in \mathbf{k} -space, wave interactions. This entails checking that the collision integral converges, when the wave action density is of KZ type, (2.111). The locality of the KZ solutions have been proven, disproven, and even logarithmically corrected if the non-locality is marginal in several WT systems. For example, local (and logarithmically corrected) KZ solutions have been proven in three-dimensional (3D) OWT and BEC [65], gravity waves [6], and capillary waves [6, 83], whilst non-local KZ solutions have been found for Rossby/drift waves [95] and for Kelvin waves in QT [9].

Our strategy for determining the locality of the KZ solutions, (2.111), is to check the convergence of the collision integral when one wave number vanishes, or when one wave number diverges to $\pm\infty$. These limits correspond to the infrared (IR) and ultraviolet (UV) regions of \mathbf{k} -space. Although the collision integral is five-dimensional (5D), the two Dirac delta functions, relating to the six-wave resonance condition, imply that integration is over a 3D surface within the 5D domain. For linear frequencies of the form, $\omega_k = Ck^2$, we can parameterise the six-wave resonance condition, (2.34), which subsequently allows us to neglect integrations in (2.94). We define our parameterisation by making two wave numbers, functions of the remaining four. Therefore, to satisfy the six-wave resonant condition, we set:

$$\mathbf{k}_2 = \frac{(\mathbf{k}_4 - \mathbf{k})(\mathbf{k}_3 - \mathbf{k}_4)}{\mathbf{k} + \mathbf{k}_3 - \mathbf{k}_4 - \mathbf{k}_6} + \mathbf{k}_6, \quad (2.112a)$$

$$\mathbf{k}_5 = \frac{(\mathbf{k}_4 - \mathbf{k})(\mathbf{k}_3 - \mathbf{k}_4)}{\mathbf{k} + \mathbf{k}_3 - \mathbf{k}_4 - \mathbf{k}_6} + \mathbf{k} + \mathbf{k}_3 - \mathbf{k}_4. \quad (2.112b)$$

2.16.1 Convergence in the Infrared Region

To check for convergence in the IR region, we must determine the scaling of the KE as one wave number, say $\mathbf{k}_6 \rightarrow 0$. Therefore, our strategy involves finding the IR scaling of each contribution in the KE. As we are still considering a general six-wave system, let us assume that the six-wave interaction coefficient has the following scaling as $k_6 \rightarrow 0$:

$$\lim_{k_6 \rightarrow 0} \mathcal{W}_{4,5,6}^{\mathbf{k},1,2} \propto k_6^\xi, \quad (2.113)$$

where $\xi \in \mathbb{R}$. Then in the same limit, the following term in the KE, behaves as

$$\begin{aligned} & \lim_{\mathbf{k}_6 \rightarrow 0} n_{\mathbf{k}} n_2 n_3 n_4 n_5 n_6 (n_{\mathbf{k}}^{-1} + n_2^{-1} + n_3^{-1} - n_4^{-1} - n_5^{-1} - n_6^{-1}) \\ & \propto n_{\mathbf{k}} n_2 n_3 n_4 n_5 n_6 (n_{\mathbf{k}}^{-1} + n_2^{-1} + n_3^{-1} - n_4^{-1} - n_5^{-1}) \propto n_6 \propto k_6^{-x}, \end{aligned} \quad (2.114)$$

where x is the spectrum exponent from (2.104). Thus, we can factor out the integral over \mathbf{k}_6 in the KE and write it as

$$\int k_6^{2\xi} n_6 d\mathbf{k}_6 \propto 2 \int_0 k_6^{2\xi-x} dk_6. \quad (2.115)$$

Therefore, convergence of the KE in the IR limit corresponds to convergence of integral (2.115) as $\mathbf{k}_6 \rightarrow 0$. Hence, convergence of the collision integral is satisfied when

$$x < 1 + 2\xi. \quad (2.116)$$

Note that all other integrals over \mathbf{k}_2 , \mathbf{k}_3 , \mathbf{k}_4 , \mathbf{k}_5 diverge in exactly the same manner as the integral over \mathbf{k}_6 . Moreover, we can check for IR divergence if two wave numbers are simultaneously small. When two wave numbers on the same side of the six-wave resonance sextet are small, i.e. \mathbf{k}_2 and \mathbf{k}_3 or \mathbf{k}_4 and \mathbf{k}_6 , then we see an integral proportional to the square of (2.115).

If the two wave numbers are on opposite sides of the sextet, then we get con-

vergence because of an additional vanishing contribution arising from:

$$\lim_{\mathbf{k}_2, \mathbf{k}_6 \rightarrow 0} (n_{\mathbf{k}}^{-1} + n_2^{-1} + n_3^{-1} - n_4^{-1} - n_5^{-1} - n_6^{-1}) \rightarrow 0. \quad (2.117)$$

Full convergence and thus locality of the KZ solutions (2.111) is only assured if we have convergence in both IR and UV limits. Therefore, if we have IR convergence, we must also check UV convergence.

2.16.2 Convergence in the Ultraviolet Region

To check UV convergence, we will consider the scaling of the collision integral as one wave number diverges. The conservation of momentum, implied by the Dirac delta function of wave numbers, means that if one wave number diverges, so must a second from the opposite side of the sextet¹⁵. This can be verified by parameterisation (2.112), where if we force \mathbf{k}_6 to diverge, then so must \mathbf{k}_2 . Indeed, due to this second divergence, we must integrate the second wave number and further check the scaling of the resulting Jacobian.

To begin, in the limit of one large wave number, let us assume that the six-wave interaction coefficient scales as

$$\lim_{\mathbf{k}_6 \rightarrow \infty} \mathcal{W}_{4,5,6}^{\mathbf{k},2,3} \propto k_6^\eta, \quad (2.118)$$

where $\eta \in \mathbb{R}$. Due to the integration of an additional wave number diverging to infinity (in this case \mathbf{k}_2), we must check the scaling of the resulting Jacobian, corresponding to the transformation between \mathbf{k}_6 and \mathbf{k}_2 . The Jacobian for \mathbf{k}_2 can be written as

$$\left| \frac{\partial \omega_{4,5,6}^{k,2,3}}{\partial \mathbf{k}_2} \right|^{-1} = \frac{1}{2|\mathbf{k} + \mathbf{k}_3 - \mathbf{k}_4 - \mathbf{k}_6|}, \quad (2.119)$$

where we have used the fact that $\mathbf{k}_5 = \mathbf{k} + \mathbf{k}_2 + \mathbf{k}_3 - \mathbf{k}_4 - \mathbf{k}_6$. Hence, the Jacobian produces a contribution to the KE $\propto k_6^{-1}$, and the following expression in the KE scales

¹⁵Divergence of two wave numbers on the same side of the sextet would violate the Dirac delta function involving frequencies.

as

$$\lim_{\mathbf{k}_6 \rightarrow \infty} \left(n_{\mathbf{k}}^{-1} + n_2^{-1} + n_3^{-1} - n_4^{-1} - n_5^{-1} - n_6^{-1} \right) n_{\mathbf{k}} n_2 n_3 n_4 n_5 n_6 \propto k_6^{-1-2x} (k_6^0 + k_6^{-2}). \quad (2.120)$$

The first term on the right-hand side is a contribution from the Jacobian and the product of $n_{\mathbf{k}}$ s. The second term stems from the difference of $n_{\mathbf{k}}$ s giving rise to two contributions. The k_6^0 scaling results from the difference of the four non-divergent $n_{\mathbf{k}}$ s, while the k_6^{-2} factor comes from the leading order Taylor expansion of the two divergent $n_{\mathbf{k}}$ s. This implies that the condition for UV convergence of the KE is

$$\max(2\eta - 2x - 2, 2\eta - 2x) < 0. \quad (2.121)$$

2.17 Linear and Nonlinear Transfer Times and The Critical Balance Regime

In this Section, we estimate the nonlinear transfer times of the KZ cascades and discuss the CB phenomenon of strong WT. The separation of timescales is essential for the construction of the WT closure (see Section 2.6). The linear timescale was previously defined in Equation (2.40). It was noted in Equation (2.42) that the nonlinear timescale, T_{NL} , is $\sim \mathcal{O}(1/\epsilon^8)$. This was an *a posteriori* estimate, that will be verified shortly. From the KE, we can define T_{NL} as

$$T_{NL} = \frac{n_{\mathbf{k}}}{\frac{\partial n_{\mathbf{k}}}{\partial t}}. \quad (2.122)$$

WT theory is applicable when there is a large separation between the linear and nonlinear timescales:

$$\frac{T_L}{T_{NL}} \ll 1. \quad (2.123)$$

The rates at which wave amplitudes evolve are wave number dependent, thus Relation (2.123) can vary significantly in different regions of \mathbf{k} -space. Therefore, it is natural to consider the k -dependence of (2.123).

Estimation of the k -dependence of the nonlinear transfer time will provide in-

formation on whether the KZ cascade is of self-accelerating or self-decelerating type, i.e. the rate of the nonlinear evolution of a self-accelerating cascade will increase as the cascade develops. The estimation of T_{NL} , with respect to k , can be achieved using the KE, (2.94), giving

$$T_{NL} \propto k^{4x-2\beta-2}. \quad (2.124)$$

Therefore, the ratio, (2.123), between the two timescales imply that

$$\frac{T_L}{T_{NL}} \propto k^{-4x+2\beta} \ll 1. \quad (2.125)$$

Relation (2.125) can be violated when either $k \rightarrow 0$ or $k \rightarrow \infty$, depending on the sign of $-4x + 2\beta$. When $T_L/T_{NL} \sim 1$, then the KE approach breaks down and we are in a regime called CB. When a system is in a CB regime, the turbulence is no longer characterised by constant fluxes, but by fluctuations and non-Gaussian statistics.

CB arises when the system possesses characteristics of strong WT, i.e the formation of non-universal features, such as condensates, solitons, vortices, collapses, shocks, etc. CB is characterised when the nonlinear evolution time, T_{NL} , is of the same order as the linear wave period, T_L , over a large range of scales. A CB scaling for the wave action density, n_k , can be made by equating T_{NL} with T_L , on a scale by scale basis, i.e.

$$\frac{T_L}{T_{NL}} \propto k^{-4x+2\beta} \sim 1, \quad (2.126)$$

implying a CB spectrum of

$$n_k^{CB} = C_{CB} k^{-\frac{\beta}{2}}, \quad (2.127)$$

where C_{CB} is a constant prefactor of the spectrum.

CB was first introduced in the context of magneto-hydrodynamics [51]. However, CB has arisen in several other applications, including gravity water waves [104], stratified turbulence [105, 106], rotating turbulence [107, 108], quasi-geostrophic turbulence [109, 110], and for Kelvin waves on quantised vortices [111].

2.18 The Differential Approximation for the Kinetic Equation

The DAM is an approximation of the KE by assuming strongly local wave interactions. This enables the construction of a partial differential equation for the evolution of the wave action density, $n_{\mathbf{k}}$. We stress that the DAM is an approximation and thus can only be used when the KZ solutions are proved local. The DAM contains both the thermodynamic and non-equilibrium KZ solutions of the KE, and can be further simplified to *reduced* DAMs, which only consider a subset of these solutions. Usefulness of the DAM can be shown with derivation of exact analytical solutions, expressions for the fluxes and finally by its computational simplicity. The DAM can also be adapted to classical turbulence theory, where it is known as the Leith model [112, 113, 114]. This has led to the DAM being used extensively in WT and classical turbulence [115, 116, 117, 118, 119, 59, 120, 7].

It is convenient for the DAM to be derived in ω -space, by angle averaging over wave vectors. Hence, the DAM will be independent from the dimension of the wave vector \mathbf{k} , allowing for a universal description. The wave action density in ω -space is defined as

$$N_{\omega} = n_{\omega} \frac{d\mathbf{k}}{d\omega_k}, \quad (2.128)$$

so that

$$\int N_{\omega} d\omega = \int n_{\mathbf{k}} d\mathbf{k}, \quad (2.129)$$

and thus the KE, (2.94) ,can be expressed as

$$\begin{aligned} \frac{\partial N_{\omega}}{\partial t} &= \int S_{4,5,6}^{\omega,2,3} n_{\omega} n_2 n_3 n_4 n_5 n_6 \left(\frac{1}{n_{\omega}} + \frac{1}{n_2} + \frac{1}{n_3} - \frac{1}{n_4} - \frac{1}{n_5} - \frac{1}{n_6} \right) \\ &\quad \times d\omega_2 d\omega_3 d\omega_4 d\omega_5 d\omega_6, \end{aligned} \quad (2.130)$$

where we have defined a new interaction coefficient given by

$$S_{4,5,6}^{\omega,2,3} = S(\omega_k, \omega_2, \omega_3, \omega_4, \omega_5, \omega_6) = \left\langle \frac{\epsilon^8 \pi}{6} |\mathcal{W}_{4,5,6}^{\mathbf{k},2,3}|^2 \delta_{4,5,6}^{\mathbf{k},2,3} \right\rangle \frac{d\mathbf{k}}{d\omega_k} \frac{d\mathbf{k}_2}{d\omega_2} \frac{d\mathbf{k}_3}{d\omega_3} \frac{d\mathbf{k}_4}{d\omega_4} \frac{d\mathbf{k}_5}{d\omega_5} \frac{d\mathbf{k}_6}{d\omega_6}. \quad (2.131)$$

$S_{4,5,6}^{\omega,2,3}$ has the same symmetry properties as $\mathcal{W}_{4,5,6}^{k,2,3}$, (see (2.26b)). Multiplication of (2.130) by some arbitrary smooth function $f(\omega) = f_\omega$, and then integration with respect to $d\omega$, with the use of the symmetry of the interaction coefficient $S_{4,5,6}^{\omega,2,3}$, gives

$$\begin{aligned} \int \dot{n}_\omega f(\omega) \omega^{-1/2} d\omega &= \frac{1}{6} \int S_{4,5,6}^{\omega,2,3} n_\omega n_2 n_3 n_4 n_5 n_6 \\ &\quad \times \left(\frac{1}{n_\omega} + \frac{1}{n_2} + \frac{1}{n_3} - \frac{1}{n_4} - \frac{1}{n_5} - \frac{1}{n_6} \right) \\ &\quad \times (f_\omega + f_2 + f_3 - f_4 - f_5 - f_6) d\omega_2 d\omega_3 d\omega_4 d\omega_5 d\omega_6, \end{aligned} \quad (2.132)$$

where $f_i = f(\omega_i)$, with $i = k, 2, 3, 4, 5, 6$. Strong locality of wave interactions imply that each ω_i with $i = 2, 3, 4, 5, 6$ can be approximated to ω_k by a small deviation, p_i , such that each frequency can be represented as $\omega_i = \omega_k(1 + p_i)$ for $i = 2, 3, 4, 5, 6$. This permits the Taylor expansion of the two brackets involving n_ω^{-1} s and f s to $\mathcal{O}(p^3)$. Furthermore, by approximating $n_\omega n_2 n_3 n_4 n_5 n_6$ by n_ω^6 and using scale invariance of $S_{4,5,6}^{\omega,2,3}$, we gain the following equation:

$$\int \dot{n}_\omega f(\omega) \omega^{-1/2} d\omega = S_0 \int \omega^{(9+2\beta)/2} n_\omega^6 \frac{\partial^2}{\partial \omega^2} \left(\frac{1}{n_\omega} \right) \frac{\partial^2 f}{\partial \omega^2} d\omega, \quad (2.133)$$

where

$$\begin{aligned} S_0 &= \frac{1}{24} \int S(1, 1 + p_2, 1 + p_3, 1 + p_4, 1 + p_5, 1 + p_6) \\ &\quad \times (p_2^2 + p_3^2 - p_4^2 - p_5^2 p_6^2)^2 \delta_{p_4, p_5, p_6}^{p_2, p_3} dp_2 dp_3 dp_4 dp_5 dp_6. \end{aligned} \quad (2.134)$$

From Integration by parts, we get

$$\int \dot{n}_\omega f(\omega) \omega^{-1/2} d\omega = S_0 \int \left(\frac{\partial^2}{\partial \omega^2} \left[\omega^{(9+2\beta)/2} n_\omega^6 \frac{\partial^2}{\partial \omega^2} \left(\frac{1}{n_\omega} \right) \right] \right) f(\omega) d\omega. \quad (2.135)$$

As $f(\omega)$ is an arbitrary function, we can equate the two integrands, resulting in the DAM:

$$\dot{n}_\omega = S_0 \omega^{1/2} \frac{\partial^2}{\partial \omega^2} \left[\omega^{\frac{9+2\beta}{2}} n_\omega^6 \frac{\partial^2}{\partial \omega^2} \left(\frac{1}{n_\omega} \right) \right]. \quad (2.136)$$

The thermodynamic solution, $n_\omega = T_c/(\omega + \mu)$ is found when

$$R_\omega = S_0 \omega^{\frac{9+2\beta}{2}} n_\omega^6 \frac{\partial^2}{\partial \omega^2} \left(\frac{1}{n_\omega} \right), \quad (2.137)$$

is equal to zero. The energy and wave action fluxes, P_ω and Q_ω , can be derived from R_ω by the following formulae:

$$P_\omega = R_\omega - \omega \frac{\partial R_\omega}{\partial \omega}, \quad (2.138a)$$

$$Q_\omega = - \frac{\partial R_\omega}{\partial \omega}. \quad (2.138b)$$

Consequently, both P_ω and Q_ω vanish upon the thermodynamic solution. By assuming the same power law scaling as (2.104), $n_\omega = C\omega^{-x/2}$, we can calculate formulae for the behaviour of the DAM with respect to ω and the exponent x :

$$\dot{n}_\omega = S_0 C^5 \frac{x}{2} \left(\frac{x}{2} - 1 \right) y (y-1) \omega^{-y-\frac{1}{2}}, \quad (2.139a)$$

$$R(\omega, x, y) = S_0 C^5 \frac{x}{2} \left(\frac{x}{2} - 1 \right) \omega^{-y+1}, \quad (2.139b)$$

$$P(\omega, x, y) = S_0 C^5 \frac{x}{2} \left(\frac{x}{2} - 1 \right) y \omega^{-y+1}, \quad (2.139c)$$

$$Q(\omega, x, y) = S_0 C^5 \frac{x}{2} \left(\frac{x}{2} - 1 \right) (y-1) \omega^{-y}, \quad (2.139d)$$

where $y = \frac{5x}{2} - \beta - \frac{3}{2}$. Stationary solutions (thermodynamic and non-equilibrium) for the DAM are observed when $\dot{n}_\omega = 0$, i.e. when $x = 0$, $x = 2$, $y = 0$ or $y = 1$. These solutions are identical to the ones determined by the KE. Relations (2.139c) and (2.139d) enable for the calculation of the sign of the KZ fluxes. Furthermore, we observe that both fluxes vanish upon reaching the thermodynamic solutions, when $x = 0$ and $x = 2$, and that the non-cascading flux on the KZ solution is zero.

2.19 The Gallavotti-Cohen Fluctuation Relation

Further analysis to the statistical properties of the flux can be achieved by investigation of fluctuation relations [121, 122, 123, 124]. Fluctuation relations are symmetries between the positive and negative non-equilibrium fluctuations and provide some measure of

how ‘non-equilibrium’ a statistical system is. The Gallavotti-Cohen fluctuation relation (GCFR) is a statistical symmetry of the PDF for an averaged non-equilibrium quantity X_τ taken from a non-equilibrium system. X_τ is defined as the time average of a physical quantity, $x(t)$, over a time window, $[t, t + \tau]$, of length τ . The quantity, $x(t)$, is usually the entropy production or energy dissipation, where the GCFR has been strictly proven in chaotic and deterministic systems that are time reversible [122, 123]. Mathematically, X_τ is defined as

$$X_\tau = \frac{1}{\tau} \int_t^{t+\tau} x(t') dt'. \quad (2.140)$$

The averaged quantity X_τ is considered positive on average, but may fluctuate to the extent that negative values can be observed. The GCFR measures the ratio of the probability of observing a positive fluctuation of magnitude σ over the probability of a negative fluctuation of size $-\sigma$. This ratio is then considered to satisfy the GCFR if it is exponential in the limit of $\tau \rightarrow \infty$. Mathematically, the quantity X_τ is said to satisfy the GCFR if

$$\lim_{\tau \rightarrow \infty} \ln \left(\frac{P(X_\tau = \sigma)}{P(X_\tau = -\sigma)} \right) = C\tau\sigma, \quad (2.141)$$

where C is a constant, independent of the averaging interval, τ .

There have been recent activity in the search for fluctuation relations in turbulent (non-time reversible) systems [125, 124]. In [124], the authors performed turbulent, 2D and 3D, Navier-Stokes simulations and showed that the PDF of the local power, obeys Relation (2.141), and is well approximated by the product of two joint normal distributed variables. However, in [125], a WT experiment was performed for waves on the surface of water and mercury. The authors presented the left-hand side of Equation (2.141), but noted that the data disagreed with the linear GCFR behaviour, but coincided with the nonlinear prediction of a Langevin-type model. The authors stated that the linear behaviour, consistent with the GCFR, is due to insufficient values for the averaged injected power in previous experiments. However, we conjecture that the nonlinear behaviour is a sign of intermittency, coherent structures, or finite box effects.

In this thesis, we study fluctuations of the energy flux over time, i.e. we take $x(t) = P(k = k_*, t)$, where k_* is a given wave number. The flux statistics are likely

to be affected by the presence of intermittency, and so the observation of Relation (2.141) may be distorted. However, we consider the application of flux statistics as a numerical experiment to see if a GCFR is satisfied. We note that there is no theory on the statistical behaviour of the flux, but we consider this as a preliminary step towards developing such a theory.

We conclude our analysis of the general six-wave system. The remainder of this thesis will be dedicated to the applications of these results to QT and OWT.

Chapter 3

Kelvin Waves in Quantum Turbulence

3.1 Introduction to Quantum Turbulence

QT is turbulence in a pure superfluid, such as superfluid helium⁴. As is well known, classical turbulence is a widespread phenomena in fluid dynamics, which poses one of the major problems for fluid dynamicists at present. It is hoped that QT, with its unique properties will aid in the understanding of classical turbulence. A superfluid, for our purposes is made by supercooling helium⁴ atoms to below 2.17K, consists of a normal fluid, described by classical hydrodynamics, coupled with an inviscid quantum fluid. At temperatures below 1K, the normal fluid component (presumably) vanishes leaving a pure superfluid. Superfluids experience severe quantum restrictions, such as irrotational flow, quantised vortices, and inviscid behaviour. QT is usually characterised by a tangle of quantised vortex lines [57, 126]. Superfluidity is similar to the concept of BEC, where quantum effects dominate. However, helium⁴ atoms are strongly coupled, unlike the atoms of a dilute gas of weakly interacting bosons that constitutes a BEC. In BEC, pure superfluidity is seen at micro-Kelvin, with the quantised vortices being relatively large in comparison to the vortices observed in superfluid helium⁴. There are many theoretical aspects to QT, but this Chapter will focus on decaying QT in pure superfluid helium. In a pure superfluid state, the fluid is irrotational, and therefore, any

circulation in the system (imposed by rotating or mixing of the fluid) is represented in a multi-connected domain by extremely thin quantised vortex lines - quantised because of the discrete values of circulation that they must take. The vortex lines are defined by vanishing density in their centre, with a usual vortex core size of $a_0 \simeq 0.1 \text{ nm}$. When these quantised vortices reconnect, they excite Kelvin waves that propagate along the 1D vortex lines. These propagating waves, lend themselves to the application of WT theory.

A pure superfluid, unlike a classical fluid, has no dissipative effects. However, it is well understood that at large scales, or scales larger than the order of the mean inter-vortex distance ℓ , the flow is of *quasi-Kolmogorov* type, i.e. the large scale flow behaves similarly to a 3D classical fluid. This is because polarised bundles of quantum vortices behave similarly to large scale eddies in classical fluids. At scales smaller than ℓ , the energy contained in the flow gets transferred to Kelvin waves on the vortex lines. The goal of this Chapter is to understand how energy is transferred via Kelvin waves to frequencies sufficiently high enough, for the energy to be dispersed by phonons. Although, not discussed here, one of the main unanswered questions in the QT community, is the understanding of how energy at large scales in the flow is transferred to the 1D vortex lines. There have been two recently proposed theories for this scenario; the first considers that energy accumulates at the inter-vortex scale ℓ - forming a bottleneck [60], whereas the second, consists of a variety of vortex interaction and reconnection mechanisms around the scale ℓ , that efficiently transfers energy to Kelvin waves without the formation of a bottleneck [127]. However, there have been little direct experimental observation or numerical simulations that favour either scenario. Let us now consider the mathematical description of QT, specifically, the modelling of quantised vortices and Kelvin waves.

3.2 Kelvin Waves and Quantised Vortices

There are two main approaches to the study of superfluid vortices. The first is to use the Gross-Pitaevskii equation (GPE) that was developed for the modelling of weakly

interacting BECs, and is defined as

$$i\hbar \frac{\partial \Psi}{\partial t} + \frac{\hbar^2}{2m_4} \nabla^2 \Psi - V(\mathbf{x}, t)\Psi - g\Psi|\Psi|^2 = 0, \quad (3.1)$$

where $\Psi(\mathbf{x}, t)$ is the 3D wave function for the condensate, $V(\mathbf{x}, t)$ is the profile of a time-dependent magnetic trap, m_4 is the mass of a helium⁴ atom and g is the coupling constant. The GPE, (3.1), is the 3D NLSE with an external potential term. The GPE can be expressed in terms of a compressible 3D Euler equation with a quantum pressure term using the Madelung transformation [128]. The GPE contains fluidic properties and vortex structures, that unlike in the 3D Euler equations, can reconnect without the formation of a singularity. This has led to a large number of numerical simulations of the GPE [129, 130, 131, 132, 133, 64, 134]. However, the GPE is more rigorously justified for the modelling of weakly interacting Bose gases than superfluid helium. This has contributed to the development of the Schwarz equation [135, 136, 134] based on the BSE. The BSE approximates infinitesimally thin quantised vortices by 1D vortex lines and is derived directly from the 3D Euler equation [137]. The BSE is of the form

$$\dot{\mathbf{r}} = \frac{\kappa}{4\pi} \int \frac{d\mathbf{s} \times (\mathbf{r} - \mathbf{s})}{|\mathbf{r} - \mathbf{s}|^3}, \quad (3.2)$$

where $\dot{\mathbf{r}} = \partial \mathbf{r} / \partial t$ is the velocity at point \mathbf{r} on the vortex, and $\kappa = 2\pi\hbar/m_4$ is the quantum of circulation. The BSE, (3.2), contains a divergence as $\mathbf{s} \rightarrow \mathbf{r}$, and as a result we must introduce a strict cut-off at $|\mathbf{s} - \mathbf{r}| > a_0$, where a_0 is some value representing the vortex core of the quantised vortex. At distances less than a_0 , the approximation to a 1D vortex line is invalid and the quantum effects of the vortex core structure become apparent.

The dispersion relation for the frequency of Kelvin waves on a hollow core vortex line, was originally proposed by Lord Kelvin [138]:

$$\omega(\mathbf{k}) = \frac{\kappa k^2}{2\pi a_0^2} \left[1 \pm \left\{ 1 + ka_0 \left[\frac{K_0(ka_0)}{K_1(ka_0)} \right] \right\}^{1/2} \right], \quad (3.3)$$

where $K_n(\cdot)$ is a modified Bessel function of order n . Formula (3.3) is usually expanded

in the limit of long-wave Kelvin waves ($ka \ll 1$), which results in the form of the dispersion relation usually observed in the modern literature:

$$\omega(\mathbf{k}) = \frac{\kappa k^2}{4\pi} \left[\ln \left(\frac{1}{ka_0} \right) + C \right], \quad (3.4)$$

where C is an $\mathcal{O}(1)$ constant that is vortex core structure dependent. For instance, $C = -\gamma + \ln(2)$ for a hollow core [139], $C = -\gamma + \ln(2) + \frac{1}{4}$ for a vortex with uniform vorticity inside a cylinder of radius a_0 [135], and $C = -\gamma - \frac{3}{2}$ for the BSE with cut-off (Equation (3.6)) [7], where γ is the Euler constant. The ambiguity and small size of the vortex core structure has led to the core being given little importance. Therefore, the BSE with its cut-off is assumed to be an accurate model for quantised vortices in superfluid helium.

The applicability of Formula (3.4) is granted for long-wave Kelvin waves on vortex lines with very thin vortex cores, which is indeed the case in superfluid helium⁴. Moreover, we see from Formula (3.4) that the dispersion is not exactly of the form of (2.28). However, the logarithmic dependence in (3.4) is slowly varying with respect to wave number \mathbf{k} , and it can be considered to be approximately constant when compared to k^2 . In Section 3.5, we consider the effect of this logarithmic dependence by calculating an adjustment to the six-wave interaction coefficient $\mathcal{W}_{4,5,6}^{1,2,3}$ to compensate for our $\omega(\mathbf{k}) \propto k^2$ approximation to Formula (3.4).

3.3 The Local Induction Approximation and Biot-Savart Hamiltonians

It was shown, that under a simple geometrical constraint, we can introduce a complex canonical coordinate $w(z, t) = x(z, t) + iy(z, t)$, which enables the BSE to be written in a Hamiltonian form of

$$i\kappa \frac{\partial w(z, t)}{\partial t} = \frac{\delta \mathcal{H}}{\delta w^*}, \quad (3.5)$$

with Hamiltonian

$$\mathcal{H} = \frac{\kappa^2}{4\pi} \int_{|z_1-z_2|>a_0} \frac{1 + \Re(w'^*(z_1)w'(z_2))}{\sqrt{(z_1-z_2)^2 + |w(z_1) - w(z_2)|^2}} dz_1 dz_2, \quad (3.6)$$

where we have used the notation of $w'(z) = \partial w / \partial z$ [10]. This is because we are able to represent the position \mathbf{r} of the vortex by a 2D parametric form $\mathbf{r} = (x(z), y(z), z)$, which corresponds to small perturbations of the straight line configuration along z , i.e. the vortex cannot fold into itself in order to preserve the single-valuedness of functions $x(z)$ and $y(z)$. The geometrical constraint of small perturbations can be represented in terms of a small parameter:

$$\epsilon(z_1, z_2) = \frac{|w(z_1) - w(z_2)|}{z_1 - z_2} \ll 1. \quad (3.7)$$

By expanding Hamiltonian (3.6) in powers of ϵ , we can express (3.6) in the form of Expansion (2.24). Kozik and Svistunov found the exact expressions for the first three even order contributions \mathcal{H}_2 , \mathcal{H}_4 and \mathcal{H}_6 [11]:

$$\mathcal{H}_2 = \frac{\kappa^2}{8\pi} \int_{|z_1-z_2|>a_0} \frac{[2\operatorname{Re}(w'^*(z_1)w'(z_2)) - \epsilon^2]}{|z_1 - z_2|} dz_1 dz_2, \quad (3.8a)$$

$$\mathcal{H}_4 = \frac{\kappa^2}{32\pi} \int_{|z_1-z_2|>a_0} \frac{[3\epsilon^4 - 4\epsilon^2 \operatorname{Re}(w'^*(z_1)w'(z_2))]}{|z_1 - z_2|} dz_1 dz_2, \quad (3.8b)$$

$$\mathcal{H}_6 = \frac{\kappa^2}{64\pi} \int_{|z_1-z_2|>a_0} \frac{[6\epsilon^4 \operatorname{Re}(w'^*(z_1)w'(z_2)) - 5\epsilon^6]}{|z_1 - z_2|} dz_1 dz_2. \quad (3.8c)$$

The divergent cut-off of the BSE is equivalent to truncation of integration in equations (3.8) at $|z_1 - z_2| > a_0$. This cut-off removes the singularity, but leaves logarithmic divergent terms, that diverge as $a_0 \rightarrow 0$. By the introduction of an arbitrary effective length scale, which for convenience we choose to be ℓ , we can follow these divergent terms at all orders with the introduction of the small parameter:

$$\Lambda_0^{-1} = \frac{1}{\ln\left(\frac{\ell}{a_0}\right)} \ll 1. \quad (3.9)$$

Therefore, we should perform a simultaneous expansion of (3.6) in both parameters ϵ and Λ_0^{-1} . Furthermore, we find that the leading order terms in Λ_0^{-1} , give an integrable model called the local induction approximation (LIA). The LIA corresponds to the approximation that a vortex element is completely influenced by its adjacent segments. This local behaviour makes the LIA significantly quicker than the BSE with regards to computational expense. However, the LIA is an integrable system, making it a poor choice in modelling nonlinear Kelvin wave interactions. The corresponding LIA Hamiltonian can be expressed as

$$\mathcal{H} = \frac{\kappa^2 \Lambda_0}{2\pi} \int \sqrt{1 + |w'(z)|^2} dz. \quad (3.10)$$

Integrability of LIA can be shown via the Hasimoto transformation leading to the 1D NLSE [140]. The LIA conserves an infinite number of invariants, and therefore, wave resonances are absent at all orders. Consequently, we have to expand Equations (3.8) in powers of Λ_0^{-1} and consider the sub-leading, non-integrable, order.

It is convenient to represent Equations (3.8) in the wave interaction representation. Therefore, we introduce the Fourier representation for variable $w(z, t)$ as

$$w(z, t) = \frac{1}{\kappa^{1/2}} \sum_{\mathbf{k}} a(\mathbf{k}, t) e^{i\mathbf{k}z}. \quad (3.11)$$

It was shown in [11], that the resulting Hamiltonian in the wave interaction representation equates to several integrals involving various cosine functions, see Appendix C. These integrals were analysed numerically in [11], however, we have analytically, computed these integrals, thus deriving complete and exact formulae for the frequency and interaction coefficients, ω_k , $T_{3,4}^{1,2}$ and $W_{4,5,6}^{1,2,3}$.

For clarity, we introduce notation to keep track for the Λ_0^{-1} -expansion of the frequency and interaction coefficients. We will denote the leading integrable order of the expansion with superscript Λ , and the proceeding $\mathcal{O}(1)$ contributions with superscript

1. Hence, we represent the linear frequency and interaction coefficients as

$$\omega_k = {}^\Lambda\omega_k + {}^1\omega_k + \mathcal{O}(\Lambda_0^{-1}), \quad (3.12a)$$

$$T_{3,4}^{1,2} = {}^\Lambda T_{3,4}^{1,2} + {}^1 T_{3,4}^{1,2} + \mathcal{O}(\Lambda_0^{-1}), \quad (3.12b)$$

$$W_{4,5,6}^{1,2,3} = {}^\Lambda W_{4,5,6}^{1,2,3} + {}^1 W_{4,5,6}^{1,2,3} + \mathcal{O}(\Lambda_0^{-1}). \quad (3.12c)$$

The analytical expressions of Equations (3.12) are expressed below as [7, 9]

$$\omega_k = \frac{\kappa k^2}{4\pi} \left[\Lambda_0 - \gamma - \frac{3}{2} - \ln(k\ell) \right], \quad (3.13a)$$

$$T_{12}^{34} = \frac{1}{16\pi} \left[\mathbf{k}_1 \mathbf{k}_2 \mathbf{k}_3 \mathbf{k}_4 (1 + 4\gamma - 4\Lambda_0) - \mathcal{F}_{3,4}^{1,2} \right], \quad (3.13b)$$

$$W_{123}^{456} = \frac{9}{32\pi\kappa} \left[\mathbf{k}_1 \mathbf{k}_2 \mathbf{k}_3 \mathbf{k}_4 \mathbf{k}_5 \mathbf{k}_6 (1 - 4\gamma + 4\Lambda_0) - \mathcal{G}_{4,5,6}^{1,2,3} \right]. \quad (3.13c)$$

The function $\mathcal{F}_{3,4}^{1,2}$ is symmetric with respect to $\mathbf{k}_1 \leftrightarrow \mathbf{k}_2$, $\mathbf{k}_3 \leftrightarrow \mathbf{k}_4$ and $\{\mathbf{k}_1, \mathbf{k}_2\} \leftrightarrow \{\mathbf{k}_3, \mathbf{k}_4\}$, whilst function $\mathcal{G}_{4,5,6}^{1,2,3}$ is symmetric with respect to $\mathbf{k}_1 \leftrightarrow \mathbf{k}_2 \leftrightarrow \mathbf{k}_3$, $\mathbf{k}_4 \leftrightarrow \mathbf{k}_5 \leftrightarrow \mathbf{k}_6$ and $\{\mathbf{k}_1, \mathbf{k}_2, \mathbf{k}_3\} \leftrightarrow \{\mathbf{k}_4, \mathbf{k}_5, \mathbf{k}_6\}$. These symmetries are required in order for the interaction coefficients to posses Properties (2.26). The full definitions of $\mathcal{F}_{3,4}^{1,2}$ and $\mathcal{G}_{4,5,6}^{1,2,3}$ are given in Appendix C.

The linear frequency (3.13a) is in the form of Relation (3.4) with $C = -\gamma - \frac{3}{2}$, albeit with the introduction of the arbitrary effective length scale ℓ . The leading contributions (the terms proportional to Λ_0) of the frequency and interaction coefficients (3.13) are none other than the frequency and interaction coefficients stemming from the LIA Hamiltonian (3.10).

Re-definition of the LIA coefficient, $\Lambda = \Lambda_0 - \gamma - 3/2$, allows us to incorporate the $\mathcal{O}(1)$ contribution in the linear frequency, (3.13a), into the LIA coefficient. Physically, this entails re-defining the vortex core radius, a_0 , to $a = a_0 e^{\gamma+3/2}$. Therefore, we can explicitly write Λ as

$$\Lambda = \ln \left(\frac{\ell}{a} \right). \quad (3.14)$$

Subsequently, Equations (3.13) become,

$$\begin{aligned}\omega_k &= {}^\Lambda\omega_k + {}^1\omega_k, \\ &= \frac{\kappa\Lambda}{4\pi}k^2 - \frac{\kappa}{4\pi}k^2 \ln(k\ell),\end{aligned}\tag{3.15a}$$

$$\begin{aligned}T_{3,4}^{1,2} &= {}^\Lambda T_{3,4}^{1,2} + {}^1T_{3,4}^{1,2}, \\ &= -\frac{\Lambda}{4\pi}\mathbf{k}_1\mathbf{k}_2\mathbf{k}_3\mathbf{k}_4 - \frac{1}{16\pi}\left(5\mathbf{k}_1\mathbf{k}_2\mathbf{k}_3\mathbf{k}_4 + \mathcal{F}_{3,4}^{1,2}\right),\end{aligned}\tag{3.15b}$$

$$\begin{aligned}W_{4,5,6}^{1,2,3} &= {}^\Lambda W_{4,5,6}^{1,2,3} + {}^1W_{4,5,6}^{1,2,3}, \\ &= \frac{9\Lambda}{8\pi\kappa}\mathbf{k}_1\mathbf{k}_2\mathbf{k}_3\mathbf{k}_4\mathbf{k}_5\mathbf{k}_6 + \frac{9}{32\pi\kappa}\left(7\mathbf{k}_1\mathbf{k}_2\mathbf{k}_3\mathbf{k}_4\mathbf{k}_5\mathbf{k}_6 - \mathcal{G}_{4,5,6}^{1,2,3}\right).\end{aligned}\tag{3.15c}$$

Note that in the full expressions for ω_k , $T_{3,4}^{1,2}$ and $W_{4,5,6}^{1,2,3}$, ℓ does not appear, but instead $\ln(1/a)$. This is natural because we have artificially introduced the auxiliary parameter ℓ . Moreover, it is important to note that it was not necessary to introduce this scale, as any effective intermediate scale ℓ_{eff} would suffice. Cancellation of ℓ provides a useful check in verifying the derivations.

3.4 The Λ^{-1} -Expansion of the Six-Wave Interaction Coefficient $\mathcal{W}_{4,5,6}^{1,2,3}$

To calculate the full interaction coefficient, we must begin by representing the Kelvin wave system in the form of the general six-wave Hamiltonian system of Chapter 2. Four-wave interactions of Kelvin waves are prohibited because there are no non-trivial solutions to the four-wave resonance condition as $\omega_k \propto k^2 \ln(k)$. Therefore, we need to apply the CT. The logarithmic dependence of the linear frequency poses a difficulty which we overcome by performing a Taylor expansion around the leading contribution ${}^\Lambda\omega_k$. To be mathematically precise, we should deal with the full six-wave resonant condition, where ω_k equals Expression (3.15a). However, the logarithmic contribution proves to be a complication to our mathematical analysis. Therefore, we consider the leading order frequency contribution, ${}^\Lambda\omega_k$ to the six-wave resonance condition, and we

denote this as the LIA resonance condition, given by

$$\mathbf{k}_1 + \mathbf{k}_2 + \mathbf{k}_3 = \mathbf{k}_4 + \mathbf{k}_5 + \mathbf{k}_6, \quad (3.16a)$$

$${}^\Lambda\omega_1 + {}^\Lambda\omega_2 + {}^\Lambda\omega_3 = {}^\Lambda\omega_4 + {}^\Lambda\omega_5 + {}^\Lambda\omega_6. \quad (3.16b)$$

Although this is not an exact expression for Kelvin wave resonances, we will subsequently correct the LIA resonance condition, (3.16), by an additional contribution to the six-wave interaction coefficient in Section 3.5. Note that the LIA resonance condition is of the same structure as the general six-wave resonance condition considered in (2.34), with ${}^\Lambda\omega_k \propto k^2$.

Application of the CT to the Kelvin wave system will give a six-wave interaction coefficient with a Λ^{-1} -expansion given by

$$\mathcal{W}_{4,5,6}^{1,2,3} = {}^\Lambda\mathcal{W}_{4,5,6}^{1,2,3} + {}^1\mathcal{W}_{4,5,6}^{1,2,3} + \mathcal{O}(\Lambda^{-1}), \quad (3.17)$$

where the first two terms are given by

$${}^\Lambda\mathcal{W}_{4,5,6}^{1,2,3} = {}^\Lambda W_{4,5,6}^{1,2,3} - \frac{1}{8} \sum_{\substack{i,j,m=1 \\ i \neq j \neq m \neq i}}^3 \sum_{\substack{p,q,r=4 \\ p \neq q \neq r \neq p}}^6 \frac{{}^\Lambda T_{p,q}^{p+q-i,i} {}^\Lambda T_{j,m}^{j+m-r,r} {}^\Lambda T_{i,j}^{i+j-p,p} {}^\Lambda T_{q,r}^{q+r-m,m}}{{}^\Lambda \omega_{j,m}^{j+m-r,r} {}^\Lambda \omega_{q,r}^{q+r-m,m}}, \quad (3.18)$$

and

$${}^1\mathcal{W}_{4,5,6}^{1,2,3} = {}^1 W_{4,5,6}^{1,2,3} + {}^1 Q_{4,5,6}^{1,2,3} + {}^1 Q_{4,5,6}^{1,2,3} + {}^1 Q_{4,5,6}^{1,2,3}, \quad (3.19a)$$

where

$${}^1 Q_{4,5,6}^{1,2,3} = -\frac{1}{8} \sum_{\substack{i,j,m=1 \\ i \neq j \neq m \neq i}}^3 \sum_{\substack{p,q,r=4 \\ p \neq q \neq r \neq p}}^6 \frac{{}^1 T_{p,q}^{p+q-i,i} {}^1 T_{j,m}^{j+m-r,r} {}^1 T_{i,j}^{i+j-p,p} {}^1 T_{q,r}^{q+r-m,m}}{{}^\Lambda \omega_{j,m}^{j+m-r,r} {}^\Lambda \omega_{q,r}^{q+r-m,m}}, \quad (3.19b)$$

$${}^2 Q_{4,5,6}^{1,2,3} = -\frac{1}{8} \sum_{\substack{i,j,m=1 \\ i \neq j \neq m \neq i}}^3 \sum_{\substack{p,q,r=4 \\ p \neq q \neq r \neq p}}^6 \frac{{}^1 T_{p,q}^{p+q-i,i} {}^\Lambda T_{j,m}^{j+m-r,r} {}^1 T_{i,j}^{i+j-p,p} {}^\Lambda T_{q,r}^{q+r-m,m}}{{}^\Lambda \omega_{j,m}^{j+m-r,r} {}^\Lambda \omega_{q,r}^{q+r-m,m}}, \quad (3.19c)$$

and

$$\begin{aligned} {}_3Q_{4,5,6}^{1,2,3} = & \frac{1}{8} \sum_{\substack{i,j,m=1 \\ i \neq j \neq m \neq i}}^3 \sum_{p,q,r=4}^6 \frac{{}^\Lambda T_{p,q}^{p+q-i,i} {}^\Lambda T_{j,m}^{j+m-r,r}}{\left({}^\Lambda \omega_{j,m}^{j+m-r,r}\right)^2} \cdot {}^1 \omega_{j,m}^{j+m-r,r} \\ & + \frac{{}^\Lambda T_{i,j}^{i+j-p,p} {}^\Lambda T_{q,r}^{q+r-m,m}}{\left({}^\Lambda \omega_{q,r}^{q+r-m,m}\right)^2} \cdot {}^1 \omega_{q,r}^{q+r-m,m}. \end{aligned} \quad (3.19d)$$

${}_i^1 Q$, where $i = 1, 2, 3$ are the $\mathcal{O}(1)$ contributions arising from the six-wave contributions stemming from the CT. Terms ${}_1^1 Q$ and ${}_2^1 Q$ originate from the product of ${}^1 T$ and ${}^\Lambda T$, divided by the leading frequency contribution ${}^\Lambda \omega_k$. Term ${}_3^1 Q$ is the correction from the Taylor expansion around the leading frequency contribution.

When the LIA resonance condition, (3.16), is satisfied, the leading contribution to the six-wave interaction coefficient, ${}^\Lambda \mathcal{W}_{4,5,6}^{1,2,3}$, vanishes, verifying the integrability of the LIA. This was achieved using the Mathematica package and parameterisation (2.112). Therefore, the leading contribution to Kelvin wave dynamics arises from the sub-leading order correction ${}^1 \mathcal{W}_{4,5,6}^{1,2,3}$.

3.5 Correction to the Local Induction Approximation Resonance Condition

Due to the logarithmic dependence of the Kelvin wave frequency, we have approximated the six-wave resonant condition (2.34) by the leading order LIA resonance condition (3.16). To compensate for this, we find an additional corrective term to the six-wave interaction coefficient, that we denote ${}^1 S_{4,5,6}^{1,2,3}$. Our strategy in finding ${}^1 S_{4,5,6}^{1,2,3}$, is to assume two corrections to the parametric formulae for wave numbers \mathbf{k}_2 and \mathbf{k}_5 in (2.112). Let us denote them as ${}^1 \mathbf{k}_2$ and ${}^1 \mathbf{k}_5$, so our new parameterisation is given by

$$\mathbf{k}_2 = {}^\Lambda \mathbf{k}_2 + {}^1 \mathbf{k}_2, \quad (3.20a)$$

$$\mathbf{k}_5 = {}^\Lambda \mathbf{k}_5 + {}^1 \mathbf{k}_5, \quad (3.20b)$$

where ${}^\Lambda \mathbf{k}_2$ and ${}^\Lambda \mathbf{k}_5$ are the right-hand sides of Equations (2.112). The wave number resonance condition for the conservation of momentum, (3.16a), fixes ${}^1 \mathbf{k}_2 = {}^1 \mathbf{k}_5$. Moreover, the frequency resonance condition implies that

$$\omega_{4,5,6}^{1,2,3} = {}^1 \mathbf{k}_2 \frac{\partial^\Lambda \omega_2}{\partial \mathbf{k}_2} - {}^1 \mathbf{k}_5 \frac{\partial^\Lambda \omega_5}{\partial \mathbf{k}_5} + {}^1 \omega_{4,5,6}^{1,2,3} + \mathcal{O}(\Lambda^{-1}) = 0, \quad (3.21)$$

where we have applied a Taylor expansion around the corrections, i.e.

$${}^\Lambda \omega({}^\Lambda \mathbf{k}_i + {}^1 \mathbf{k}_i) \approx {}^\Lambda \omega({}^\Lambda \mathbf{k}_i) + {}^1 \mathbf{k}_i \frac{\partial^\Lambda \omega_i}{\partial \mathbf{k}_i}, \quad (3.22)$$

for $i = 2, 5$. Therefore, to the leading order in Λ , our corrections to the parameterisation, (2.112), are

$${}^1 \mathbf{k}_2 = {}^1 \mathbf{k}_5 \approx \frac{2\pi {}^1 \omega_{4,5,6}^{1,2,3}}{\Lambda \kappa(\mathbf{k}_5 - \mathbf{k}_2)}. \quad (3.23)$$

This enables us to express the correction to $\mathcal{W}_{4,5,6}^{1,2,3}$ as

$$\begin{aligned} {}^1 S_{4,5,6}^{1,2,3} &= {}^1 \mathbf{k}_2 \frac{\partial^\Lambda \mathcal{W}_{4,5,6}^{1,2,3}}{\partial \mathbf{k}_2} - {}^1 \mathbf{k}_5 \frac{\partial^\Lambda \mathcal{W}_{4,5,6}^{1,2,3}}{\partial \mathbf{k}_5} + \mathcal{O}(\Lambda^{-1}), \\ &\approx \frac{2\pi {}^1 \omega_{4,5,6}^{1,2,3}}{\Lambda \kappa(\mathbf{k}_5 - \mathbf{k}_2)} \left(\frac{\partial^\Lambda \mathcal{W}_{4,5,6}^{1,2,3}}{\partial \mathbf{k}_2} + \frac{\partial^\Lambda \mathcal{W}_{4,5,6}^{1,2,3}}{\partial \mathbf{k}_5} \right). \end{aligned} \quad (3.24)$$

Instead of using wave numbers, \mathbf{k}_2 and \mathbf{k}_5 , in (3.20), we could have chosen any pair, \mathbf{k}_i and \mathbf{k}_j with $i = 1, 2, 3$ and $j = 4, 5, 6$. Considering this fact, we can write a fully symmetric, with respect to these wave number permutations, expression for ${}^1 S_{4,5,6}^{1,2,3}$:

$${}^1 S_{4,5,6}^{1,2,3} = \frac{2\pi}{9\kappa\Lambda} {}^1 \omega_{4,5,6}^{1,2,3} \sum_{\substack{i=1,2,3 \\ j=4,5,6}} \frac{\left(\frac{\partial}{\partial \mathbf{k}_i} + \frac{\partial}{\partial \mathbf{k}_j} \right) {}^\Lambda \mathcal{W}_{4,5,6}^{1,2,3}}{(\mathbf{k}_j - \mathbf{k}_i)}. \quad (3.25)$$

Therefore, the corrected six-wave interaction coefficient for describing Kelvin wave dynamics takes the form:

$${}^c \mathcal{W}_{4,5,6}^{1,2,3} = {}^1 \mathcal{W}_{3,4,5}^{1,2,3} + {}^1 S_{4,5,6}^{1,2,3}, \quad (3.26)$$

with ${}^1 \mathcal{W}_{3,4,5}^{1,2,3}$ from (3.19) and ${}^1 S_{4,5,6}^{1,2,3}$ from (3.25).

Unfortunately, ${}^c\mathcal{W}_{4.5.6}^{1,2,3}$ comprises of a large number of terms, making its analytical use inconvenient. However, we find that ${}^c\mathcal{W}_{4.5.6}^{1,2,3}$ has remarkably simple asymptotics, which we demonstrate in the next Section.

3.6 Asymptotics of ${}^c\mathcal{W}_{4.5.6}^{1,2,3}$

In this Section, we examine the asymptotic limit of the corrected six-wave interaction coefficient for Kelvin waves, (3.26). ${}^c\mathcal{W}_{4.5.6}^{1,2,3}$ consists of five contributions given by formulae (3.19) and (3.25). The explicit form of (3.26) involves $\simeq 2 \times 10^4$ terms, making any analytical expression cumbersome. However, we will consider the behaviour of ${}^c\mathcal{W}_{4.5.6}^{1,2,3}$ in various asymptotical regimes, analysed using *Mathematica*. We study ${}^c\mathcal{W}_{4.5.6}^{1,2,3}$ on the LIA resonant condition, (3.16), allowing for the application of parameterisation (2.112).

If the smallest wave number, say \mathbf{k}_6 , is smaller than the largest, say \mathbf{k}_1 , then we have the following asymptotic property of ${}^c\mathcal{W}_{4.5.6}^{1,2,3}$:

$${}^c\mathcal{W}_{4.5.6}^{1,2,3} \rightarrow -\frac{3}{4\pi\kappa} \mathbf{k}_1 \mathbf{k}_2 \mathbf{k}_3 \mathbf{k}_4 \mathbf{k}_5 \mathbf{k}_6, \quad (3.27a)$$

as

$$\frac{\min\{k_1, k_2, k_3, k_4, k_5, k_6\}}{\max\{k_1, k_2, k_3, k_4, k_5, k_6\}} \rightarrow 0. \quad (3.27b)$$

For Expression (3.27a) to hold, it is enough that the smallest wave number be less than the largest, and not all of the remaining five in the sextet. This was established using *Mathematica* and the Taylor expansion of ${}^c\mathcal{W}_{4.5.6}^{1,2,3}$ with respect to one, two and four wave numbers¹. These limits give the same expression as (3.27a). The analysis of these asymptotic limits can be found in Appendix D.

Numerical evaluation of ${}^c\mathcal{W}_{4.5.6}^{1,2,3}$ on a set of 2^{10} randomly chosen wave numbers, different from each other at most by a factor of two, indicate that the most important contributions to ${}^c\mathcal{W}_{4.5.6}^{1,2,3}$ are from the IR region - where the asymptotic expression (3.27a) is exact. Therefore, for most purposes we can approximate the corrected six-wave

¹The limit of three wave numbers tending to zero is not allowed by the six-wave resonance condition.

interaction coefficient, ${}^c\mathcal{W}_{4.5.6}^{1,2,3}$, with its asymptotical expression, (3.27a).

3.7 The Local Nonlinear Equation

By considering Hamiltonian (2.37) with the asymptotic expression as its six-wave interaction coefficient, Equation (3.27a), and reverting back into physical space gives:

$$\mathcal{H}^{LNE} = \frac{\kappa^2}{4\pi} \int \Lambda \left| \frac{\partial w}{\partial z} \right|^2 - \frac{1}{12} \left| \frac{\partial w}{\partial z} \right|^6 dz. \quad (3.28)$$

Notice that the nonlinear part of the energy, \mathcal{H}_4 , in (3.28) is a purely negative quantity.

Applying Relation (3.5), we get a dynamical evolution equation for $w(z, t)$ given by

$$i \frac{\partial w}{\partial t} = -\frac{\kappa}{4\pi} \frac{\partial}{\partial z} \left[\left(\Lambda - \frac{1}{4} \left| \frac{\partial w}{\partial z} \right|^4 \right) \frac{\partial w}{\partial z} \right]. \quad (3.29)$$

We denote Equation (3.29) as the LNE. Like the BSE, the LNE conserves the energy (3.28), and wave action $\mathcal{N} = \int |w|^2 dz^2$. The LNE is a competent model for the description Kelvin wave dynamics in QT, without relying on the computational expense of the BSE, (3.2). The LNE includes the leading contribution obtained from local elements (LIA) and in addition, the nonlinear interactions of Kelvin waves, whilst being simpler than the BSE itself. The LNE is isomorphic to the TLIA model [7] in the limit of weakly nonlinear Kelvin waves. However, unlike the TLIA model, which was introduced by *ad hoc* reasoning, the LNE was systematically derived from the BSE.

A direct comparison of the LNE to the BSE would provide a useful and important verification of the LNE dynamics. Not only for the WT scenario, but also for larger amplitude waves, where the non-locality of the BSE plays an important role. The LNE dynamics could easily be tested by performing an identical numerical simulation with the same initial condition on the BSE.

²The consideration of a single quantised vortex line, as in this case for the LNE (Equation (3.29)) and in the previous case of the BSE Hamiltonian (Equation (3.6)), the total linear and angular momenta of the corresponding flow are conserved.

3.8 The Truncated Local Induction Approximation Model

The TLIA model was introduced as a simple model for Kelvin wave dynamics that contained the same scaling properties as the BSE [7]. The model arises from a truncation of the LIA Hamiltonian, (3.10). For small Kelvin wave amplitudes, $|w'| \ll 1$, the LIA Hamiltonian can be expanded in powers of $|w'|$:

$$\mathcal{H}^{LIA} = \frac{\kappa^2 \Lambda_0}{2\pi} \int \left(1 + \frac{1}{2}|w'|^2 - \frac{1}{8}|w'|^4 + \dots \right) dz. \quad (3.30)$$

The TLIA model is found by truncating the LIA Hamiltonian, (3.30), at the quartic order in w' .

$$\mathcal{H}^{TLIA} = \mathcal{H}_0 + \mathcal{H}_2 + \mathcal{H}_4 = \frac{\kappa^2 \Lambda_0}{2\pi} \int \left(1 + \frac{1}{2}|w'|^2 - \frac{1}{8}|w'|^4 \right) dz. \quad (3.31)$$

The truncation breaks the integrability of the LIA Hamiltonian, thereby allowing non-trivial energy transfer in Kelvin wave interactions. Neglecting the constant term \mathcal{H}_0 , which only contributes a constant value to the Hamiltonian. The TLIA Hamiltonian has the following interaction coefficients when represented in form (2.25):

$$\omega_k = \frac{\kappa \Lambda_0 k^2}{4\pi}, \quad (3.32a)$$

$$T_{3,4}^{1,2} = -\frac{\Lambda_0}{16\pi} \mathbf{k}_1 \mathbf{k}_2 \mathbf{k}_3 \mathbf{k}_4, \quad (3.32b)$$

$$W_{4,5,6}^{1,2,3} = 0. \quad (3.32c)$$

Similarly to the BSE, the TLIA model cannot produce any non-trivial four-wave resonances as $\omega_k \propto k^2$. Therefore, we should apply the CT from Chapter 2. After eliminating the four-wave resonances, we result in a six-wave interaction coefficient given by

$$\mathcal{W}_{4,5,6}^{1,2,3} = -\frac{\Lambda_0}{32\pi\kappa} \mathbf{k}_1 \mathbf{k}_2 \mathbf{k}_3 \mathbf{k}_4 \mathbf{k}_5 \mathbf{k}_6. \quad (3.33)$$

Formula (3.33) is of similar form as the six-wave interaction coefficient in the LNE. Moreover, (3.33) is of opposite sign to the six-wave contribution that would arise from the first term after the truncation in (3.30). This is expected, as the LIA Hamiltonian,

(3.10), is an integrable model, and therefore after application of the the CT, all orders of interaction coefficients should be zero.

3.9 The Kozik-Svistunov Spectrum

To calculate the Kelvin wave spectrum, we must find the homogeneity coefficient of the six-wave interaction coefficient for the BSE. However the six-wave interaction coefficient, (3.26), is not scale invariant. The slowly varying logarithmic contribution can be approximated as constant with the change of wave number \mathbf{k} . Moreover, this is supported by the fact that (3.26) has an asymptotic limit of (3.27a), with no logarithmic dependence. This was the case when the KZ solution, corresponding to a constant energy flux, $P_{\mathbf{k}}$, was derived using a dimensional analysis argument from the six-wave KE assuming that the scaling property of the six-wave interaction coefficient was assumed to be a product of six wave numbers [11]. The neglected logarithmic terms were followed, but assumed to be small in [60], and additional missing terms account for in [7, 9]. The resulting wave action spectrum for energy is known as the Kozik-Svistunov (KS) spectrum, given by

$$n_{\mathbf{k}}^{\mathcal{H}} = C_{\mathcal{H}} \kappa^{2/5} P_{\mathbf{k}}^{1/5} k^{-17/5}. \quad (3.34a)$$

The corresponding wave action spectrum for the inverse cascade yields a scaling of

$$n_{\mathbf{k}}^{\mathcal{N}} = C_{\mathcal{N}} \kappa^{1/5} Q_{\mathbf{k}}^{1/5} \Lambda^{-1/5} k^{-3}. \quad (3.34b)$$

Here we have added the dimensional quantities to the power law, so that the constant in each spectrum is of $\mathcal{O}(1)$. We emphasise, that the KZ solutions (3.34) are only valid solution if they correspond to local wave interactions. If not, then the solutions are meaningless and a non-local description is required.

3.10 Non-locality of Kelvin Wave Turbulence

We apply the strategy in Chapter 2 for determining the locality of the two KZ spectra for Kelvin wave turbulence.

3.10.1 Infrared Convergence

To check the convergence property in the IR region we need to compute the asymptotic limit of ${}^c\mathcal{W}_{4,5,6}^{1,2,3}$, for $k_6 \ll k, k_2, k_3, k_4, k_5$. We find from (3.27a) that

$$\lim_{k_6 \rightarrow 0} {}^c\mathcal{W}_{4,5,6}^{1,2,3} \propto k_6. \quad (3.35)$$

Therefore, $\xi = 1$ in Equation (2.113), and we find that the formula for convergence, (2.116), reads

$$x < 3. \quad (3.36)$$

Therefore, the KS spectrum, (3.34a), with $x = 17/5$, does not imply convergence of the collision integral. Moreover, we find that the inverse spectrum, (3.34b), is borderline divergent. As these KZ solutions do not make the collision integral convergent, they are physically unrealisable. Divergence in the IR region is sufficient to dismiss the two Kelvin wave spectra, (3.34), as valid solutions of the KE.

3.10.2 Ultraviolet Convergence

Although we have already shown that the two Kelvin wave KZ solutions, (3.34), are non-local, for completeness we will check UV convergence. In the limit of one large wave number, the interaction coefficient scales as

$$\lim_{k_6 \rightarrow \infty} {}^c\mathcal{W}_{4,5,6}^{1,2,3} \propto k_6^0. \quad (3.37)$$

Hence the criterion for convergence in the UV limit, (2.121), becomes

$$\max(4 - 2x, 2 - 2x) < 0. \quad (3.38)$$

We see from (3.38), that both the KS and inverse spectra, (3.34), imply UV convergence. However, this does not change the fact that both spectra, (3.34), are non-local. The inverse spectrum, (3.34b), is on the border of convergence, therefore, we consider a logarithmic dependence to the power law to invoke convergence of the collision integral.

3.11 Logarithmic Corrections to the Inverse Wave Action Spectrum

In the IR limit, the inverse wave action spectrum, (3.34b), conveyed logarithmic divergence of the collision integral. Although divergent, the rate is slow enough for the spectrum to be corrected by considering a logarithmic dependence. The same scenario occurs for the inverse enstrophy cascade for 2D turbulence, proposed by Kraichnan [101, 102]. For the case of the inverse cascade for Kelvin waves, this implies looking for a solution of the form:

$$n_{\mathbf{k}}^N = C_N k^{-3} \ln^{-y}(k\ell), \quad (3.39)$$

where ℓ is the scale at which wave action is injected. The logarithmic power law exponent is calculated by assuming that the wave action flux, $Q_{\mathbf{k}}$, remains \mathbf{k} -independent when considering that all wave numbers have the same magnitude, i.e. $k_1, k_2, k_3, k_4, k_5 \propto k$. Then the wave action flux can be written as

$$Q_{\mathbf{k}} = \int^{\mathbf{k}} \dot{n}_{\mathbf{k}} d\mathbf{k} \propto \int^{\mathbf{k}} k^{14} n_{\mathbf{k}}^5 d\mathbf{k} \propto \int^{\mathbf{k}} k^{-1} \ln^{-5y}(k\ell) d\mathbf{k}, \quad (3.40)$$

where we have used the fact that the collision integral of (2.94) scales as $\dot{n}_{\mathbf{k}} \propto k^{14} n_{\mathbf{k}}^5$. Relation (3.40) is independent of \mathbf{k} if we set $y = 1/5^3$, therefore our corrected spectrum is given by

$$n_{\mathbf{k}}^N = C \kappa^{1/5} Q_{\mathbf{k}}^{1/5} k^{-3} \ln^{-1/5}(k\ell), \quad (3.41)$$

With this logarithmic correction, the inverse wave action spectrum produces a convergent collision integral, and thus becomes physically observable.

3.12 The L'vov-Nazarenko Spectrum

Non-locality of the KS spectrum and subsequent divergence of the collision integral has prompted a new non-local Kelvin WT theory to be proposed and consequently a new wave action spectrum for the direct cascade derived called the L'vov-Nazarenko (LN)

³The wave action flux is actually proportional to $Q_{\mathbf{k}} \propto \ln(\ln(k\ell))$.

spectrum [85]. In [85], the authors claim that the biggest divergence of the KS spectrum arises when two wave numbers go to zero and as such the KS spectrum is unrealisable. However, they develop an argument to derive a wave action spectrum away from the small \mathbf{k} region, when two wave numbers go to zero. Subsequently, this corresponds to local four-wave interaction describing $1 \leftrightarrow 3$ processes upon vortices with random large-scale curvature. This process yields a new wave action spectrum, $n_{\mathbf{k}}$, with a constant energy flux, $P_{\mathbf{k}}$, of the form:

$$n_{\mathbf{k}}^{\mathcal{H}} = C_{LN} P_{\mathbf{k}}^{1/3} \Psi^{-2/3} k^{-11/3}, \quad (3.42)$$

where Ψ is a dimensionless quantity denoting the mean-square angle of deviation from a straight vortex line and where

$$\Psi = \frac{2}{\kappa} \int_{1/\ell} k^2 n_{\mathbf{k}} dk. \quad (3.43)$$

Whether the KS or the LN spectra are correct has remained a discussion point for theorists. The exponents of both spectra are relatively close to each other, making it difficult to distinguish between the spectra observed in numerical simulations [58, 99]. High resolution numerical simulations or experimental observations are essential for the verification of either spectrum, and more importantly, the physics that determine them.

The numerical simulation for the direct cascade of the full BSE Hamiltonian, (3.6), was performed by Kozik and Svistunov to confirm the scaling in (3.34a) [99]. However they used a scale separation scheme, that seems to artificially force locality of wave interactions, and furthermore, they observe the scaling in a quasi-stationary state from an initial condition close to the observed spectrum. This implies that the results presented in [99] may still be in transition, and the agreement to spectrum (3.34a), may be coincidental. A numerical scheme of high resolution that allows for a spectrum in a statistically stationary state, with the ability to measure the energy flux is essential. The energy flux for the KS spectrum was estimated in [11], however, its value was surprisingly small. Due to the difference in the physics for the derivation of the LN spectrum, the value of the energy fluxes for the KS and LN spectra should be fundamentally different.

Therefore, the measurement of energy flux may be more insightful in determining which theory is correct, than the exponent of the spectrum.

3.13 Numerical Results

In this Section, we present some numerical simulations of the TLIA model and the LNE. The TLIA model was computed by Davide Dezzani [7]. In [7], the motivation was to compare the TLIA model with the simulations of the BSE. The reasoning was that the easily computable TLIA model contains the same WT predictions as the BSE, and would provide a useful and time efficient way of modelling Kelvin wave dynamics.

Both the TLIA model and LNE are numerically simulated with forcing and dissipation. The forcing is narrow-band (in Fourier space), which allows for an inertial range to be produced between the forcing and dissipation regions where neither have an effect. However, it should be noted that in reality, Kelvin waves are forced by vortex reconnections, which force the system at discrete times and produce a forcing that is largely non-local in Fourier space. It is thus a numerical simplification to use a continuous local forcing to enable an inertial range, thus allowing for the better observation of the WT scenario. The presence of dissipation at low wave numbers can also be considered somewhat artificial. Numerically this is required to avoid condensation of wave action (and the subsequent break down of the WT regime) at the lowest modes, but in reality self-reconnections and the generation of vortex rings could be a natural dissipation mechanism.

3.13.1 The Truncated Local Induction Approximation Model

We begin by performing a direct numerical simulation of the dynamical equation, stemming from the TLIA model, (3.31), given by

$$\frac{\partial w}{\partial t} = \frac{i\kappa\Lambda_0}{4\pi} \left[w' \left(1 - \frac{1}{2}|w'|^2 \right) \right]' - \nu_{\text{hyper}} \left(\frac{\partial}{\partial z} \right)^8 w - \nu_{\text{friction}} w + F_{\mathbf{k}}. \quad (3.44)$$

The aim is to perform the simulation until a stationary non-equilibrium turbulent cascade has developed. To achieve this we apply additive forcing to the system in the form of

$F_{\mathbf{k}} = F(\mathbf{k}, t)$, acting on a narrow-band of wave numbers around a given wave number, k_f . To prevent any accumulation or bottlenecks of an invariant appearing, we apply friction in the form of $-\nu_{\text{friction}} w$ acting at low wave numbers, to remove wave action and hyper-viscosity at high wave numbers to remove energy. Physically, the forcing can be interpreted as waves generated from vortex reconnections. The dissipation at low wave numbers can be interpreted as friction with the normal fluid component at a rate ν_{friction} . At high wave numbers the hyper-viscosity term simulates the removal of energy by heat radiation from phonons at a rate proportional to ν_{hyper} .

In ideal conditions, we would prefer to observe the dual cascade scenario in one numerical simulation. However, due to computational and time restrictions, we are forced to run separate simulations for each turbulent cascade.

The numerical code integrates the equation of motion, (3.44), using a pseudo-spectral method for a periodic vortex filament of length 2π , with a resolution of 2^{11} spatial points. The linear and dissipative terms are integrated exactly, whilst the nonlinear term is progressed in time by a second order Runge-Kutta method. The vortex filament is initially a straight line and a long time integration is performed until a stationary regime is achieved⁴. The ratio of the linear \mathcal{H}_2 and the nonlinear \mathcal{H}_4 energies is $\mathcal{H}_2/\mathcal{H}_4 \simeq 20$, confirming *a posteriori* the validity of the Perturbation (3.30) and the condition of small amplitude Kelvin waves, where $\epsilon \ll 1$.

The first set of simulations is devoted to the study of the direct cascade. Energy fluctuations are injected at a forcing scale, $k_f \simeq 2$, and the friction coefficient is set to be $\nu_{\text{friction}} = 4$. Energy is removed at small scales by hyper-viscosity, which restricts the range of dissipation to the wave number in a close vicinity of k_{\max} .

In Figure 3.1, we plot the wave action spectrum for the direct cascade simulation, averaged over time in stationary conditions. A well developed power law spectrum is observed close to the theoretical prediction (3.34a), for over more than one decade (see inset). However, we note that the resolution of these numerical simulations are not sufficient for the comparison to the LN spectrum of non-local Kelvin WT.

We now consider the simulation for the inverse cascade regime. To observe an

⁴This is checked via stationarity of the energy \mathcal{H} and wave action \mathcal{N} .

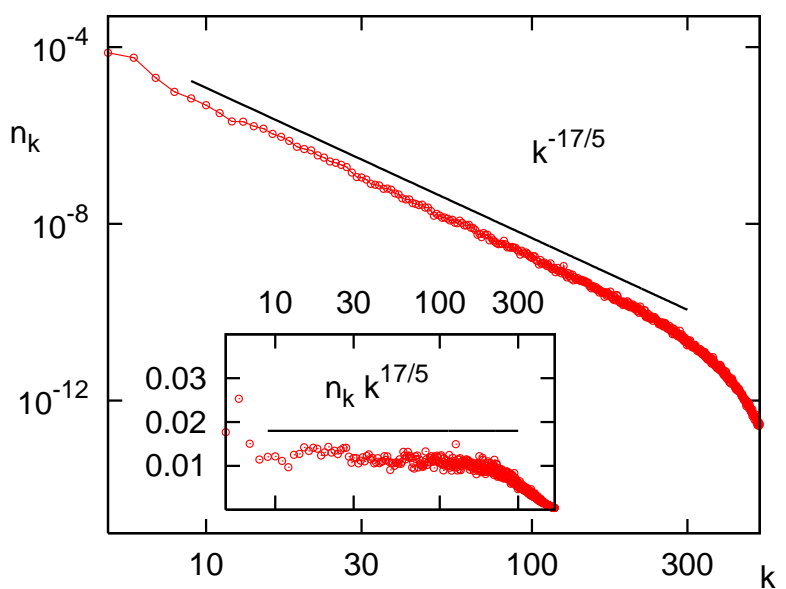


Figure 3.1: The averaged wave number spectrum n_k for a simulation of the direct cascade in stationary conditions, courtesy of Davide Dezzani. The straight line represents the KE prediction $n_k \propto k^{-17/5}$. The inset shows the spectrum compensated with the theoretical prediction.

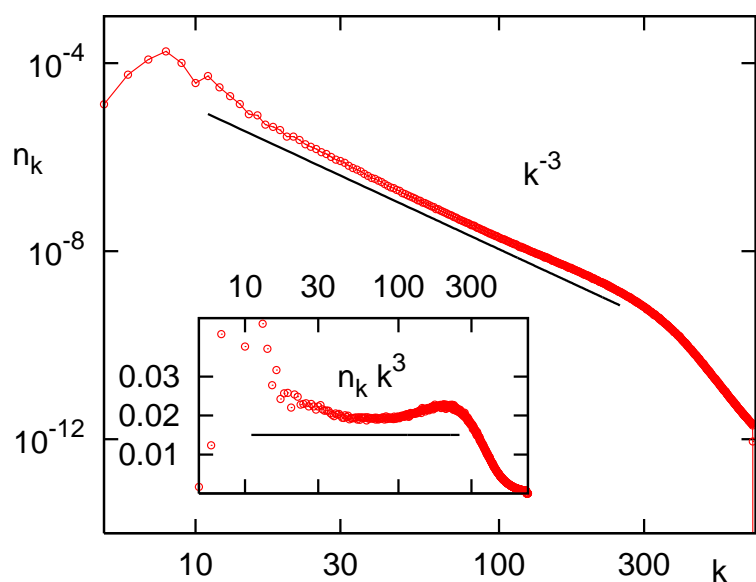


Figure 3.2: The averaged wave number spectrum, n_k , for a simulation of the inverse cascade in stationary conditions, courtesy of Davide Dezzani. The straight line represents the KE prediction, $n_k \propto k^{-3}$. The inset shows the spectrum compensated with the theoretical prediction.

inverse cascade, we apply forcing to small scales, around $k_f = 300$. In order to avoid finite size effects and accumulation at the largest scales [141], the friction coefficient $\nu_{\text{friction}} \simeq 100$ is chosen in such a way as to remove wave action at large scales. Figure 3.2 shows the spectrum for this inverse cascade in stationary conditions. In the compensated plot, a small deviation from the power law scaling at small wave numbers is observed, possibly due to the presence of condensate at the zeroth mode.

3.13.2 The Local Nonlinear Equation

We perform a numerical simulation of the LNE to check the power law scaling of the energy spectrum for Kelvin WT. We use a pseudo-spectral method with 2^{14} spatial points in a periodic box of size $L = 2\pi$. The time step of the simulation is set to $\Delta t = 1 \times 10^{-4}$. We numerically solve the LNE with the addition of forcing and dissipation, giving the numerical model as

$$i \frac{\partial w}{\partial t} = -\frac{\kappa}{4\pi} \frac{\partial}{\partial z} \left[\left(\Lambda - \frac{1}{4} \left| \frac{\partial w}{\partial z} \right|^4 \right) \frac{\partial w}{\partial z} \right] + i (F_{\mathbf{k}} - D_{\mathbf{k}}). \quad (3.45)$$

The conservation of the energy and wave action is checked in the absence of forcing and dissipation, providing a numerical verification of our numerical code.

We include additive forcing, $F_{\mathbf{k}}$, with a profile of

$$F_{\mathbf{k}} = \begin{cases} A \exp(i\theta_{\mathbf{k}}) & \text{if } 8 \leq k < 16 \\ 0 & \text{otherwise ,} \end{cases} \quad (3.46)$$

where $A = 1 \times 10^3$ is a constant amplitude and $\theta_{\mathbf{k}}$ is a random variable sampled from a uniform distribution on $[0, 2\pi)$ for each \mathbf{k} , and at each time step. We add dissipation at both ends of the \mathbf{k} -space to enable us to reach a non-equilibrium steady state, and to avoid any bottleneck effects. The dissipation profile $D_{\mathbf{k}} = D_{\mathbf{k}}^L + D_{\mathbf{k}}^H$, is the sum of a low wave number friction and hyper-viscosity term acting at high wave numbers given by

$$D_{\mathbf{k}}^L = \begin{cases} \nu_{\text{friction}} \psi_{\mathbf{k}} & \text{if } 0 \leq k \leq 6 \\ 0 & \text{otherwise,} \end{cases}$$

and

$$D_{\mathbf{k}}^H = \nu_{\text{hyper}} k^4 \psi_{\mathbf{k}},$$

where, $\nu_{\text{friction}} = 1 \times 10^{-3}$ and $\nu_{\text{hyper}} = 1 \times 10^{-9}$ are the viscosity coefficients

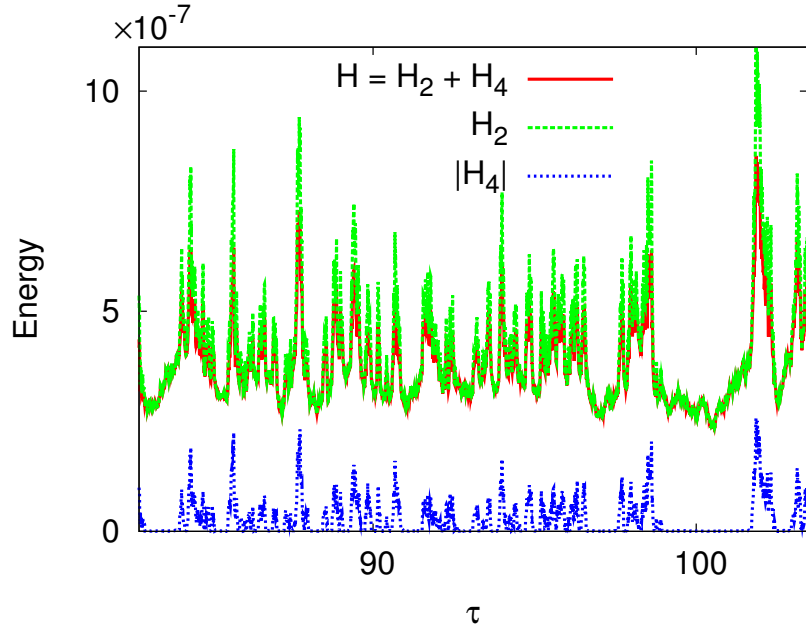


Figure 3.3: We plot the magnitude of the linear, \mathcal{H}_2 , the nonlinear, \mathcal{H}_4 , and the total, \mathcal{H} energies of the simulation at late times in units of the linear timescale of the forcing mode, τ . Note that \mathcal{H}_2 is strictly non-negative and \mathcal{H}_4 is strictly non-positive. We observe a statistically stationary state of the energy. However, we also observe sharp jumps, peaks and troughs in the energy values.

Initially, the system is at rest and we allow the simulation to evolve until it has reached a statistically non-equilibrium steady state. We verify this by observing stationarity of the system's energy, see Figure 3.3. Although statistically stationary, the energy contains intermittent bursts. The cause of such behaviour may be down to finite-box effects, giving rise to a sand-pile effect seen in mesoscopic turbulence [27, 82]. In Figure 3.4, we plot the numerical wave action spectrum and compare against both the KS, (3.34a), and LN, (3.42), spectra. We observe an agreement with the LN scaling and note that there is a clear deviation to the KS slope. We believe this supports the LN spectrum and the non-local theory for Kelvin WT. In Figure 3.5, we plot three wave

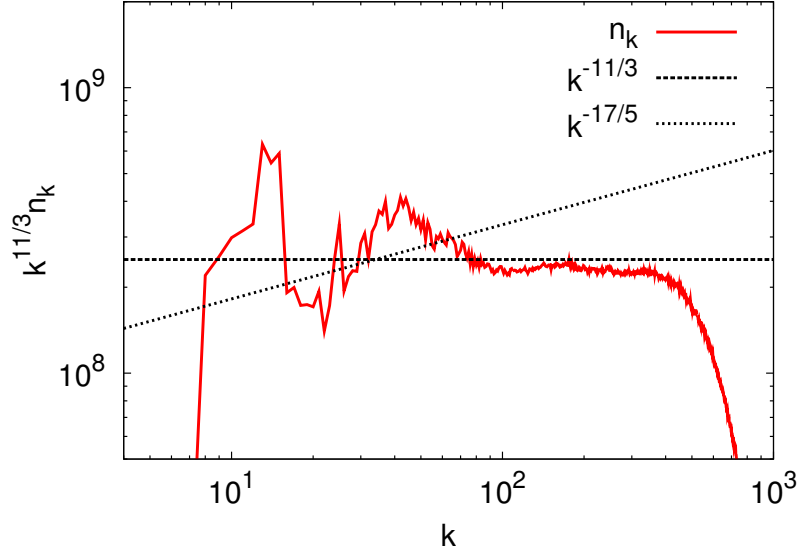


Figure 3.4: Averaged wave action spectrum n_k for the LNE compensated by $k^{11/3}$. The spectrum has been averaged over a long time window once the steady state is reached. We plot the theoretical predictions of the KS and LN spectra.

action spectra at different τ , where $\tau = 8\pi^2/\kappa\Lambda k_f^2$ is the unit of the linear time scale of our forcing mode $k_f \approx 10$. We average two spectra, over a small time window around the time of consideration, and compare with the fully averaged spectrum of Figure 3.4. The first spectrum is at $\tau = 84$, which is taken when the energy of Figure 3.3 is at a peak. The spectrum is well developed of slightly higher magnitude to the fully average spectrum, but with a similar power law slope to the averaged spectrum. At $\tau = 100$, we plot the spectrum when the energy is at a local minimum. The spectrum at this time does not saturate fully to the high wave number region and a clear accumulation at low wave numbers is apparent. As energy fluctuates between peaks and troughs, we observe oscillations of the wave action spectrum between the specific time states in Figure 3.5. We believe that this behaviour is down to the sand-pile behaviour of mesoscopic WT. By taking a long time average, we see a clear power law behaviour of the spectrum in Figure 3.5 (identical to the spectrum in Figure 3.4).

In Figure 3.6, we plot the statistically averaged energy flux, P_k , of the simulation. We observe that at the forcing scale, the energy flux reaches a non-zero value

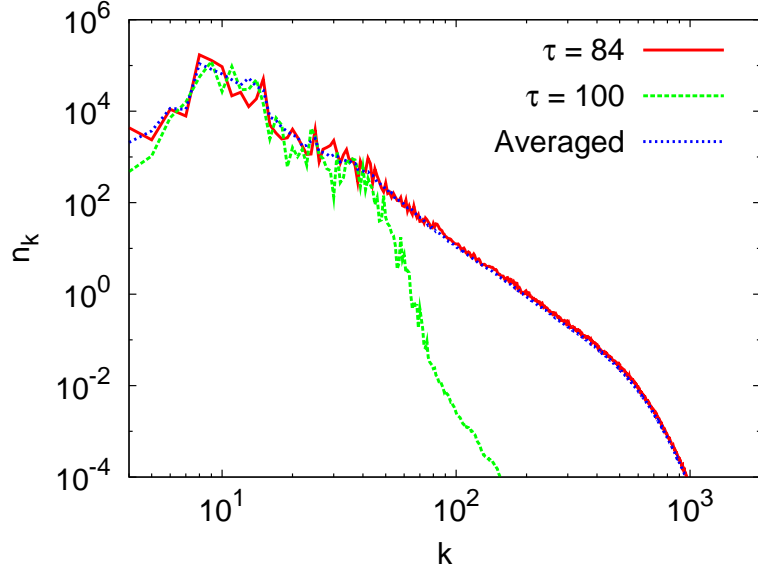


Figure 3.5: We plot the wave action spectrum, n_k , at two times $\tau = 84$ and $\tau = 100$, where the energy at peka and in a trough respectively. We compare these two spectra with the fully averaged wave action spectrum of Figure 3.4.

and remains constant until approximately $k = 30$. After this point the value of P_k declines and converges to a negative constant. Ideally, the energy flux should be constant over a large inertial range, and then return to zero around the dissipation scale at high wave numbers. However this is not the case in Figure 3.6, we believe this is because numerically P_k is only the *linear* energy flux. Conservation of energy and the Kolmogorov-Richardson cascade picture implies that the total, (linear plus nonlinear), energy flux is constant over the inertial range. Therefore, this decline of P_k could be accounted by the absence of the nonlinear energy flux contribution.

In Figure 3.7, we plot the intensity PDF of the system and compare to a straight line, corresponding to a Gaussian wave field, (see Section 2.12). We observe a good agreement at low intensities to a Gaussian wave field. However at at large intensities, the PDF deviates from the straight line - this corresponds to WT intermittency. The deviation corresponds to an increase in the probability of observing intermittent high amplitude events or rogue waves, which break the WT assumptions and inhibit the WT regime.

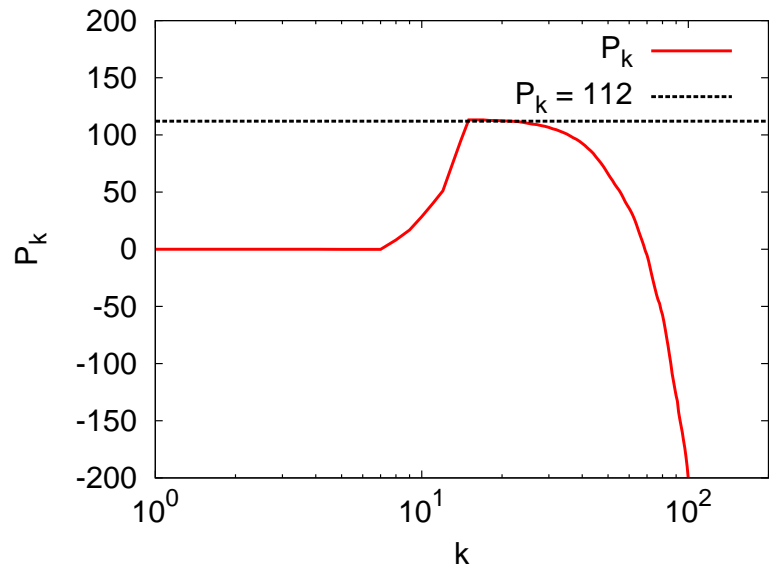


Figure 3.6: We plot the averaged linear energy flux, P_k , verses k in a stationary state. We observe a short inertial range where P_k is constant corresponding to the KZ solution.

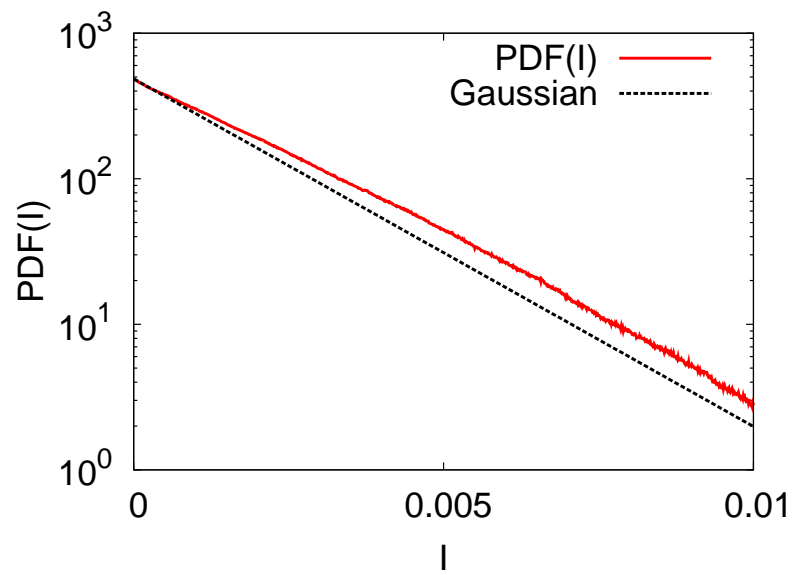


Figure 3.7: We plot the PDF of the intensity of the wave field from physical space. We compare with the Gaussian fit of a straight line.

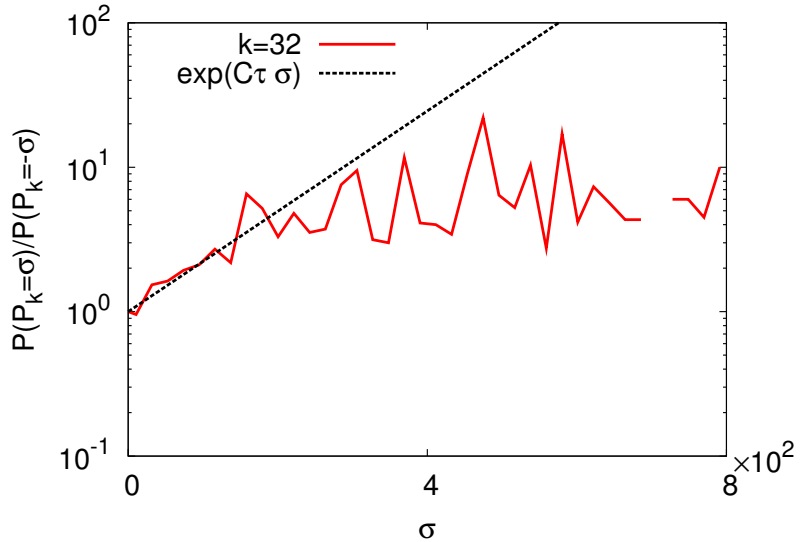


Figure 3.8: We plot the GCFR for the LNE for time fluctuations in the energy flux P_k . We superimpose a straight line corresponding to Relation (2.141). The length of the average τ is taken over a window corresponding to 285 linear time periods of the mode $k = 32$.

In Figure 3.8, we plot the ratio $P(P_k = \sigma)/P(P_k = -\sigma)$ at wave number $k = 32$, and plot the corresponding GCFR prediction using the constant C as a fitting parameter. We average over a range τ of length 285 linear time periods of the mode $k = 32$, once the system has reached a non-equilibrium steady state. Figure 3.8 is consistent with the GCFR at low fluctuations. However, at larger fluctuations, the curve deviates from the GCFR prediction. We note, that the numerical data may not be sufficiently averaged. However, there is a distinct possibility that this deviation may be a consequence of some nonlinear behaviour [125], thus further investigation is needed.

In this Chapter, we have considered the role of Kelvin waves in QT. We have systematically calculated analytical expressions for the BSE Hamiltonian, and used WT theory presented in Chapter 2 to derive the KZ solutions to the KE. With further investigation, we found that the KS spectrum for the direct energy cascade in Kelvin waves is actually non-local. This implies that the KS spectrum is physically irrelevant. We discuss the proposed non-local theory to Kelvin waves, and perform numerical simulations of the LNE that supports the predictions of the non-local theory.

Chapter 4

Optical Wave Turbulence

OWT is the study of WT in light waves propagating in a nonlinear medium. OWT demonstrates similar behaviour to fluid dynamics, such as vortex-like solutions [69, 70], shock waves [68], and statistical properties of weakly interacting nonlinear random waves [20]. Although there have been numerous theoretical and numerical studies of OWT [65, 142, 143, 144, 62], there have been few experimental observations to date [8]. OWT was theoretically predicted to exhibit dual cascade properties when two conserved quantities cascade to opposite ends of wave number space [65]. This is analogous to 2D turbulence, where we observe an inverse cascade of energy and a direct cascade of enstrophy [101, 102]. In the context of OWT, energy cascades to high wave numbers, while wave action cascades towards low wave numbers [65, 142, 143, 144]. An interesting property of OWT is the inverse cascade of wave action which in the optical context implies the condensation of photons - the optical analogue of BEC.

Experimental implementation of BEC in alkali atoms was first achieved in 1995, and subsequently awarded the 2001 Nobel prize [145, 146]. This work involved developing a sophisticated cooling technique to micro-Kelvin temperatures, in order to make the de Broglie wave length exceed the average inter-particle distance. This is known as the BEC condition. Photons were actually the first bosons introduced by Bose in 1924 [147], and the BEC condition is easily satisfied by light at room temperature. However, there was the belief that optical BEC would be impossible, because of the fundamental difference between atoms, whose numbers are conserved and photons which can be ran-

domly emitted and absorbed. However, we can think of situations where light is neither emitted nor absorbed, e.g. light in an optical cavity, reflected back and forth by mirrors [148], or light freely propagating through a transparent medium. In the latter, the movement of photons to different energy states (specifically the lowest one corresponding to BEC) can be achieved by nonlinear wave interactions. The mechanism for these nonlinear wave interactions is provided by the Kerr effect which permits wave mixing.

When the nonlinearity of the system is weak, OWT can be described by WT theory [6], with the prediction of two KZ states in a dual cascade system. One aspect of OWT is the inverse cascade of wave action, with the progression of wave action towards large scales, where the nonlinearity of the system is predicted to grow. This will eventually lead to a violation of the weak nonlinearity assumption of WT theory. The high nonlinearity at low wave numbers will lead to the formation of coherent structures [65, 143, 62, 72, 84, 73]. In OWT this corresponds to the formation of solitons and collapses for focusing nonlinearity [8], or a quasi-uniform condensate and vortices in the de-focusing case [62]. Experimentally, OWT is produced by propagating light through a nonlinear medium, such as a liquid crystal (LC). However, the nonlinearity is typically very weak and it is a challenge to make it overpower the dissipation of the LC. This is the main obstacle regarding the photon condensation setup in a 2D optical Fabry-Perot cavity, theoretically suggested in [148] but never experimentally implemented.

In this Chapter, we present the first ever conducted experimental setup for OWT. We compare the experimental observations with the predictions of WT theory. The key feature in our setup is to trade one spatial dimension for a time axis, i.e. we consider a time-independent 2D light field where the principal direction of the light propagation acts as time. This allows us to use a nematic LC, which provides a high level of tunable optical nonlinearity [149, 150]. The slow relaxation time of the reorientational dynamics is not a restriction of our setup because the system is steady in time. Similar experiments were first reported in [151], where a beam propagating inside a nematic layer undergoes a strong self-focusing effect followed by filamentation, soliton formation and an increase in light intensity. Recently, a renewed interest in the same setup has led to further studies on optical solitons and modulational instability (MI) regimes [152, 153, 154]. However,

the previous experiments used a high input intensity, implying a strong nonlinearity of the system, and therefore the soliton condensate appears immediately, bypassing the WT regime.

In our experiment, we set up an initial condition of weakly nonlinear waves situated towards high wave numbers from a laser beam. We randomise the phase of the beam, so that we produce a wave field as close to RPA as possible. The nonlinearity of the system is provided by the LC, controlled by a voltage applied across the LC cell. This provides the means for nonlinear wave mixing via the Kerr effect. The LC we use is of a focusing type, causing any condensate that forms to become unstable and the formation of solitons to occur via a MI.

Experimentally we cannot force the system, therefore we consider a decaying setup - with the initial condition relaxing as the beam propagates through the LC cell. Fortunately, this does not pose a problem, as the inverse cascade spectrum is of a finite capacity type - i.e. that only a finite amount of the cascading invariant (wave action in this case) is needed to fill the infinite inertial range. In these cases the turbulent systems have a long transient en route to the final thermodynamic equilibrium state, in which the scaling is of KZ type. This is because the initial condition serves as a huge reservoir of the cascading invariant. Note, that the situation here is not specific to WT and is generally valid for turbulence. For example, it is valid for Navier-Stokes turbulence, e.g. the Kolmogorov-Obukhov spectrum is also finite capacity. We emphasise that our work is on the turbulent non-equilibrium transition leading to the thermalised state and not the thermodynamic equilibrium itself.

The final thermalised state was extensively theoretically studied in various settings for non-integrable Hamiltonian systems starting with the pioneering paper by Zakharov *et al* [155], and then subsequently in [156, 157, 158, 159, 160, 161, 162, 163, 164, 165]. The final state, with a single soliton and small scale noise, was interpreted as a statistical attractor, and an analogy was pointed out to the over-saturated vapour system, where the solitons are similar to droplets and the random waves behave as molecules [165]. Here, small droplets evaporate whilst large droplets gain in size from free molecules, resulting in a decrease in the number of droplets.

4.1 The Experimental Setup

The experimental apparatus is shown in Figure 4.1a. It consists of a LC cell, inside which a laminar shaped beam propagates. The input beam is prepared in such a way, as to have an initial condition of weakly nonlinear random waves. The LC cell is made by sandwiching a nematic layer, (E48), of thickness $d = 50 \mu m$, between two $20 \times 30 mm^2$, glass windows and is schematically depicted in Figure 4.1b. On the interior, the glass walls are coated with indium-tin-oxide transparent electrodes. We have pre-treated the indium-tin-oxide surfaces with polyvinyl-alcohol, polymerised and then rubbed, in order to align all the molecules parallel to the confining walls. When a voltage is applied across the cell, LC molecules tend to orientate in such a way as to become parallel to the direction of the electric field. By applying a $1 kHz$ electric field with a rms voltage of $V_0 = 2.5 V$ we preset the molecular director to an average tilt angle Θ .

The LC layer behaves as a positive uni-axial medium, where $n_{||} = n_z = 1.7$ is the extraordinary refractive index and $n_{\perp} = 1.5$, the ordinary refractive index [150]. LC molecules tend to align along the applied field and the refractive index, $n(\Theta)$, follows the distribution of the tilt angle θ . When a linearly polarised beam is injected into the cell, the LC molecules orientate towards the direction of the incoming beam polarisation. The input light comes from a diode pumped, solid state laser, with $\lambda = 473 nm$, polarised along y and shaped as a thin laminar Gaussian beam of $30 \mu m$ thickness. The beam evolution inside the cell is monitored with an optical microscope and a CCD camera. The light intensity is kept very low, with an input intensity of $I = 30 \mu W/cm^2$ to ensure the weakly nonlinear regime. A spatial light modulator (SLM), at the entrance of the cell is used to produce suitable intensity masks for injecting random phased fields with large wave numbers.

Figure 4.2 depicts how the input light beam is prepared before entering the LC cell. The beam is expanded and collimated through the spatial light filter shown in Figure 4.2. The objective, OB, focuses the light into the $20 \mu m$ pinhole, PH, the lens L_1 collimates the beam with a waist of $18 mm$. After that, the light passes through the SLM, which is a LCD screen working in transmission with a resolution of 800×600 , with 8 bits pixels, of size $14 \mu m$. Each pixel is controlled through a personal computer PC,

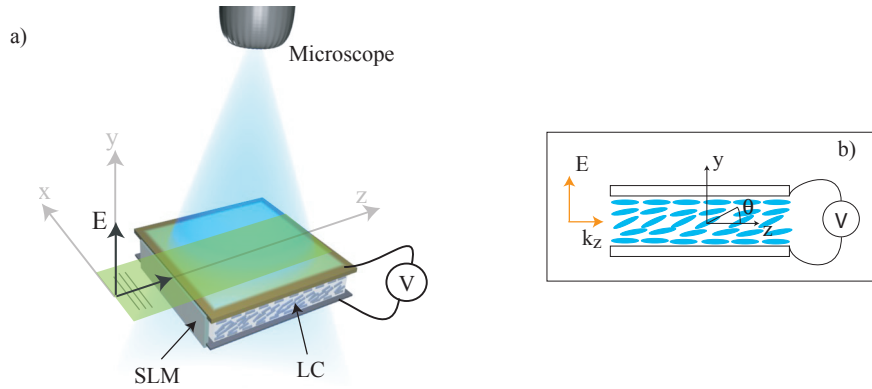


Figure 4.1: a) Sketch of the experimental setup: a laminar shaped input beam propagates inside the LC layer; random phase modulations are imposed at the entrance of the cell by means of a SLM. b) Schematic of the LC cell. Figure courtesy of Umberto Bortolozzo and Stefania Residori.

to ensure that the outgoing light is intensity modulated. In our case we use a cosinus modulation having a coloured noise envelope. The lenses, L_3 and L_4 , are used to focus the image from the LCD screen at the entrance of the LC cell. The half wave-plate, W, together with the polariser, P, are used to control the intensity and the polarisation, which is linear along the y -axis. The circular aperture is inserted in the focal plane to filter out the diffraction given by the pixelisation of the SLM and the diffuser, PH, is inserted to spatially randomise the phase of the light. In order to inject the light inside the LC cell, we use a cylindrical lens, L_4 , close to the entrance of the LC layer.

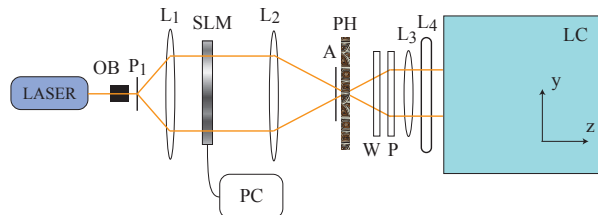


Figure 4.2: Detailed representation of the experimental setup, showing the initialisation of the input laser beam. Figure courtesy of Umberto Bortolozzo and Stefania Residori.

4.2 Equations for Optical Wave Turbulence

Theoretically, the experimental setup can be modelled by an evolution equation for the input beam, coupled to a relaxation equation for the LC dynamics given by

$$2iq\frac{\partial\psi}{\partial z} + \frac{\partial^2\psi}{\partial x^2} + k_0^2 n_a^2 a\psi = 0, \quad (4.1a)$$

$$\frac{\partial^2 a}{\partial x^2} - \frac{1}{l_\xi^2} a + \frac{\varepsilon_0 n_a^2}{4K} |\psi|^2 = 0, \quad (4.1b)$$

where $\psi(x, z)$ is the complex amplitude of the input beam propagating along the time axis z ; x is the coordinate across the beam; $a(x, z)$ is the LC reorientation angle; $n_a = n_e - n_o$ is the birefringence of the LC; k_0 is the optical wave number; ε_0 is the vacuum permittivity; and $l_\xi = \sqrt{\pi K / 2\Delta\varepsilon}(d/V_0)$ is the electrical coherence length of the LC [166], with K being the elastic constant, $q^2 = k_0^2 (n_o^2 + n_a^2/2)$ and $\Delta\varepsilon$ is the dielectric anisotropy. Note that l_ξ fixes the typical dissipation scale, limiting the extent of the inertial range in which the OWT cascade develops. In other contexts, (see [152, 153, 154]), such a spatial diffusion of the molecular deformation has been denoted as a non-local effect. In our experiment, when $V_0 = 2.5$ V, we have that $l_\xi = 9$ μm . The typical value of K in the experiment is of the order ~ 10 pN, thus we can derive a typical dissipation length scale of the order ~ 10 μm .

4.2.1 The Evolution Equation

The evolution equations, (4.1), can be simplified by de-coupling the complex amplitude of the input beam, $\psi(x, z)$, to the LC reorientation angle, $a(x, z)$. This can be achieved by formally inverting the operator on $a(x, z)$ in Equation (4.1b), yielding a single equation for the evolution of $\psi(x, z)$ along the LC cell. Equation (4.1b) implies that

$$a(x, z) = \frac{\varepsilon_0 n_a^2}{4K} \left(\frac{1}{l_\xi^2} - \frac{\partial^2}{\partial x^2} \right)^{-1} |\psi|^2. \quad (4.2)$$

Substituting this expression for $a(x, z)$ into Equation (4.1a), we eliminate the dependence on variable $a(x, z)$. This gives

$$2iq\frac{\partial\psi}{\partial z} + \frac{\partial^2\psi}{\partial x^2} + \frac{k_0^2 n_a^4 \varepsilon_0}{4K} \psi \left(\frac{1}{l_\xi^2} - \frac{\partial^2}{\partial x^2} \right)^{-1} |\psi|^2 = 0. \quad (4.3)$$

Equation (4.3) is a single equation modelling the evolution of the complex amplitude, $\psi(x, z)$. Scale invariance of the system is a necessary property for the application of WT theory. If we apply the procedures of Chapter 2, we find that Equation (4.3) does not lead to a scale invariant nonlinear interaction coefficient. There are two ways in which we can proceed, although we reach the same final outcome regardless. Firstly, we could derive a KE for (4.3), and then take a limit of long and short wave numbers ($kl_\xi \ll 1$ and $1 \ll kl_\xi$ respectively). Secondly, we could take the long- and short-wave limits of Equation (4.3), deriving new evolution equations for $\psi(x, z)$ in each limit, and then apply the WT approach¹. Here, we use the latter procedure. The limitations imposed by the dissipation of the LC prevent the experimental implementation in the short-wave limit. However, we will continue to investigate this limit theoretically and numerically.

4.2.2 The Long-Wave Equation

The long-wave approximation to Equation (4.3) corresponds to the light wave length $\lambda \propto 1/k$ being greater than the electrical coherence length of the LC, l_ξ . In physical space, this limit corresponds to $l_\xi \partial/\partial x \ll 1$, which we can use to expand the nonlinear operator of Equation (4.3) to give us

$$\left(\frac{1}{l_\xi^2} - \frac{\partial^2}{\partial x^2} \right)^{-1} = l_\xi^2 \left(1 + l_\xi^2 \frac{\partial^2}{\partial x^2} + l_\xi^4 \frac{\partial^4}{\partial x^4} + \dots \right). \quad (4.4)$$

Taking the leading order of this expansion yields

$$2iq\frac{\partial\psi}{\partial z} = -\frac{\partial^2\psi}{\partial x^2} - \frac{\varepsilon_0 n_a^4 l_\xi^2 k_0^2}{4K} \psi |\psi|^2. \quad (4.5)$$

¹It has been checked by us that both ways yield the same interaction coefficients in each limit.

Equation (4.5) is the 1D NLSE. Unfortunately, this would be a poor model for OWT, as the 1D NLSE is an integrable model. The 1D NLSE can be exactly solved by the inverse scattering transform [167], resulting in solutions that correspond to solitary waves or solitons. Integrability of a system implies that wave turbulent interactions are not possible. To overcome this, we must consider the sub-leading contribution of Expansion (4.4). This extra nonlinear term breaks the integrability of the system, giving rise to

$$2iq \frac{\partial \psi}{\partial z} = -\frac{\partial^2 \psi}{\partial x^2} - \frac{\varepsilon_0 n_a^4 l_\xi^2 k_0^2}{4K} \left(\psi |\psi|^2 + l_\xi^2 \psi \frac{\partial^2 |\psi|^2}{\partial x^2} \right). \quad (4.6)$$

We refer to Equation (4.6) as the LWE. As a consequence of Expansion (4.4), the additional nonlinear term is of smaller order than the leading nonlinear term. Moreover, note that the additional nonlinear contribution is smaller than the linear term in the weak nonlinearity setting. Therefore, although we have lost integrability, the system will remain close to the integrable one, (4.5). As a result, we expect to observe, in the final condensed state, soliton-like solutions close to the exact solutions of (4.5). Exact soliton solutions of Equation (4.5), do not change shape and have the ability to pass through one another unchanged. We can postulate that in the LWE, (4.6), we will observe similar solitons, but the non-integrability will allow solitons to interact with other solitons, and with the weakly nonlinear random wave background.

4.2.3 The Short-Wave Equation

Before we apply the WT description of Chapter 2, let us consider the opposite limit of Equation (4.3), when $1 \ll l_\xi^2 \partial^2 / \partial x^2$. The nonlinear operator of Equation (4.3) can be represented in terms of a Taylor expansion as

$$\left(\frac{1}{l_\xi^2} - \frac{\partial^2}{\partial x^2} \right)^{-1} = - \left(\frac{\partial^2}{\partial x^2} \right)^{-1} + \frac{1}{l_\xi^2} \left(\frac{\partial^2}{\partial x^2} \right)^{-2} - \dots \quad (4.7)$$

It is sufficient for us to approximate the nonlinear operator of Equation (4.3) with just the leading order term in Expansion (4.7), as integrability is not a factor. Therefore, we

get an equation of the form:

$$2iq \frac{\partial \psi}{\partial z} = -\frac{\partial^2 \psi}{\partial x^2} + \frac{\varepsilon_0 n_a^4 k_0^2}{4K} \psi \left(\frac{\partial^2}{\partial x^2} \right)^{-1} |\psi|^2. \quad (4.8)$$

We denote Equation (4.8) as the SWE. Consequently, we have derived two equations from the long- and short-wave limits of system (4.3). We will proceed, by applying the WT description to both the LWE and the SWE and compare the predictions with experimental and numerical observations.

4.3 The Hamiltonian Formulation

Systems (4.6) and (4.8) conserve two quantities, energy \mathcal{H} and wave action \mathcal{N} . If we define the equation for a Hamiltonian system as

$$2iq \frac{\partial \psi}{\partial z} = \frac{\delta \mathcal{H}}{\delta \psi^*}, \quad (4.9)$$

then the LWE possesses a Hamiltonian of

$$\begin{aligned} \mathcal{H}^L &= \mathcal{H}_2 + \mathcal{H}_4^L, \\ &= \int \left| \frac{\partial \psi}{\partial x} \right|^2 - \frac{\varepsilon_0 n_a^4 l_\xi^2 k_0^2}{8K} \left[|\psi|^4 - l_\xi^2 \left(\frac{\partial |\psi|^2}{\partial x} \right)^2 \right] dx. \end{aligned} \quad (4.10a)$$

In the nonlinear energy term \mathcal{H}_4 , the term that is quartic with respect to ψ , we have added a superscript L to denote that this quartic term corresponds to the LWE, (4.6). Similarly, the SWE can be written in Hamiltonian form:

$$\begin{aligned} \mathcal{H}^S &= \mathcal{H}_2 + \mathcal{H}_4^S, \\ &= \int \left| \frac{\partial \psi}{\partial x} \right|^2 - \frac{\varepsilon_0 n_a^4 k_0^2}{8K} \left(\frac{\partial^{-1} |\psi|^2}{\partial x^{-1}} \right)^2 dx. \end{aligned} \quad (4.10b)$$

In both the LWE and the SWE, the linear, (quadratic), energy \mathcal{H}_2 is of the same form. In addition to energy conservation, there is a second invariant of both equation, the wave action, \mathcal{N} . This is a consequence arising from the fact that both equations

correspond to even order wave interactions².

The total wave action, \mathcal{N} , is defined as

$$\mathcal{N} = \int |\psi|^2 dx. \quad (4.11)$$

Hamiltonians (4.10) can be written in the form of Equation (2.25), by applying the Fourier representation (2.16) to function $\psi(x, z)$. Subsequently, Hamiltonian (4.10a) possesses the following interaction coefficients:

$$\omega_k = k^2, \quad (4.12a)$$

$$\begin{aligned} {}^L T_{3,4}^{1,2} &= {}^1 T_{3,4}^{1,2} + {}^2 T_{3,4}^{1,2} \\ &= -\frac{\varepsilon_0 n_a^4 l_\xi^2 k_0^2}{2K} + \frac{\varepsilon_0 n_a^4 l_\xi^4 k_0^2}{4K} (\mathbf{k}_1 \mathbf{k}_4 + \mathbf{k}_2 \mathbf{k}_3 + \mathbf{k}_2 \mathbf{k}_4 + \mathbf{k}_1 \mathbf{k}_3 \\ &\quad - 2\mathbf{k}_3 \mathbf{k}_4 - 2\mathbf{k}_1 \mathbf{k}_2), \end{aligned} \quad (4.12b)$$

$$W_{4,5,6}^{1,2,3} = 0. \quad (4.12c)$$

We denote the two contributions to ${}^L T_{3,4}^{1,2}$, from both nonlinear terms in (4.6), as ${}^1 T_{3,4}^{1,2}$ and ${}^2 T_{3,4}^{1,2}$, where the first arises from the usual cubic nonlinearity seen in the 1D NLSE, and the second from the sub-leading correction. Similarly, the SWE yields the following coefficients:

$$\omega_k = k^2, \quad (4.13a)$$

$${}^S T_{3,4}^{1,2} = \frac{\varepsilon_0 n_a^4 l_\xi^4 k_0^2}{4K} \left(\frac{1}{\mathbf{k}_1 \mathbf{k}_3} + \frac{1}{\mathbf{k}_2 \mathbf{k}_3} + \frac{1}{\mathbf{k}_1 \mathbf{k}_4} + \frac{1}{\mathbf{k}_2 \mathbf{k}_4} - \frac{2}{\mathbf{k}_1 \mathbf{k}_2} - \frac{2}{\mathbf{k}_3 \mathbf{k}_4} \right) \quad (4.13b)$$

$$W_{4,5,6}^{1,2,3} = 0. \quad (4.13c)$$

We have expressed the LWE and SWE in terms of the six-wave Hamiltonian system of Chapter 2. We mentioned in Subsection 4.2.1 that the full evolution equation, (4.3), also emits a Hamiltonian structure. For completeness, we derive the corresponding interaction coefficients for Equation (4.3) and show that we can recover (4.12) and (4.13) by taking limits.

²This is a consequence of an extra symmetry property of the equation. The $U(1)$ gauge symmetry or invariance with respect to a phase shift: $\psi(x, z) \rightarrow \psi(x, z) \exp(i\phi)$.

4.4 The Hamiltonian Representation for the Evolution Equation

We mentioned previously that a KE for Equation (4.3) can be directly calculated. This is because (4.3) also possesses a Hamiltonian formulation with interaction coefficients given by

$$\omega_k = k^2, \quad (4.14a)$$

$$\begin{aligned} {}^F T_{3,4}^{1,2} &= -\frac{\varepsilon_0 n_a^4 l_\xi^2 k_0^2}{8K} \left(\frac{1}{l_\xi^2 (\mathbf{k}_4 - \mathbf{k}_1)^2 + 1} + \frac{1}{l_\xi^2 (\mathbf{k}_3 - \mathbf{k}_1)^2 + 1} \right. \\ &\quad \left. + \frac{1}{l_\xi^2 (\mathbf{k}_4 - \mathbf{k}_2)^2 + 1} + \frac{1}{l_\xi^2 (\mathbf{k}_3 - \mathbf{k}_2)^2 + 1} \right), \end{aligned} \quad (4.14b)$$

$$W_{4,5,6}^{1,2,3} = 0. \quad (4.14c)$$

A further verification, that the LWE and the SWE are correct, is given by checking the asymptotic limit of ${}^F T_{3,4}^{1,2}$ in the limits of $kl_\xi \ll 1$ and $1 \ll kl_\xi$. Indeed, we find that

$$\lim_{kl_\xi \rightarrow 0} {}^F T_{3,4}^{1,2} = {}^L T_{3,4}^{1,2}, \quad (4.15a)$$

$$\lim_{kl_\xi \rightarrow \infty} {}^F T_{3,4}^{1,2} = {}^S T_{3,4}^{1,2}, \quad (4.15b)$$

i.e. that the long- and short-wave limits of the Equation (4.3) are exactly the LWE and SWE respectively, either before or after the formulation of the Hamiltonian.

4.5 The Nonlinearity Parameter

To verify that experimental and numerical simulations are in a weakly nonlinear regime, we need to quantify the linearity and nonlinearity within the system. In this Section, we present the nonlinear parameter, J , which is determined by the ratio of the linear term to the nonlinear term within the dynamical equations.

The nonlinear parameter from the LWE (4.6) is defined as

$$J^L = \frac{4Kk^2}{\varepsilon_0 n_a^4 k_0^2 l_\xi^2 I}. \quad (4.16)$$

This is derived from the ratio of the linear term and the first of the two nonlinear terms. Here, $I = \langle |\psi(x, 0)|^2 \rangle$ is the average value of the input intensity. Similarly, the SWE, (4.8) yields a parameter of

$$J^S = \frac{4Kk^4}{\varepsilon_0 n_a^4 k_0^2 I}. \quad (4.17)$$

Calculation of J^L and J^S act as a verification of the weak nonlinear assumption of WT, especially in the context of the experimental setup.

4.6 Scale Invariance of $\mathcal{W}_{4,5,6}^{1,2,3}$

Scale invariance of the interaction coefficients are essential for the prediction of the KZ solutions of the KE. First, we consider the LWE. The four-wave interaction coefficient of the LWE, (4.12b), contains two terms, each with a different scaling in wave number k , where all four wave numbers are of the same order, i.e. $k_1, k_2, k_3, k_4 \propto k$. This does not necessarily pose a problem, however, let us consider the structure of the final six-wave interaction coefficient, $\mathcal{W}_{4,5,6}^{1,2,3}$, after we have applied the CT, (2.38). In fact, for the LWE, we can represent the final six-wave interaction coefficient as a sum of three contributions:

$${}^L\mathcal{W}_{4,5,6}^{1,2,3} = {}^1\mathcal{W}_{4,5,6}^{1,2,3} + {}^2\mathcal{W}_{4,5,6}^{1,2,3} + {}^3\mathcal{W}_{4,5,6}^{1,2,3}, \quad (4.18a)$$

where

$${}^1\mathcal{W}_{4,5,6}^{1,2,3} = -\frac{1}{8} \sum_{\substack{i,j,m=1 \\ i \neq j \neq m \neq i}}^3 \sum_{\substack{p,q,r=4 \\ p \neq q \neq r \neq p}}^6 \frac{{}^1T_{p,q}^{p+q-i,i} {}^1T_{j,m}^{j+m-r,r}}{\omega_{j,m}^{j+m-r,r}} + \frac{{}^1T_{i,j}^{i+j-p,p} {}^1T_{q,r}^{q+r-m,m}}{\omega_{q,r}^{q+r-m,m}}, \quad (4.18b)$$

$${}^2\mathcal{W}_{4,5,6}^{1,2,3} = -\frac{1}{8} \sum_{\substack{i,j,m=1 \\ i \neq j \neq m \neq i}}^3 \sum_{\substack{p,q,r=4 \\ p \neq q \neq r \neq p}}^6 \left[\frac{{}^1T_{p,q}^{p+q-i,i} {}^2T_{j,m}^{j+m-r,r}}{\omega_{j,m}^{j+m-r,r}} + \frac{{}^1T_{i,j}^{i+j-p,p} {}^2T_{q,r}^{q+r-m,m}}{\omega_{q,r}^{q+r-m,m}} \right. \\ \left. + \frac{{}^2T_{p,q}^{p+q-i,i} {}^1T_{j,m}^{j+m-r,r}}{\omega_{j,m}^{j+m-r,r}} + \frac{{}^2T_{i,j}^{i+j-p,p} {}^1T_{q,r}^{q+r-m,m}}{\omega_{q,r}^{q+r-m,m}} \right], \quad (4.18c)$$

and

$${}^3\mathcal{W}_{4,5,6}^{1,2,3} = -\frac{1}{8} \sum_{\substack{i,j,m=1 \\ i \neq j \neq m \neq i}}^3 \sum_{\substack{p,q,r=4 \\ p \neq q \neq r \neq p}}^6 \frac{{}^2T_{p,q}^{p+q-i,i} {}^2T_{j,m}^{j+m-r,r}}{\omega_{j,m}^{j+m-r,r}} + \frac{{}^2T_{i,j}^{i+j-p,p} {}^2T_{q,r}^{q+r-m,m}}{\omega_{q,r}^{q+r-m,m}}. \quad (4.18d)$$

The three contributions have different orders in kl_ξ - the small parameter arising from the long-wave limit. Therefore, ${}^1\mathcal{W}_{4,5,6}^{1,2,3} \propto (kl_\xi)^4$ is the leading contribution to the six-wave dynamics, followed by ${}^2\mathcal{W}_{4,5,6}^{1,2,3} \propto (kl_\xi)^6$ and finally ${}^3\mathcal{W}_{4,5,6}^{1,2,3} \propto (kl_\xi)^8$.

The first term in Expansion (4.18), ${}^1\mathcal{W}_{4,5,6}^{1,2,3}$, is generated from the coupling of the leading cubic, nonlinear term of (4.6) with itself. If we were to consider the 1D NLSE, then the six-wave interaction coefficient would only consist of the contribution ${}^1\mathcal{W}_{4,5,6}^{1,2,3}$, as ${}^2T_{3,4}^{1,2} \equiv 0$. Integrability of the 1D NLSE implies that ${}^1\mathcal{W}_{4,5,6}^{1,2,3}$ is zero when the six-wave resonance condition is satisfied. We verify this by using parameterisation, (2.112), in Mathematica.

The main contribution to the six-wave dynamics arises from the first non-zero term in (4.18), ${}^2\mathcal{W}_{4,5,6}^{1,2,3}$. This contribution, with the use of (2.112), gives a \mathbf{k} -independent result:

$$L\mathcal{W}_{4,5,6}^{1,2,3} \approx {}^2\mathcal{W}_{4,5,6}^{1,2,3} = \frac{9\varepsilon_0^2 n_a^8 l_\xi^6 k_0^4}{16K^2}. \quad (4.19)$$

Conversely, from the SWE, we see that the four-wave interaction coefficient, ${}^S T_{3,4}^{1,2}$, is scale invariant and scales as $\propto k^{-2}$ when considering $k_1, k_2, k_3, k_4 \propto k$. Formula (2.38), implies that the homogeneity coefficients for the LWE and SWE are $\beta^L = 0$ and $\beta^S = -6$ respectively. We omit the explicit expression for ${}^S\mathcal{W}_{4,5,6}^{1,2,3}$ as it extremely long. With these homogeneity coefficients, we are able to determine the solutions to the KE.

4.7 The Kolmogorov-Zakharov Solutions of Optical Wave Turbulence

With the aid of the homogeneity coefficients calculated in the previous Section, we can derive the energy and wave action KZ solutions for a non-equilibrium stationary state in the LWE and the SWE. Results (2.111) imply that the KZ solutions for the LWE are given by

$${}^L n_k^{\mathcal{H}} = C_{\mathcal{H}}^L \left(\frac{P_{\mathbf{k}} K^4}{\varepsilon_0^4 n_a^{16} l_{\xi}^{12} k_0^8} \right)^{1/5} k^{-1}, \quad (4.20a)$$

$${}^L n_k^{\mathcal{N}} = C_{\mathcal{N}}^L \left(\frac{Q_{\mathbf{k}} K^4}{\varepsilon_0^4 n_a^{16} l_{\xi}^{12} k_0^8} \right)^{1/5} k^{-3/5}, \quad (4.20b)$$

where ${}^L n_k^{\mathcal{H}}$, is the KZ spectrum for the direct energy cascade, and ${}^L n_k^{\mathcal{N}}$ is the inverse wave action spectrum. Here, $C_{\mathcal{H}}^L$ and $C_{\mathcal{N}}^L$ are constant prefactors of the spectra. The same analysis implies that the SWE contains the following KZ solutions:

$${}^S n_k^{\mathcal{H}} = C_{\mathcal{H}}^S \left(\frac{P_{\mathbf{k}} K^4}{\varepsilon_0^4 n_a^{16} l_{\xi}^{16} k_0^8} \right)^{1/5} k^{7/5}, \quad (4.21a)$$

$${}^S n_k^{\mathcal{N}} = C_{\mathcal{N}}^S \left(\frac{Q_{\mathbf{k}} K^4}{\varepsilon_0^4 n_a^{16} l_{\xi}^{16} k_0^8} \right)^{1/5} k^{9/5}, \quad (4.21b)$$

where, $C_{\mathcal{H}}^S$ and $C_{\mathcal{N}}^S$ are constant coefficients of $\mathcal{O}(1)$.

Solutions (4.20) and (4.21) are valid only if they correspond to local wave interactions, therefore we must check that the collision integral converges for both systems.

4.8 Locality of Optical Wave Turbulence

In this Section, we will investigate whether the KZ solutions for OWT correspond to local wave interactions. This is achieved by checking if the collision integral converges, whilst assuming a KZ solution. We begin by investigating locality in the LWE. The six-wave interaction coefficient ${}^L \mathcal{W}_{4,5,6}^{1,2,3}$ was shown (at leading order) to be constant in Equation (4.19). This implies that in the IR limit, ${}^L \mathcal{W}_{4,5,6}^{1,2,3}$ remains constant, i.e. $\xi = 0$.

Hence, the condition for IR convergence becomes

$$x < 1, \quad (4.22)$$

when x is the exponent for n_k . For KZ solutions, (4.20), we have that the direct cascade of energy, when $x = 1$, implies divergence. However, the cascade only contradicts Relation (4.22) at equality, resulting in slow logarithmic divergence of the collision integral (see Chapter 3). This implies that by taking into account a logarithmic dependence to Spectrum (4.20a), we can prevent divergence of the collision integral. The inverse cascade of wave action, with $x = 3/5$, implies convergence in the IR region.

Before a spectrum is deemed convergent, we must check for convergence in the UV region. Due to Relation (4.19), we also have that $\eta = 0$, and therefore, the condition for UV convergence is given by

$$\max(-2x - 2, -2x) < 0. \quad (4.23)$$

For both long-wave KZ solutions, (4.20), Condition (4.23) is satisfied. Thus giving total convergence of the inverse cascade, and only convergence of the direct cascade in the UV limit.

Consideration of the SWE in the IR region, implies that the six-wave interaction coefficient, ${}^S\mathcal{W}_{4,5,6}^{1,2,3}$, behaves as

$$\lim_{k_6 \rightarrow 0} {}^S\mathcal{W}_{4,5,6}^{1,2,3} \propto k_6^{-1}, \quad (4.24)$$

giving $\xi = -1$. Therefore, the condition for IR convergence of the KZ solutions becomes

$$x < -1. \quad (4.25)$$

For both KZ solutions, (4.21), where $x = -7/5$ and $x = -9/5$ for the direct and inverse spectra respectively, we have IR convergence. For total convergence, we must also have that both KZ solutions are convergent in the UV region. Interaction coefficient ${}^S\mathcal{W}_{4,5,6}^{1,2,3}$

in the limit of $\mathbf{k}_6 \rightarrow \infty$ scales as

$$\lim_{\mathbf{k}_6 \rightarrow \infty} {}^S\mathcal{W}_{4,5,6}^{1,2,3} \propto k_6^0, \quad (4.26)$$

thus $\eta = 0$. This implies that the UV condition for convergence is the same as Relation (4.23). Both short-wave KZ solutions, (4.21) do not satisfy the UV convergence condition. Therefore, both short-wave KZ solutions are non-local spectra. Non-locality of the KZ solutions implies that the local wave interaction assumption is incorrect, and thus the approach taken to predict these spectra is invalid. However, the development of a non-local theory to OWT for the SWE may yield further insight.

4.9 Logarithmic Corrections to the Direct Energy Spectrum

In the previous Section, the direct energy cascade in the LWE, (4.20a), was shown to be marginally divergent in the IR limit. This is to say, that the collision integral diverges at a logarithmic rate in the limit of one vanishing wave number. However, by considering a logarithmic dependence to the KZ solution, we can produce a convergent collision integral. Following Kraichnan's argument [101, 102], let us assume a correction of the form:

$${}^L n_{\mathbf{k}}^{\mathcal{H}} = C_{\mathcal{H}}^L \left(\frac{P_{\mathbf{k}} K^4}{\varepsilon_0^4 n_a^{16} l_{\xi}^{12} k_0^8} \right)^{1/5} k^{-1} \ln^{-y}(k\ell), \quad (4.27)$$

where y is some power law to be found and ℓ is the scale of energy injection. The exponent of the logarithmic power law, y , is calculated by assuming that the energy flux, $P_{\mathbf{k}}$, remains \mathbf{k} -independent. Subsequently, the energy flux can be expressed as

$$P_{\mathbf{k}} = \int^{\mathbf{k}} \omega_k \frac{\partial n_{\mathbf{k}}}{\partial t} d\mathbf{k} \propto \int^{\mathbf{k}} k^4 n_{\mathbf{k}}^5 d\mathbf{k} \propto \int^{\mathbf{k}} k^{-1} \ln^{-5y}(k\ell) d\mathbf{k}, \quad (4.28)$$

where we have used that the collision integral, (2.94), with interaction coefficients (4.12), scales as $\dot{n}_{\mathbf{k}} \propto k^2 n_{\mathbf{k}}^5$. Therefore, $P_{\mathbf{k}}$ remains \mathbf{k} -independent³ when $y = 1/5$.

³The energy flux is actually proportional to $P_{\mathbf{k}} \propto \ln(\ln(k\ell))$.

This implies that the logarithmically corrected direct energy KZ spectrum is given by

$${}^L n_{\mathbf{k}}^{\mathcal{H}} = C_{\mathcal{H}}^L \left(\frac{P_{\mathbf{k}} K^4}{\varepsilon_0^4 n_a^{16} l_{\xi}^{12} k_0^8} \right)^{1/5} k^{-1} \ln^{-1/5}(k\ell). \quad (4.29)$$

Hence, by considering a logarithmic contribution, Spectrum (4.20a) is a local KZ solution of the KE and thus physically realisable.

4.10 Flux Directions in Optical Wave Turbulence

The Fjørtoft argument of Section 2.14, showed the directions of \mathbf{k} -space in which energy and wave action are permitted to flow. However, the direction of the invariant cascade is ultimately determined by the sign of the invariant's flux. Therefore, it is essential that the direction of the flux agrees with the analysis of Fjørtoft's argument.

We use the formulation of the DAM in Section 2.18, to determine the directions of the energy and wave action fluxes P_{ω} and Q_{ω} within the LWE. Non-locality of the KZ solution (4.21) of the SWE implies that constant flux cascades do not occur and thus the analysis of this Section does not apply.

By plotting formulae (2.139c) and (2.139d) for P_{ω} and Q_{ω} against the exponent of the KZ solution, x , we can qualitatively determine the sign of the fluxes. When the exponent is that of both thermodynamic solutions (2.109), then both fluxes should vanish. Moreover, to agree with Fjørtoft's argument, when $x = 1$, the energy flux should be *positive* and the wave action flux zero. Similarly, when the exponent agrees with the KZ exponent of the inverse cascade, (4.20b), Fjørtoft's argument implies that the wave action flux should be *negative*.

In Figure 4.3, we plot Equations (2.139), for P_{ω} and Q_{ω} . we observe that at $x = 0, 2$ corresponding to the two thermodynamic equilibrium solutions, we have both the energy and wave action fluxes identically zero. At $x = 3/5$, corresponding to the wave action cascade, we have that the energy flux P_{ω} is zero, whilst the wave action flux Q_{ω} is *positive*. When $x = 1$, the exponent for the energy cascade, we have the wave action flux Q_{ω} is zero, and the energy flux P_{ω} *negative*.

From Formulae (2.139c) and (2.139d), we have wave action flowing to small scales, whilst the energy flows to large scales. However, the weak nonlinear regime restricts the flow of the invariants in these directions. The authors of [65] suggest that in such situations, we might expect to observe a *finite temperature* KZ solution. This solution is predominantly a thermodynamic solution similar to (2.110), but with a finite flux contribution of the form:

$$n_{\mathbf{k}} = \frac{T_c}{\omega_k + \mu + \phi(\omega_k, P_{\mathbf{k}}, Q_{\mathbf{k}})}, \quad (4.30)$$

where $\phi(\cdot)$ is a function of the linear frequency and the energy and wave action fluxes, and $\phi \ll \omega_k, \mu$. This results in a mixed solution of the thermodynamic equilibrium and the non-equilibrium parts.

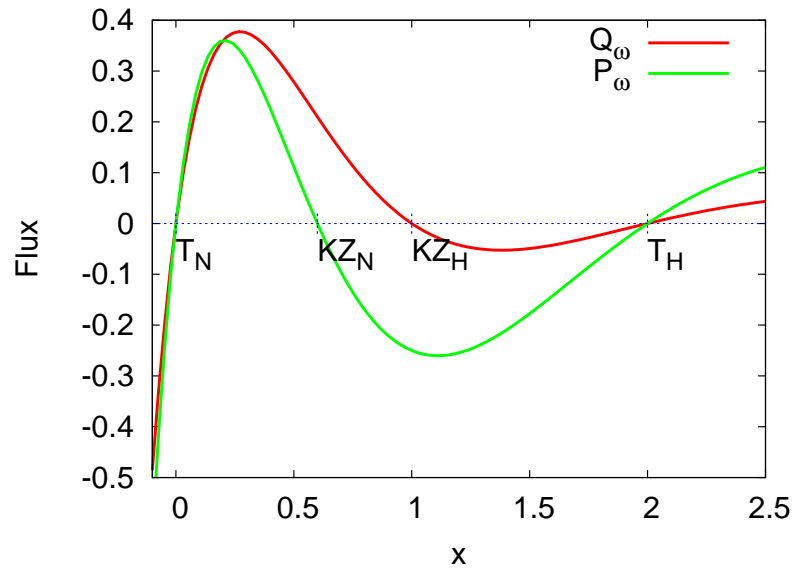


Figure 4.3: Plot of the energy flux P_{ω} and wave action flux Q_{ω} against the exponent x of the power law distribution of $n_{\omega} = C\omega^{-x/2}$ in the DAM representation of the LWE.

4.11 Modulational Instability and the Creation of Solitons in the Long-Wave Equation

The similarity of Equation (4.6) to the integrable 1D NLSE (4.5) means that we should expect not only random waves but also soliton-like coherent structures. During the inverse cascade, solitons appear naturally as wave action reaches the lowest wave numbers. Indeed, the KE description, (2.94) becomes invalid, and the MI of the wave field occurs resulting in the filamentation of light and its condensation into solitons.

Solitons are permanent localised (in physical space) structures resulting from the balance between the dispersion of the wave and the nonlinear wave breaking effect of the focusing medium. Solitons appear in several nonlinear wave equations, with the 1D NLSE an example. The 1D NLSE can be solved exactly by the inverse scattering transform, resulting in exact analytical soliton solutions of the form:

$$\begin{aligned}\psi(x, z) = & \sqrt{\frac{8K}{\varepsilon_0 k_0^2 n_a^4 l_\xi^2}} A \operatorname{sech} \left(Ax - \frac{ABz}{q} + C_1 \right) \\ & \times \exp \left(i \left[Bx + \frac{(A^2 - B^2)z}{2q} + C_2 \right] \right),\end{aligned}\quad (4.31)$$

where A , B , C_1 and C_2 are constants. The soliton solution is a consequence of the integrability of the 1D NLSE. Unlike Equation (4.5), the LWE, (4.6), is non-integrable, and thus, will not possess exact analytical solutions. However, the LWE's deviation from integrability is small, so we would expect to observe coherent structures of the LWE to be qualitatively similar to (4.31). Moreover, solitons of integrable systems possess the property of passing through one another without being changed. However, when integrability is slightly violated, we expect to observe weak nonlinear interactions of solitons. This may be viewed as possible merging events, oscillations in profile, or collapses.

In Figure 4.4, we plot the profile of soliton (4.31), with the corresponding wave action spectrum given in Figure 4.5. The intensity profile of the soliton in Figure 4.4 corresponds to a value of the nonlinearity parameter (4.16) of $J^L \sim 1$, which clearly makes sense if we consider solitons being the balance between linear dispersion and the

nonlinearity. In Figure 4.5, we observe a scaling of $n_k \propto k^0$ towards low wave numbers, with a decline of the spectrum at large k . However, a $n_k \propto k^0$ scalings is also observed from the equipartition of wave action (2.109). Therefore, by mere observation of the wave action spectrum, n_k , it will be difficult to determine if the wave field is comprised of equilibrated random waves or if is in the presence of solitons. To distinguish between these two states, we can numerically produce a (k, ω) -plot, that involves an additional Fourier transform over a time window. This method separates the random waves from the coherent component by observation of the dispersion relation, ω_k [8, 62, 64].

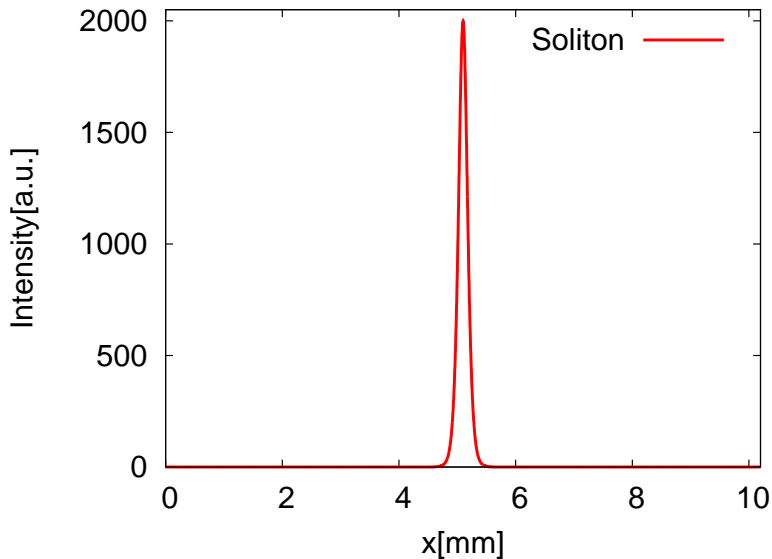


Figure 4.4: Intensity profile of the 1D NLSE soliton profile given in Equation (4.31).

The inverse cascade of photons is an essential step in the creation of solitons from a weakly nonlinear random wave field. The cascade provides the means, via nonlinear wave interaction, for wave action to reach large scales. As the inverse cascade develops, the nonlinearity of the system increases and a condensate forms, resulting in the dynamics of random waves deviating from the linear dispersion relation to one that is Bogoliubov modified. If wave amplitudes at low wave numbers increase sufficiently, then the Bogoliubov dispersion relation can become complex. The imaginary component of the Bogoliubov wave frequency then instigates unstable exponential growth of the wave amplitudes and thus we experience an instability of the wave packet known as MI. MI

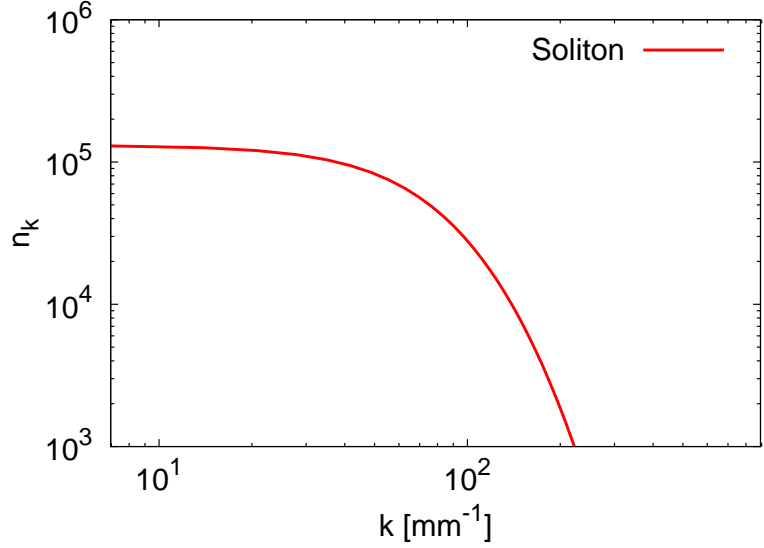


Figure 4.5: The corresponding wave action spectrum for the soliton profile in Figure 4.4

was first discovered in the context of water waves, where it was originally known as the Benjamin-Feir instability [168].

To derive an expression for the Bogoliubov dispersion relation, we must first expand the wave function $\psi(x, z)$ around a homogeneous condensate solution. The condensate solution describes the behaviour of the zeroth mode. The Bogoliubov dispersion relation then comprises of the wave frequency for the disturbances on the condensate and the rotation frequency of the condensate .

To derive an expression for the condensate, we consider an x -independent solution to the LWE, (4.6), i.e. a solution of the form $\psi(x, z) = \psi_c(z)$. Then $\psi_c(z)$ is given by

$$\psi_c(z) = \psi_0 \exp(-i\omega_c z), \quad (4.32)$$

with $\omega_c = -\varepsilon_0 n_a^4 l_\xi^2 k_0^2 I_0 / 8qK$ and where $I_0 = |\psi_0|^2$ is the intensity of the zeroth mode. Solution $\psi_c(z)$ describes the background rotation of a uniform condensate in (4.6) with a rotation frequency of ω_c .

We consider a small perturbation, $\phi(x, z)$ around this condensate and study the

linearised evolution of perturbation, where

$$\psi(x, z) = \psi_c(z) [1 + \phi(x, z)], \quad (4.33)$$

with $|\phi(x, z)| \ll 1$. Substituting Relation (4.33) into the LWE, (4.6), and linearising to the first order in $\phi(x, z)$, gives a linear evolution equation for $\phi(x, z)$. Assuming disturbance $\phi(x, z)$ takes the form of a single monochromatic plane wave:

$$\phi(x, z) = A \exp(ikx - i\Omega_k z) + A^* \exp(-ikx + i\Omega_k z), \quad (4.34)$$

where A is a complex amplitude of the wave and Ω_k is the frequency of waves on the condensate. Then by equating both types of exponentials, we can derive the dispersion relation for weakly nonlinear waves on the condensate given by

$$2q\Omega_k = \sqrt{\left(1 + \frac{\varepsilon_0 n_a^4 l_\xi^4 k_0^2 I_0}{2K}\right) k^4 - \frac{\varepsilon_0 n_a^4 l_\xi^2 k_0^2 I_0}{2K} k^2}. \quad (4.35)$$

To obtain the Bogoliubov frequency of the original wave function $\psi(x, z)$, we must include the frequency in which the condensate is rotating, ω_c . Therefore, the Bogoliubov dispersion relation for a weakly nonlinear wave is given by

$$\begin{aligned} \omega_k &= \omega_c + \Omega_k, \\ &= -\frac{\varepsilon_0 n_a^4 l_\xi^2 k_0^2 I_0}{8qK} + \frac{1}{2q} \sqrt{\left(1 + \frac{\varepsilon_0 n_a^4 l_\xi^4 k_0^2 I_0}{2K}\right) k^4 - \frac{\varepsilon_0 n_a^4 l_\xi^2 k_0^2 I_0}{2K} k^2}. \end{aligned} \quad (4.36)$$

Formation of solitons occurs with the assistance of MI. The instability allows for the growth of the wave amplitude to sufficient levels that the nonlinearity balances with the dispersion. Frequency (4.36) becomes complex when the term inside the square root turns negative. This gives an estimation to which wave numbers undergo MI. For a specific condensate intensity I_0 , we can estimate for which wave numbers are effected by MI using

$$k^2 < \frac{\varepsilon_0 n_a^4 l_\xi^2 k_0^2 I_0}{2K + \varepsilon_0 n_a^4 l_\xi^4 k_0^2 I_0}. \quad (4.37)$$

Hence all wave numbers smaller than the right-hand side of (4.37) will be subject to MI.

4.12 The Numerical Method

For the numerical computation of the LWE and the SWE, we implement a pseudo-spectral method [169, 170], with a resolution of $N = 2^{12}$ Fourier modes. The scheme utilises the fast Fourier transform to convert physical space vectors into their Fourier representation, where differentiation of the wave field is transformed to algebraic multiplication by wave number \mathbf{k} . The linear terms are solved exactly in Fourier space and then converted back into physical space with the aid of integrating factors, to greatly improve the numerical stability. Nonlinear terms are more complicated. Multiplications involving $\psi(x, z)$, have to be performed in physical space. Moreover, multiplication produces aliasing errors, due to the periodicity of the Fourier series expansion of the solution. These errors can be removed by artificially padding the Fourier mode representation with wave number modes of zero amplitude at either ends of \mathbf{k} -space. The amount of de-aliasing is subject to the degree of nonlinearity of the equation. For us, this entails that half of the wave number resolution for the solution needs to be zero - a quarter at each end of \mathbf{k} -space [170].

For the LWE we perform two types of numerical simulation, one without forcing and dissipation, and one with. Experimentally, the system is decaying from an initial condition with natural dissipation resulting from scattering at the edge of the cell and from the natural dissipation of the LC. However, this natural dissipation is relatively weak, so we perform an idealised decaying numerical simulation with no forcing and dissipation. Ideally, the WT regime is best observed in a non-equilibrium stationary steady state with the formation of coherent structures inhibited, hence we perform an additional simulations for the LWE and the SWE in this scenario. The low wave number dissipation allows for the removal of the wave action and suppression of solitons, whilst the high wave number dissipation allows for the removal of energy.

We evolve the simulations in time by using the fourth order Runge-Kutta method

[170], using a time step that is small enough so that it satisfies the Courant-Friedrichs-Lowy (CFL) condition of

$$\max_{\mathbf{k}} \left(\frac{\partial \omega_k}{\partial \mathbf{k}} \right) \Delta t < \Delta x, \quad (4.38)$$

where $\Delta x = L/N$ is the spacing of our spatial grid and $L = 32\pi$, is the length of our periodic box. Numerically we compute the non-dimensionalised equation given by

$$i \frac{\partial \psi}{\partial z} = - \frac{\partial^2 \psi}{\partial x^2} + N(\psi) + i(F_{\mathbf{k}} - D_{\mathbf{k}}), \quad (4.39)$$

where $N(\psi)$ represents the nonlinear part of our equations. Appendix F includes the derivation of the non-dimensional versions of both the LWE and SWE. The non-dimensional LWE contains an adjustable parameter α , defined in Appendix F. For the decaying setup, we set $\alpha = 128$, so that the numerical simulation is in the same regime as the experiment. For the forced and dissipated cases, we set $\alpha = 1024$, so that the long-wave limit is better realised. $F_{\mathbf{k}} = F(\mathbf{k})$ is the forcing profile, where energy and wave action are injected into the system. We define this in Fourier space, over a specific range of wave numbers. For the direct cascade simulations we use a forcing profile given by

$$F_{\mathbf{k}}^{\text{direct}} = \begin{cases} A \exp(i\theta_{\mathbf{k}}) & \text{if } 9 \leq k \leq 11 \\ 0 & \text{otherwise,} \end{cases} \quad (4.40)$$

where A is the amplitude of forcing and $\theta_{\mathbf{k}}$ is a random variable chosen from a uniform distribution on $[0, 2\pi)$ at each wave number and at each time step. For the inverse cascade simulations, we apply forcing over a small range of wave numbers situated in the high wave number region. However, we must allow for some Fourier modes larger than the forcing scale, as to not restrict the development of the inverse cascade, and for dissipation purposes. Our forcing profile for the inverse cascade simulations is given by

$$F_{\mathbf{k}}^{\text{inverse}} = \begin{cases} A \exp(i\theta_{\mathbf{k}}) & \text{if } \frac{N}{16} - 10 \leq k \leq \frac{N}{16} + 10 \\ 0 & \text{otherwise.} \end{cases} \quad (4.41)$$

In all simulations, we dissipate at high wave numbers by adding a hyper-viscosity term of the order $\propto k^4 \psi_{\mathbf{k}}$. We use the fourth power of \mathbf{k} , so that the dissipation profile is not

too steep for the formation of a bottleneck, or too shallow as to prevent a large enough inertial range developing. At low wave numbers, we use two types of dissipation profile. Firstly, we can use a hypo-viscosity term $\propto k^{-4} \psi_{\mathbf{k}}$. However, this type of dissipation profile has led to the WT description becoming invalid and a CB regime to develop [64]. In these situations, the CB scenario is avoided by the use of low wave number friction.

The numerical dissipation profile $D_{\mathbf{k}} = D(\mathbf{k})$, removes wave action and energy from the system at low and high wave numbers. For clarity, we split $D_{\mathbf{k}}$ into the low and high wave number contributions $D_{\mathbf{k}}^L$ and $D_{\mathbf{k}}^H$. At high wave numbers our hyper-viscosity profile is defined as

$$D_{\mathbf{k}}^H = \nu_{\text{hyper}} k^4 \psi_{\mathbf{k}}, \quad (4.42a)$$

where ν_{hyper} is the coefficient for the rate of dissipation. If we apply hypo-viscosity at low wave numbers, then $D_{\mathbf{k}}^L$ is given by

$$D_{\mathbf{k}}^L = \begin{cases} \nu_{\text{hypo}} k^{-4} \psi_{\mathbf{k}} & \text{if } \mathbf{k} \neq 0 \\ \psi_{\mathbf{k}} = 0 & \text{if } \mathbf{k} = 0, \end{cases}$$

where ν_{hypo} is the coefficient for the rate of dissipation at low wave numbers. However, in situations where we use friction, then $D_{\mathbf{k}}^L$ is defined as

$$D_{\mathbf{k}}^L = \begin{cases} \nu_{\text{friction}} \psi_{\mathbf{k}} & \text{if } 0 \leq k \leq 6 \\ 0 & \text{otherwise,} \end{cases}$$

where ν_{friction} is the rate of friction dissipation.

4.13 Results

We present the experimental and numerical results for OWT. We divide this Section into two main parts, firstly, we consider the system described by the LWE, in both experimental and numerical aspects. We begin this Subsection by considering the decaying setup with condensation at the lowest wave numbers. Then we move on to the numerical simulations of the LWE in the forced and dissipated regime. In the second

Subsection, we present the numerical results for the SWE.

4.13.1 The Long-Wave Equation

The Decaying Inverse Cascade with Condensation

The decaying simulation leading to photon condensation was originally reported by us in [8]. Both experimental and numerical setups are configured for decaying OWT, where an initial condition is set up and allowed to develop in the absence of any forcing or artificial dissipation. We perform the numerical simulation with the same parameters as the experiment, and present results in dimensional units for comparison.

The inverse cascade spectrum is of a finite capacity type, in a sense that only a finite amount of the cascading invariant (wave action in this case) is needed to fill the infinite inertial range. Indeed, this is determined as the integral of the wave action spectrum $n_{\mathbf{k}}$ converges at $\mathbf{k} = 0$, i.e.

$$\int_0 n_{\mathbf{k}} dk \propto \int_0 k^{-3/5} dk < \infty. \quad (4.43)$$

For finite capacity spectra, the turbulent systems have a long transient (on its way to the final thermal equilibrium state) in which the scaling is of the KZ type. This is because the initial condition serves as a huge reservoir of the cascading invariant.

Experimentally, the initial condition is setup by injecting photons at small spatial scales by modulating the intensity of the input beam with a patterned intensity mask. We randomise the phases by the use of a phase modulator. This is made by creating a random distribution of diffusing spots with the average size $\simeq 35 \mu m$ through the SLM. This is done in order to create an initial condition close to an RPA wave field required by the theory. The numerical initial condition is more idealised. We restrict the initial condition to a localised region at small scales. The initial profile is given by

$$\psi_{\mathbf{k}}(0) = \begin{cases} A \exp(i\theta_{\mathbf{k}}) & \text{if } \frac{N}{16} - 5 < k < \frac{N}{16} \\ \psi_{\mathbf{k}}(0) = 0 & \text{otherwise,} \end{cases} \quad (4.44)$$

where $A = 4.608 \times 10^3$ is the amplitude of forcing and $\theta_{\mathbf{k}}$ is a random variable chosen from a uniform distribution on $[0, 2\pi)$ at each wave number. In dimensional units, this corresponds to an initial condition in the region around $k_f \approx 1.5 \times 10^2 \text{ mm}^{-1}$. Moreover, we apply a Gaussian filter in physical space to achieve a beam profile comparable to that of the experiment.

Applicability of the WT approach is verified by the calculation of the nonlinear parameter ${}^L J$ for the numerical simulation, which agrees with the experiment and is of the order ${}^L J \simeq 100$. Experimentally, we measure the light intensity $I(x, z) = |\psi|^2$ and not the phases of ψ . Therefore the wave action spectrum $n_{\mathbf{k}}$ is not directly accessible. Instead, we measure the intensity spectrum, $N(\mathbf{k}, z) = |I_{\mathbf{k}}(z)|^2$, where the k -scaling for $N_{\mathbf{k}}$ in the inverse cascade state is easily obtained from the KZ solution (4.20b) and the random phase condition, (see Appendix E). This procedure gives an intensity spectrum of

$$N_{\mathbf{k}} \propto k^{-1/5}. \quad (4.45)$$

The wave action spectrum from the numerical simulation is shown in Figure 4.6 at two different distances, we see at $z = 0 \text{ mm}$ the peak from the initial condition at high wave numbers, then at $z = 63 \text{ mm}$ we see evidence of an inverse cascade, as the majority of the wave action is situated towards low wave numbers. However, at low wave numbers we do not see the spectrum matching our theoretical KZ prediction (4.20b). We showed in Section 4.10, that the wave action flux, $Q_{\mathbf{k}}$, corresponding to the KZ solution (4.20b), has the incorrect sign for an inverse cascade. Therefore, we noted that the inverse cascade spectrum would correspond to a mixed thermal solution with a finite flux contribution. This is the probable cause for the lack of agreement with the KZ solution. We observe from Figure 4.6, that $n_{\mathbf{k}} \propto k^0$ at low wave numbers, which may account for the mixed thermal solution (as this scaling corresponds to the equipartition of wave action (2.109a)) or for the presence of solitons (c.f. Figure 4.5).

The experimental and numerical intensity spectra are shown in Figures. 4.7 and 4.8 respectively. In both plots, we observe an inverse cascade, resulting in a good agreement with the WT prediction for the intensity spectrum (4.45). This agreement may be coincidental, as we have shown that the flux directions are insufficient for a

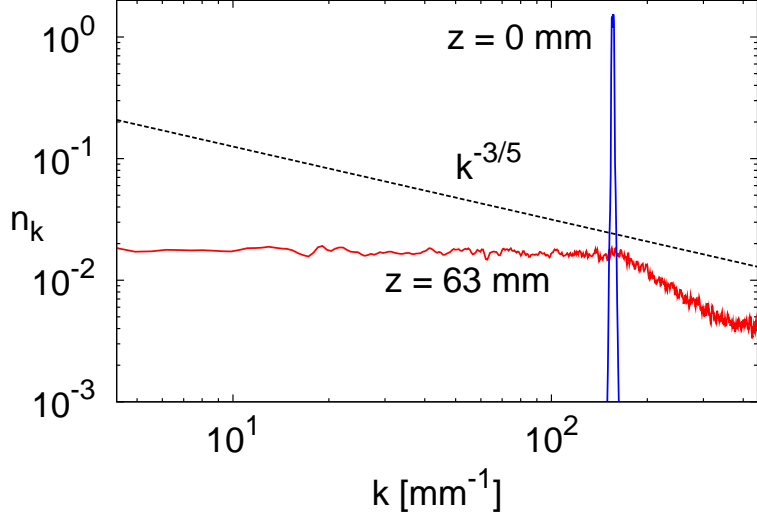


Figure 4.6: Numerical spectrum of the wave action, n_k , at distances $z = 0 \text{ mm}$ and $z = 63 \text{ mm}$.

KZ wave action cascade. However, the intensity spectrum is a non-local quantity, and therefore may not be affected by the lack of wave action flux. We can only confidently say that we still do not fully understand the agreement.

Verification of the long-wave limit $kl_\xi \ll 1$ and deviation from integrability is checked by considering the ratio of the two nonlinear terms in the LWE (4.6), which we denote as R , and is estimated in Fourier space as $R \propto k^2 l_\xi^2$. We observe from Figures 4.7 and 4.8 that the inverse cascade is approximately in the region $k \sim 10^4 - 10^5 \text{ m}^{-1}$, giving an estimation of $R \sim 10^{-2} - 1$. Note, that if R is too small, then we are close to an integrable system, which would be dominated by solitons and lack cascade dynamics, and if R is too high, then the LWE is a poor approximation for 1D OWT.

The inverse cascade can be observed directly in the physical experiment by inspecting the light pattern in the (x, z) plane of the LC cell. Two magnified images of the intensity distribution, $I(x, z)$, showing the beam evolution during propagation in the experiment are displayed in Figure 4.9. For comparison, in Figure 4.9a and b, we show the beam evolution in the linear and in the weakly nonlinear regimes, respectively. In Figure 4.9a, we set a periodic initial condition with a uniform phase and apply no volt-

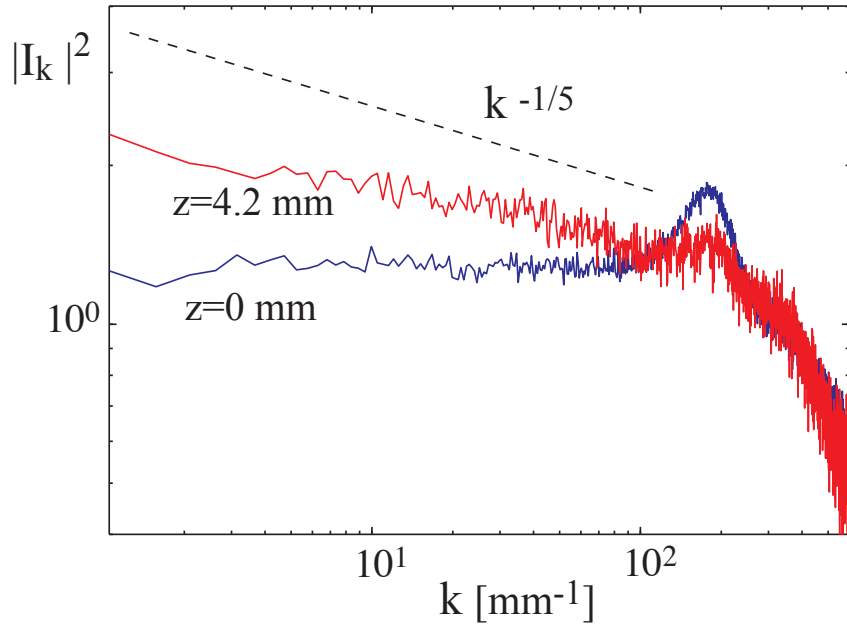


Figure 4.7: Experimental spectrum of the light intensity, $N_k = |I_k|^2$ at two different distances z . Figure courtesy of Umberto Bortolozzo and Stefania Residori.

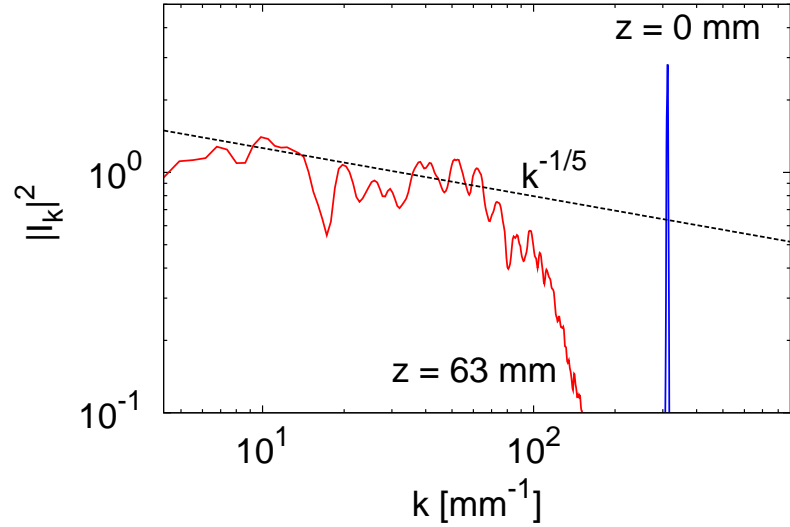


Figure 4.8: Numerical spectrum of the light intensity, $N_k = |I_k|^2$ at two different distances z . Averaging is done over a small finite time window and over ten realisations.

age to the LC cell. We see that the linear propagation is characterised by the periodic recurrence of the pattern with the same period, a phase slip occurring at every Talbot

distance. This is defined by p^2/λ , with p , the period of the initial condition and λ , the laser wave length [171]. In Figure 4.9b, we apply a voltage, $V = 2.5$ V to the LC cell. The initial condition is periodic with the same period as in Figure 4.9a, but now with random phases. We observe that the initial period of the pattern is becoming larger as the light beam propagates along z .

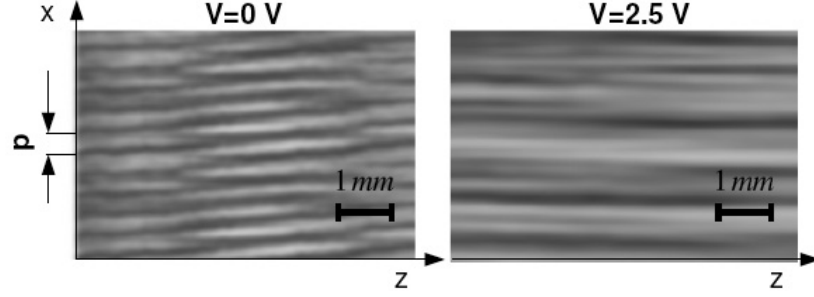


Figure 4.9: Intensity distribution $I(x, z)$ showing the beam evolution during propagation; a) linear case, b) weakly nonlinear case. Figure courtesy of Umberto Bortolozzo and Stefania Residori.

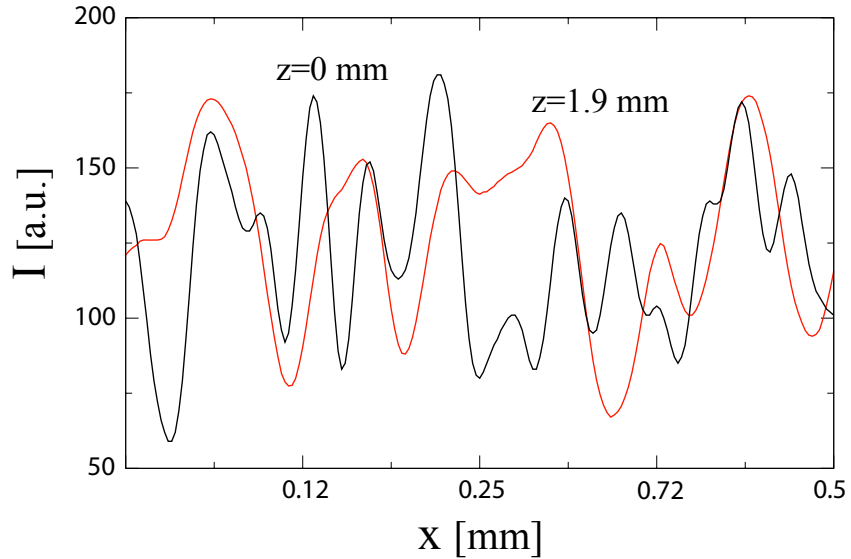


Figure 4.10: Two intensity profiles $I(x)$ recorded at $z = 0$ and $z = 1.9$ mm in the weakly nonlinear regime, with $V = 2.5$ V, showing the smoothing associated with the inverse cascade. Figure courtesy of Umberto Bortolozzo and Stefania Residori.

While the linear propagation in Figure 4.9a, forms Talbot intensity carpets [172], with the initial intensity distribution reappearing periodically along the propagation di-

rection z , the weak nonlinearity in Figure 4.9b, leads to wave interactions, with different spatial frequencies mixing and the periodic occurrence of the Talbot carpet being broken.

In Figure 4.10, we show two intensity profiles taken in the nonlinear case at two different stages of the beam propagation. The inverse cascade is accompanied by a smoothing of the intensity profile and the amplification of low wave number components.

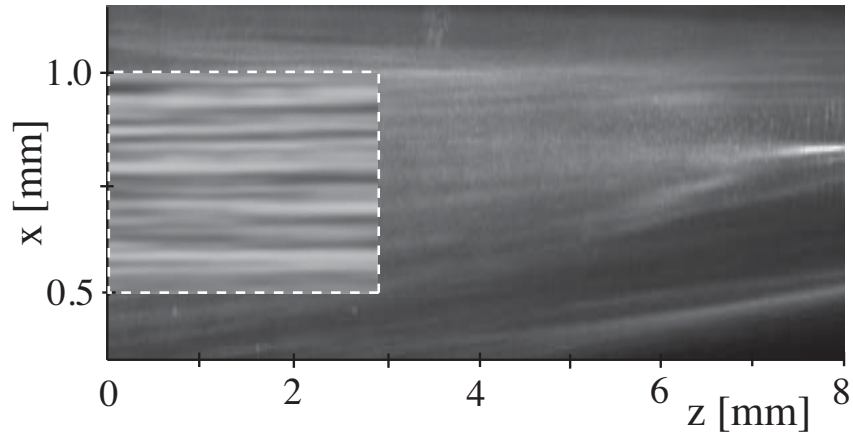


Figure 4.11: Experimental results for intensity distribution $I(x, z)$. The area marked by the dashed line is shown at a higher resolution (using a larger magnification objectif). Figure courtesy of Umberto Bortolozzo and Stefania Residori.

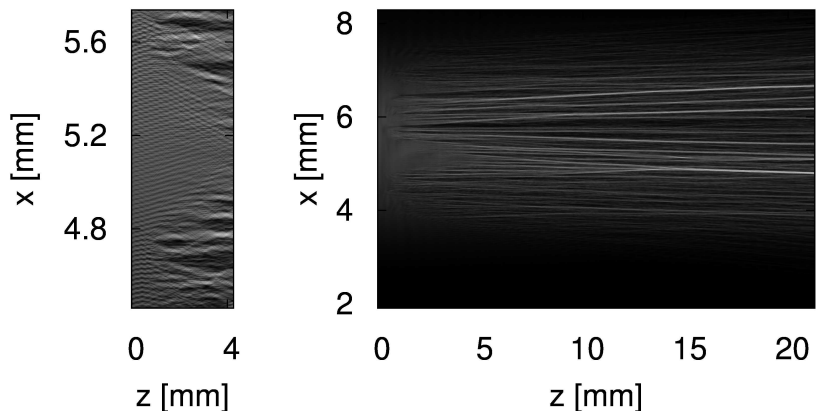


Figure 4.12: Numerical results for intensity distribution $I(x, z)$. The frame on the left is a magnified section of the initial propagation of the beam.

The intensity distribution, $I(x, z)$, showing the beam evolution during propagation in the experiment and in the numerical simulation are displayed in Figures 4.11

and 4.12, respectively. In the high resolution inset of Figure 4.11, we can observe that the typical wave length of the waves increases along the beam which corresponds to an inverse cascade process. Furthermore, one can see the formation of coherent solitons out of the random initial wave field, such that in the experiment, one strong soliton is dominant at the largest distance z . Both the experimental and the numerical results in Figures 4.11 and 4.12 indicate that the total number of solitons reduces. The observed increase of the scale and formation of coherent structures represents the condensation of light. Experimentally, the condensation into one dominant soliton is well revealed by the linear intensity profiles $I(x)$ taken at different propagation distances, as shown in Figure 4.13 for $z = 0.3, 4.5$ and 7.5 mm . Note that the amplitude of the final dominant soliton is three orders of magnitude larger than the amplitude of the initial periodic modulation.

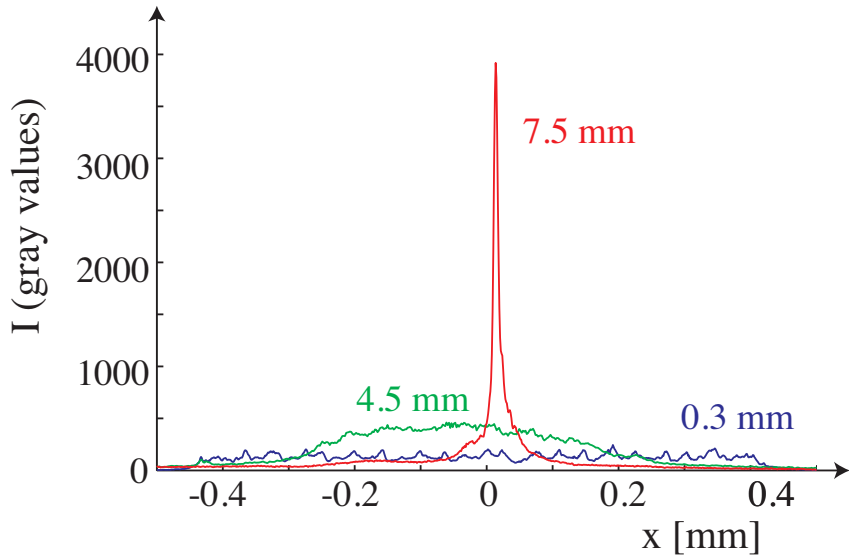


Figure 4.13: Linear intensity profiles $I(x)$ taken at different propagation distances, $z = 0.3, 4.5$ and 7.5 mm . Figure courtesy of Umberto Bortolozzo and Stefania Residori.

Figure 4.14 displays three profiles of the PDF of the wave intensity along the cell at distances $z = 0\text{ mm}$, $z = 3\text{ mm}$ and $z = 8\text{ mm}$. In a pure Gaussian wave field, we would observe a straight profile of the PDF tail. However, in Figure 4.14, non-Gaussianity is observed with the deviation from the straight lines, indicating a slower than exponential decay of the PDF tails. Non-Gaussianity corresponds to *intermittency*

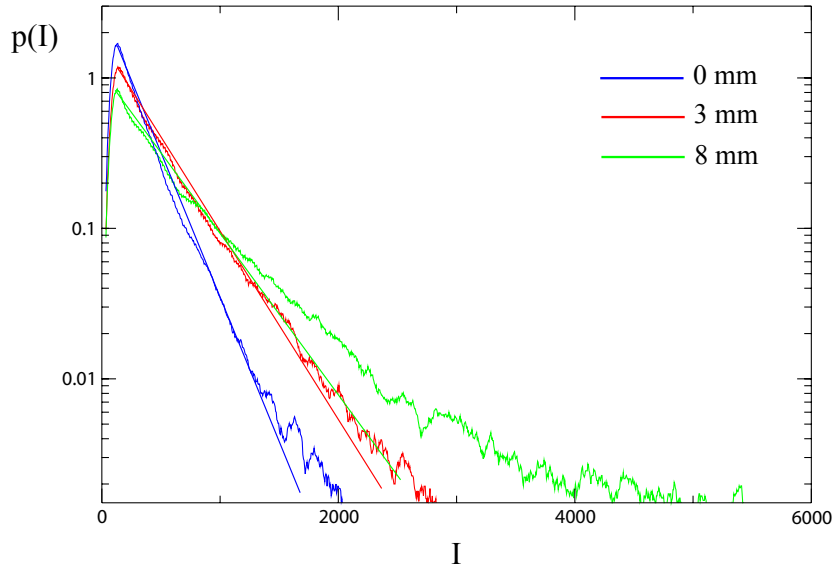


Figure 4.14: PDFs of the wave intensity within the experimental cell at three different distances along the cell, $z = 0 \text{ mm}$, $z = 3 \text{ mm}$ and $z = 8 \text{ mm}$. Straight lines have been fitted to each PDF to show Gaussianity. Figure courtesy of Umberto Bortolozzo and Stefania Residori.

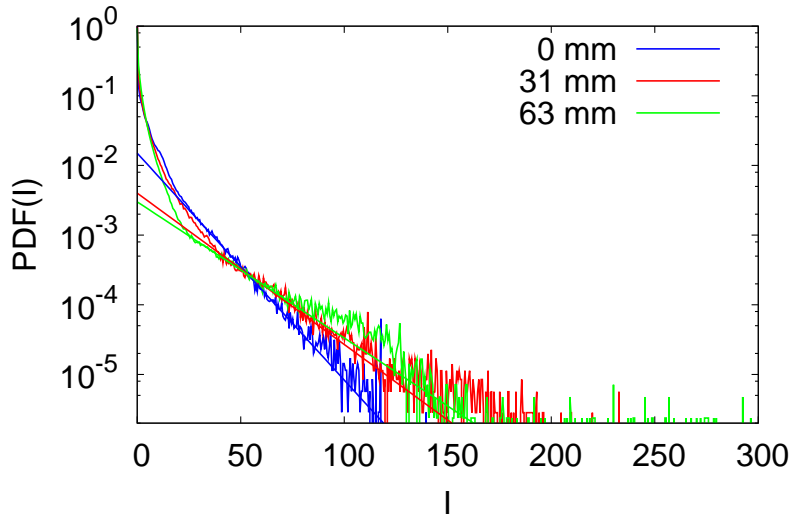


Figure 4.15: PDFs of the wave intensity within the numerical cell at three different distances along the cell, $z = 0 \text{ mm}$, 31 mm and 63 mm . Straight lines have been fitted to each PDF to show Gaussianity.

of WT. Intermittency implies that there is a significantly higher occurrence of high intensity structures compared to that predicted by a Gaussian wave field. We see a

similar scenario in Figure 4.15, showing the intensity PDFs of the numerical simulation. We plot three PDFs at distances $z = 0 \text{ mm}$, $z = 31 \text{ mm}$ and $z = 63 \text{ mm}$. The observation of intermittency could be a sign of the development of coherent structures in the system. To be certain of the presence of any coherent structures, we should produce a (\mathbf{k}, ω) -plot.

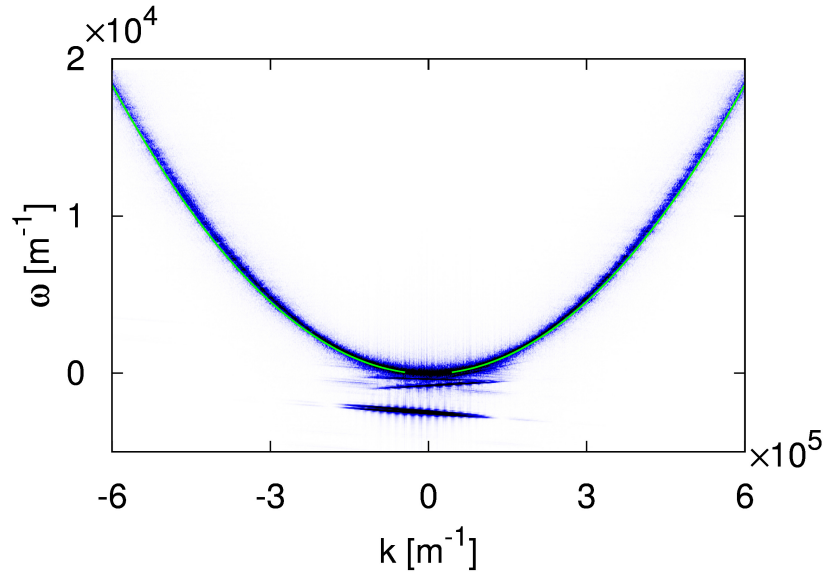


Figure 4.16: The (\mathbf{k}, ω) -plot of the wave field at $z = 10 \text{ m}$. The Bogoliubov dispersion relation is shown by the solid green line.

We perform an additional decaying simulation with a lower initial intensity, to allow us to capture the inverse cascade dynamics in more detail and to enable us to analyse the relationship between solitons and incoherent waves. However, to compensate for the lower intensity initial condition, we must run the simulation for much larger times. Separation of the random wave and the coherent soliton components can be achieved by performing an additional Fourier transform with respect to z over a finite z -window [62, 8].

The numerically obtained (\mathbf{k}, ω) -plot enables the direct observation of the dispersion relation of random waves, and is shown in Figure 4.16. Here, the incoherent wave component is distributed around the wave dispersion relation, which is Bogoliubov-modified by the condensate (4.35), and is shown by the solid line in Figure 4.16. The

distribution of the dispersion relation is centred around the theoretical prediction. We observe that the width of the dispersion relation is narrow for large \mathbf{k} , a sign of weak nonlinearity, and progressively gets wider as it approaches smaller wave numbers. This broadening, is an indication that the nonlinearity of the system increases towards smaller \mathbf{k} , as was theoretically predicted in [65]. At wave numbers around zero, we see that the theoretical Bogoliubov curve vanishes, corresponding to the region defined by Equation (4.37), where the frequency becomes complex. For such wave numbers, MI of the wave packets occurs and the WT description breaks down. Below the region where the Bogoliubov relation becomes complex, we observe slanted lines. Each of these lines corresponds to a coherent soliton, whose speed is equal to the inclination of the slope. We observe that the formation of solitons is seen in the (\mathbf{k}, ω) -plot as straight lines ‘peeling’ from the dispersion curve with a gradient tangential to the dispersion curve. Moreover, we observe the gradual migration of these lines to higher negative frequencies, as the solitons begin to grow in size by the absorption energy from surrounding waves or by merging with other solitons.

Further analysis can be achieved by separating the wave and soliton components of the (\mathbf{k}, ω) -plot by cutting along the $\omega_k = 0$ axis. Then, by inverting the Fourier transforms of each half-plane, we can recover the wave field, $\psi(x, z)$, for each half of the (\mathbf{k}, ω) -plot. This enables us to compare the soliton ($\omega_k < 0$) and wave ($\omega_k \geq 0$) components of the intensity profile, Figure 4.17, and the wave action spectrum, Figure 4.18. In Figure 4.17, we plot the intensity profile of light in real space for the soliton and wave components. We see that separating the negative and positive parts of the (\mathbf{k}, ω) -plot isolates the coherent solitons from the random wave background and we observe that the main soliton is at least an order of magnitude greater than the random wave field.

In Figure 4.18, we observe that the soliton component of the wave action spectrum, is heavily situated towards the low wave number region and scales as $\propto k^0$. This profile is qualitatively similar to the wave action spectrum of the exact soliton of the 1D NLSE, seen in Figure 4.4. The wave component of the wave action spectrum is more widely distributed in \mathbf{k} -space. However, we still do not observe a KZ scaling,

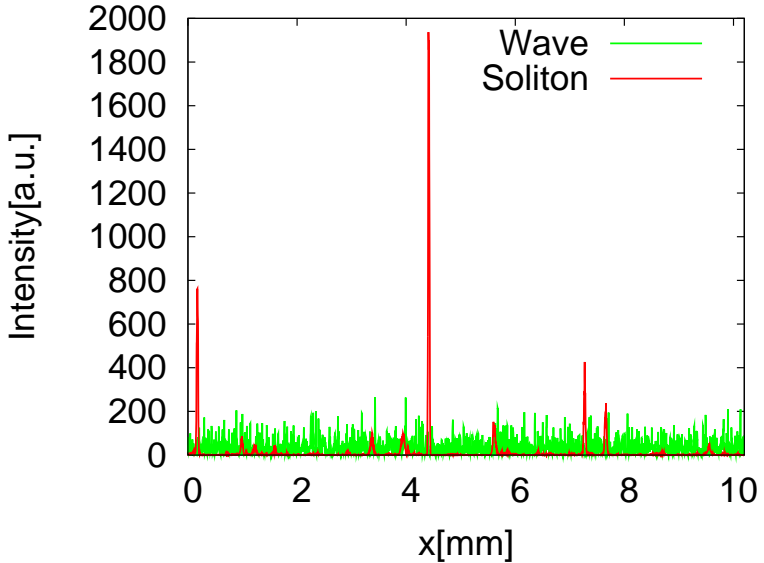


Figure 4.17: Plot of the intensity profile at $z = 10\text{ m}$ of both the soliton and wave components

but this is largely down to the incompatibility of the flux to the KZ solution. In other wave systems, the separation of the coherent and wave components, may be a useful technique in observing the KZ scaling otherwise masked by the presence of coherent structures. From the same simulation, we plot the (x, z) -plot for the intensity distribution, $I(x, z)$, in Figure 4.19. With the longer propagation distance, we observe the formation and evolution of solitons from the weakly nonlinear background. In the initial stages of the simulation, we observe the formation of solitons out of the random wave background, characterised by the increase in wave intensity and the deviation from the linear wave propagation direction. As the simulation progresses, the solitons become more pronounced and begin to behave independently from the waves, with an almost random movement through the numerical box. A large number of solitons are produced at the beginning of the simulation, but over long evolution times, the number of solitons reduces, with the remaining solitons being of increasing amplitude. Indeed, there are a large number of merging events between solitons, in Figure 4.20b we see a magnified section of a merging event from Figure 4.19. At late times, Figure 4.19 shows a single dominant soliton in the system that has subsequently grown by absorption of energy from

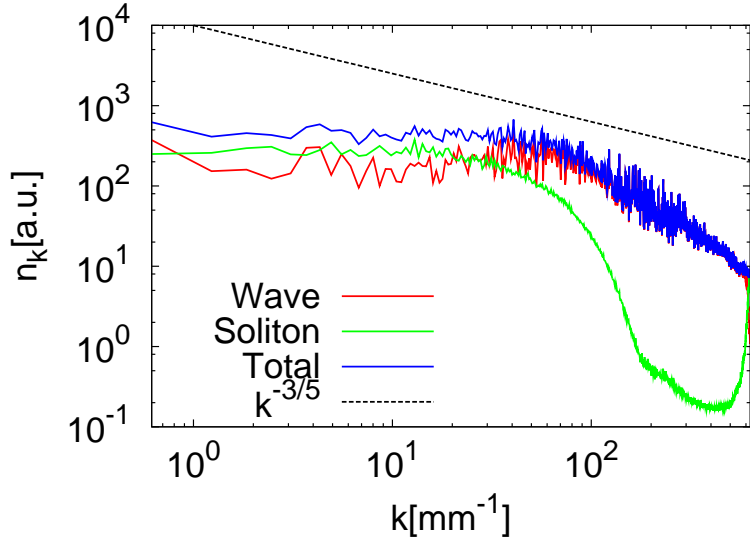


Figure 4.18: The wave action spectrum of both soliton and wave components of the spectrum, with the KZ prediction for comparison.

fellow solitons and the background wave field. This final state, is also observed in the experiment (Figure 4.11), albeit at a much shorter propagation distance. In Figure 4.20, we plot three zoomed in sections of Figure 4.11. In Figure 4.20a, we observe several solitons passing through one another with little deviation in their trajectories. Moreover, the weaker solitons (light grey in colour), have almost straight trajectories, like freely propagating linear waves, whilst the stronger solitons' movement is more erratic.

In Figure 4.20b, we magnify a merging event between two solitons. The larger soliton engulfs the smaller soliton without any deviation in its trajectory. Therefore, in the numerical simulation, large solitons absorb energy from smaller solitons, reducing the total number within the system. In addition, we also observe at $z = 11.5 \text{ m}$, a soliton bouncing off the larger soliton. As the weaker soliton approaches the larger soliton, it slows, before moving away at a fast speed. The understanding of when two solitons merge or if they repel is a key question that still remains to be answered. Finally, in Figure 4.20c, we observe two weak solitons propagating together, until around $z = 13 \text{ m}$, when they both repel each other and disperse back into the random wave field. This shows the break up of the coherent structures and the subsequent re-injection of wave

action into high frequency waves.

In Figures 4.21 and 4.22, we plot the maximum of the intensity and the energy of the system with z . To begin, we note that the maximum of the intensity of the wave field is always growing, and moreover, we observe that there is a sharp increase in the maximum at around $z = 11 \text{ m}$. This jump corresponds to the merging event seen in Figure 4.20b. Thus, the dominant soliton instantly grows in size once it absorbs the other soliton. This merging event is also noticed in Figure 4.22, where we observe a similar sharp increase to the linear and nonlinear energies at $z = 11 \text{ m}$, showing that as the dominant soliton's amplitude increases, there is a significant increase in the nonlinearity of the system.

From the beginning, the nonlinear energy from the first nonlinear term, grows almost an order of magnitude in size, compared to just under double in size for the linear contribution. This indicates that the inverse cascade and the subsequent soliton development is associated with an increase in the nonlinearity of the system, and hence the breakdown of the WT description. Moreover, we note that the total energy remains conserved, verifying that our simulation is well-resolved.

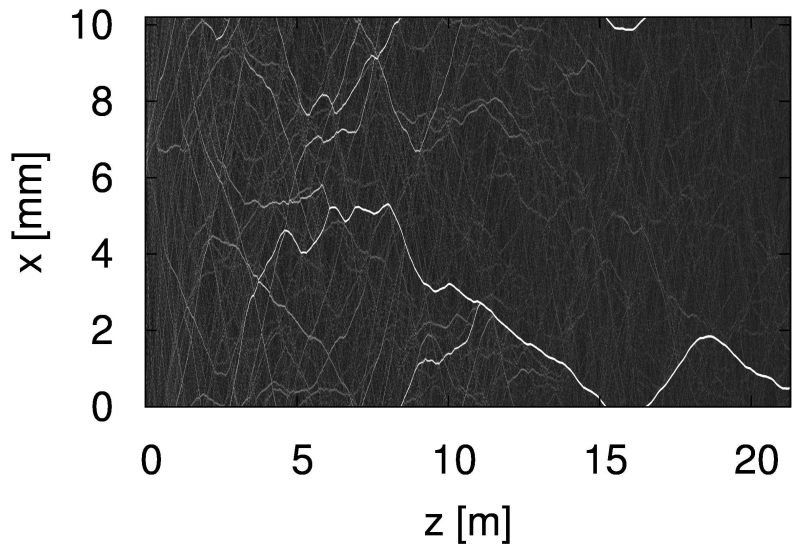


Figure 4.19: Numerically obtained (x, z) -plot for a long time simulation with a low intensity initial condition to see the inverse cascade and soliton merging.

In Figure 4.23, we plot the intensity PDF in k -space for two wave numbers,

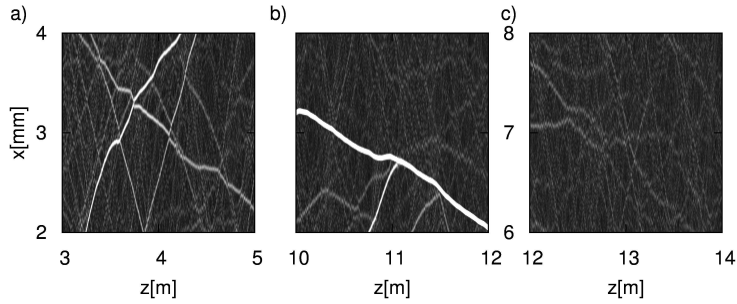


Figure 4.20: Three close-ups at different propagation distances showing solitons a) passing through each other, b) merging and c) dissipating.

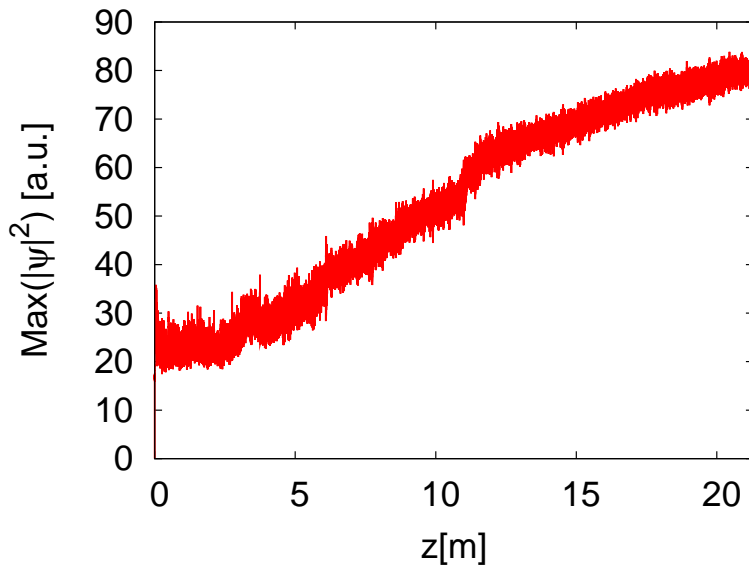


Figure 4.21: Plot of the maximum of the wave intensity in physical space versus z .

$k = 9.8 \text{ mm}^{-1}$, and $k = 3.8 \times 10^2 \text{ mm}^{-1}$. These two wave numbers are situated in the low wave number and high wave number regions respectively. We observe that both PDFs in the low intensity region are in good agreement with the Gaussian fit. However, at higher amplitudes, we observe that in the PDF at $k = 9.8 \text{ mm}^{-1}$, there is a depletion of the probability with regards to the Rayleigh distribution. This corresponds to a lower likelihood of observing high intensity structures. In the context of the analysis in Section 2.12, this implies that we are observing a positive probability flux, \mathcal{F} , with a flow from small to large J_k . Conversely, the PDF at $k = 3.8 \times 10^2 \text{ mm}^{-1}$, we

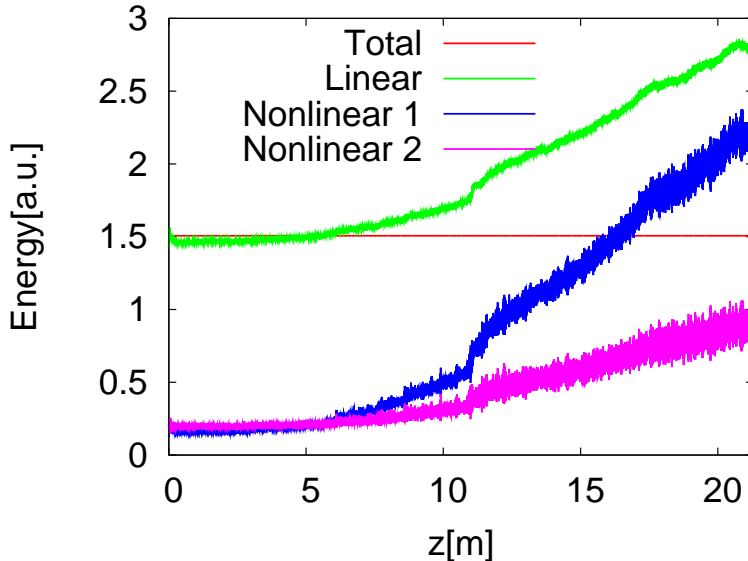


Figure 4.22: Plot of the magnitude of the energies for the long time simulation. We see the conservation of the total energy, the growth of the linear and both nonlinear energies (corresponding to the two nonlinear terms in equation (4.10a)). Note that the first nonlinear energy is strictly a non-positive quantity, therefore we have plotted the magnitude of the value in this Figure.

we observe an increase in probability from the Gaussian fit at high intensities. This behaviour corresponds to a negative probability flux, \mathcal{F} and flow from large to small J_k . This can be interpreted as a wave breaking process at low wave numbers. The inverse cascade transports wave action to small k and to higher J_k , as the inverse cascade is associated with an increase in nonlinearity of the system. As wave action accumulates at large scales, solitons form, with wave action spreading along the soliton spectrum $n_k \propto k^0$. Periodically, solitons will interact allowing for the emission of energy and wave action to incoherent waves, resulting in a reversal of the probability flux \mathcal{F} . This continuous transport of wave action can be seen as a WTLC for 1D OWT [30, 1]. A diagram for the WTLC is presented in Figure 4.24. Here we see that wave action is injected at high wave numbers, which subsequently gets transported to low k by an inverse cascade. When the amplitude at low k is sufficiently high, MI causes the formation of coherent nonlinear solitons. Solitons are a coherence of a broad range of wave modes situated at low wave numbers. Non-integrability of the system allows for

solitons to interact with surrounding structures, that enable energy exchange, and the possible ejection of energy and wave action back into the wave field. This supplies the random wave field with more wave action for the inverse cascade to transport, and the cycle begins again.

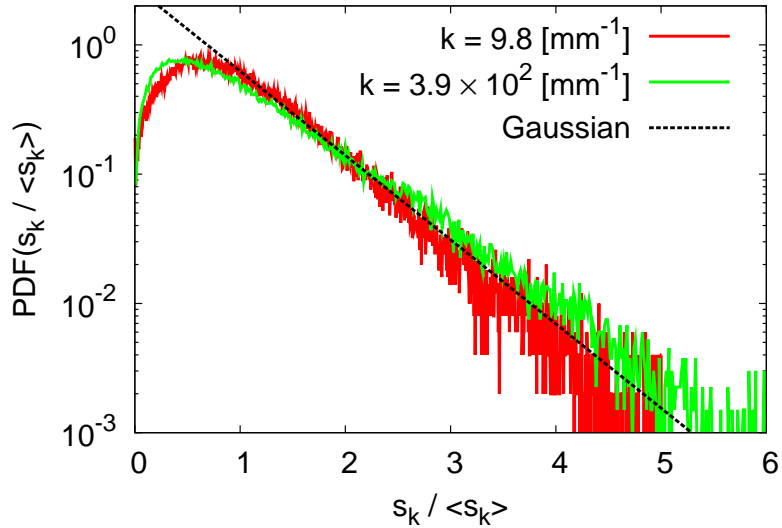


Figure 4.23: We plot the intensity PDF for variable $s_k = J_k$, at two wave numbers, $k = 9.8 \text{ mm}^{-1}$, and $k = 3.8 \times 10^2 \text{ mm}^{-1}$. We fit a black dashed straight line that corresponds to a Gaussian wave field.

Forced and Dissipated Simulations

In this Subsection, we explore numerical simulations of the LWE and SWE with forcing and dissipation. This allows the system to reach a non-equilibrium stationary state, where the observation of the KZ solutions, (4.20), can be made. In an infinite sized system, both KZ solutions can be realised in the same simulation, with forcing acting at an intermediate scale and two inertial ranges either side (see Figure 2.3). However, computational and time restrictions make it impractical to perform such a simulation. Therefore, we simulate each cascade separately, by performing two simulations with forcing at either ends of \mathbf{k} -space, allowing for just one inertial range. For both the direct and inverse cascade setups, we set the low wave number dissipation profile, D_k^L , to be friction, defined by (4.42b), with the friction coefficient of $\nu_{\text{friction}} = 5 \times 10^0$

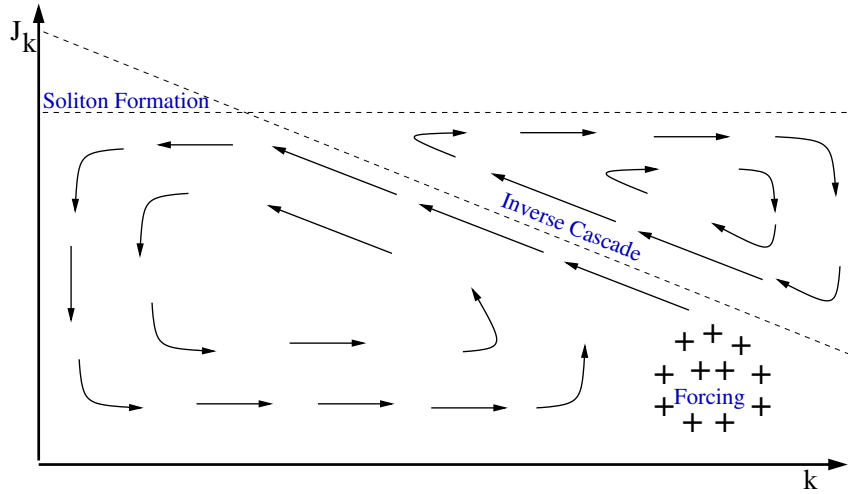


Figure 4.24: We depict the WTLC for 1D OWT. High wave number forcing injects wave action, that subsequently gets transferred to low k by the inverse cascade. At low k , solitons form resulting in a $n_k \propto k^0$ spectrum. The emission of waves from merging or dissipating solitons re-injects wave action at low intensities.

for the direct simulation, and $\nu_{\text{friction}} = 2 \times 10^0$ for the inverse simulation. We use hyper-viscosity at high wave numbers with a coefficient of $\nu_{\text{hyper}} = 1 \times 10^{-9}$ for the direct and $\nu_{\text{hyper}} = 1 \times 10^{-8}$ for the inverse setup. The forcing is situated at large scales for the direct cascade defined by Equation (4.40), with amplitude $A = 3.2 \times 10^3$ and at small scales for the inverse cascade, defined by Equation (4.41), with amplitude $A = 1.6 \times 10^3$. We numerically solve the non-dimensionalised equation in Appendix F, with $\alpha = 1024$. We run the simulations with a time step of $\Delta t = 1 \times 10^{-4}$ in a box of length $L = 32\pi$, with spatial resolution of $N = 2^{12}$, until we are at a non-equilibrium steady state. This is checked by observing stationarity of the total energy \mathcal{H} and wave action \mathcal{N} in the system.

Once the simulations reach a statistically non-equilibrium steady state, we analyse the statistics by performing time averages over this steady state regime. We have plotted the wave action spectrum, n_k , for both the direct, Figure 4.25, and inverse, Figure 4.26 cascades.

In Figure 4.25, we observe the direct wave action spectrum for the LWE, with the theoretical prediction also plotted. We do not observe any agreement with the WT prediction (4.29). However, this is to be expected, as it was shown in Section 4.10 that

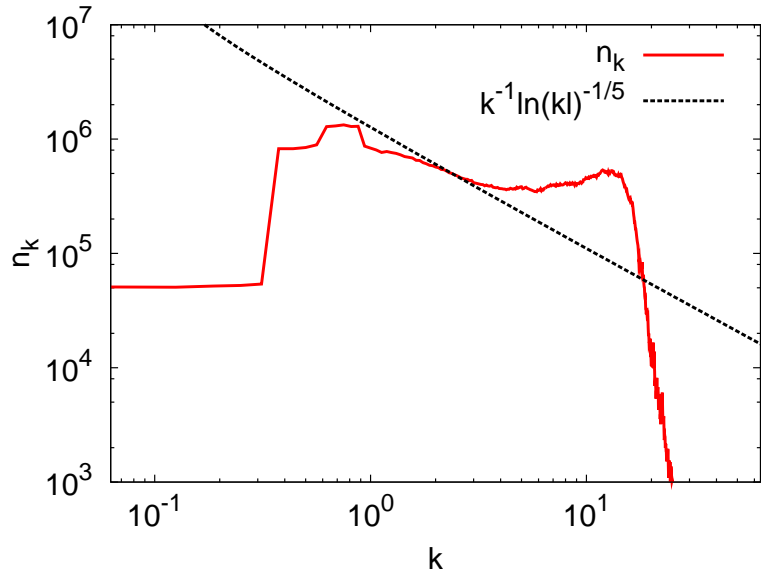


Figure 4.25: The wave action spectrum n_k in a statistically non-equilibrium stationary state for the direct cascade simulation of the LWE. The straight line represents the WT prediction of the KZ solution of $n_k \propto k^{-1} \ln(k\ell)$.

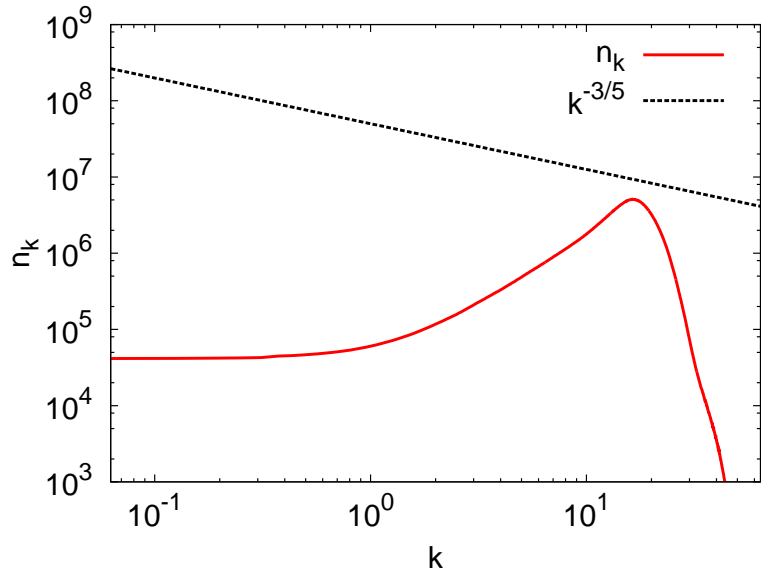


Figure 4.26: The wave action spectrum, n_k , in a statistically non-equilibrium stationary state for the inverse cascade simulation of the LWE. The straight line represents the WT prediction of the KZ solution of $n_k \propto k^{-3/5}$.

the direction of the energy flux does not coincide with Fjørtoft's argument. Moreover,

we see the formation of an accumulation of energy, or a bottleneck in the high wave number region. This could be caused by over-dissipation at high wave numbers, or a hyper-viscosity profile that is too steep.

The inverse wave action spectrum is shown in Figure 4.26. We observe that there is a build up of wave action around the forcing scale, $k \approx 16$, however, there seems to be no inverse cascade to low wave numbers. Although not surprising as the wave action flux is positive, this does contradict the observation of the decaying simulation, where an inverse cascade was observed. Over-dissipation at low wave numbers may be inhibiting the inverse cascade, however dissipation only acts on the first six wave modes.

In Figures 4.27 and 4.28, we plot the averaged energy and wave action fluxes corresponding to the two wave action spectra of Figures 4.25 and 4.26 respectively. In Figure 4.27, we observe a constant-like energy flux just after the forcing region $k \approx 0.8$, however, it does not last long before it becomes negative and noisy. The noise is probably down to an insufficient time average due to a lack of numerical data. A key observation is that the flux immediately to the right of the forcing scale is positive, contradicting the analysis of the DAM. Moreover, the energy flux becomes negative in the region where we observe the bottleneck in the spectrum. This negative flux could be down to the reflection of the flux due to over dissipation, or the physics of the system. In a non-equilibrium steady state, the total flux of an invariant should be zero. However, in the case of the energy flux P_k , this is not the case. A possible reason for this, is that the definition of P_k implies it is the linear energy flux. Therefore, only the total energy flux (including the nonlinear contribution to the flux) is conserved, and so we expect that this non-zero total flux is attributed to us not taking into account the nonlinear contribution⁴.

In Figure 4.28, we observe a noisy wave action flux, Q_k . At low wave numbers, the wave action flux is negative, which is inconsistent with the analysis of Section 4.10. However, near the forcing scale at $k \approx 16$, we see some volatility of the flux, where it is changing rapidly in \mathbf{k} -space from positive to negative. Indeed, this may be down to an

⁴The weak nonlinear regime implies that the total energy can be approximated by the linear energy, and likewise with the flux. Moreover, it is a numerical difficulty to compute the nonlinear contribution to the energy flux.

insufficient time average, or simply the behaviour of the flux - fluctuating around zero because the wave action cannot flow to either end of \mathbf{k} -space as it is restricted by the flux direction and the Fjørtoft argument.

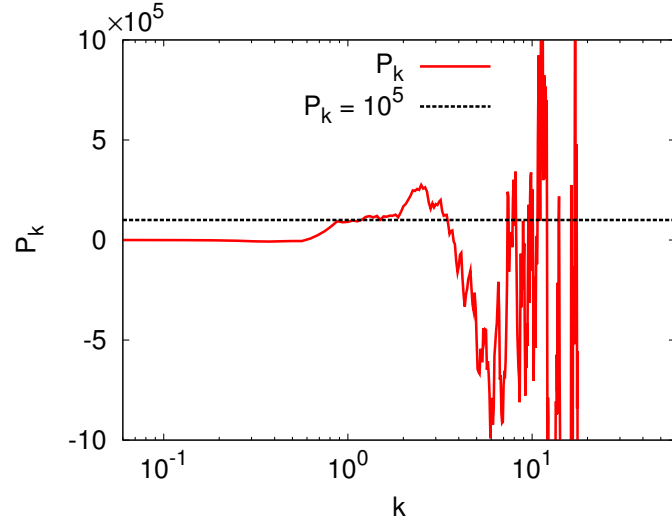


Figure 4.27: Averaged energy flux P_k versus wave number k in the direct cascade simulation of the LWE. A KZ solution implies that P_k should be a non-zero constant in the inertial range

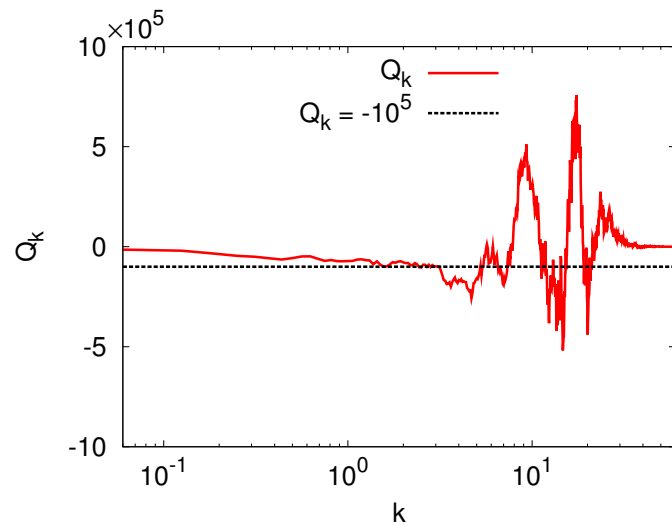


Figure 4.28: Averaged wave action flux Q_k versus wave number k in the inverse cascade simulation of the LWE. A KZ solution implies that Q_k should be a non-zero constant in the inertial range

Finally, we plot the intensity PDFs for the direct and inverse cascades in Figures 4.29 and 4.30 respectively. In both plots we superimpose a straight line in log-lin coordinates, corresponding to a Gaussian distribution for the wave field. In Figure 4.29, we observe a good agreement with the Gaussian fit. However, there is a slight deviation from Gaussianity at high intensities. In Figure 4.30, the intensity PDF for the inverse cascade deviates significantly from the Gaussian fit. This corresponds to strong WT intermittency, and the possible presence of coherent structures. Also, the restriction to the movement of wave action (Fjørtoft's argument and wrong flux sign), would result in the accumulation of wave action at the forcing scale. This pile up would increase the wave amplitudes in this region and been seen in the intensity PDF.

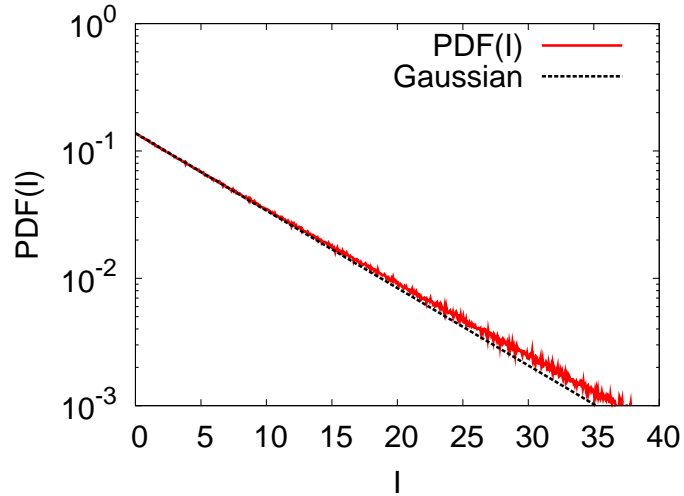


Figure 4.29: PDF of the wave intensity in the direct cascade simulation of the LWE. The straight line corresponds to a Gaussian distribution predicted by WT theory.

4.13.2 The Short-Wave Equation

We investigate the SWE, (4.8) by numerical simulations of the non-dimensionalised model of Appendix F. We apply the same forcing and dissipation profiles that are described in Section 4.12. We dissipate at low wave numbers using a hypo-viscosity profile, while using hyper-viscosity at high wave numbers. The dissipation rates we use are $\nu_{\text{hypo}} = 1 \times 10^{-2}$, $\nu_{\text{hyper}} = 1 \times 10^{-11}$ for the direct simulation and $\nu_{\text{hypo}} = 1 \times 10^0$, $\nu_{\text{hyper}} = 1 \times 10^{-8}$ for the inverse. For the direct cascade, we force the system with the

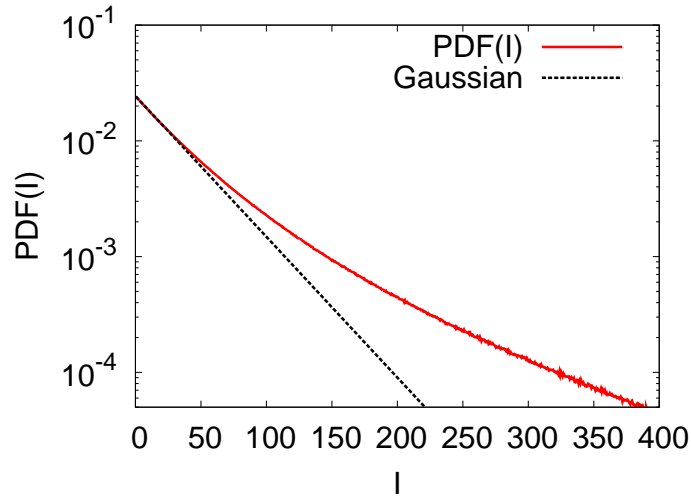


Figure 4.30: PDF of the wave intensity in the inverse cascade simulation of the LWE. The straight line corresponds to a Gaussian distribution predicted by WT theory.

profile (4.40), with amplitude $A = 1.6 \times 10^2$ and for the inverse cascade with profile (4.41), with amplitude $A = 4.8 \times 10^2$.

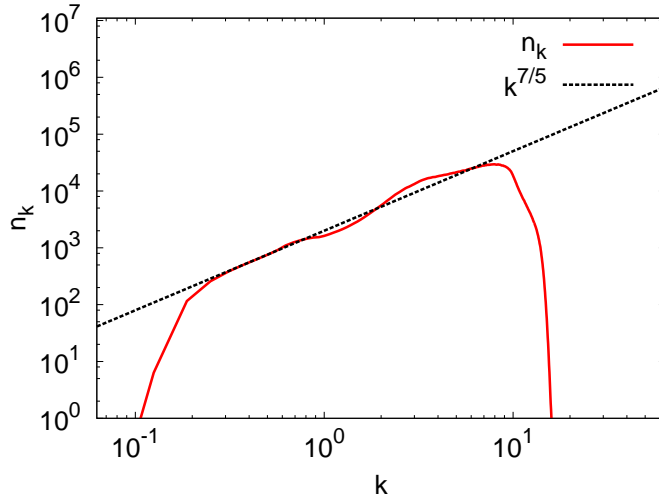


Figure 4.31: The wave action spectrum n_k in a statistically non-equilibrium stationary state for the direct cascade simulation of the SWE. The straight line represents the WT prediction of the KZ solution of $n_k \propto k^{7/5}$.

In Figure 4.31 we plot the wave action spectrum for the direct cascade averaged over a time window once the system has reached a statistically non-equilibrium steady

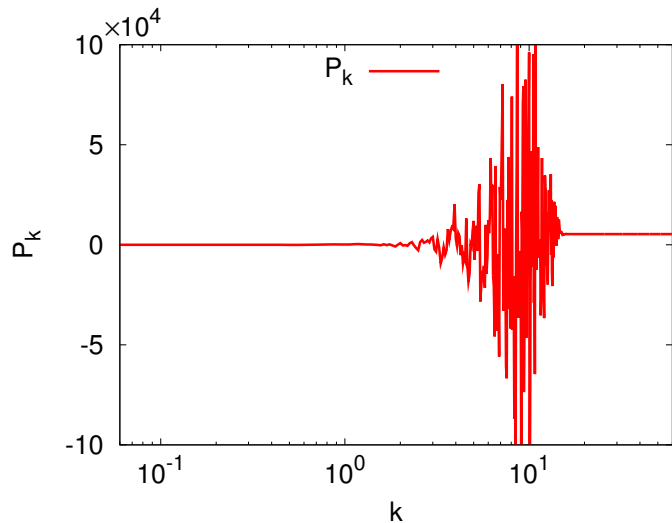


Figure 4.32: Averaged energy flux P_k versus wave number k in the direct cascade simulation of the SWE. A KZ solution implies that P_k should be a non-zero constant in the inertial range

state. We observe a good agreement to the WT prediction (4.21a). However, notice that there is some slight deviation of the spectrum in the middle of the inertial range. This is likely to be caused by an insufficient time average of the statistics. The agreement is surprising, as we showed that the KZ solution, (4.21a), does not produce convergence of the collision integral in the UV limit. However, we may be observing a non-local spectrum that is close to the local WT prediction. Investigation of the flux would provide a useful check, as a constant flux would determine if we are observing a local KZ spectra. In Figure 4.32, we plot the averaged energy flux, P_k , corresponding to the wave action spectrum of Figure 4.31. We observe an extremely noisy flux, that does not show any signs of a constant flux relation. Moreover, note that the flux oscillates wildly between positive and negative values, with almost identical occurrence. From Figure 4.32, we can state that we do not observe a constant flux and therefore, the wave action spectrum does not correspond to a local transfer of constant energy flux.

We present the averaged wave action spectrum for the inverse cascade in Figure 4.33. We observe a good agreement, for almost a decade in \mathbf{k} -space, with the theoretical prediction (4.21b). At low wave numbers, we observe a slight accumulation of wave action before the dissipation occurs. In Figure 4.34, we plot the corresponding

wave action flux, Q_k , for the wave action spectrum. We observe that there is almost a constant negative flux for about a decade in k -space, in the inertial range where we see the wave action spectrum close to the prediction (4.21b). These observations indicate that we have a local KZ spectrum of the form (4.21b). However, analysis of the locality, showed that the inverse KZ solution is invalid, raising many questions that need to be investigated further.

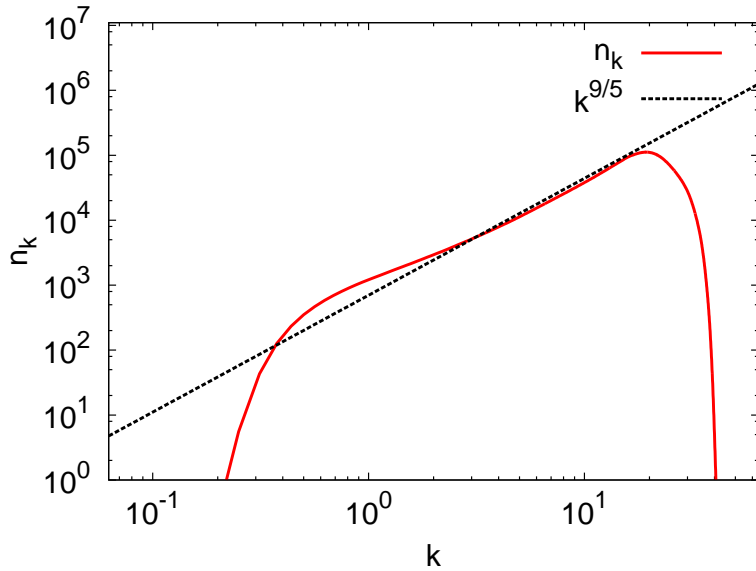


Figure 4.33: The wave action spectrum n_k in a statistically non-equilibrium stationary state for the inverse cascade simulation for the SWE. The straight line represents the WT prediction of the KZ solution of $n_k \propto k^{9/5}$.

In Figures 4.35 and 4.36, we present the intensity PDFs for the direct and inverse setups for the SWE. In both Figures, we observe a clear positive deviation from the Gaussian fit of a straight line. This indicates the presence of WT intermittency, with a significantly higher occurrence of high intensity structures than what is expected from a Gaussian wave field. The larger tails of the intensity PDFs imply that these systems are in a wave turbulence regime in the presence of a wave breaking process that is restricting the progression of the WT cascades and building up the wave intensity around the wave breaking scale.

In trying to tackle OWT, we have ended with more questions than answers. We presented an experimental setup for OWT that shows an inverse cascade of wave action

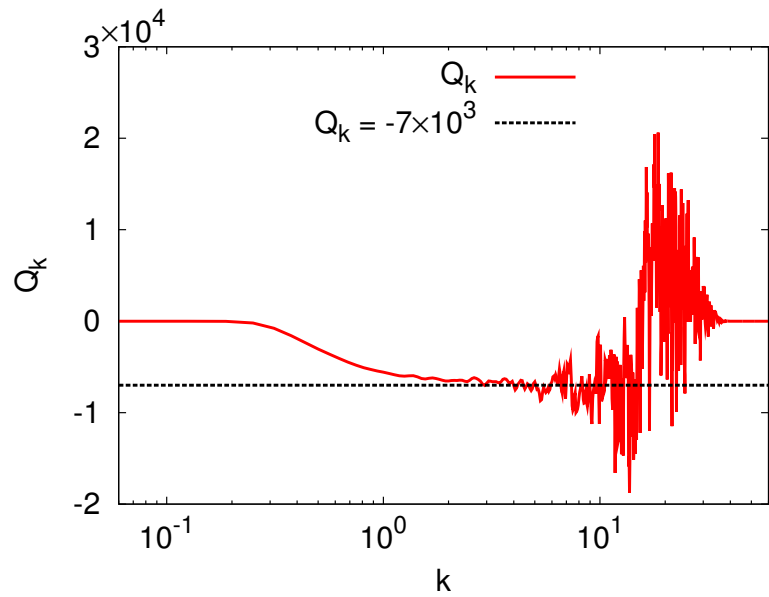


Figure 4.34: Averaged wave action flux Q_k versus wave number k for the inverse cascade simulation of the SWE. A KZ solution implies that Q_k should be a non-zero constant in the inertial range

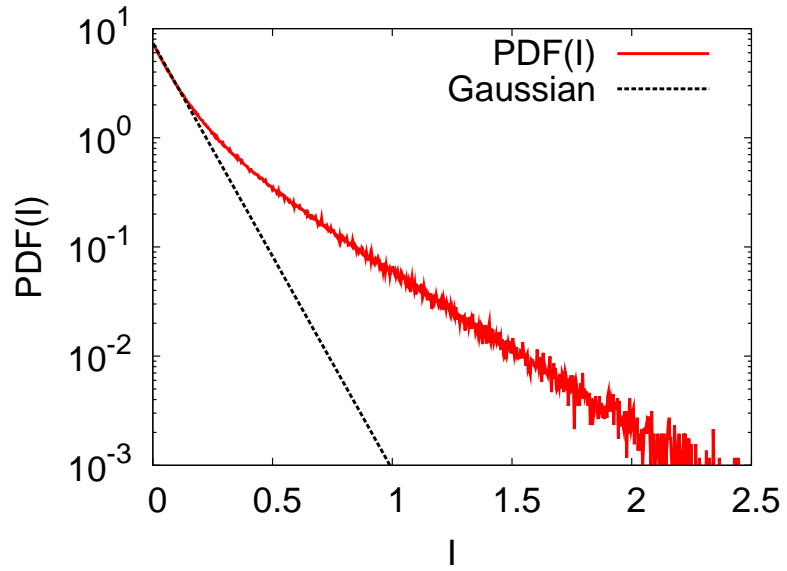


Figure 4.35: PDF of the wave intensity in the direct cascade simulation of the SWE. The straight line corresponds to a Gaussian distribution predicted by WT theory.

(in agreement with the intensity spectrum prediction), and subsequent development of solitons. However, analysis of the energy and wave action fluxes, reveals that the LWE

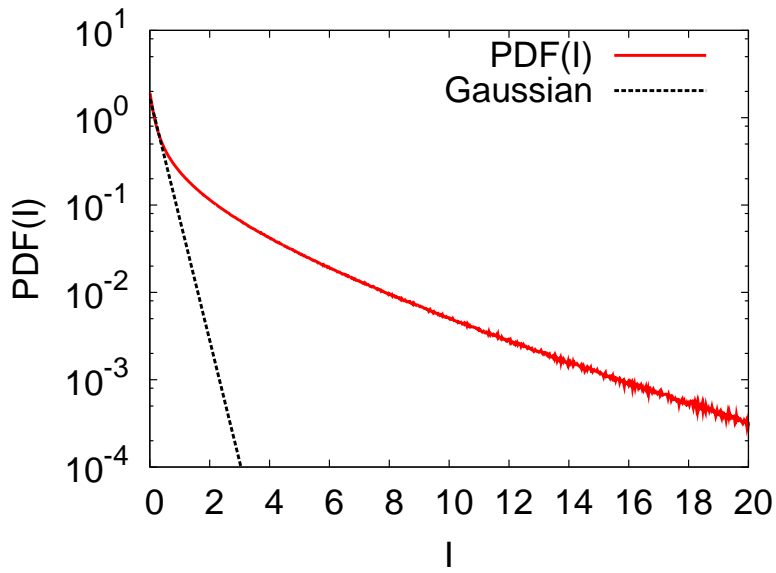


Figure 4.36: PDF of the wave intensity in the inverse cascade simulation of the SWE. The straight line corresponds to a Gaussian distribution predicted by WT theory.

does not permit the realisation of KZ solutions. This is supported by a lack of KZ spectra in the numerical simulations, Figures 4.25 and 4.26. Moreover, we observe good agreements to the KZ solution in the numerical simulations for the SWE, although, the non-local analysis of the spectra showed that they are not viable solutions. Additional investigation into 1D OWT is needed before any concrete statements can be made.

Chapter 5

Conclusions

Our main objective for this thesis, was to present a clear and concise description of six-wave WT systems. The majority of wave systems can be explained in terms of three and four-wave interactions, with only a few examples of six-wave systems known. We introduced a generic 1D six-wave system that contains two invariants and systematically applied WT theory in Chapter 2. With the general formulation set, we proceeded by considering specific physical six-wave systems, namely, QT and 1D OWT. The layout of the thesis, grants for the separation of the technical analysis of WT to the physical aspects of real world problems, allowing for a transparent and straightforward approach.

In Chapter 2, we began by introducing the necessary statistical construction for the development of WT. This took the form of the RPA field description and the subsequent definitions of the amplitude PDFs and the GF. We began by considering a general six-wave Hamiltonian system containing four-wave and six-wave contributions. Moreover, we assumed that the system contained a linear frequency that does not permit non-trivial solutions to the four-wave resonance condition. This invokes the application of a CT to remove the leading non-resonance order, resulting in a re-definition of the six-wave interaction coefficient. At this point, we used an iterative method from the evolution equation for the wave amplitude to average over the fast linear timescale and compute a nonlinear evolution equation for the GF. Subsequently, from this equation, we derived evolution equations for the amplitude PDF and the KE. The main objective in Chapter 2, was to analysis the stationary solutions of both the PDF equation and

the KE. For the KE, we derived the thermodynamic and KZ solutions by applying the ZT to the collision integral. The KZ solutions can only be realised if they in turn imply convergence of the collision integral. We acquired necessary conditions for convergence of the collision integral for the KZ solutions. Finally, we obtained a DAM for the six-wave system by assuming super local wave interactions and determined the qualitative behaviour of the fluxes.

In Chapter 3, we investigated the application of WT theory to Kelvin waves in QT. Kelvin waves have been shown to interact via a six-wave process and we began by introducing the original analysis of Kozik and Svistunov. However, with the aid of the results of Chapter 2, we examined in more detail, the BSE description of Kelvin waves. By introducing the LIA parameter, Λ , we were able to explicitly compute the leading order contribution to Kelvin wave dynamics in the KE. Moreover, we noticed that the Kelvin wave KE is considered on the LIA resonance surface, which is an approximation to the real Kelvin wave resonance condition. We compensated for this, by deriving a correction to the interaction coefficient, ${}^1S_{4,5,6}^{1,2,3}$. Indeed, we find that because the leading LIA contribution is integrable, this correction has a leading order effect on the dynamics of Kelvin waves - an essential step missed out in the previous analysis of [11]. We found that the KS spectrum forces the collision integral to diverge, and therefore is not a valid and realisable solution to the KE. Initially, this posed a problem, as the energy transfer in Kelvin waves had been assumed to be local process. Fortunately, L'vov and Nazarenko proposed a non-local theory for Kelvin waves, resulting in the LN spectrum for the energy cascade. This has led to a debate on the non-locality analysis of the KS spectrum and the subsequent non-local theory. We believe that due to the complexity of the Kelvin wave theory, a numerical approach to be more suitable in settling the debate.

The full expression for the interaction coefficient for Kelvin waves is extremely long, preventing any direct analysis, theoretically or numerically. This focused us to examine the asymptotic limit in the region of one vanishing wave number. The asymptotic expression implied a drastic simplification of the interaction coefficient and led to the LNE. As a high resolution numerical calculation of the BSE was beyond the scope of this thesis, we numerically implemented the LNE and the TLIA model. In Subsec-

tion 3.13.1, we observed a good agreement to the KS spectrum for the direct energy cascade, however, it was of insufficient resolution for the distinction between the two competing energy spectra. Nevertheless, in Subsection 3.13.2, we observed an excellent agreement of the wave action spectrum to the non-local LN spectrum, supporting the non-local analysis of the KS spectrum and the subsequent non-local theory for Kelvin WT. Despite this, we observed sand-pile behaviour in the LNE, an indication of mesoscopic WT. One factor contributing to this would be a lack of wave resonances, due to an insufficient resolution - a fact not helped by the one-dimesionality of the problem. The LNE would provide an interesting model for the investigation of mesoscopic WT and would help understand the bursty behaviour we observe.

Although the wave action spectrum is important, it is only one indication of WT. Further analysis in determining the constant prefactor of the energy flux is essential, as both spectra involve different numerical prefactors. Ideally, this should be undertaken in a high resolution direct numerical simulation of the unapproximated BSE. We plan on implementing such an approach in the near future and hope to resolve the debate about whether Kelvin wave interactions are local or not.

Finally in Chapter 3, we investigated a possible fluctuation relation for the time fluctuations of the energy flux. We noted that the GCFR for entropy production has been considered in various non-equilibrium systems and confirmed, however, a contradictory nonlinear relation has also been suggested. Indeed, the subsequent analysis from the LNE suggests a possible agreement with the GCFR at low disturbances. However, the result is not of sufficient smoothness to determine any possible relation at high fluctuations. This gives a positive indication that a high resolution and well averaged simulation, with a possible extension to the theory to fluxes, would be beneficial.

In Chapter 4, we introduced the field of OWT, where waves of light propagating through a nonlinear medium weakly interact. One intriguing aspect of OWT is the inverse cascade, where wave action is transported to large scales. This process is analogous to BEC in super-cooled alkali gases. We demonstrated this process with the first experimental implementation of 1D OWT. We showed that by injecting high frequency waves into a nonlinear LC cell, we observed a wave turbulent inverse cascade, followed by

the condensation of photon into coherent solitons. Moreover, we supported the experimental findings by performing numerical simulation of the LWE. Analysis of the inverse cascade by WT theory predicted that a pure KZ state was not realisable. However, we determined that the inverse cascade can be described by a mixed wave action spectrum of thermal and non-equilibrium parts. The inverse cascade is associated with the growth of nonlinearity of the system, gradually resulting in the formation of solitons by MI. We observed solitons in both the experiment and numerical simulations, and found that the system relaxes to a state of a single dominant soliton. During the transition to this final state, we observed interactions between solitons and the random wave background. With the aid of WT theory, we developed a strong WT description for the behaviour of the system in the form of a WTLC. The WTLC diagrammatically represents the coexistence of coherent solitons and the incoherent random wave background.

In addition to the experimental setup, we performed numerical simulations of the LWE and SWE in non-equilibrium stationary regimes. This allowed for the subsequent observation of the KZ solutions. Theoretically we discovered that the LWE emits fluxes of opposite sign to what is necessary for the KZ states, and this was further verified by a lack of agreement of the wave action spectrum to the KZ solutions. Conversely, this problem does not occur for the SWE. However, we showed that both the KZ for the SWE are non-local and thus, non-realisable. Surprisingly, we observed good agreements to the KZ predictions for both the direct and inverse cascades. Further investigation into the fluxes yielded a non-constant energy flux for the direct cascade - a constant flux being an essential requirement for a local KZ solution. This indicates that we observed a possible non-local wave action spectrum and if so, we are led to ask what non-local process determines this power law? The answer to this can be determined with a development of a non-local theory for 1D OWT in the short-wave limit - which is a future goal of ours. The inverse cascade for the SWE yielded an excellent agreement to the KZ solution and a good indication of a constant negative flux of wave action. This suggests that the inverse cascade is of KZ type, contradicting the non-locality analysis of Section 4.8 and thus raising questions in itself. Thus further analysis of the numerical prefactor of the wave action spectrum is required and a possible explanation

of the observations via a non-local theory.

We consider Chapter 4 as an initial investigation to OWT. Our analysis has raised several new questions that need to be addressed with additional experiments and numerical simulations. There is yet an experimental investigation into higher dimensional OWT, which we believe is a natural extension to the research presented in this thesis. In addition, the description of the evolution of solitons, with the possible understanding of their behaviour and manipulation would be valuable to any future industrial applications in nonlinear optics. Several applications of OWT have been recently suggested, including a WT laser - the random coherence of light through weakly nonlinear wave interactions and to applications in noise filtering and image reconstruction, which we plan on pursuing in the near future.

Appendix A

The Canonical Transformation

The CT enables the elimination of the non-resonant four-wave interactions, and the subsequent description of the leading resonant six-wave interactions. The CT is derived from an auxiliary Hamiltonian (2.29). The coefficients of the CT, (2.30), are derived by applying formulae (2.31) to the auxiliary Hamiltonian. The first coefficient of the CT,

(2.31a), is given by

$$\begin{aligned}
\left(\frac{\partial c(\mathbf{k}, t)}{\partial t} \right)_{t=0} = & -i \left[\frac{1}{2} \sum_{1,2} \tilde{V}_{\mathbf{k}}^{1,2} \delta_{\mathbf{k}}^{1,2} c_1 c_2 + 2 \left(\tilde{V}_2^{\mathbf{k},1} \right)^* \delta_2^{\mathbf{k},1} c_1^* c_2 \right. \\
& + \frac{1}{2} \sum_{1,2} \left(\tilde{U}^{\mathbf{k},1,2} \right)^* \delta^{\mathbf{k},1,2} c_1^* c_2^* + \frac{1}{2} \sum_{1,2,3} \tilde{W}_{\mathbf{k},3}^{1,2} \delta_{\mathbf{k},3}^{1,2} c_1 c_2 c_3^* \\
& + \frac{1}{6} \sum_{1,2,3} \tilde{X}_{\mathbf{k}}^{1,2,3} \delta_{\mathbf{k}}^{1,2,3} c_1 c_2 c_3 + 3 \left(\tilde{X}_3^{\mathbf{k},1,2} \right)^* \delta_3^{\mathbf{k},1,2} c_1^* c_2^* c_3 \\
& + \frac{1}{6} \sum_{1,2,3} \left(\tilde{Y}^{\mathbf{k},1,2,3} \right)^* \delta^{\mathbf{k},1,2,3} c_1^* c_2^* c_3^* \\
& + \frac{1}{24} \sum_{1,2,3,4} \left(\tilde{A}^{\mathbf{k},1,2,3,4} \right)^* \delta^{\mathbf{k},1,2,3,4} c_1^* c_2^* c_3^* c_4 \\
& + \frac{1}{24} \sum_{1,2,3,4} \tilde{B}_{\mathbf{k}}^{1,2,3,4} \delta_{\mathbf{k}}^{1,2,3,4} c_1 c_2 c_3 c_4 + 4 \left(\tilde{B}_4^{\mathbf{k},1,2,3} \right)^* \delta_4^{\mathbf{k},1,2,3} c_1^* c_2^* c_3^* c_4 \\
& + \frac{1}{12} \sum_{1,2,3,4} 2 \tilde{C}_{\mathbf{k},4}^{1,2,3} \delta_{\mathbf{k},4}^{1,2,3} c_1 c_2 c_3 c_4^* + 3 \left(\tilde{C}_{3,4}^{\mathbf{k},1,2} \right)^* \delta_{3,4}^{\mathbf{k},1,2} c_1^* c_2^* c_3 c_4 \\
& + \frac{1}{12} \sum_{1,2,3,4,5} \tilde{T}_{\mathbf{k},4,5}^{1,2,3} \delta_{\mathbf{k},4,5}^{1,2,3} c_1 c_2 c_3 c_4^* c_5^* \\
& + \frac{1}{120} \sum_{1,2,3,4,5} \tilde{Q}_{\mathbf{k}}^{1,2,3,4,5} \delta_{\mathbf{k}}^{1,2,3,4,5} c_1 c_2 c_3 c_4 c_5 \\
& + 5 \left(\tilde{Q}_5^{\mathbf{k},1,2,3,4} \right)^* \delta_5^{\mathbf{k},1,2,3,4} c_1^* c_2^* c_3^* c_4^* c_5 \\
& + \frac{1}{48} \sum_{1,2,3,4,5} 2 \tilde{R}_{\mathbf{k},5}^{1,2,3,4} \delta_{\mathbf{k},5}^{1,2,3,4} c_1 c_2 c_3 c_4 c_5^* \\
& + 4 \left(\tilde{R}_{4,5}^{\mathbf{k},1,2,3} \right)^* \delta_{4,5}^{\mathbf{k},1,2,3} c_1^* c_2^* c_3^* c_4 c_5 \\
& \left. + \frac{1}{6} \sum_{1,2,3,4,5} \left(\tilde{S}^{\mathbf{k},1,2,3,4,5} \right)^* \delta^{\mathbf{k},1,2,3,4,5} c_1^* c_2^* c_3^* c_4^* c_5^* \right]. \tag{A.1}
\end{aligned}$$

The second coefficient, (2.31b), is derived by taking the time derivative of coefficient (A.1). Then each time derivative of variable $c_{\mathbf{k}}$ can then be subsequently replaced by using Formula (A.1).

Appendix B

The Zakharov Transform

The ZT acts on six regions of the domain of the collision integral. It enables for five of the regions to be transformed onto just one region with the aid of the symmetries in the collision integral. In Chapter 2, we have already presented one transform. In this Appendix, we give the four remaining transformations, given by

$$\tilde{\mathbf{k}}_1 = \frac{\tilde{\mathbf{k}}\tilde{\mathbf{k}}'_1}{\tilde{\mathbf{k}}'_2}, \quad \tilde{\mathbf{k}}_2 = \frac{\tilde{\mathbf{k}}^2}{\tilde{\mathbf{k}}'_2}, \quad \tilde{\mathbf{k}}_3 = \frac{\tilde{\mathbf{k}}\tilde{\mathbf{k}}'_3}{\tilde{\mathbf{k}}'_2}, \quad \tilde{\mathbf{k}}_4 = \frac{\tilde{\mathbf{k}}\tilde{\mathbf{k}}'_4}{\tilde{\mathbf{k}}'_2} \quad \text{and} \quad \tilde{\mathbf{k}}_5 = \frac{\tilde{\mathbf{k}}\tilde{\mathbf{k}}'_5}{\tilde{\mathbf{k}}'_2}, \quad (\text{B.1a})$$

with Jacobian $J = -\left(\tilde{\mathbf{k}}/\tilde{\mathbf{k}}'_2\right)^6$.

$$\tilde{\mathbf{k}}_1 = \frac{\tilde{\mathbf{k}}\tilde{\mathbf{k}}'_4}{\tilde{\mathbf{k}}'_3}, \quad \tilde{\mathbf{k}}_2 = \frac{\tilde{\mathbf{k}}\tilde{\mathbf{k}}'_5}{\tilde{\mathbf{k}}'_3}, \quad \tilde{\mathbf{k}}_3 = \frac{\tilde{\mathbf{k}}^2}{\tilde{\mathbf{k}}'_3}, \quad \tilde{\mathbf{k}}_4 = \frac{\tilde{\mathbf{k}}\tilde{\mathbf{k}}'_1}{\tilde{\mathbf{k}}'_3} \quad \text{and} \quad \tilde{\mathbf{k}}_5 = \frac{\tilde{\mathbf{k}}\tilde{\mathbf{k}}'_2}{\tilde{\mathbf{k}}'_3}, \quad (\text{B.1b})$$

with Jacobian $J = -\left(\tilde{\mathbf{k}}/\tilde{\mathbf{k}}'_3\right)^6$.

$$\tilde{\mathbf{k}}_1 = \frac{\tilde{\mathbf{k}}\tilde{\mathbf{k}}'_5}{\tilde{\mathbf{k}}'_4}, \quad \tilde{\mathbf{k}}_2 = \frac{\tilde{\mathbf{k}}\tilde{\mathbf{k}}'_3}{\tilde{\mathbf{k}}'_4}, \quad \tilde{\mathbf{k}}_3 = \frac{\tilde{\mathbf{k}}\tilde{\mathbf{k}}'_2}{\tilde{\mathbf{k}}'_4}, \quad \tilde{\mathbf{k}}_4 = \frac{\tilde{\mathbf{k}}^2}{\tilde{\mathbf{k}}'_4} \quad \text{and} \quad \tilde{\mathbf{k}}_5 = \frac{\tilde{\mathbf{k}}\tilde{\mathbf{k}}'_1}{\tilde{\mathbf{k}}'_4}, \quad (\text{B.1c})$$

with Jacobian $J = -\left(\tilde{\mathbf{k}}/\tilde{\mathbf{k}}'_4\right)^6$.

$$\tilde{\mathbf{k}}_1 = \frac{\tilde{\mathbf{k}}\tilde{\mathbf{k}}'_3}{\tilde{\mathbf{k}}'_5}, \quad \tilde{\mathbf{k}}_2 = \frac{\tilde{\mathbf{k}}\tilde{\mathbf{k}}'_4}{\tilde{\mathbf{k}}'_5}, \quad \tilde{\mathbf{k}}_3 = \frac{\tilde{\mathbf{k}}\tilde{\mathbf{k}}'_1}{\tilde{\mathbf{k}}'_5}, \quad \tilde{\mathbf{k}}_4 = \frac{\tilde{\mathbf{k}}\tilde{\mathbf{k}}'_2}{\tilde{\mathbf{k}}'_5} \quad \text{and} \quad \tilde{\mathbf{k}}_5 = \frac{\tilde{\mathbf{k}}^2}{\tilde{\mathbf{k}}'_5}, \quad (\text{B.1d})$$

with Jacobian $J = -\left(\tilde{\mathbf{k}}/\tilde{\mathbf{k}}_5'\right)^6$.

Appendix C

Derivation of the Interaction Coefficients for the Biot-Savart Equation

In this Appendix, we derive the interaction coefficients for the Hamiltonian description for the BSE. Recall from Chapter 3 that the BSE Hamiltonian can be written as

$$\mathcal{H}_2 = \frac{\kappa}{8\pi} \int \frac{[2\Re(w'^*(z_1)w'(z_2)) - \epsilon^2]}{|z_1 - z_2|} dz_1 dz_2, \quad (\text{C.1a})$$

$$\mathcal{H}_4 = \frac{\kappa}{32\pi} \int \frac{[3\epsilon^4 - 4\epsilon^2\Re(w'^*(z_1)w'(z_2))]}{|z_1 - z_2|} dz_1 dz_2, \quad (\text{C.1b})$$

$$\mathcal{H}_6 = \frac{\kappa}{64\pi} \int \frac{[6\epsilon^4\Re(w'^*(z_1)w'(z_2)) - 5\epsilon^6]}{|z_1 - z_2|} dz_1 dz_2. \quad (\text{C.1c})$$

We would like to deal with Hamiltonian (C.1), in Fourier space by introducing the wave amplitude variable $a_{\mathbf{k}}$. Using the Fourier representation, (2.16), we introduce additional integration variables, the wave numbers. Moreover, invoking a cut-off at $a_0 < |z_1 - z_2|$, to avoid the singularity in the BSE (3.2), we derive the coefficients of \mathcal{H}_2 , \mathcal{H}_4 and \mathcal{H}_6 in terms of cosines in Fourier space [11]. Once Equations (C.1) are written in terms of wave amplitudes, we can transform to variables z_- and z_+ , defined as $z_- = |z_1 - z_2|$, which ranges from the vortex core radius a_0 to ∞ , and $z_+ = z_1 + z_2$,

ranging from $-\infty$ to ∞ . Cosine functions arise due to the collection of exponentials with powers in variable z_- . Subsequently, the remaining exponentials with powers of variable z_+ can be integrated out with respect to z_+ , yielding the corresponding delta function for the conservation of wave numbers $\delta_{4,5,6}^{1,2,3}$. The explicit formulae of the four-wave, $T_{3,4}^{1,2}$, and the six-wave, $W_{4,5,6}^{1,2,3}$, interaction coefficients can be expressed as [11]

$$\omega_k = \frac{\kappa}{2\pi} [A - B], \quad (\text{C.2a})$$

$$T_{3,4}^{1,2} = \frac{1}{4\pi} [6D - E], \quad (\text{C.2b})$$

$$W_{4,5,6}^{1,2,3} = \frac{9}{4\pi\kappa} [3P - 5Q], \quad (\text{C.2c})$$

where A , B , D , E , P and Q are integrals of cosines:

$$A = \int_{a_0}^{\infty} \frac{1}{z_-} k^2 C^k dz_-, \quad (\text{C.3a})$$

$$B = \int_{a_0}^{\infty} \frac{1}{z_-^3} [1 - C^k] dz_-, \quad (\text{C.3b})$$

$$D = \int_{a_0}^{\infty} \frac{1}{z_-^5} [1 - C_1 - C_2 - C^3 - C^4 + C_2^3 + C^{43} + C_2^4] dz_-, \quad (\text{C.3c})$$

$$E = \int_{a_0}^{\infty} \frac{1}{z_-^3} [\mathbf{k}_1 \mathbf{k}_4 (C^4 + C_1 - C^{43} - C_2^4) + \mathbf{k}_1 \mathbf{k}_3 (C^3 + C_1 - C^{43} - C_2^3) + \mathbf{k}_3 \mathbf{k}_2 (C^3 + C_2 - C^{43} - C_1^3) + \mathbf{k}_4 \mathbf{k}_2 (C^4 + C_2 - C^{43} - C_2^3)] dz_-, \quad (\text{C.3d})$$

$$P = \int_{a_0}^{\infty} \frac{1}{z_-^5} \mathbf{k}_6 \mathbf{k}_2 [C_2 - C_2^5 - C_{23} + C_{23}^5 - C_2^4 + C_2^{45} + C_{23}^4 - C_1^6 + C^6 - C^{56} - C_3^6 + C_3^{56} - C^{46} + C^{456} + C_3^{46} - C_{12}] dz_-, \quad (\text{C.3e})$$

$$Q = \int_{a_0}^{\infty} \frac{1}{z_-^7} [1 - C^4 - C_1 + C_1^4 - C^6 + C^{46} + C_1^6 - C_1^{46} - C^5 + C^{45} + C_1^5 - C_1^{45} + C^{65} - C^{456} - C_1^{56} + C_{23} - C_3 + C_3^4 + C_{13} - C_{13}^4 + C_3^6 - C_3^{46} - C_{13}^6 + C_2^5 + C_3^5 - C_3^{45} - C_{13}^5 + C_2^6 - C_3^{56} + C_{12} + C_2^4 - C_2] dz_-, \quad (\text{C.3f})$$

where the variable, $z_- = |z_1 - z_2|$ and the expressions C , are cosine functions such that $C_1 = \cos(\mathbf{k}_1 z_-)$, $C_1^4 = \cos((\mathbf{k}_4 - \mathbf{k}_1) z_-)$, $C_1^{45} = \cos((\mathbf{k}_4 + \mathbf{k}_5 - \mathbf{k}_1) z_-)$, $C_{12}^{45} =$

$\cos((\mathbf{k}_4 + \mathbf{k}_5 - \mathbf{k}_1 - \mathbf{k}_2)z_-)$ and so on.

The trick used for explicit calculation of the analytical form of these integrals was suggested and used in [7]. First, we apply integration by parts to all the cosine integrals, so they can be expressed in the form of $\int_{a_0}^{\infty} \frac{\cos(z)}{z} dz$. Then, we use the following cosine identity for this integral [173], given by

$$\begin{aligned} \int_{a_0}^{\infty} \frac{\cos(z)}{z} dz &= -\gamma - \ln(a_0) - \int_0^{a_0} \frac{\cos(z) - 1}{z} dz, \\ &= -\gamma - \ln(a_0) - \sum_{i=1}^{\infty} \frac{(-a_0^2)^i}{2i(2i)!}, \\ &= -\gamma - \ln(a_0) + \mathcal{O}(a_0^2). \end{aligned} \quad (\text{C.4})$$

For example, let us consider the following general cosine expression that can be found in Equation (C.3c): $\int_{a_0}^{\infty} z^{-3} \cos(\mathcal{K}z) dz$, where \mathcal{K} is an expression that involves a linear combination of wave numbers, i.e. $\mathcal{K} = \mathbf{k}_1 - \mathbf{k}_4$. Therefore, applying integration by parts to this integral yields

$$\begin{aligned} \int_{a_0}^{\infty} \frac{\cos(\mathcal{K}z)}{z^3} dz &= \left[-\frac{\cos(\mathcal{K}z)}{2z^2} \right]_{a_0}^{\infty} + \left[\frac{\mathcal{K} \sin(\mathcal{K}z)}{2z} \right]_{a_0}^{\infty} - \frac{\mathcal{K}}{2} \int_{a_0}^{\infty} \frac{\cos(\mathcal{K}z)}{z} dz, \\ &= \frac{\cos(\mathcal{K}a_0)}{2a_0^2} - \frac{\mathcal{K} \sin(\mathcal{K}a_0)}{2a_0} - \frac{\mathcal{K}^2}{2} \int_{\mathcal{K}a_0}^{\infty} \frac{\cos(y)}{y} dy. \end{aligned} \quad (\text{C.5})$$

Subsequently, we consider the Taylor expansion $\cos(\mathcal{K}a_0)$ and $\sin(\mathcal{K}a_0)$ in powers of small a_0 , and apply the cosine formula, (C.4), to the last integral. This method give the final expression of

$$\int_{a_0}^{\infty} \frac{\cos(\mathcal{K}z)}{z^3} dz = \frac{1}{2a_0^2} - \frac{3\mathcal{K}^2}{4} + \frac{\mathcal{K}^2}{2} [\gamma + \ln(|\mathcal{K}a_0|)] + \mathcal{O}(a_0^2). \quad (\text{C.6})$$

With a similar application to the other cosine integrals, we produce an expansion of the interaction coefficients (C.3) in terms of the cut-off parameter, a_0 . After the summation of each contribution we find that all negative powers of a_0 (that will diverge in the limit $a_0 \rightarrow 0$) cancel in the final expression for each interaction coefficient. Neglecting,

terms of $\mathcal{O}(a_0)$ or higher¹, our final expression for the interaction coefficients involve the leading logarithmic divergent and the $\mathcal{O}(1)$ contributions given by [7]

$$\Lambda_0 = \ln(\ell/a_0), \quad (\text{C.7a})$$

$$\omega_k = \frac{\kappa k^2}{4\pi} \left[\Lambda_0 - \gamma - \frac{3}{2} - \ln(k\ell) \right], \quad (\text{C.7b})$$

$$T_{3,4}^{1,2} = \frac{1}{16\pi} \left[\mathbf{k}_1 \mathbf{k}_2 \mathbf{k}_3 \mathbf{k}_4 (1 + 4\gamma - 4\Lambda_0) - \mathcal{F}_{3,4}^{1,2} \right], \quad (\text{C.7c})$$

$$W_{4,5,6}^{1,2,3} = \frac{9}{32\pi\kappa} \left[\mathbf{k}_1 \mathbf{k}_2 \mathbf{k}_3 \mathbf{k}_4 \mathbf{k}_5 \mathbf{k}_6 (1 - 4\gamma + 4\Lambda_0) - \mathcal{G}_{4,5,6}^{1,2,3} \right], \quad (\text{C.7d})$$

where $\mathcal{F}_{3,4}^{1,2}$ and $\mathcal{G}_{4,5,6}^{1,2,3}$ are defined in the next Section.

C.1 The Four-Wave Function $\mathcal{F}_{3,4}^{1,2}$

A rather cumbersome calculation, presented above, results in an explicit equation for the four-wave interaction function $\mathcal{F}_{3,4}^{1,2}$ in Equation (3.13b) and Equation (C.7c). Function $\mathcal{F}_{3,4}^{1,2}$ is a symmetrical version of $F_{3,4}^{1,2}$: $\mathcal{F}_{3,4}^{1,2} = \{F_{3,4}^{1,2}\}_S$ where the operator $\{\dots\}_S$ implies symmetry with respect to $\mathbf{k}_1 \leftrightarrow \mathbf{k}_2$, $\mathbf{k}_3 \leftrightarrow \mathbf{k}_4$ and $\{\mathbf{k}_1, \mathbf{k}_2\} \leftrightarrow \{\mathbf{k}_3, \mathbf{k}_4\}$. The definition of $F_{3,4}^{1,2}$ is given by

$$F_{3,4}^{1,2} \equiv \sum_{\mathcal{K} \in \mathcal{K}_1} \mathcal{K}^4 \ln(|\mathcal{K}| \ell) + 2 \sum_{i,j} \sum_{\mathcal{K} \in \mathcal{K}_{ij}} \mathbf{k}_i \mathbf{k}_j \mathcal{K}^2 \ln(|\mathcal{K}| \ell) . \quad (\text{C.8})$$

In Equation (C.8), $\sum_{i,j}$ denotes sum of four terms with respect to $(i,j) = \{(4,1), (3,1), (3,2), (4,2)\}$, and \mathcal{K} is either a single wave number or a linear combination of wave numbers that belong to one of the following sets:

$$\mathcal{K}_1 = \{-[1], -[2], -[3], -[4], +[3], +[4]\}, \quad (\text{C.9a})$$

$$\mathcal{K}_{41} = \{+[4], +[1], -[43], -[2]\}, \quad (\text{C.9b})$$

$$\mathcal{K}_{31} = \{+[3], +[1], -[43], -[2]\}, \quad (\text{C.9c})$$

$$\mathcal{K}_{32} = \{+[3], +[2], -[43], -[1]\}, \quad (\text{C.9d})$$

$$\mathcal{K}_{42} = \{+[4], +[2], -[43], -[1]\}. \quad (\text{C.9e})$$

¹These terms will vanish in the limit as $a_0 \rightarrow 0$.

Here we have used the following notations with $\alpha, \beta, \gamma = 1, 2, 3, 4$: $[\alpha] = \mathbf{k}_\alpha$, $[\beta] = -\mathbf{k}_\beta$, $[\alpha] = \mathbf{k}_\alpha - \mathbf{k}_\beta$, $[\alpha\gamma] = \mathbf{k}_\alpha + \mathbf{k}_\gamma$, $[\beta\gamma] = -\mathbf{k}_\beta - \mathbf{k}_\gamma$. The $+$ or $-$ before $[\dots]$ refer to prefactors $+1$ or -1 in the corresponding terms in the sum, e.g.

$$\begin{aligned} \mathcal{K}^4 \ln(|\mathcal{K}| \ell) \text{ for } \mathcal{K} \in \{-[1]\} \text{ is } & -k_1^4 \ln(|\mathbf{k}_1| \ell), \\ \mathcal{K}^4 \ln(|\mathcal{K}| \ell) \text{ for } \mathcal{K} \in \{+[4][2]\} \text{ is } & +(k_4 - k_2)^4 \ln(|\mathbf{k}_4 - \mathbf{k}_2| \ell), \\ \mathbf{k}_i \mathbf{k}_j \mathcal{K}^2 \ln(|\mathcal{K}| \ell) \text{ for } i = 4, j = 1, & \\ \mathcal{K} \in \{-[43]\} \text{ is } & -\mathbf{k}_4 \mathbf{k}_1 (\mathbf{k}_4 + \mathbf{k}_3)^4 \ln(|\mathbf{k}_4 + \mathbf{k}_3| \ell). \end{aligned}$$

C.2 The Six-Wave Function $\mathcal{G}_{4,5,6}^{1,2,3}$

Function $\mathcal{G}_{4,5,6}^{1,2,3} = \left\{ G_{4,5,6}^{1,2,3} \right\}_S$ is the symmetric version of function $G_{4,5,6}^{1,2,3}$. The operator $\{\dots\}_S$ denotes symmetry with respect to $\mathbf{k}_1 \leftrightarrow \mathbf{k}_2 \leftrightarrow \mathbf{k}_3$, $\mathbf{k}_4 \leftrightarrow \mathbf{k}_5 \leftrightarrow \mathbf{k}_6$ and $\{\mathbf{k}_1, \mathbf{k}_2, \mathbf{k}_3\} \leftrightarrow \{\mathbf{k}_4, \mathbf{k}_5, \mathbf{k}_6\}$. The definition of $G_{4,5,6}^{1,2,3}$ is derived from the previous Section and is given by

$$G_{4,5,6}^{1,2,3} \equiv \sum_{\mathcal{K} \in \mathcal{K}_3} \mathbf{k}_6 \mathbf{k}_2 \mathcal{K}^4 \ln(|\mathcal{K}| \ell) + \frac{1}{18} \sum_{\mathcal{K} \in \mathcal{K}_4} \mathcal{K}^6 \ln(|\mathcal{K}| \ell), \quad (\text{C.10a})$$

where

$$\begin{aligned} \mathcal{K}_3 = & \left\{ +[2], -[5], -[23], +[5][23], -[4][2], +[45][2], +[4][23], -[6][1], +[6], -[56], -[6][3], \right. \\ & \left. +[56][3], -[46], +[456], +[46], -[12] \right\}, \end{aligned} \quad (\text{C.10b})$$

$$\begin{aligned} \mathcal{K}_4 = & \left\{ -[4], -[1], +[4][1], -[6], +[46], +[6][1], -[46][1], -[5], +[45], +[5][1], -[45][1], \right. \\ & +[65], -[456], -[56][1], +[23], -[3], +[4][3], +[13], -[4][13], +[6][3], -[46][3], \\ & \left. -[6][13], +[5][2], +[5][3], -[45][3], -[5][13], +[6][2], -[65][3], +[12], +[4][2], -[2] \right\}. \end{aligned} \quad (\text{C.10c})$$

Appendix D

The Asymptotic Expansion of ${}^c\mathcal{W}_{4,5,6}^{1,2,3}$

D.1 The Analytical Expression for ${}^c\mathcal{W}_{4,5,6}^{1,2,3}$ with Two Small Wave Numbers

In this Section, we will consider the asymptotic limit of ${}^c\mathcal{W}_{4,5,6}^{1,2,3}$ when two wave numbers tend to zero. In order to achieve this, we will use the terms of the interaction coefficient ${}^c\mathcal{W}_{4,5,6}^{1,2,3}$ given in Equations (3.19) and (3.25), and apply the consider the parametrisation of the LIA resonance condition (2.112). We presented in Section 3.6, using the Mathematica package, the Taylor expansion of ${}^c\mathcal{W}_{4,5,6}^{1,2,3}$ with respect to one wave number, e.g. \mathbf{k}_6 , we obtain a remarkably simple result - expression (3.27a).

Now we will consider the asymptotical limit when two of the wave numbers, say \mathbf{k}_3 and \mathbf{k}_6 (let them be on the opposite sides of the resonance condition), are less than the other wave numbers in the sextet. Again, by using Mathematica, we can compute the Taylor expansion of ${}^c\mathcal{W}_{4,5,6}^{1,2,3}$ with respect to two small wave numbers, \mathbf{k}_3 and \mathbf{k}_6 , giving

$$\lim_{\substack{\mathbf{k}_3 \rightarrow 0 \\ \mathbf{k}_6 \rightarrow 0}} {}^c\mathcal{W}_{4,5,6}^{1,2,3} = -\frac{3}{4\pi\kappa} k_1^2 \mathbf{k}_3 k_4^2 \mathbf{k}_6. \quad (\text{D.1})$$

Simultaneously, in the same limit, the parametrisation for the LIA resonance condition, (2.112), implies

$$\lim_{\begin{array}{c} \mathbf{k}_3 \rightarrow 0 \\ \mathbf{k}_6 \rightarrow 0 \end{array}} \mathbf{k}_2 = \mathbf{k}_4, \quad \lim_{\begin{array}{c} \mathbf{k}_3 \rightarrow 0 \\ \mathbf{k}_6 \rightarrow 0 \end{array}} \mathbf{k}_5 = \mathbf{k}_1. \quad (\text{D.2})$$

Therefore, Equation (D.1) coincides with Equation (3.27a). Note, that this was not obvious *a priori*, because formally, Equation (3.27a), was obtained when \mathbf{k}_6 was much less than the rest of the wave numbers, including \mathbf{k}_3 .

For reference, we provide expressions for the different contributions to the full six-wave interaction coefficient, ${}^c\mathcal{W}_{4,5,6}^{1,2,3}$, given in Equations (3.19) and (3.25). Then in the limits of $\mathbf{k}_3, \mathbf{k}_6 \rightarrow 0$, each contribution to the full six-wave interaction coefficient

can be expressed as

$$\begin{aligned} {}^1W_{4,5,6}^{1,2,3} &\rightarrow -\frac{3}{4\pi\kappa}k_1^2\mathbf{k}_3k_4^2\mathbf{k}_6 \left[\frac{3}{2}\ln(k\ell) - \frac{1}{24} \right. (49) \\ &- \frac{(1-x)^2(7+10x+7x^2)}{x^2} \ln|1-x| \\ &+ \left. 2x(12+7x)\ln|x| - 7\frac{(1+x)^4}{x^2}\ln|1+x| \right], \end{aligned} \quad (\text{D.3a})$$

$$\begin{aligned} {}^1Q_{4,5,6}^{1,2,3} = {}^2Q_{4,5,6}^{1,2,3} &\rightarrow -\frac{3}{4\pi\kappa}k_1^2\mathbf{k}_3k_4^2\mathbf{k}_6 \left[-\frac{3}{2}\ln(k\ell) + \frac{1}{48} \right. (59) \\ &- \frac{(1-x)^2(9+10x+9x^2)}{x^2} \ln|1-x| \\ &+ 2\left(9x^2+14x-6+\frac{2}{1-x}\right)\ln|x| \\ &- \left. 9\frac{(1+x)^4}{x^2}\ln|1+x| \right], \end{aligned} \quad (\text{D.3b})$$

$$\begin{aligned} {}^3Q_{4,5,6}^{1,2,3} &\rightarrow -\frac{3}{4\pi\kappa}k_1^2\mathbf{k}_3k_4^2\mathbf{k}_6 \left[\frac{3}{2}\ln(k\ell) + \frac{1}{48}(7 \right. \\ &+ \frac{(1-x)^2(1+x^2)}{x^2}\ln|1-x| \\ &+ 2\left(\frac{1-5x+x^3}{1-x}\right)\ln|x| + \left. \frac{(1+x)^4}{x^2}\ln|1+x| \right], \end{aligned} \quad (\text{D.3c})$$

$${}^1S_{4,5,6}^{1,2,3} \rightarrow -\frac{3}{4\pi\kappa}k_1^2\mathbf{k}_3k_4^2\mathbf{k}_6 \left[\frac{1}{6}\left(\frac{1+x}{1-x}\right)\ln|x| \right], \quad (\text{D.3d})$$

$$\begin{aligned} {}^1\mathcal{W}_{4,5,6}^{1,2,3} &\rightarrow -\frac{3}{4\pi\kappa}k_1^2\mathbf{k}_3k_4^2\mathbf{k}_6 \left[1 - \frac{1}{6}\left(\frac{1+x}{1-x}\right)\ln|x| \right], \quad (\text{D.3e}) \\ x &= \mathbf{k}_4/\mathbf{k}_1. \end{aligned}$$

The other possibility is for the two vanishing wave numbers to be on the same side of the sextet. We have checked that when the LIA resonance condition is satisfied, it also implies (3.27a).

D.2 The Analytical Expression for ${}^c\mathcal{W}_{4,5,6}^{1,2,3}$ with Four Small Wave Numbers

We calculate the asymptotic behaviour of ${}^c\mathcal{W}_{4,5,6}^{1,2,3}$ when four wave numbers are smaller than the remaining two. Again we utilise the Mathematica package and note, that the parametrisation for the LIA resonance condition automatically implies $k_2, k_3, k_4, k_6 \ll k_1, k_5$ from Equations (D.2). Therefore, we have

$$\lim_{\mathbf{k}_{2,3,4,6} \rightarrow 0} {}^c\mathcal{W}_{4,5,6}^{1,2,3} = -\frac{3}{4\pi\kappa} k_1^2 \mathbf{k}_3 k_4^2 \mathbf{k}_6. \quad (\text{D.4})$$

Thus, we have obtained an expression which coincides with (3.27a). We conclude that Equation (3.27a) is valid when \mathbf{k}_6 is much smaller than just one other wave number in the sextet, say \mathbf{k} , and not only when it is smaller than all of the remaining five wave numbers.

For reference, we present the term by term results for each contribution of ${}^c\mathcal{W}_{4,5,6}^{1,2,3}$, in the limit $k_2, k_3, k_4, k_6 \ll k_1, k_5$:

$$\begin{aligned} {}^1W_{4,5,6}^{1,2,3} &\rightarrow -\frac{3}{4\pi\kappa} k_1^2 \mathbf{k}_3 k_4^2 \mathbf{k}_6 \left[-1 + \frac{3}{2} \ln(k\ell) + 0 \right], \\ {}^1Q_{4,5,6}^{1,2,3} &\rightarrow -\frac{3}{4\pi\kappa} k_1^2 \mathbf{k}_3 k_4^2 \mathbf{k}_6 \left[\frac{1}{2} - \frac{3}{2} \ln(k\ell) - \frac{1}{6} \ln\left(\frac{k_4}{k_1}\right) \right], \\ {}^2Q_{4,5,6}^{1,2,3} &\rightarrow -\frac{3}{4\pi\kappa} k_1^2 \mathbf{k}_3 k_4^2 \mathbf{k}_6 \left[\frac{1}{2} - \frac{3}{2} \ln(k\ell) - \frac{1}{6} \ln\left(\frac{k_4}{k_1}\right) \right], \\ {}^3Q_{4,5,6}^{1,2,3} &\rightarrow -\frac{3}{4\pi\kappa} k_1^2 \mathbf{k}_3 k_4^2 \mathbf{k}_6 \left[1 + \frac{3}{2} \ln(k\ell) + \frac{1}{6} \ln\left(\frac{k_4}{k_1}\right) \right], \\ {}^1S_{4,5,6}^{1,2,3} &\rightarrow -\frac{3}{4\pi\kappa} k_1^2 \mathbf{k}_3 k_4^2 \mathbf{k}_6 \left[0 + 0 + \frac{1}{6} \ln\left(\frac{k_4}{k_1}\right) \right]. \end{aligned}$$

Hence the sum of these contributions give

$${}^c\mathcal{W}_{4,5,6}^{1,2,3} \rightarrow -\frac{3}{4\pi\kappa} k_1^2 \mathbf{k}_3 k_4^2 \mathbf{k}_6 [1 + 0 + 0]. \quad (\text{D.5})$$

Appendix E

The Intensity Spectrum

Experimentally, due to the difficulty in measuring the phase of $\psi(x, z)$, we cannot calculate $n_{\mathbf{k}}$ easily. However, we can measure the spectrum of Intensity $N_{\mathbf{k}} = |(|\psi|^2)_{\mathbf{k}}|^2$. Theoretically, we are able to relate the scaling of $N_{\mathbf{k}}$ with that of the KZ solution derived from the KE, (2.94). In this Appendix, we present the derivation of this relationship. Firstly, we must consider the expression for the light intensity in \mathbf{k} -space. Using the usual definition for the Fourier transform in \mathbb{R} , this implies

$$I_{\mathbf{k}} = (|\psi|^2)_{\mathbf{k}} = \int \psi(x)\psi^*(x)e^{-i\mathbf{k}x} dx, \quad (\text{E.1a})$$

$$= \int a_1 a_2^* \delta_1^{\mathbf{k},2} d\mathbf{k}_1 d\mathbf{k}_2. \quad (\text{E.1b})$$

Hence, for the intensity spectrum $N_{\mathbf{k}} = \langle |I_{\mathbf{k}}|^2 \rangle$ this gives

$$\langle |I_{\mathbf{k}}|^2 \rangle = \int \langle a_1 a_2 a_3^* a_4^* \rangle \delta_1^{\mathbf{k},4} \delta_3^{\mathbf{k},2} d\mathbf{k}_1 d\mathbf{k}_2 d\mathbf{k}_3 d\mathbf{k}_4. \quad (\text{E.2})$$

The next step is to average over phases, using our definition of an RPA field. This implies that only wave number pairings $\mathbf{k}_1 = \mathbf{k}_4$, $\mathbf{k}_2 = \mathbf{k}_3$ and $\mathbf{k}_1 = \mathbf{k}_3$, $\mathbf{k}_2 = \mathbf{k}_4$ will contribute to the intensity spectrum. Therefore, the intensity spectrum can be expressed

as

$$N_{\mathbf{k}} = \int \langle |a_1|^2 \rangle \langle |a_2|^2 \rangle \delta^{\mathbf{k}} \delta^{\mathbf{k}} d\mathbf{k}_1 d\mathbf{k}_2 + \int \langle |a_1|^2 |a_2|^2 \rangle \delta_1^{\mathbf{k},2} \delta_1^{\mathbf{k},2} d\mathbf{k}_1 d\mathbf{k}_2 \quad (\text{E.3a})$$

$$= \left(\int n_1 \delta^{\mathbf{k}} d\mathbf{k}_1 \right)^2 + \int n_1 n_2 \delta_1^{\mathbf{k},2} d\mathbf{k}_1 d\mathbf{k}_2. \quad (\text{E.3b})$$

We will examine the intensity spectrum, when the system is in a statistically non-equilibrium stationary state and the KZ solution is realised. Therefore, we can assume that the wave action spectrum is of the KZ form, i.e. $n_{\mathbf{k}} = Ck^{-x}$, where C is a constant determining the amplitude of the spectrum and x is the spectrum exponent. The first term of Equation (E.3b) contains a Dirac delta function, centred around $\mathbf{k} = 0$. Therefore, this implies that the contribution from this term will only appear at the zeroth mode¹. Conversely, the second term in Equation (E.3b) will contribute to the whole of \mathbf{k} -space, and will determine the scaling for the intensity spectrum. We can manipulate the second term, by using the Dirac delta function to eliminate one of the integration variables, i.e.

$$\begin{aligned} \int n_1 n_2 \delta_1^{\mathbf{k},2} d\mathbf{k}_1 d\mathbf{k}_2 &= \int n_1 n_{1-\mathbf{k}} d\mathbf{k}_1 \\ &= C^2 \int k_1^{-x} |\mathbf{k}_1 - \mathbf{k}|^{-x} d\mathbf{k}_1. \end{aligned} \quad (\text{E.4})$$

If Expression (E.4) converges on the KZ solution, then the integral will yield the intensity spectrum power law. To check for convergence, we change the integration variable to a non-dimensional variable $s = \mathbf{k}_1/\mathbf{k}$. Then, the intensity spectrum can be approximated by the integral:

$$\begin{aligned} N_{\mathbf{k}} &\approx C^2 k^{-2x+1} \int_{-\infty}^{\infty} s^{-x} |s - 1|^{-x} ds. \\ &\approx C^2 k^{-2x+1} \int_0^{\infty} s^{-x} (|s - 1|^{-x} + |s + 1|^{-x}) ds. \end{aligned} \quad (\text{E.5})$$

¹Numerically and experimentally this may be seen as a contribution around $\mathbf{k} = 0$.

Convergence must be checked in the regions where $s \rightarrow 0$ and $s \rightarrow \infty$. Therefore, as $s \rightarrow 0$, Relation (E.5) behaves as

$$\int_0^{\infty} s^{-x} (|s-1|^{-x} + |s+1|^{-x}) ds \propto \int_0^{\infty} s^{-x} ds, \quad (\text{E.6})$$

and therefore, the integral converges for $x < 1$.

In the limit when $s \rightarrow \infty$, integral (E.5) can be expressed as

$$\int_0^{\infty} s^{-x} (|s-1|^{-x} + |s+1|^{-x}) ds \propto \int_0^{\infty} s^{-2x} ds. \quad (\text{E.7})$$

The right-hand side of Expression (E.7) converges for $x > 1/2$. Therefore, the intensity spectrum integral, (E.5), is convergent in the region:

$$1/2 < x < 1, \quad (\text{E.8})$$

Experimentally, we can only set up the inverse cascade scenario. Subsequently, we only measure the intensity spectrum in the inverse cascade regime. The exponent of the KZ solution for the inverse cascade is given in Equation (4.20b), which lies inside the region of convergence (E.8), and corresponds to an intensity spectrum of

$$N_{\mathbf{k}} \propto k^{-1/5}. \quad (\text{E.9})$$

Appendix F

Non-Dimensionalisation of the Optical Wave Turbulence Models

The dimensional models for OWT contain several physical constants and parameters. For convenience and clarity, it is preferred to consider dimensionless models. Therefore, we present our non-dimensional descriptions for the LWE, (4.6) and the SWE, (4.8). We follow the non-dimensionalisation that was performed in [154], where the authors introduced the following dimensionless variables:

$$\psi = (\psi_c / \sqrt{\alpha}) \psi^*(x^*, z^*), \quad x^* = x/x_c \sqrt{\alpha}, \quad z^* = z/z_c \alpha \quad (\text{F.1})$$

with $\psi_c^2 = 2K/\varepsilon_0 k_0^2 n_a^4 l_\xi^4$, $z_c = 2ql_\xi^2$ and $x_c = l_\xi$. The electrical coherence length of the LC was already introduced in Chapter 4 and is defined as $l_\xi = \sqrt{\pi K/2\Delta\varepsilon}(d/V_0)$.

Non-dimensionalisation (F.1), expresses the LWE in the form:

$$i \frac{\partial \psi}{\partial z} = -\frac{\partial^2 \psi}{\partial x^2} - \frac{1}{2} \psi |\psi|^2 - \frac{1}{2\alpha} \psi \frac{\partial^2 |\psi|^2}{\partial x^2}, \quad (\text{F.2})$$

where α is a tunable parameter that adjusts the strength of the second nonlinear term. The weak nonlinearity of the system can be adjusted by the amplitude of $\psi(x, z)$, however, parameter α , provides additional control on the balance of the two nonlinear terms. This is important as the long-wave limit implies that $(k^*)^2 / \alpha \ll 1$, where k^* is

the dimensionless wave number.

Similarly, we can derive a non-dimensional model for the SWE. Using the same dimensionless variables, (F.1), we can represent the SWE in the dimensionless form:

$$i \frac{\partial \psi}{\partial z} = -\frac{\partial^2 \psi}{\partial x^2} + \frac{1}{2} \psi \frac{\partial^{-2} |\psi|^2}{\partial x^{-2}}. \quad (\text{F.3})$$

Bibliography

- [1] S. Nazarenko, *Wave Turbulence*. Springer-Verlag, 2010.
- [2] Y. Choi, Y. L'vov, and S. Nazarenko, "Wave Turbulence," *Recent Res. Devel. Fluid Dynamics*, no. 5, 2004.
- [3] Y. Choi, Y. L'vov, S. Nazarenko, and B. Pokorni, "Anomalous Probability of High Amplitudes in Wave Turbulence," *Physical Review A*, vol. 339, no. 3-5, pp. 361–369, 2004.
- [4] Y. Choi, Y. L'vov, and S. Nazarenko, "Joint Statistics of Amplitudes and Phases in Wave Turbulence," *Physica D*, no. 201, pp. 121–149, 2005.
- [5] Y. Choi, G. Jo, H. Kim, and S. Nazarenko, "Aspects of Two-Mode Probability Density Function in Weak Wave Turbulence," *Journal of the Physical Society of Japan*, vol. 78, no. 084403, 2009.
- [6] V. Zakharov, V. Lvov, and G. Falkovich, *Kolmogorov Spectra of Turbulence I: Wave Turbulence*. Springer, 1992.
- [7] G. Boffetta, A. Celani, D. Dezzani, J. Laurie, and S. Nazarenko, "Modeling Kelvin Wave Cascades in Superfluid Helium," *Journal of Low Temperature Physics*, no. 3-6, pp. 193–214, 2009.
- [8] U. Bortolozzo, J. Laurie, S. Nazarenko, and S. Residori, "Optical Wave Turbulence and the Condensation of Light," *Journal of Optical Society of America B*, vol. 26, no. 12, pp. 2280–2284, 2009.

- [9] J. Laurie, V. L'vov, S. Nazarenko, and O. Rudenko, "Interaction of Kelvin Waves and Non-Locality of the Energy Transfer in Superfluids," *Physical Review B*, vol. 81, no. 10, 2010.
- [10] B. Svistunov, "Superfluid Turbulence in the Low-Temperature Limit," *Physical Review B*, vol. 52, no. 3647, 1995.
- [11] E. Kozik and B. Svistunov, "Kelvin-Wave Cascade and Decay of Superfluid Turbulence," *Physical Review Letters*, vol. 92, no. 3, 2004.
- [12] R. Peierls, "Zur Kinetischen Theorie der Wärmeleitung in Kristallen," *Annalen den Physik* 3, pp. 1055–1101, 1929.
- [13] A. Vedenov, *Reviews of Plasma Physics*. Consultants Bureau, New York, 1967, vol. 3, ch. Theory of Weakly Turbulent Plasma, p. 229.
- [14] A. Galeev and R. Sagdeev, *Review of Plasma Physics*. Consultants Bureau, New York, 1979, vol. 7.
- [15] K. Hasselmann, "On the Nonlinear Energy Transfer in a Gravity Wave Spectrum: Part 1," *Journal of Fluid Mechanics*, vol. 12, pp. 481–500, 1962.
- [16] ——, "On the Nonlinear Energy Transfer in a Gravity Wave Spectrum: Part 2," *Journal of Fluid Mechanics*, vol. 15, pp. 273–281, 1963.
- [17] D. Benney and P. Saffman, "Nonlinear Interaction of Random Waves in a Dispersive Medium," *Proceedings of the Royal Society A*, vol. 289, no. 1418, pp. 301–320, 1966.
- [18] D. Benney and A. Newell, "Random Wave Closures," *Studies in Applied Mathematics*, vol. 48, pp. 29–53, 1969.
- [19] V. Zakharov and N. Filonenko, "The Energy Spectrum for Stochastic Oscillation of a Fluid's Surface," *Doklady Akademii Nauk*, vol. 170, pp. 1292–1295, 1966.
- [20] ——, "Weak Turbulence of Capillary Waves," *J. Appl. Mech. Tech. Phys.*, vol. 4, pp. 506–515, 1967.

- [21] V. Zakharov, "Weak Turbulence in Media with Decay Spectrum," *Journal of Applied Mechanics and Technical Physics*, vol. 6, no. 4, pp. 22–24, 1965.
- [22] A. Kolmogorov, "The Local Structure of Turbulence in Incompressible Viscous Fluid for Very Large Reynolds Numbers," *C. R. Acad. Sci. URSS*, vol. 30, pp. 301–305, 1941.
- [23] M. Onorato, A. Osborne, M. Serio, D. Resio, A. Pushkarev, V. Zakharov, and C. Brandini, "Freely Decaying Weak Turbulence for Sea Surface Gravity Waves," *Physical Review Letters*, vol. 89, no. 144501, 2002.
- [24] S. Annenkov and V. Shrira, "Numerical Modelling of Water-Wave Evolution Based on the Zakharov Equation," *Journal of Fluid Mechanics*, vol. 449, pp. 341–371, 2001.
- [25] ——, "Role of Non-Resonant Interactions in the Evolution of Nonlinear Random Water Wave Fields," *Journal of Fluid Mechanics*, vol. 561, pp. 181–207, 2006.
- [26] ——, "Direct Numerical Simulation of Downshift and Inverse Cascade for Water Wave Turbulence," *Physical Review Letters*, vol. 96, no. 204501, 2006.
- [27] S. Nazarenko, "Sandpile Behaviour in Discrete Water-Wave Turbulence," *Journal of Statistical Mechanics*, no. L02002, 2006.
- [28] P. Denissenko, S. Lukaschuk, and S. Nazarenko, "Gravity Wave Turbulence in a Laboratory Flume," *Physical Review Letters*, vol. 99, no. 014501, 2007.
- [29] S. Lukaschuk, S. Nazarenko, S. McLelland, and P. Denissenko, "Gravity Wave Turbulence in Wave Tanks: Space and Time Statistics," *Physical Review Letters*, vol. 103, no. 044501, 2009.
- [30] ——, "Statistics of Surface Gravity Wave Turbulence in the Space and Time Domains," *Journal of Fluid Mechanics*, vol. 642, pp. 395–420, 2010.
- [31] Y. L'vov, S. Nazarenko, and B. Pokorni, "Discreteness and its Effects on Water-Wave Turbulence," *Physica D*, vol. 218, pp. 24–35, 2006.

- [32] C. Connaughton, S. Nazarenko, and A. Pushkarev, “Discreteness and Quasi-Resonances in Weak Turbulence of Capillary Waves,” *Physical Review E*, vol. 63, no. 046306, 2001.
- [33] E. Falcon, C. Laroche, and S. Fauve, “Observation of Gravity-Capillary Wave Turbulence,” *Physical Review Letters*, vol. 98, no. 094503, 2007.
- [34] E. Falcon, S. Fauve, and C. Laroche, “Observation of Intermittency in Wave Turbulence,” *Physical Review Letters*, vol. 98, no. 154501, 2007.
- [35] C. Falcón, E. Falcon, U. Bortolozzo, and S. Fauve, “Capillary Wave Turbulence on a Spherical Fluid Surface in Low Gravity,” *Europhysics Letters*, vol. 86, no. 14002, 2009.
- [36] P. Caillol and V. Zeitlin, “Kinetic Equations and Stationary Energy Spectra of Weakly Nonlinear Internal Gravity Waves,” *Dynamics of Atmospheres and Oceans*, vol. 32, pp. 81–112, 2000.
- [37] Y. L’vov and E. Tabak, “Hamiltonian Formalism and the Garrett-Munk Spectrum of Internal Waves in the Ocean,” *Physical Review Letters*, vol. 87, no. 168501, 2001.
- [38] S. Galtier, “Weak Inertial-Wave Turbulence Theory,” *Physical Review E*, vol. 68, no. 015301, 2003.
- [39] M. Longuet-Higgins, A. Gill, and K. Kenyon, “Resonant Interactions between Planetary Waves and Discussion,” *Proceedings of the Royal Society of London A*, vol. 299, no. 1456, pp. 120–144, 1967.
- [40] V. Zakharov and L. Piterbarg, “Canonical Variables for Rossby Waves and Plasma Drift Waves,” *Physics Letters A*, vol. 126, no. 8–9, pp. 497–500, 1988.
- [41] A. Morin and L. Piterbarg, “On the Kinetic Equation of Rossby-Blinova Waves,” *Doklady Akademii Nauk SSSR*, vol. 295, pp. 816–820, 1987.

- [42] A. Balk and S. Nazarenko, "On the Physical Realizability of Anisotropic Kolmogorov Spectra of Weak Turbulence," *JETP Letters*, vol. 70, pp. 1031–1041, 1990.
- [43] A. Balk, S. Nazarenko, and V. Zakharov, "On the Nonlocal Turbulence of Drift Type Wave," *Physics Letters A*, vol. 146, pp. 217–221, 1990.
- [44] ——, "New Invariant for Drift Turbulence," *Physics Letters A*, vol. 152, no. 5–6, pp. 276–280, 1991.
- [45] P. Iroshnikov, "Turbulence of a Conducting Fluid in a Strong Magnetic Field," *Soviet Astronomy*, vol. 7, pp. 566–571, 1964.
- [46] E. Falgarone and T. Passot, Eds., *Turbulence and Magnetic Fields in Astrophysics*. Lecture Notes in Physics, Springer, 2003.
- [47] S. Galtier, S. Nazarenko, A. Newell, and A. Pouquet, "A Weak Turbulence Theory for Incompressible MHD," *Journal of Plasma Physics*, vol. 63, pp. 447–488, 2000.
- [48] ——, "Anisotropic Turbulence of Shear-Alfvén Waves," *The Astrophysical Journal Letters*, vol. 564, pp. 49–52, 2002.
- [49] S. Galtier, S. Nazarenko, and A. Newell, "On Wave Turbulence in MHD," *Non-linear processes in Geophysics*, vol. 8, pp. 141–150, 2001.
- [50] S. Galtier and S. Nazarenko, "Large-Scale Magnetic Field Re-Generation by Resonant MHD Wave Interactions," *Journal of Turbulence*, vol. 9, no. 40, pp. 1–10, 2008.
- [51] P. Goldreich and S. Sridhar, "Toward a Theory of Interstellar Turbulence. 2: Strong Alfvénic Turbulence," *Astrophysical Journal*, vol. 438, no. 2, pp. 763–775, 1995.
- [52] S. Nazarenko, "2D Enslaving of MHD Turbulence," *New Journal of Physics*, vol. 9, no. 307, 2007.
- [53] B. Bigot, S. Galtier, and H. Politano, "An Anisotropic Turbulent Model for Solar Coronal Heating," *Astronomy and Astrophysics*, vol. 490, pp. 325–337, 2008.

- [54] A. Alexakis, B. Bigot, H. Politano, and S. Galtier, “Development of Anisotropy in Incompressible Magnetohydrodynamic Turbulence,” *Physical Review E*, vol. 78, no. 066301, 07.
- [55] J. Saur, H. Politano, A. Pouquet, and W. Matthaeus, “Evidence for Weak MHD Turbulence in the Middle Magnetosphere of Jupiter,” *Astronomy and Astrophysics*, vol. 386, pp. 699–708, 2002.
- [56] J. Saur, “Turbulent Heating of Jupiter’s Middle Magnetosphere,” *The Astrophysical Journal Letters*, vol. 602, no. 2, pp. 137–140, 2004.
- [57] W. Vinen and J. Niemela, “Quantum Turbulence,” *Journal of Low Temperature Physics*, vol. 128, no. 516, 2002.
- [58] W. Vinen, M. Tsubota, and A. Mitani, “Kelvin-Wave Cascade on a Vortex in Superfluid He4 at Very Low Temperature,” *Physical Review Letters*, vol. 91, no. 135301, 2003.
- [59] S. Nazarenko, “Differential Approximation for Kelvin-Wave Turbulence,” *JETP Letters*, vol. 83, p. 198, 2006.
- [60] V. L’vov, S. Nazarenko, and O. Rudenko, “Bottleneck Crossover between Classical and Quantum Superfluid Turbulence,” *Physical Review B*, vol. 76, no. 024520, 2007.
- [61] ——, “Gradual Eddy-Wave Crossover in Superfluid Turbulence,” *Journal of Low Temperature Physics*, vol. 153, pp. 140–161, 2008.
- [62] S. Nazarenko and M. Onorato, “Wave Turbulence and Vortices in Bose-Einstein Condensation,” *Physica D*, vol. 219, pp. 1–12, 2006.
- [63] ——, “Freely Decaying Turbulence and Bose-Einstein Condensation in Gross-Pitaevskii Model,” *Journal of Low Temperature Physics*, vol. 146, pp. 31–46, 2007.
- [64] D. Proment, S. Nazarenko, and M. Onorato, “Quantum Turbulence Cascades in the Gross-Pitaevskii Model,” *Physical Review A*, vol. 80, no. 051603, 2009.

- [65] S. Dyachenko, A. Newell, A. Pushkarev, and V. Zakharov, "Optical Turbulence: Weak Turbulence, Condensates and Collapsing Filaments in the Nonlinear Schrödinger Equation," *Physica D*, vol. 57, p. 96, 1992.
- [66] R. Sagdeev and A. Galeev, *Nonlinear Plasma Theory*, ser. Frontiers in Physics. W.A. Benjamin, New York, 1969.
- [67] G. Düring, C. Josserand, and S. Rica, "Weak Turbulence for a Vibrating Plate: Can One Hear a Kolmogorov Spectrum?" *Physical Review Letters*, vol. 97, no. 025503, 2006.
- [68] C. Barsi, W. Wan, C. Sun, and J. W. Fleischer, "Dispersive Shock Waves with Nonlocal Nonlinearity," *Optics Letters*, vol. 32, pp. 2930–2932, 2007.
- [69] F. Arecchi, G. Giacomelli, P. Ramazza, and S. Residori, "Vortices and Defect Statistics in Two-Dimensional Optical Chaos," *Physical Review Letters*, vol. 67, pp. 3749–3752, 1991.
- [70] G. Swartzlander Jr. and C. Law, "Optical Vortex Solitons Observed in Kerr Nonlinear Media," *Physical Review Letters*, vol. 69, pp. 2503–2506, 1992.
- [71] S. Nazarenko, S. Lukaschuk, S. McLelland, and P. Denissenko, "Statistics of Surface Gravity Wave Turbulence in the Space and Time domains," *Journal of Fluid Mechanics*, vol. 642, pp. 395–420, 2010.
- [72] A. Majda, D. McLaughlin, and E. Tabak, "A One-Dimensional Model for Dispersive Wave Turbulence," *Journal of Nonlinear Science*, vol. 6, pp. 9–44, 1997.
- [73] V. Zakharov, F. Dias, and A. Pushkarev, "One-Dimensional Wave Turbulence," *Physics Reports*, vol. 398, pp. 1–65, 2004.
- [74] E. Kartashova, "Partitioning of Ensembles of Weakly Interaction Dispersive Waves in Resonators into Disjoint Classes," *Physica D*, vol. 46, pp. 43–56, 1990.
- [75] ——, "On Properties of Weakly Nonlinear Wave Interactions in Resonators," *Physica D*, vol. 54, pp. 125–134, 1991.

- [76] ——, “Weakly Nonlinear Theory of Finite-Size Effects in Resonators,” *Physical Review Letters*, vol. 73, pp. 2013–2016, 1994.
- [77] ——, “Clipping A New Investigation Method for PDEs in Compact Domains,” *Theoretical and Mathematical Physics*, vol. 99, no. 3, pp. 675–680, 1994.
- [78] ——, *Nonlinear Waves and Weak Turbulence*. Springer-Verlag, 1998, ch. Wave Resonances in Systems with Discrete Spectra, p. 95.
- [79] E. Kartashova and G. Mayrhofer, “Cluster Formation in Mesoscopic Systems,” *Physica A: Statistical Mechanics and its Applications*, vol. 385, pp. 527–542, 2007.
- [80] E. Kartashova, S. Nazarenko, and O. Rudenko, “Resonant Interactions of Nonlinear Water Waves in a Finite Basin,” *Physical Review E*, vol. 78, no. 016304, 2008.
- [81] A. Pushkarev, “On the Kolmogorov and Frozen Turbulence in Numerical Simulation of Capillary Waves,” *European Journal of Mechanics - B/Fluids*, vol. 18, pp. 345–351, 1999.
- [82] V. Zakharov, A. Korotkevich, A. Pushkarev, and A. Dyachenko, “Mesoscopic Wave Turbulence,” *JETP Letters*, vol. 82, no. 8, pp. 487–491, 2005.
- [83] A. Pushkarev and V. Zakharov, “Turbulence of Capillary Waves - Theory and Numerical Simulation,” *Physica D*, vol. 135, pp. 98–116, 2000.
- [84] D. Cai, A. Majda, D. McLaughlin, and E. Tabak, “Dispersive Wave Turbulence in One Dimension,” *Physica D*, vol. 152–153, pp. 551–572, 2001.
- [85] V. L’vov and S. Nazarenko, “Spectrum of Kelvin-Wave Turbulence in Superfluids,” *JETP Letters*, vol. 91, no. 8, pp. 428–434, 2010.
- [86] H. Wyld, “Formulation of the Theory of Turbulence in an Incompressible Fluid,” *Annals of Physics*, vol. 14, pp. 143–165, 1961.

- [87] V. L'vov, Y. L'vov, A. Newell, and V. Zakharov, "Statistical Description of Acoustic Turbulence," *Physical Review E*, vol. 56, no. 390–405, 1997.
- [88] V. Zakharov and V. L'vov, "The Statistical Description of the Nonlinear Wave Fields," *Radiophysics and Quantum Electronics*, vol. 18, no. 10, pp. 1084–1097, 1975.
- [89] A. Newell, "The Closure Problem in a System of Random Gravity Waves," *Reviews of Geophysics*, vol. 6, no. 1, pp. 1–31, 1968.
- [90] R. Davidson, *Methods in Nonlinear Plasma Theory*. Academic Press, New York, 1972.
- [91] C. Connaughton, "New Directions in Wave Turbulence," Ph.D. dissertation, University of Warwick, 2002.
- [92] Y. Choi, Y. L'vov, and S. Nazarenko, "Probability Densities and Preservation of Randomness in Wave Turbulence," *Physical Review A*, no. 332, 2004.
- [93] Y. L'vov and S. Nazarenko, "Noisy Spectra, Long Correlations and Intermittency in Wave Turbulence," *Physical Review E*, vol. 69, no. 066608, 2004.
- [94] S. Nazarenko and B. Quinn, "Triple Cascade Behavior in Quasi-geostrophic and Drift Turbulence and Generation of Zonal Jets," *Physical Review Letters*, vol. 103, no. 118501, 2009.
- [95] A. Balk, S. Nazarenko, and V. Zakharov, "On the Structure of the Rossby/Drift Turbulence and Zonal Flows," *Proceedings of the International Symposium Generation of Large-Scale Structures in Continuous Media, Perm-Moscow, USSR*, no. 34–35, 1990.
- [96] V. Krasitskii, "On Reduced Equations in the Hamiltonian Theory of Weakly Nonlinear Surface Waves," *Journal of Fluid Mechanics*, vol. 272, pp. 1–20, 1994.
- [97] V. Zakharov, "Statistical Theory of Gravity and Capillary Waves on the Surface of a Finite-Depth Fluid," *European Journal Mechanics B/Fluids*, vol. 18, no. 3, pp. 327–344, 1999.

- [98] ——, “Stability of Periodic Waves of Finite Amplitude on the Surface of a Deep Fluid,” *J. Appl. Mech. Tech. Phys.*, vol. 9, pp. 190–194, 1968.
- [99] E. Kozik and B. Svistunov, “Scale-Separation Scheme for Simulating Superfluid Turbulence: Kelvin-Wave Cascade,” *Physical Review Letters*, vol. 94, no. 025301, 2005.
- [100] A. Newell and V. Zakharov, “The Role of the Generalized Phillips’ Spectrum in Wave Turbulence,” *Physical Review A*, vol. 372, no. 23, pp. 4230–4233, 2008.
- [101] R. Kraichnan, “Inertial Ranges in Two Dimensional Turbulence,” *Physics of Fluids*, vol. 10, p. 1417, 1967.
- [102] ——, “Inertial-Range Transfer in Two- and Three-Dimensional Turbulence,” *Journal of Fluid Mechanics*, vol. 47, pp. 525–535, 1971.
- [103] R. Fjørtoft, “On the Changes in the Spectral Distribution of Kinetic Energy for Two-Dimensional Nondivergent Flow,” *Tellus*, vol. 5, pp. 225–230, 1953.
- [104] O. Phillips, “The Equilibrium Range in the Spectrum of Wind Generated Waves,” *Journal of Fluid Mechanics*, vol. 4, pp. 426–434, 1958.
- [105] E. Dewan, “Saturated-Cascade Similitude Theory of Gravity Wave Spectra,” *Journal of Geophysical Research*, vol. 102, no. D25, pp. 29 799–29 817, 1997.
- [106] P. Billant and J. Chomaz, “Self-Similarity of Strongly Stratified Inviscid Flows,” *Physics of Fluids*, vol. 13, pp. 1645–1651, 2001.
- [107] L. Smith and F. Waleffe, “Transfer of Energy to Two-Dimensional Large Scales in Forced, Rotating Three-Dimensional Turbulence,” *Physics of Fluids*, vol. 11, no. 6, pp. 1608–1622, 1999.
- [108] C. Cambon, R. Rubinstein, and F. Godeferd, “Advances in Wave Turbulence: Rapidly Rotating Flows,” *New J. Phys.*, vol. 6, p. 73, 2004.
- [109] P. Rhines, “Waves and Turbulence on a Beta-Plane,” *Journal of Fluid Mechanics*, vol. 69, p. 417, 1975.

- [110] B. Galperin, S. Sukoriansky, and H.-P. Huang, “Universal n^5 Spectrum of Zonal Flows on Giant Planets,” *Physics of Fluids*, vol. 13, pp. 1545–1548, 2001.
- [111] W. Vinen, “Classical Character of Turbulence in a Quantum Liquid,” *Physical Review B*, vol. 61, pp. 1410–1420, 2000.
- [112] C. Leith, “Diffusion Approximation to Inertial Energy Transfer in Isotropic Turbulence,” *Physics of Fluids*, vol. 10, p. 1409, 1967.
- [113] ——, “Diffusion Approximation for Turbulent Scalar Fields,” *Physics of Fluids*, vol. 11, p. 1612, 1968.
- [114] C. Connaughton and S. Nazarenko, “Warm Cascades and Anomalous Scaling in a Diffusion Model of Turbulence,” *Physical Review Letters*, vol. 92, no. 044501, 2004.
- [115] S. Hasselmann and K. Hasselmann, “Computations and Parameterizations of the Nonlinear Energy Transfer in Gravity Wave Apectrum,” *Journal of Physical Oceanography*, vol. 15, pp. 1369–1377, 1985.
- [116] R. Iroshnikov, “Possibility of a Non-Isotropic Spectrum of Wind Waves by their Weak Nonlinear Interaction,” *Soviet Physics. Dokl.*, vol. 30, p. 126, 1985.
- [117] V. Zakharov and A. Pushkarev, “Diffusion Model of Interacting Gravity Waves on the Surface of Deep Fluid,” *Nonlinear Processes in Geophysics*, vol. 6, pp. 1–10, 1999.
- [118] V. L'vov, S. Nazarenko, and G. Volovik, “Energy Spectra of Developed Superfluid Turbulence,” *JETP Letters*, vol. 80, p. 535, 2004.
- [119] V. L'vov and S. Nazarenko, “Differential Models for 2D Turbulence,” *JETP Letters*, vol. 83, pp. 635–639, 2006.
- [120] V. L'vov, S. Nazarenko, and L. Skrbek, “Energy Spectra of Developed Turbulence in Helium Superfluids,” *Journal of Low Temperature Physics*, vol. 145, p. 125, 2006.

- [121] D. Evans, E. Cohen, and G. Morriss, "Probability of Second Law Violations in Shearing Steady States," *Physical Review Letters*, vol. 71, no. 15, pp. 2401–2404, 1993.
- [122] D. Evans and D. Searles, "Equilibrium Microstates which Generate Second Law Violating Steady States," *Physical Review E*, vol. 50, no. 2, pp. 1645–1648, 1994.
- [123] G. Gallavotti and E. Cohen, "Dynamical Ensembles in Stationary States," *Journal of Statistical Physics*, vol. 80, pp. 931–970, 1995.
- [124] M. Bandi, S. Chumakov, and C. Connaughton, "Probability Distribution of Power Fluctuations in Turbulence," *Physical Review E*, vol. 79, no. 016309, 2009.
- [125] E. Falcon, S. Aumaître, C. Falcón, C. Laroche, , and S. Fauve, "Fluctuations of Energy Flux in Wave Turbulence," *Physical Review Letters*, vol. 100, no. 064503, 2008.
- [126] E. Kozik and B. Svistunov, "Theory of Decay of Superfluid Turbulence in the Low-Temperature Limit," *Journal of Low Temperature Physics*, vol. 156, pp. 215–267, 2009.
- [127] ——, "Kolmogorov and Kelvin Wave Cascades of Superfluid Turbulence at $T = 0$: What is in between?" *Physical Review B*, vol. 77, no. 060502, 2008.
- [128] E. Madelung, "Quantetheorie in Hydrodynamischer Form," *Zeit. F. Phys*, vol. 40, pp. 322–326, 1927.
- [129] J. Koplik and H. Levine, "Vortex Reconnection in Superfluid Helium," *Physical Review Letters*, vol. 71, pp. 1375–1378, 1993.
- [130] N. Berloff and B. Svistunov, "Scenario of Strongly Non-Equilibrated Bose-Einstein Condensation," *Physical Review A*, vol. 66, no. 13603, 2002.
- [131] C. Nore, M. Abid, and M. Brachet, "Decaying Kolmogorov Turbulence in a Model of Superflow," *Physics of Fluids*, vol. 9, pp. 2644–2669, 1997.

- [132] M. Kobayashi and M. Tsubota, “Kolmogorov Spectrum of Superfluid Turbulence: Numerical Analysis of the Gross-Pitaevskii Equation with a Small-Scale Dissipation,” *Physical Review Letters*, vol. 94, no. 65302, 2005.
- [133] ——, “Kolmogorov Spectrum of Quantum Turbulence,” *Physical Society of Japan*, vol. 74, pp. 3248–3258, 2005.
- [134] S. Alamri, A. Youd, and C. Barenghi, “Reconnection of Superfluid Vortex Bundles,” *Physical Review Letters*, vol. 101, no. 215302, 2008.
- [135] K. Schwarz, “Three-Dimensional Vortex Dynamics in Superfluid ^4He : Line-line and Line-Boundary Interactions,” *Physical Review B*, vol. 31, pp. 5782–5804, 1985.
- [136] ——, “Three-Dimensional Vortex Dynamics in Superfluid ^4He : Homogeneous Superfluid Turbulence,” *Physical Review B*, vol. 38, pp. 2398–2417, 1988.
- [137] R. Donnelly, *Quantized Vortices in Helium II*. Cambridge University Press, 1991.
- [138] W. Thomson, “Vibrations of a columnar vortex,” *Phil Mag*, vol. 10, pp. 155–168, 1880.
- [139] C. Barenghi, R. Hänninen, and M. Tsubota, “Anomalous Translational Velocity of Vortex Ring with Finite-Amplitude Kelvin Waves,” *Physical Review E*, vol. 71, no. 046303, 2006.
- [140] H. Hasimoto, “Superfluid Turbulence in the Low-Temperature Limit,” *Journal of Fluid Mechanics*, vol. 51, no. 477, 1972.
- [141] L. Smith and V. Yakhot, “Finite-Size Effects in Forced Two-Dimensional Turbulence,” *Journal of Fluid Mechanics*, vol. 274, pp. 115–138, 1994.
- [142] S. Musher, A. Rubenchik, and V. Zakharov, “Hamiltonian Approach to the Description of Nonlinear Plasma Phenomena,” *Physics Reports*, vol. 129, pp. 285–366, 1985.

- [143] S. Nazarenko and V. Zakharov, "Dynamics of the Bose-Einstein Condensation," *Physica D*, vol. 201, pp. 203–211, 2005.
- [144] C. Connaughton, C. Josserand, A. Picozzi, Y. Pomeau, and S. Rica, "Condensation of Classical Nonlinear Waves," *Physical Review Letters*, vol. 95, no. 236901, 2005.
- [145] M. Anderson, J. Ensher, M. Matthews, C. Wieman, and E. Cornell, "Observation of Bose-Einstein Condensation in a Dilute Atomic Vapor," *Science*, vol. 269, pp. 198–201, 1995.
- [146] L. Pitaevskii and S. Stringari, *Bose-Einstein Condensation*. Clarendon Press, Oxford, 2003.
- [147] S. Bose, "Plancks Gesetz und Lichtquantenhypothese," *Zeitschrift für Physik*, vol. 26, pp. 178–181, 1924.
- [148] R. Chiao and J. Boyce, "Bogoliubov Dispersion Relation and the Possibility of Superfluidity for Weakly Interacting Photons in a Two-Dimensional Photon Fluid," *Physical Review A*, vol. 60, pp. 4114–4121, 1999.
- [149] N. Tabiryan, A. Sukhov, and V. Zeldovich, "The Orientational Optical Nonlinearity of Liquid Crystals," *Molecular Crystals and Liquid Crystals*, vol. 136, p. 1, 1986.
- [150] I. Khoo, *Liquid Crystals: Physical Properties and Nonlinear Optical Phenomena*. Wiley, 1995.
- [151] E. Braun, L. Faucheux, and A. Libchaber, "Strong Self Focusing in Nematic Liquid Crystals," *Physical Review A*, vol. 48, pp. 611–622, 1993.
- [152] M. Peccianti, C. Conti, G. Assanto, A. D. Luca, and C. Umeton, "Routing of Anisotropic Spatial Solitons and Modulational Instability in Liquid Crystals," *Nature*, vol. 432, p. 733, 2004.
- [153] M. Peccianti, C. Conti, and G. Assanto, "Optical Modulational Instability in a Nonlocal Medium," *Physical Review E*, vol. 68, no. 025602, 2003.

- [154] C. Conti, M. Peccianti, and G. Assanto, “Complex Dynamics and Configurational Entropy of Spatial Optical Solitons in Nonlocal Media,” *Optics Letters*, vol. 31, no. 13, pp. 2030–2032, 2006.
- [155] V. Zakharov, A. Pushkarev, V. Shvets, and V. Yan’kov, “Soliton Turbulence,” *JETP Letters*, vol. 48, no. 2, pp. 83–87, 1988.
- [156] B. Rumpf and A. Newell, “Coherent Structures and Entropy in Constrained, Modulationally Unstable, Nonintegrable Systems,” *Physical Review Letters*, vol. 87, p. 5, 2001.
- [157] ——, “Localization and Coherence in Nonintegrable Systems,” *Physica D*, vol. 184, pp. 162–191, 2003.
- [158] B. Barviau, B. Kibler, A. Kudlinski, A. Mussot, H. Millot, and A. Picozzi, “Experimental Signature of Optical Wave Thermalization Through Supercontinuum Generation in Photonic Crystal Fiber,” *Optical Express*, vol. 17, p. 7392, 2009.
- [159] A. Eisner and B. Turkington, “Nonequilibrium Statistical Behavior of Nonlinear Schrödinger Equations,” *Physica D*, vol. 213, pp. 85–97, 2006.
- [160] R. Jordan and C. Josserand, “Self-Organization in Nonlinear Wave Turbulence,” *Physical Review E*, vol. 61, p. 1, 2000.
- [161] T. C. K.Ø. Rasmussen and P. Kevrekidis, “Statistical Mechanics of a Discrete Nonlinear System,” *Physical Review Letters*, vol. 84, p. 17, 2000.
- [162] R. Jordan, B. Turkington, and C. Zirbel, “A Mean-Field Statistical Theory for the Nonlinear Schrödinger Equation,” *Physica D*, vol. 137, pp. 353–378, 2000.
- [163] A. Picozzi, S. Pitois, and G. Millot, “Spectral Incoherent Solitons: a Localized Soliton Behavior in the Frequency Domain,” *Physical Review Letters*, vol. 101, no. 093901, 2008.
- [164] S. Pitois, S. Langrange, H. Jauslin, and A. Picozzi, “Velocity Locking of Incoherent Nonlinear Wave Packets,” *Physical Review Letters*, vol. 97, no. 033902, 2006.

- [165] V. Petviashvili and V. Yan'kov, "Solitons and Turbulence," *Reviews of Plasma Physics*, vol. 14, 1987.
- [166] P. D. Gennes and J. Prost, *The Physics of Liquid Crystals*. Oxford Science Publications, 1992.
- [167] V. Zakharov and S. Manakov, "On the Complete Integrability of a Nonlinear Schrödinger Equation," *Journal of Theoretical and Mathematical Physics*, vol. 19, pp. 551–559, 1974.
- [168] T. Benjamin and J. Feir, "The Disintegration of Wave Trains on Deep Water Part 1. Theory," *Journal of Fluid Mechanics*, vol. 27, pp. 417–430, 1967.
- [169] B. Fornberg, *A Practical Guide to Pseudospectral Methods*. Cambridge University Press, 1998.
- [170] C. Canuto, M. Hussaini, A. Quarteroni, and T. Zang, *Spectral Methods: Fundamentals in Single Domains*. Springer, 2006.
- [171] H. Talbot, "Facts Relating to Optical Science," *Phil. Mag.*, vol. 9, pp. 401–407, 1836.
- [172] M. Berry, I. Marzoli, and W. Schleich, "Quantum Carpets, Carpets of Light," *Physics World*, pp. 1–6, 2001.
- [173] I. Gradstein and I. Ryzhik, *Table of Integrals, Series, and Products*. Academic Press, 1980.